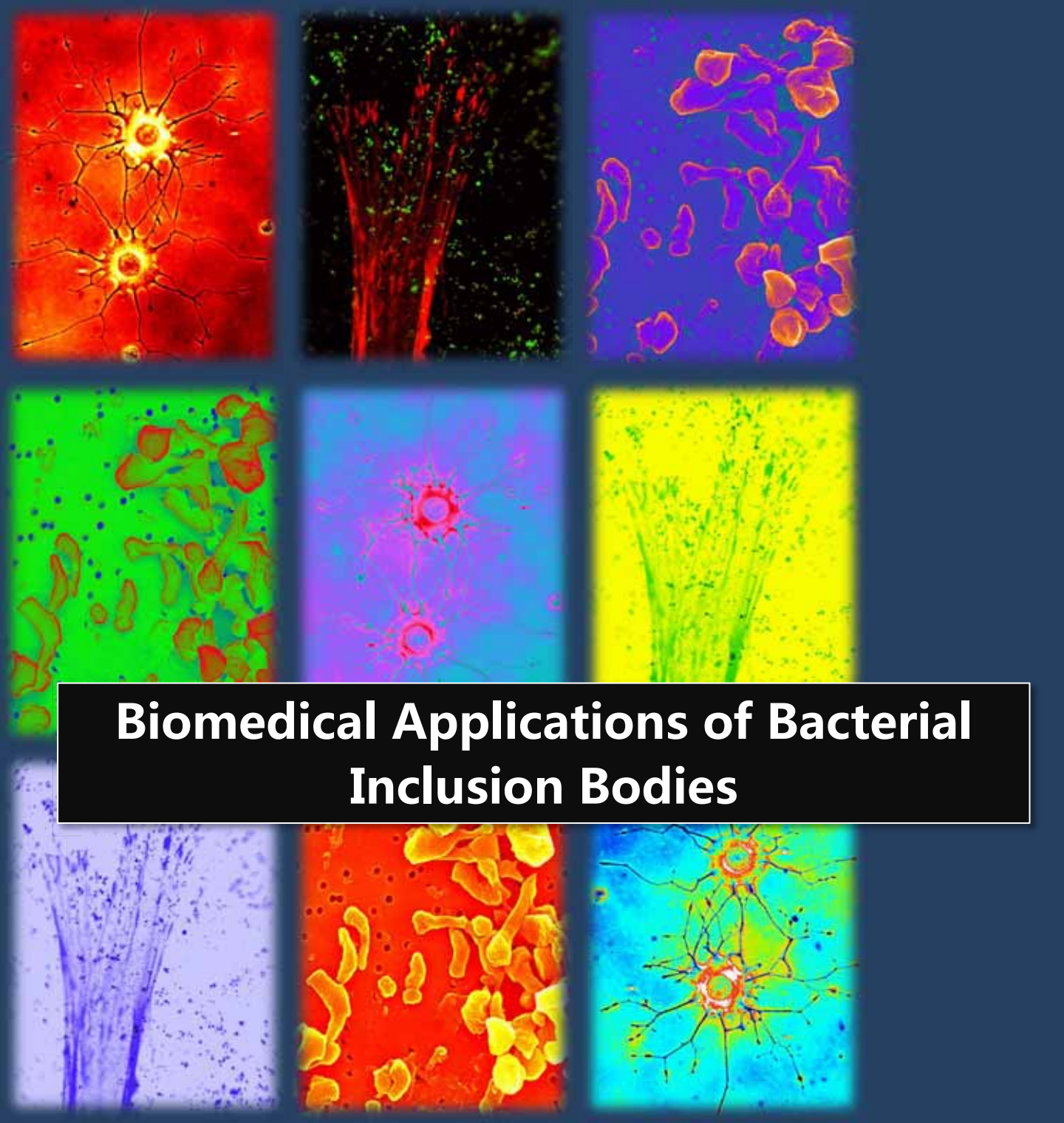

Biomedical Applications of Bacterial Inclusion Bodies

PhD Thesis
Joaquin Seras Franzoso

Directors:
Elena García Fruitós, Antonio Villaverde Corrales i Esther Vazquez Gomez

Facultat de Biociències / Dept. De Genètica i de Microbiologia
Institut de Biotecnologia i de Biomedicina
Universitat Autònoma de Barcelona

UAB
Universitat Autònoma de Barcelona

Contents

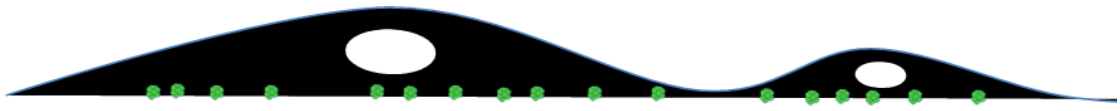

Introduction

Biological life is possible mainly thanks to the combined action of organic molecules such as carbohydrates, lipids and proteins that carry out essential functions supporting organisms existence. Among them, proteins are probably the most complex and interesting macromolecules due to the immense number of activities they can develop. It is well known the key role that proteins play in all living organisms even if a high amount of them remain still undiscovered or their biological significance unidentified. Proteins are responsible for the metabolic reactions carried out within the cells, are structural components, take part in the signaling process, are involved in the respiratory chain, are the motor of cell movement in both unicellular and pluricellular organisms and form the basis of the immune system, just to mention some of their functions. Thus, proteins have a great deal of importance regarding the good performance of any organism. In fact, the lack of a specific protein, the failure in reaching its proper structure or the misregulation of its activity can derive in many cases in disease. Some examples of protein-linked diseases are: cystic fibrosis, diabetes, Alzheimer or Parkinson.

In this scenario it is obvious the interest that the protein universe rise for biotechnological and biomedical applications. Many protein activities have been proved extremely useful for industry. From diary[1] to mining industry[2] we can find examples of processes carried out by purified enzymes, proteins acting as catalysers of a specific reaction, or microorganisms, pointing out that there are enzymes within the microorganisms which are responsible for the mentioned reaction. Industry has been largely benefited by the stereoselectivity and substrate specificity of enzymes as well as by the ability of proteins for performing reactions in friendlier conditions than the ones provided by classical chemistry, improving in most of the cases the safety of the process and reducing the amount of possible hazardous by-products. But also, proteins have been considered the final product themselves; such is the case of lipases and other enzymes that we commonly find in detergents[3].

In the medical field we can find examples of proteins with a high relevance in human health too. In this regard many proteins have been successfully marketed such as insulin, cytokines, interferon and immunoglobulins with many uses in disease treatment, diagnosis processes and research of new treatments.

1. Protein synthesis and folding

Protein synthesis occurs in ribosomes by the combination of 20 amino acids linked through the formation of peptide bonds. The sequence of amino acids or polypeptide chain can differ in length and composition and represents the primary structure of the forming protein. However, this chain needs to be folded to achieve its three dimensional (3D) structure and thus protein functionality.

A completely folded protein shows several levels of structural complexity being the unfolded protein the simplest one. We also find secondary structure in which inter-residue interactions are established conferring a certain degree of stability, among the most common secondary structures found in proteins are α-helix and β-sheet. Then, these structures are organized and maintained in a stable 3D structure by disulphide bonds, ionic bonds, hydrophobic interactions, hydrogen bonds and Van der Waals forces within the amino acids of the protein backbone resulting in tertiary structure. An extra level of complexity appears when, in order to carry out its biological activity, a protein needs to interact with other proteins or subunits; these complexes constitute the quaternary structure. However, protein folding shouldn't be seen as a sequential pathway, in which a predetermined series of interactions and transitional structures must occur before reaching the native conformation rather than as a unique process in which different type of interactions guide the polypeptide chain to a functional 3D structure.

To better understand how protein folding takes place it is important to note that all the information required for the proper protein folding is encoded within the amino acid sequence[4]. However, so far the complexity of this process has not been elucidated. It is known that proteins don't fold randomly since the time required to try every possible conformation till ending by chance into the native structure will be extremely long[5]. The most accepted model to describe protein folding pathway combine the formation of secondary structure, restricting the number of combinations in which residues within the polypeptide chain could interact, and the hydrophobic collapse. The last mentioned event is induced by interactions established between non-polar residues that would situate themselves in the core of the protein, leaving in the external part the most hydrophilic zones (molten globule state). Thus, a folding nucleus is created, around

which the remainder structure condenses rapidly[6, 7]. From a thermodynamic point of view this process would lead unfolded protein through an energetic landscape till arriving to a stable state where the free energy is the lowest (figure 1). This minimum corresponds to the protein native structure. However, several depressions of free energy could be found along the pathway, being more frequent the bigger and complex is the folding protein. These transient minimums of free energy show the semi-stable folding intermediates adopted by the polypeptide chain during its folding process[8].

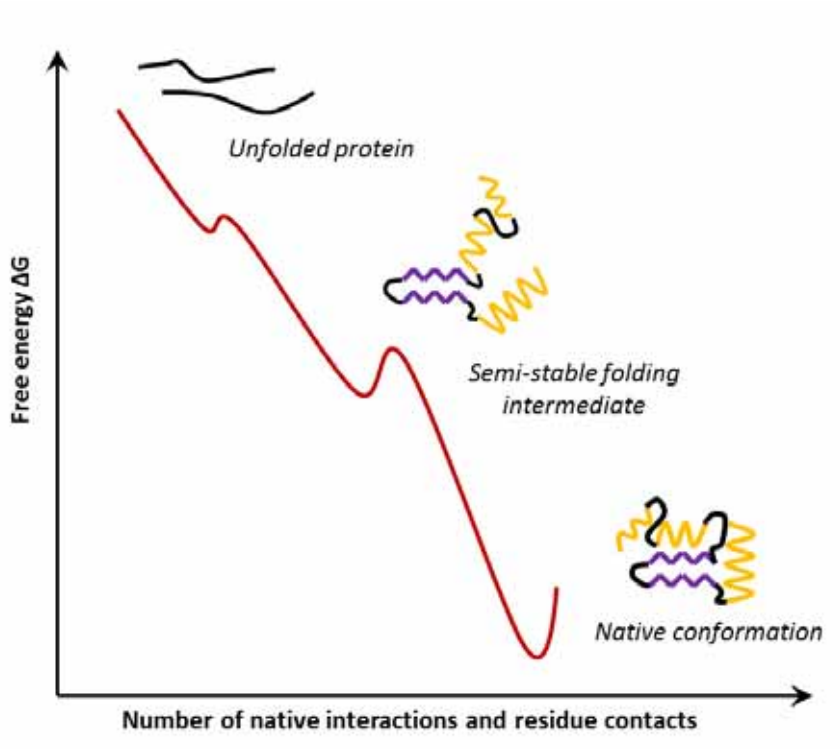

Figure 1 Schematic representation of the protein folding energetic landscape.

Nevertheless, due to the complexity of the folding process in which so diverse variables intervene (including aminoacid sequence, environmental conditions, cell metabolism or interaction with other proteins), not all the synthesized polypeptide chains reach their native conformation. These protein species are known as misfolded proteins. Misfolded species often expose on their surface hydrophobic patches that should be situated in the core of the protein when they are in their native form. This results in highly unstable molecules when they are placed in an aqueous environment such as the cell cytosol[9]. Thus, misfolded species will tend to bury their exposed hydrophobic regions by the interaction between two or more misfolded proteins through their hydrophobic patches originating *protein aggregation*. When protein

aggregation occurs in recombinant bacteria, it results in amorphous protein deposits named bacterial Inclusion bodies (IBs) (see section 3), but also eukaryotic cells can be subjected to protein aggregation. In this case two different types of aggregates can be formed, aggresomes in which misfolded proteins are deposited around the microtubule organizing center and show similar morphology with IBs[10] and amyloid fibrils. These misfolded protein fibrils are composed by polypeptides that adopt β-sheet structure and assembly in a fibril structure by the interaction of repetitive monomers, oriented perpendicularly to the fibril axis, by hydrogen bonds[11] (figure 2).

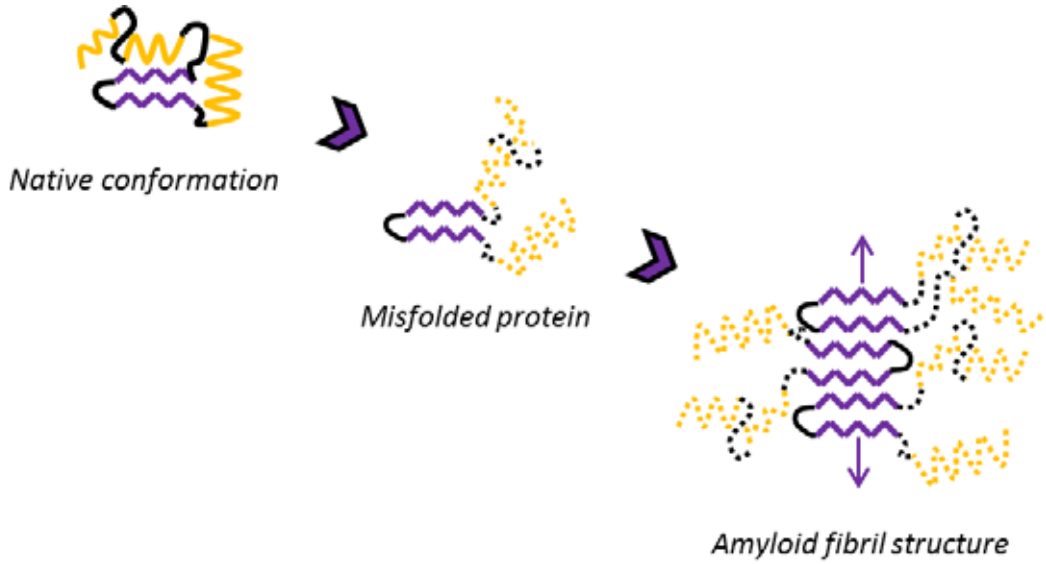

Figure 2 Schematic representation of amyloid fibril formation.

Protein aggregation is one of the major bottlenecks in protein production industry when using bacterial platforms as expression system, being *Escherichia coli* (*E. coli*) the most exploited of them. This phenomenon causes great losses by either reducing the amount of soluble protein obtained or increasing the production cost by the need to implement complex and not always effective re-folding processes to return misfolded species to their native structure. However, protein aggregation has a great incidence also in disease. In human health, several pathologies have been found to be related with amyloid fibrils or plaques formation such as Alzheimer, Parkinson, Huntington and transmissible spongiform encephalopathies like mad cow disease, Kuru disease or Creutzfeldt-Jakob disease[11]. Nevertheless, it is believed that the pathogenic form of the above mentioned diseases are the oligomer intermediates found in the aggregation process rather than the mature fibril, which in fact could be acting as a

resistance mechanism to avoid the free circulation of the toxic species. Moreover, amyloid fibril formation is not always linked to protein misfolding. Some naturally occurring proteins are shown to require amyloid fibril formation to achieve their native and therefore biological active state. That is the case of Curli[12] and Chaplins[13] proteins in bacteria or some hormones in which secretion is done in form of amyloid aggregates from which soluble protein is steady released[14].

2. Recombinant protein production

The development of recombinant genetics in the seventies provided the tools that allowed engineering DNA sequences by copying, cutting and covalently linking small fragments of DNA. These three actions were crucial for recombinant protein production origin, since they made possible to introduce genes codifying for proteins of interest in expression vectors and to synthetize the protein in a different system than the source organism. This fact supposed the possibility of obtaining significant amounts of product overcoming the low availability of protein in their natural environment and allowing taking advantage of the huge spectrum of functions that these molecules can offer. Thus, proteins could be produced and their biological activity exploited in sectors so diverse such as the textile industry in which enzymes are used for instance to soften cotton fabric or the human health where proteins are commonly applied for diagnosis and treatment of many diseases.

Several factors play an important role in the success of recombinant protein production being the choice of the producing organism the one which will determine the subsequent strategy. Nowadays, it is possible to produce heterologous proteins in microorganisms like bacteria, yeast or fungi, in insect cells, mammalian cells or even in complex organisms like plants or animals. Despite the advantages offered by eukaryotic cell cultures, it is important to note that the production process difficulty and therefore its cost are proportional to the producing system complexity. However, protein production yield usually decrease while increasing the intricacy of the producing platform.

Therefore, a priori, one would choose the simplest platform to perform recombinant protein production. Nevertheless, it is important to consider the features of the protein of interest, since production in lower organisms, like bacteria, is impaired for the production of proteins requiring specific post-translational modifications to achieve their biological activity. Among these modifications we can find glycosylations, phosphorylations or the formation of disulfide bonds. In some cases it is possible to overcome these barriers by using genetic engineered strains[15] (see section 2.2.2).

However, these approaches are not always successful and in some cases the protein production in complex systems cannot be avoided.

In summary even if some proteins can only be produced in a functional form in biologically complex production systems, the first option to set a recombinant production process are still microorganisms, mainly *E. coli*, due to its a priori high protein production yield, growth speed, and low cost.

2.1 Protein production in *E. coli*

E. coli is a Gram-negative enterobacteria naturally found in the gut of warm blood organisms. Being part of the normal intestinal flora, *E. coli* helps in preventing the establishment of pathogenic organisms and providing vitamin K_2[16]. However, several serotypes have been shown to be pathogenic, being one of the major causes of foodborne disease[17].

In the laboratory context, *E. coli* has been widely used and studied to elucidate regulatory genetic networks, protein functions or to develop metabolism studies[18, 19]. The extensive investigation of this model organism has provided a huge amount of tools also applicable in recombinant protein production. Nowadays, it is available a wide spectrum of cloning and protein expression vectors, efficient systems for the introduction and manipulation of exogenous DNA as well as *E. coli* mutant strains, optimized to carry out specific activities. In addition, the vast knowledge of *E. coli* metabolism and physiology allows the optimization of the bacterial cell growing and protein expression conditions, and also favors an efficient scaling-up of the process when necessary.

2.2 Relevant factors in *E. coli* recombinant protein production.

Several factors have to be considered in order to establish an efficient protein production strategy in *E. coli*, being crucial the choice of the expression vector as well as the producing strain.

2.2.1 Vector

Vectors are the entities responsible of carrying and transfer genetic information from one organism to another. In protein production are used to provide to the

microbial cell factory with the gene encoding the protein of interest. The most common vectors used for protein production in *E. coli* are plasmids, but other vectors can be found such as phagemids[20]. Bacterial plasmids are small circular extrachromosomal double stranded DNA (dsDNA) molecules that replicate autonomously in the cell. They are defined by several features or elements that will determine their utility.

Origin of replication (ori). The origin of replication is the sequence where plasmid replication starts and will determine the plasmid number of copies. Depending on the case it would be interesting to use either low or high copy number plasmids (from one to several hundreds of molecules per cell). High copy number plasmids show higher stability within the cell during cell division but, on the other hand, cells tend to grow slower than the ones containing low copy number plasmids. In addition, ori also define plasmid compatibility since two different plasmids sharing the same ori cannot co-exist. This fact is particularly important for applications in which more than one plasmid is required. Some commonly used ori in protein production are ColE1, p15A or pMB1[21].

Promoter: A promoter is a DNA region situated upstream of a gene devoted to regulate the gene expression. It can be composed by more than one DNA sequence. In bacteria, they are usually formed by two short DNA sequences (6-7 nucleotides) situated at -10 (Pribnow box) and at -35 from the transcription start site. Pribnow is an evolutively conserved box essential in order to start the transcription reaction. Nevertheless, this box exhibits a certain degree of plasticity regarding the forming nucleotides. -35 sequence increase RNA polymerase transcription rate. The variability between elements involved in the promoter structure as well as their nucleotide composition allows this regulatory region to finely modulate gene expression by changing the affinity of these sequences to RNA polymerase and transcription factors. These factors also recognize the promoter and regulates transcription rate by enhancing or blocking RNA polymerase recruitment[22].

In protein production, in which usually high production yields are pursued, it is common to use strong promoters to control the expression of the gene of interest, achieving the amount of recombinant protein in some cases up to 30 % of the total cellular protein[23]. In this context, it is important to note that most of the promoters used in protein expression plasmids are inducible by an external agent or condition. That

means one can control the exact moment to switch on protein expression. This external control is crucial when the protein of interest is detrimental for the microbial host. In addition, an ideal promoter for protein production should have a low level of basal expression since an incomplete repression of the protein production could cause plasmid instability or slower cell growth representing a decrease of the production yield.

At the laboratory scale and more precisely along this work, two common promoters have been used for protein production and IB deposition, Ptrc and T7 RNA polymerase promoter based system. Ptrc is a synthetic promoter formed by the combination of the Tryptophan -35 region and LAC -10 region, it is a strong promoter inducible by lactose and its analogues such as isopropyl-β-D-thiogalactopyranoside (IPTG)[24]. pET expression plasmids are based in the T7 RNA polymerase and its promoter, which exhibits high levels of protein expression. The gene of interest is placed in a plasmid under control of the T7 RNA polymerase promoter and transformed to a specific *E. coli* strain (DE3), containing in its chromosome the λDE3 prophage with the T7 RNA polymerase gene under control of a lacUV5 promoter[25]. Thus, in presence of lactose or IPTG, T7 RNA polymerase production is induced, which in turn transcribes the gene of interest. Both promoters contain lac operators, so they are repressed in absence of inducer.

However, despite these systems perform efficiently at the laboratory scale, it is advisable to use other types of promoters in larger productions such as promoters inducible by temperature (e.g λp_L)[24] or inexpensive chemicals (e.g trp, pBAD)[26] since IPTG, despite being a strong inducer, it is expensive and could be toxic at high concentrations.

Selection markers: Selection markers are genes placed in the plasmid sequence which products confer to the cells containing these plasmids prevalence against the ones who lack them. The most used selection markers in the laboratory are genes conferring resistance to determined antibiotics such as ampicillin, kanamycin, chloramphenicol or tetracycline. In industry the use of antibiotics is largely contraindicated due to the prize and, depending on the product, the potential harm for human health. In these cases gene selection by auxotrophies, extensively used in yeast[27], is more suitable.

2.2.2 Strain

Nowadays thanks to the development of recombinant genetics it is available a huge variety of engineered strains, each one of them devoted to carry out a specific function. In this sense, the most common strains used for protein production are those which allow overcoming one or more of the possible bottlenecks found along the process. Some examples of *E. coli* strains are: BL21(DE3)[28] knock out for Lon and OmpT proteases that may degrade the produced recombinant protein. In addition, the presence of the prophage λDE3 enables the use of the T7 RNA polymerase system for protein expression. Rosetta strain, which supplies through a pRARE plasmid several tRNA for strange codons that often hinder the production of eukaryotic proteins in microbial platforms. Origami strains, which are negative mutants for trx and gor genes providing an oxidizing cytosol that favors the formation of disulfide bonds[29] (**see annex 1**) and C41 (DE3) and C43 (DE3)[30], BL21 (DE3) derivatives that have been selected for their capacity of expressing membrane proteins otherwise toxic for the host cell. Another interesting example is the use of strains that reproduce the eukaryotic glycosylation pathway. In this strategy the bacterial strain is engineered by introducing part of the eukaryotic glycosylation set of genes[31].

Besides, the possibility of easily modifying the *E. coli* genome, allows tailoring the producing strains towards a desired field of study. Also, mutant strains for specific genes can be obtained and used to produce proteins with unpredictable features[32]. It is the case of the K-12 derivatives, defective for DnaK, ClpA and ClpP protein quality modulators, used in these work to obtain physico-chemically distinct bacterial inclusion bodies (**see annex 2**).

2.3 Protein quality control network in *E. coli*

Protein synthesis and folding is a highly regulated process that can be unbalanced by stress conditions such as high temperatures, strong induction of protein synthesis or the presence of determined chemicals, among others. In such circumstances is when the quality control machinery is more critical in order to prevent protein misfolding and aggregation. Here is presented a summary of how this quality control system works in *E. coli*, being one of the most studied model organisms and the

first choice for recombinant protein production, process closely related with protein misfolding and aggregation.

This machinery acts mainly by two pathways, trying to recover the proper structure of misfolded polypeptide chains and destroying those misfolded proteins that cannot be properly refold, and may represent a potential danger to the cell. The first activity is accomplished by a type of proteins named chaperones while the proteolysis of misfolded proteins is carried out by proteases (figure 3). However, these two activities are not completely independent since in many cases chaperones can act cooperatively with proteases by providing the misfolded protein in a proteolytic-competent state.

2.3.1 Chaperones

Chaperones are a family of structurally diverse and highly conserved proteins devoted to assist proper protein folding. Despite being constitutively expressed to help in the folding of newly synthesized polypeptides, many of them are up-regulated under stress conditions such as an increase in the temperature. Due to its significant incidence in the protein folding process, this family of temperature inducible chaperones has been traditionally known as heat shock proteins (Hsps)[33].

Chaperones can be classified regarding activity in: folding, holding and disaggregating chaperones.

Folding chaperones actively promote the folding of their substrates in an energy-dependent manner, being ATP the molecule responsible of providing the required energy. In *E. coli* there are three systems of folding chaperones: trigger factor[34], DnaK-DnaJ-GrpE and GroEL-GroES[35].

Holding chaperones maintain proteins partially folded preventing these molecules from aggregating and providing the time to folding chaperones to carry out their function. Some examples of holding chaperones are ibpA and ibpB[36].

Disaggregating chaperones are responsible of dissolving protein aggregates when they occur. Once misfolded proteins are detached from the aggregate surface can be directed either to refolding pathway or proteolysis. The most studied disaggregating chaperone in *E. coli* is ClpB[37].

2.3.2 Proteases

Proteases are the proteins in charge of degrading misfolded polypeptides. This proteolytic process is an energy dependent reaction mediated by ATP in which soluble but also aggregated misfolded species are destroyed, releasing the amino acids to be reused by the cell. The most important proteases in *E. coli* are Lon[38] and ClpP[39].

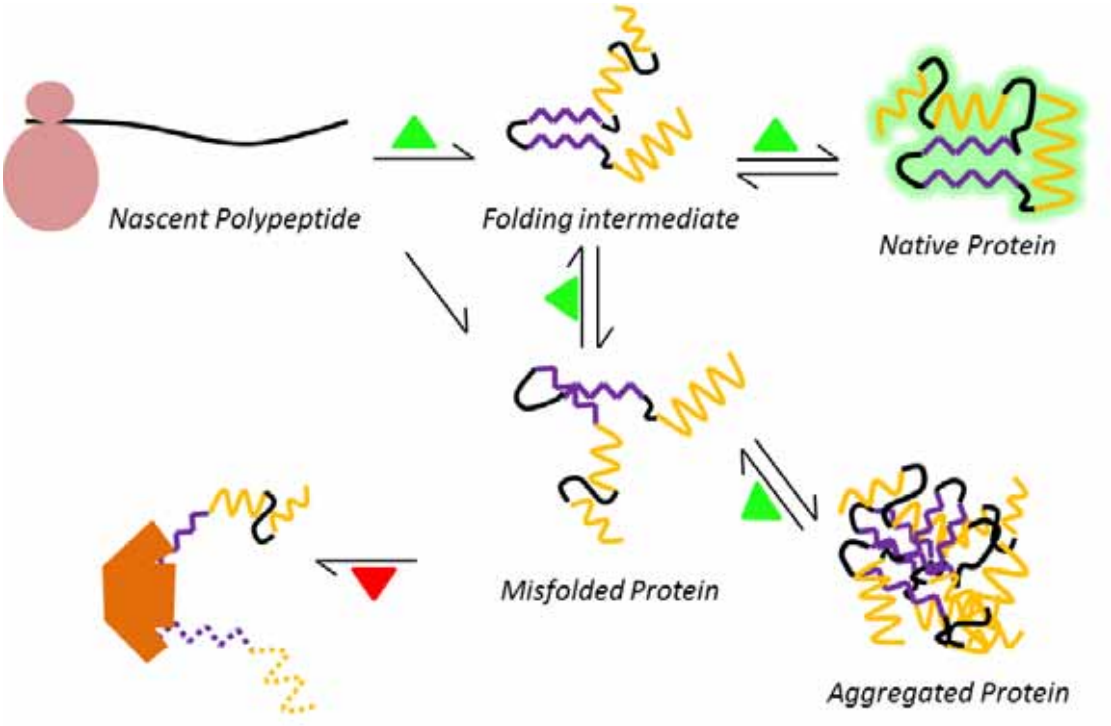

Figure 3 Protein folding and misfolding pathway. Steps marked by green triangles indicate chaperone favoured processes. Red triangles indicate polypeptide degradation mediated by proteases.

3. Bacterial Inclusion Bodies (IBs)

Inclusion bodies are non-enveloped protein aggregates which are frequently observed in microbial factories over-expressing heterologous protein[40]. At first, these granules were thought to be protein deposits mainly formed by misfolded and therefore inactive protein, thus they were considered as non-desired by-products of the recombinant protein production process. Nowadays, this perception is changing thanks to the steady comprehension increase of the physiology of these protein aggregates. Currently, is largely accepted that IBs are able to retain a certain degree of biological activity, depending mainly on the forming protein nature[41, 42]. Interestingly, we can find examples such as β-galactosidase, in which IBs exhibit very similar specific activities than their soluble equivalent[43]. Recent studies have also demonstrated that IB formation is not apart from the cell protein quality control network, but closely related with folding modulators[44] and proteases. Moreover, evidence provided by our and other groups prompted the appearance of a new model that breaks the dogma by which protein conformational quality is directly linked with protein solubility. In this model, proteins present in either soluble or insoluble fraction are equally sensitive to be modulated in terms of conformational quality[45]. This fact is extremely important, since allows increasing IB protein conformational quality and therefore biological activity by changing process variables such as protein production temperature[46]. Thus, bacterial IBs have passed in a lapse of 10 years from being regarded as waste by-products, due to their supposed lack of biological activity, to be seen as biofunctional particles capable of performing their biological activity and which production process can be engineered in order to optimize the conformational quality of the resulting aggregates.

3.1 Origin and formation

Polypeptide deposition as IBs is mainly a direct consequence of protein overproduction. In such situations, commonly observed during recombinant protein production processes in which the use of strong promoters or high inducer concentrations are regularly applied to achieve the highest production yields, protein quality control network can become saturated by the exceeding amount of nascent

polypeptides and misfolded proteins. Therefore, proteins in several folding states are deposited in protein aggregates. These misfolded polypeptides expose hydrophobic patches which interact to other exposed regions forming the insoluble particle[47]. However, contrarily to what was believed, it has been proved that the aggregation in IBs is a rather specific, plastic and dynamic process[48]. Thus, IB formation should be understood as a balance between the self-assembly through stereospecific interactions of misfolded or partially misfolded proteins around exclusive nucleation cores and the release of solubilized and properly refolded proteins from the particle to the environment. When the incorporation rate of polypeptides to the IBs is bigger than the release, what happens under protein overproduction conditions, IB formation occurs. In addition, the inverse transition is also possible. It is has been observed how in absence of new protein synthesis, for instance, when protein synthesis is arrested by the addition of chloramphenicol, IBs are resolubilized in few hours and a transition of polypeptides from the insoluble to the soluble fraction is detected in terms of increasing the amount and biological activity of the protein present in the last one[49, 49]. Thus IBs can be seen as a transient reservoir of protein in which the forming polypeptide can go from the insoluble aggregate to the soluble fraction and viceversa.

From a physiological point of view, it has also been speculated that IB's origin could be the consequence of a protective mechanism of the host cells. Some studies have revealed many resemblances between amyloid fibril formation and IB deposition, being both rich in inter molecular β-sheet structure, exhibiting aggregation hot spots, a seeding-driven aggregation process and tropism for amyloids binding dyes[50-52]. In this regard, it is plausible to think that, as it happens in amyloid aggregation diseases, IB could be selectively recruiting and immobilizing soluble misfolded species or aggregation intermediates. Being proved that the most harmful species are those with exposed hydrophobic patches circulating through the cell, IB body formation could be the result of a highly conserved protective strategy against misfolded protein derived damage[53].

3.2 IB structure

IB particles are found in the insoluble fraction of prokaryotic cells, usually associated with a protein overexpression process, especially when these proteins are from mammalian or viral origin. One, eventually two, IBs are produced per cell in a polar

situation, showing a high refractivity under optic microscope. However, secreted proteins can also aggregate forming IB placed in the periplasmic space[54].

These particles are non-enveloped, porous and highly hydrated structures with variable size between 50 nm to 2 µm[55, 56]. IB size is determined by the combination of several factors such as the producing protein sequence, the genetic background of the host cell, or process variables like temperature or induction time among others. Once purified, these aggregates commonly exhibit spherical or cylindrical morphology[56, 57].

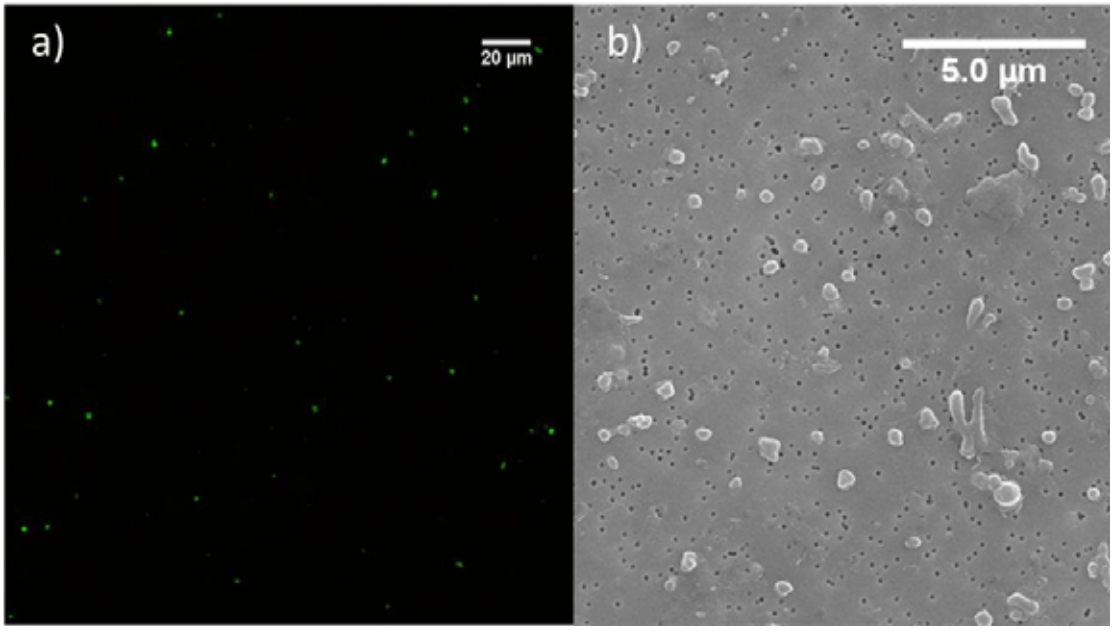

Figure 4 Purified VP1GFP IBs. A) Fluorescence microscopy image of VP1GFP IBs. B) Scanning electron microscopy (SEM) micrograph of VP1GFP IBs.

Due to the stereo-specificity of the IB deposition, these particles result in highly pure protein deposits that can reach 95% of the recombinant protein content[58]. Nevertheless, minor amounts of other cell proteins can be found as well as other contaminants that have unspecifically precipitated such as lipids, DNA and RNA molecules[59, 60]. In addition, folding modulators have also been regularly identified as IB components.

Polypeptides within the aggregate coexist in several conformational states. In fact, the presence of biological activity in IBs proves that at least part of the embedded protein is in its native or native-like conformation. In addition, some studies have shown the ability of releasing soluble active globular protein from the aggregate[42]. On the other hand, during the last years several works have provided evidence of the presence of β-

amyloid structure in these particles, identifying amyloid resistant fibrils by transmission electron microscopy after proteinase K digestion of the globular species[53].

3.3 Bacterial IB plasticity

What determines if a protein is prone to aggregate as a IB when produced in a microbial host is still unknown, although some evidences suggest that the own protein sequence could be playing an important role in protein aggregation by the presence of particular regions known as aggregation "hot spots". The incidence of these regions has been used to develop computational approaches to study protein tendency to aggregate[61].

Despite polypeptide sequence influence in the IB aggregation pattern, other variables can affect this pathway such as the genetic background and process parameters. In that sense, process variables and more specifically protein expression temperature has been shown to alter protein deposition process by modulating the protein expression rate. Therefore, different aggregates, regarding their structure and composition, can be obtained (see table 1)[62-64].

Temperature	IB features
<Physiological T°	More fragile. Sensitive to mild detergent treatments. Higher extent of biologically active protein.
=Physiological T°	Stable protein deposits. Presence of biologically active protein.
>Physiological T°	Unspecific aggregation due to the mild denaturing conditions of the production. Lower level of biological activity. Poorly pure particles.

Table 1 Aggregate features regarding their producing temperature.

Besides, IB deposition it is also determined by the molecular environment during the aggregation process, being especially critical the presence of the proper folding regulators. Thus, when fabricating IB in *E. coli* strains defective for key genes of the protein quality control network, the resulting aggregates also exhibit different features regarding their chemistry and mechanical integrity. (**see annex 2**).

3.4 IB purification process

Classically, IBs have been easily isolated by its high density from other cell contaminants using ultrasonication or enzymatic treatments to disrupt cells and release the particles, followed by centrifugation procedures. Depending on production scale, also French press and high pressure homogenization can be used. After that, several simple treatments can be carried out to remove possible impurities coprecipitated with the IBs. These washing steps usually consist in mild detergents such as Triton-X or NP40 treatments, DNAase treatment or the addition at low concentrations of chaotropic agents (see figure 5).

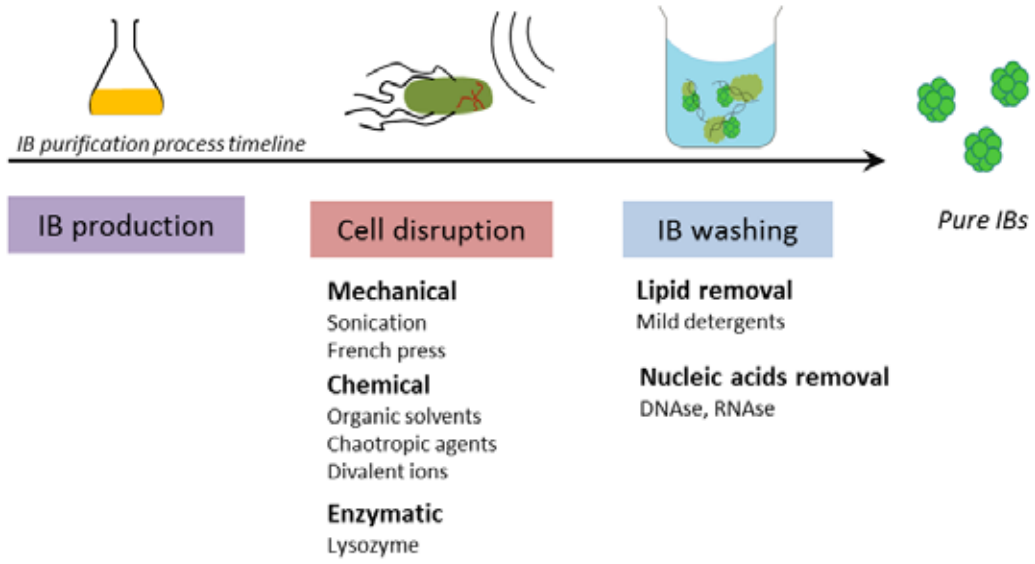

Figure 5 Typical approaches for IB purification.

However, the raising spectrum of IB applications and the increasing understanding of the aggregates structure have raised the need of more specific and efficient purification methods regarding the ultimate application of the produced material. For instance, harsh disruption methods and detergent treatments should be avoided when producing IB at low temperatures or when the resulting IB structures present high tendency to be resolubilized[65], since they exhibit lower levels of mechanical stability and such treatments would represent a significant loss of functional protein[62]. Thus, when applying one or other purification process, several factors must be taken into account. Depending on the IB mechanical stability, the producing microbial host and the final application of the material, the purification procedure should be optimized in

order to release as many particles as possible without compromising IB integrity and completely removing microbial cell contamination when required (**see annex 3**).

4. Biotechnological applications of IBs

Bacterial IBs have been regarded as waste by-products of recombinant protein production since they first were identified. However, the extensive study of IB deposition process during the last decade raised the appearance of new applications for these protein deposits.

4.1 Source of soluble protein

Bacterial IBs, being highly pure protein deposits can be used as source of protein from which the forming polypeptides can be extracted to obtain the protein of interest in their soluble form. However, usually IB resolubilization procedures require protein denaturalization and technically complex, and not always efficient, *in vitro* refolding protocols[66]. In this regard, some studies have shown that lowering the protein production temperature is possible to obtain aggregates with higher extents of biologically active polypeptides that are sensitive to resolubilization under mild detergent treatments simplifying enormously the protein extraction process[46, 62].

4.2 Protein aggregation model

Similarities between IB structure and formation with mammalian amyloid fibrils aggregation promote the use of IBs as model platform to study the physiology of prionic[67] and amyloid-related diseases, which have every day increasing incidence in human health in the developed countries[68]. An interesting example of the use of IBs as a model has been provided by Villar and co-workers, in which they used bacterial IBs as a screening platform to test amyloid aggregation inhibitors[69].

4.3 Biocatalysts

The use of IBs as immobilized biocatalysts is probably the most exploited application. Enzyme immobilization as IBs present many advantages compared to the classical immobilization methods in which pure soluble protein is required. IB intrinsic features such as their ability to retain biological activity, high purity grade and its simple purification process, allow reducing the production process cost enormously by

producing the enzyme of interest in IB insoluble form. In this regard several studies have successfully fabricated IBs and used them straight forward as immobilized enzyme for biocatalysis. Some examples are β-galactosidase[41], human dihydrofolate reductase (hDHFR)[41], polyphosphate kinase (PPK)[70], D-aminoacid oxidase (DAO)[71] and sialic acid aldolase (SAA)[72] . In addition, IBs exhibit promising features for their use in industrial-scale bioreactions, since these particles are mechanically stable, highly hydrated and only minor amounts of the IB forming protein are released to the aqueous environment during the first minutes of incubation[42]. After that period, IBs remain stable in terms of size and biological activity[73]. Therefore, IBs formed by enzymes can be used in several cycles with only a small decrease of their biological activity[74].

5. Regenerative medicine

Humanity has been exposed to disease and injury since the beginning of its existence. This fact early raised the need to develop treatments to help in the recovery of ill people or to ease the pain. At first, a very rudimentary, often mixed with mysticism, practice was carried out based on the observation and use of some plants and other natural elements such as animal parts or minerals, but with time empirical knowledge and experience lead to work out useful tools for the medical tasks. In fact, there is evidence that in the ancient Egypt surgical procedures were applied. From that time point to the current medicine countless advances have been done in the understanding of the human anatomy and physiology, but it has been the study at the cellular and molecular level, started in the last century, what has really changed the approaches used to treat diseases. Thus several medical fields have risen being regenerative medicine one of the most promising disciplines.

Regenerative medicine is a term referred to the integration of different biomedical approaches intended to restore or establish normal cell or tissue function in damaged cells or tissues. This area can be divided in three main fields: gene therapy, cell therapy, and tissue engineering. Within cell therapy, an especial mention is deserved to stem cell based therapies since combined with tissue engineering approaches represent the most promising alternative to restore tissue functionality

5.1 Gene Therapy

Gene therapy consists in the delivery of nucleic acids to cells in order to restore their functionality. Cell activity can be impaired by several causes: the lack of a specific gene product, misregulation of gene expression or injury. Thus, regarding, the nature of the damage, different strategies can be implemented. For instance, the lack of an specific gene can be overcome by delivering the gene of interest in a protein expression vector[75]. Up regulation of genes can be treated by delivering siRNA[76]. Injured tissue can be restored by the delivery of genes encoding growth factors able to stimulate the own tissue repair or when complemented with cell therapy[77], leading stem cells to differentiate into the damaged tissue lineage.

In gene therapy approaches is extremely important the choice of the delivering vector since it will determine the efficiency and toxicity of the technique (see figure 6).

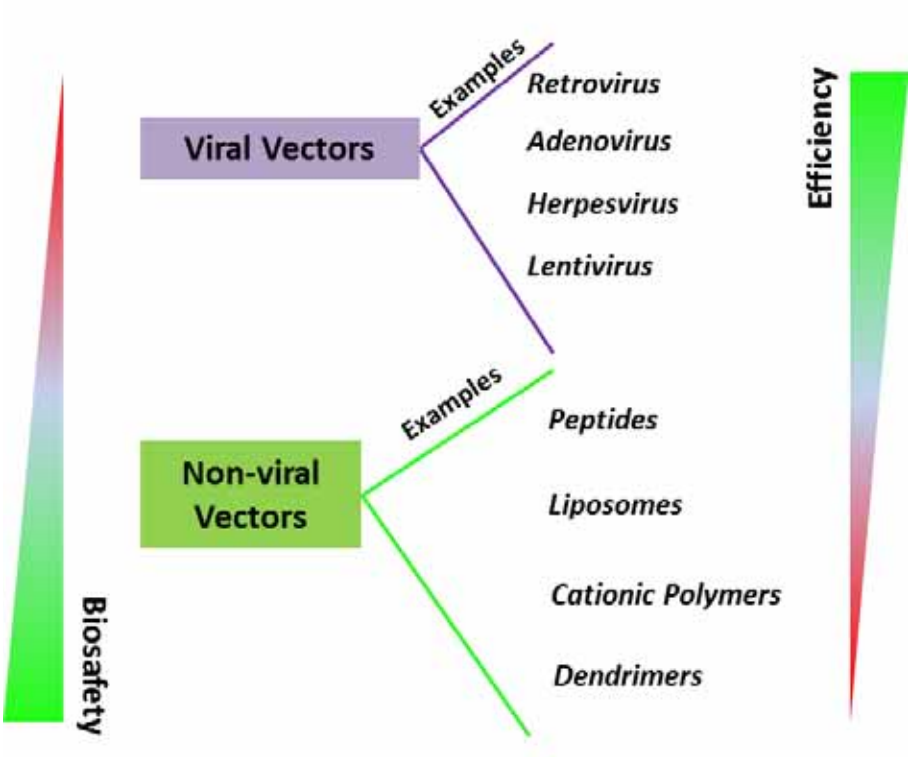

Figure 6 General classification of typical vectors used for gene therapy**.**

5.2 Cell therapy

Cell therapy is directed to restore a tissue or organ by introducing cells capable of developing the function of the mentioned tissue or by stimulating other cells to do it. In this regard different approaches under study comprise: autologous cell therapy, allogeneic cell therapy and xenotransplantation.

Autologous cell therapy consists basically in the harvesting, *ex vivo* expansion and reintroduction in a damaged site of a specific cell type. In that sense, some treatments are being studied including chondrocytes for cartilage repair[78], keratinocytes for burned damaged tissues[79] or myocytes for myocardial repair[80] among many others. This strategy would be ideal in terms of immunocompatibility but also shows limitations related to the availability of tissue in order to isolate an amount enough of cells for an effective therapy. Moreover, primary cultures can suffer a significant decrease in cell viability or dedifferentiate during the culture period.

On the contrary *allogeneic cell therapy* doesn't present this shortage in cell availability but makes necessary to combine immunosuppressant treatment to avoid graft rejection.

Xenotransplantation, also known as cross species transplantation, has been extensively investigated in the last 20 years in order to overcome immunogenic derived problems and cross-species pathogen infectivity. In this regard transgenesis has allowed tailoring gene expression towards a human pattern while suppressing the expression of endogenous genes in pigs[81, 82]. Thus, since the fabrication of artificial organs are still far from optimized, mainly due to the difficulty of scaling up the *in vitro* forming organ, xenotransplantation should be taken into account as a possible alternative.

5.3 Stem cell based therapies

Stem cell is a term used to define cells that have the distinctive ability of self-renewal, being able to go through numerous cell divisions without losing their undifferentiated state. Moreover, almost all of these cells are able to originate through differentiation processes distinct cell types.

Stem cells can be found in small amounts in most human tissues. However, tissues are formed, mainly by differentiated, specialized cells that have a limited life span. Thus, a steady income of new cells to maintain tissue functionality is required. In this regard, stem cells are devoted to provide a source of cells, able to differentiate in the needed tissue cell type for their renewal.

One can distinguish between embryonic stem cells (ESCs) and adult stem cells (ASCs). ESCs can be isolated from early stage embryos and show the ability to origin all three primary germ layers derived cells, known as pluripotency[83]. On contrary, ASCs are multipotent cells obtained from different tissues of adult organisms. Multipotent cells have a more restricted scope than pluripotent cells regarding the possible progenies they can generate. ASCs can be classified depending on the tissue source. Thus, a considerable spectrum of adult stem cell can be obtained: hematopoietic, mesenchymal, neural and epithelial stem cells from bone marrow (the first and second), brain and intestine respectively[84], but also some reports revealed umbilical cord tissue[85], primary teeth[86], adipose tissue[87] and human placenta[88] as a potential source for stem cell extraction.

From this range of cells, a special attention should be paid to mesenchymal stem cells (MSCs). MSCs has become one of the most promising tools in cell therapy and tissue engineering applications due to their easy isolation, their high expansion potential in *ex vivo* cultures and their ability to develop a broader number of cell types than other ASCs. For instance, MSCs has been shown to form *in vitro* adipocytes[89], osteoblasts[89], chondrocytes[90], myocytes[91], insulin producing cells[92] and neuron-like cells[93].

In the last years, some studies have shown a new promising type of pluripotent cells known as induced pluripotent stem cells (iPSCs). Takahashi and co-workers generated for the first time iPSCs by retroviral reprogramming of mouse fibroblasts, observing that the resulting cells exhibited a similar pluripotency state to the one shown for ESCs[94]. Since then, also human iPSCs have been successfully obtained making possible to produce disease models with the patient specific phenotype when iPSC are differentiated to functional cells[95, 96]. This fact has prompted the appearance of new insights in drug screening, toxicology, disease models and regenerative medicine. However, even iPSCs show some advantages compared to ESCs and ASCs (see table 2), there is still concern about their safety for regenerative medicine. Thus further research regarding how the reprogramming process can affect the resulting iPSC should be addressed.

Progenitor cell type	Advantages	Disadvantages
Adult Stem cells (ASCs)	• Multipotency • Possible application of autologous therapies • Self-renewal capacity	• They cannot provide all cell lineages • In some cases are difficult to isolate
Embryonic Stem cells (ESCs)	• Pluripotency • Self-renewal capacity	• Ethical concerns derived from ESC origin • Impossibility to obtain patient cells, limiting their application to

		allogeneic therapies • Extremely high growth rate could derive in teratoma formation[97]
Induced pluripotent stem cells (iPSCs)	• Pluripotency • Self-renewal capacity • Possible application of autologous therapies	• Possible tumorigenic effect[98]

Table 2 Stem cell classification, advantages and disadvantages.

In summary, although stem cells in all their variants represent a huge step ahead towards personalized regenerative medicine, more specifically in tissue and organ repair, and they overcome the main problems of other cell therapies thanks to their self-renewal and pluri or mutlipotency characteristics, two main challenges remain to be fully faced. Guarantee the safety of the cell used for human engraftment and optimize cell differentiation process to a specific cell type.

6. Tissue engineering

Nowadays, there are a steady increasing number of surgical procedures intended to replace or reconstruct damaged tissues and organs as a consequence of injuries, disease and malformations. In this regard, tissue engineering approaches aim to provide the necessary supply of these tissues and organs by their *in vitro* fabrication. This notable goal results highly appealing from a medical sight, and despite their clinical application is still quite limited, tissue engineering has experienced an important progress in the last years.

Tissue engineering has largely benefited by the knowledge developed in stem cell biology (see section 5.3) as well as in material sciences. Therefore it can be considered that tissue engineering approaches are based in the production of a scaffold in which stem cells are cultured and differentiated, usually by the addition of inductive factors, in order to obtain the final implant[99]. In that sense, scaffold should mimic tissue architecture and responses being able of integrating with the surrounding tissue and actively stimulating regeneration of normal tissue.

6.1 Biomaterials in tissue engineering

Biomaterials for tissue engineering have evolved since their first application as inert scaffolds in which seed cells. Nowadays, materials used in tissue engineering should ideally fulfill several requirements such as biocompatibility, controlled porosity and permeability, mechanical features and degradation kinetics comparable to the targeted tissue, support cell attachment and proliferation and additionally direct cell response at a molecular level. In this regard, extensive investigation has been carried out in both material development as well as addition of nanotopograhies or functionalization with bioactive molecules for cell response tailoring.

Currently, the number of materials in use or under study for tissue engineering is enormous. They can be classified in natural and synthetic. Natural materials such as collagen, gelatin, alginates, silk or chitosan are formed by extra cellular matrix (ECM) components and allow mimicking the extracellular environment in a quite accurate

manner. However, they can show some disadvantages regarding their mechanical integrity, degradation and toxicity of the generated sub-products[100-102].

Besides, also decellularized tissues such as dermis for treatment of burnt patients[103] or blood vessels for vascular surgery applications[104] have been investigated with promising results.

On the other hand, synthetic materials can be divided in metals, ceramics and polymers. The most used metal materials are Titanium and its alloys. They have been widely used for generating osteogenic implants[105, 106]. However, this kind of material raises concern regarding its permanent implantation due to a possible toxicity derived from the accumulation of metal ions released by corrosion. Ceramics potential for implantation has been largely exploited. Ca-phosphate ceramics[107, 108], Zirconia[109] have shown to be useful for generating tissue engineering scaffold due to their biocompatibility and capacity for generating mechanical strong scaffolds able to withstand high load forces, especially important in some bone implants. However, ceramics features are highly dependent on the production process and can become fragile when fabricating scaffolds with high porosity values. Polymers show some advantages when compared with metal or ceramics scaffolds. Unlike metal materials, polymer scaffolds are bio-absorbable, avoiding classical inconvenient of these permanent implants or the need of extra surgical procedures for the implant removal. In addition, polymeric matrices also allow generating scaffolds with a high degree of structural precision to finely control their physico-chemical properties such as degradation kinetics, stiffness or porosity. Poly-L-lactic acid (PLLA)[110], poly-lactic-co-glycolic acid (PLGA)[111], poly-ε-caprolactone (PCL)[112], poly-vinyl alcohol (PVA)[113] and poly-hidroxybutyrate (PHB)[114] are the most studied polymers for tissue engineering purposes. However, polymeric materials are limited for some applications by their relatively low mechanical strength. Moreover, it has been described that polymeric scaffolds can locally lower the environmental pH due to the autocatalytic ester breakdown derived from degradation. In such conditions cell growth would be impaired[115, 116].

6.2 Nanostructure surface modification and scaffold functionalization

As mentioned before, biomaterials used in tissue engineering should allow control of the cell response at the molecular level in order to direct cell differentiation to the specific target tissue, while stimulating cell adhesion and growth. In this regard, two different strategies can be implemented, namely the addition of nanostructures for mechanical stimulation or the scaffold functionalization by incorporating bioactive molecules.

6.2.1 Nanostructured materials

It has been widely accepted that cells can interact and effectively sense their environmental distribution or topography at the nano-scale[117]. Moreover, this kind of mechanical stimuli is able to raise important cell responses such as increase cell adhesion, proliferation or direct differentiation[118].

The addition of nano-topographies to conventional materials has become a usual practice in order to promote cell functionalities. For instance some studies have shown that nanostructured surface of titanium implant favor cell differentiation to osteoblasts, improving calcium deposition and the implant integration[119, 120]. Others have proved that nanostructured PLGA promote adhesion and proliferation of chondrocytes accelerating also ECM formation[121, 122] or that PLGA vascular graft exhibiting a nanoscale surface roughness enhance endothelial differentiation[123]. These studies among many others have confirmed the usefulness of the scaffold surface nano-modification as a tool to tailor a specific cell response.

The addition of nano-cues to direct cell response can be achieved by highly diverse strategies: lithographic methods[117] (usually applied to generate nano-pits or nano-grooves), particle deposition, electrospinning[124] (extensively used for fabricating nano-fiber matrices), or chemical growth[125] are the most common of them.

In this regard, particle deposition results highly appealing since it allows generating nanotopographies in already fabricated scaffolds by an easy and versatile method that can be implemented in combination with the other strategies. Some examples of this strategy are deposition of ceramic particles[126] to enhance osteogenic

response in PLLA scaffolds or the use of carbon nanotubes to modify tungsten and stainless steel wire surface in order to enhance electrical stimulation of neurons[127].

6.2.2 Surface functionalization

Cell response can also be affected by numerous molecules such as adhesive peptides, growth factors and other proteins with incidence in the cell functionality and differentiation pathways. Thus, tissue engineering approaches has taken advantage of such molecules to direct cellular response at the molecular level. Some examples of surface functionalization with biologically active molecules comprise the use of epidermal growth factor (EGF)[128], fibroblast growth factor-1 (FGF-1)[129], fibroblast growth factor-2 (FGF-2)[130], nerve growth factor-β (NGF-β)[131], vascular endothelial growth factor (VEGF)[130], bone morphogenic proteins (BMP)[132] as well as vitronectin[133] and RGD peptides[134, 135] among others. Every protein or peptide can be potentially immobilized onto a surface or engineered to provide a controlled release of the molecule from the scaffold to the environment, becoming available for the cells. This fact supposes a great tool for tissue engineering devices in order to generate scaffolds able to direct specific responses and widening the spectrum of activities that the biomaterial can carry out.

Scaffold functionalization and addition of nanostructure are not exclusive processes. For instance Berner and co- workers recently developed a PCL nanofiber mesh scaffold coated with Ca-phospate ceramics that in addition contained BMP-7 for bone regeneration[136].

6.2.3 Protein and peptide nanostructures

Another interesting approach consists in using bioactive peptides with self-assembly capability to origin a nanostructure *per se*. In this regard, several studies have been carried out to investigate nano-fibril, nano-tube or nano-sphere formation from a wide spectrum of peptides, including cyclic peptides[137], peptide amphipiles and bolamphipiles[138, 139], surfactant-like peptides[140], aromatic dipeptides[141] and hydrophobic dipeptides[142]. All of them have the capacity of generating nanostructures by spontaneous self-assembly process, producing high ordered structures comparable to that observed for amyloid fibrils. Indeed, both peptide nanostructures and amyloids,

share the same general principles of geometric restriction in their interactions as well as very appealing properties such as spontaneous supramolecular assembly in mild conditions, low cost production compared to inorganic nano-fibers, allow engineering additional functionalities and exhibit very special mechanical properties such as a high resistance degree while maintaining their flexibility as well as thermal and chemical endurance[143].

Besides, amyloid fibrils (see section 1) have also been envisaged as nanostructured material able to provide a controlled released of the building blocks forming the supramolecular self-assembly.

Bacterial IBs are also self-assembly protein particles, sharing many features with amyloid and amyloid-like nanostructures regarding their *in vivo* formation and final structure that are starting to be studied as a potential biomaterial with uses in the biomedical field[73].

Protein or peptide nanostructures allow to synergistically combine stimuli from the surface nano-modification as well as exploit a bioactive effect of the own peptide or protein while being biologically compatible, and thermally and chemically stable but biodegradable. Thus, they can be considered as a powerful tool for future applications in tissue engineering.

Objectives

This study is aimed to determine the suitability of bacterial IBs as a biomaterial with an effective application in regenerative medicine. In this regard, this work is mainly focused to evaluate surface modification for cell culture by the addition of nano-topographies and surface functionalization based on IBs. Also, it has been involved the analysis of cell response to the IB-based topographies in terms of cell adhesion, growth and differentiation. In order to reach these goals, several specific issues have been addressed.

1. The study of IB tuneability regarding their morphology and other physicochemical properties when fabricating this particulate material in E. coli strains with different genetic backgrounds. Specifically, those strains were deficient in genes that are key regulators of the protein quality control network such as DnaK-, ClpA- and ClpP-.

2. The assessment of the IB capability to stimulate cell proliferation and adhesion, in immortalized cell lines, when acting as surface nano-topographical modifiers.

3. The in vitro comparison of cell growth and adhesion on physicochemically distinct IB-based topographies.

4. The exploration of the cell growth stimulation mechanism focusing in the identification of elements present in the mechanotransductive cascade.

5. The comparison of different mammalian cell types response when cultured on IB-based topographies.

6. The study of hMSCs response to IB-based topographies by gene expression and metabolomic analysis.

7. The exploration of bacterial IBs as bioactive surface nano-topographical modifiers.

Results

Paper 1

Tunable geometry of bacterial inclusion bodies as substrate materials for tissue engineering

Elena García-Fruitós*, Joaquin Seras-Franzoso*, Esther Vazquez and Antonio Villaverde

*Equally contributed

Nanotechnology, 21, 2010

Bacterial inclusion bodies (IBs) have been commonly described as pseudo-spherical protein deposits with a highly stable shape. Nevertheless, some hints regarding IB morphological plasticity have been widely observed, for instance these particles size can be tailored by modifying fabrication process variables such as protein expression time or temperature, indicating the possibility of altering the protein deposition process with a clear incidence in the final particle structure. In this work we have identified an *E. coli* gene, *clpP,* encoding for one of the major proteases of the protein quality control network, playing also an important role as regulator of the IB fabrication process. Moreover, we have observed how in absence of this regulator the balance between properly folded protein, misfolded protein and proteolysis that defines the IB formation dynamics is perturbed, originating IBs with abnormal morphologies. Specifically, IBs produced in *E. coli clpP*$^{-}$ strain are particles with tear-shape morphology with higher surface-volume ratios not observed in other *E. coli* knock outs lacking regulatory elements of the protein quality control network. Additionally, we have provided evidences that mammalian cells when cultured in IB-based topographies exhibit higher rates of cell growth as well as they can sense the difference between topographies fabricated with morphologically distinct IBs and response in consequence. Thus, genetic control of the IB fabrication process opens the possibility of producing IBs with geometries on demand to tailor the final cell response.

IOP Publishing Nanotechnology
Nanotechnology **21** (2010) 205101 (8pp) doi:10.1088/0957-4484/21/20/205101

Tunable geometry of bacterial inclusion bodies as substrate materials for tissue engineering

Elena García-Fruitós[1], Joaquín Seras-Franzoso[1], Esther Vazquez and Antonio Villaverde[2]

CIBER en Bioingeniería, Biomateriales y Nanomedicina, Bellaterra, 08193 Barcelona, Spain
and
Institut de Biotecnologia i de Biomedicina and Departament de Genètica i de Microbiologia, Universitat Autònoma de Barcelona, 08193 Bellaterra (Cerdanyola del Vallès), Barcelona, Spain

Received 26 February 2010, in final form 5 April 2010
Published 23 April 2010
Online at stacks.iop.org/Nano/21/205101

Abstract
A spectrum of materials for biomedical applications is produced in bacteria, and some of them, such as metals or polyhydroxyalkanoates, are straightforwardly obtained as particulate entities. We have explored the biofabrication process of bacterial inclusion bodies, particulate proteinaceous materials (ranging from 50 to 500 nm in diameter) recently recognized as suitable for surface topographical modification and tissue engineering. Inclusion bodies have been widely described as spherical or pseudo-spherical particles with only minor morphological variability, mostly restricted to their size. Here we have identified a cellular gene in *Escherichia coli* (*clpP*) that controls the *in vivo* fabrication process of inclusion bodies. In the absence of the encoded protease, the dynamics of protein deposition is perturbed, resulting in unusual tear-shaped particles with enhanced surface–volume ratios. This fact modifies the ability of inclusion bodies to promote mammalian cell attachment and differentiation upon surface decoration. The implications of the genetic control of inclusion body geometry are discussed in the context of their biological fabrication and regarding the biomedical potential of these protein clusters in regenerative medicine.

1. Introduction

Many materials with applicability in nanomedicine are produced in microbial cells, including a range of soluble substances, polymers and particulate entities. Bacteria produce alginates [1], polyhydroxyalkanoates [2] and other polymers, which have long been used in the biotechnology industry and progressively implemented in biomedicine and nanomedicine. [3]. Also, some bacterial species synthesize metal [4] or magnetic particles [5] with wide applications in imaging, diagnosis, bioseparation and molecular therapies [6]. Upon convenient cloning and expression of structural genes from selected viruses, bacteria also produce virus-like particles (VLPs) [7], empty, highly organized protein cages that mimic the original symmetry of the wild type infectious particle. They are mainly used for vaccination purposes [8], but upon filling them with drugs or nucleic acids they are observed as highly promising tools for gene therapy and drug delivery [8–10].

Bacteria expressing recombinant genes often produce inclusion bodies (IBs), namely spherical or ovoid-shaped aggregates of the encoded protein with high compositional purity [11]. While IBs have been traditionally associated with protein misfolding problems and considered undesirable by-products of protein production processes [12, 13], they are contemporarily observed as protein clusters with a high level of molecular organization and formed by functional protein species [14–18]. This fact has attracted the attention of biotechnologists, as IBs, when formed by enzymes, are promising biocatalyzers [19–22]. Very recently [23], we have shown that bacterial IBs can also be observed as mechanically stable, highly biocompatible particulate materials with sizes ranging from around 50–500 nm in diameter, and that they stimulate mammalian cell proliferation

[1] Equally contributed.
[2] Author to whom any correspondence should be addressed.

Table 1. Representative studies on morphology and size of cytoplasmic IBs.

Forming polypeptide	Bacteria, strain	Culture conditions and culture media	Reported morphology and methodology	Reference and Figure number
Granulocyte colony-stimulating factor	*E. coli* BL21(DE3)	Shake flask, 25 and 42 °C GYSP rich medium	Spherical, SEM Purified	[26] figure 2
Δ(4–23) TEM-β-lactamase	*E. coli* K12 strain HMS174 (DE3)	20 l bioreactor 30 and 37 °C minimal salt medium	Spherical with slight variations tending to ellipsoids and cylinders), TEM Purified	[25] figure 3
mGFP	*E. coli* K12 strain MC4100 and derivatives	Shake flask, 37 °C, LB rich medium	Spherical with slight variations tending to ellipsoids), SEM and AFM Purified	[23] figure 2
β-lactamase	*E. coli* K12 strain RB791	Shake flask, 37 °C, M9 minimal medium	Cylindrical SEM and TEM Purified	[27] figure 3
Porcine somatotropine		Shake flask, 42 °C, LB rich medium	Spherical-like. TEM, ultra-thin sections, *in vivo*	[57] figure 3

and differentiation when used for the bottom-up modification of surface topologies. For this purpose, and in the context of other potential nanomedical applications, the production of IBs with tailored sizes and morphologies would be highly convenient. This must necessarily be done during their *in vivo* fabrication, by targeting conditions that affect their construction process. However, the possibility of modulating the morphological properties of IBs has been so far unexplored. In fact, even when formed by different polypeptides and produced under diverse bacterial growth conditions, IBs have been described as spherical-like particles (eventually including short cylinders and paracrystalline forms) [24–28], with extremely poor morphological variety (table 1). Here, we have explored different *E. coli* genetic backgrounds (relevant to the protein quality control) in order to identify those genes involved in the morphological control of IB construction. Despite the high coincidence in the forms that IBs adopt in these strains, cells deficient in the ClpP protease produce unusually tear-shaped IBs with refined properties regarding mammalian cell growth stimulation. The role of the protease ClpP in the *in vivo* fabrication process is discussed in the context of the genetic determination of IB architecture, and the consequent biological impact of these variant particles when used as biomaterials.

2. Materials and methods

2.1. Strains and plasmids

The *Escherichia coli* strains used in this work were MC4100 (*araD139*Δ*(argF-lac) U169 rpsL150 relA1 flbB5301 deoC1 ptsF25 rbsR*) [29] as a wild type, and its derivatives JGT3 (Δ*clpB::kan*), JGT4 (*clpA::kan*), JGT6 (*zjd::Tn10 groES30*), JGT17 (Δ*ibp::kan*), JGT19 (*clpP::cat*), JGT20 (*dnak756 thr::Tn10*) [30], BB4564 (*groEL140 zjd::Tn10 zje::*Ω*Spc*^{r}*/Str*^{r}) [31, 32], and JGT32 (*dnak756 thr::Tn10*Δ *clpB::kan*) [30]. These strains carried pTVP1GFP [18], encoding a misfolding-prone fusion version of GFP (mGFP), in which the VP1 capsid protein of foot-and-mouth disease virus is fused to the amino termini of GFP and produced under the control of the *trc* promoter. For determination of proteolytic stability, cell protein synthesis was arrested by the addition of chloramphenicol at 200 μg ml^{-1}, and the cells further cultured under the same conditions.

2.2. Culture conditions and cell fractioning

Production of mGFP was carried out in shake flask bacterial cultures growing at 37 °C in LB rich medium at 250 rpm [33], in the presence of 100 μg ml^{-1} ampicillin. Expression of the recombinant gene was induced when the OD_{550} reached around 0.5, by the addition of 1 mM IPTG. Cell samples were collected at different times after induction of gene expression for further analysis.

Bacterial cells from 10 ml samples were collected by low-speed centrifugation (for 15 min at 15 000 g) and resuspended in 2 ml PBS buffer with one tablet of protease inhibitor cocktail (Roche, ref. 1 836 170). These mixtures were jacketed in ice, sonicated for 5 min at 50 W under 0.5 s cycles as described [34] and centrifuged for 15 min at 15 000 g. The supernatant was directly used for the analysis of the soluble cell fraction. IBs were purified by a standard detergent–lysozyme–sonication protocol.

2.3. Flow cytometry and fluorescence determination

Flow cytometry was performed on bacterial cell samples fixed with 0.1% formaldehyde O/N at 4 °C. Fluorescence was acquired through a 530/30 nm bandpass filter (FL1) in logarithmic mode, in a FACSCalibur system (Becton Dickinson), with 488 nm excitation from a 15 mW air-cooled argon-ion laser. Fluorescence was also manually determined at 510 nm in a Cary Eclipse Fluorescence Spectrophotometer (Variant) by using an excitation wavelength of 450 nm.

2.4. Quantitative protein analysis

Samples were resuspended or dissolved in denaturing buffer [35]. After boiling for 15 min (for the soluble fraction) or 25 min (for inclusion bodies), appropriate volumes were loaded onto denaturing gels for Western blot determination, using polyclonal antibodies directed against GFP and a commercial anti-GFP secondary antibody. Dried blots were scanned at high resolution and bands quantified with the Quantity One software from Bio Rad. Appropriate protein dilutions of commercial GFP were used as controls and determinations were always done within the linear range. Data were statistically evaluated by nested ANOVAs.

2.5. Confocal microscopy

For confocal image analysis, bacterial cells producing mGFP were fixed with 0.2% formaldehyde in phosphate saline buffer (PBS) and purified IBs were resuspended in PBS + Tween 0.5%. Samples were examined using a Leica SP2 AOBS confocal fluorescence microscope (Leica Microsystems Heidelberg GmbH, Mannheim, Germany), at an excitation wavelength of 488 nm and at an emission wavelength between 500 and 600 nm (63×, NA 1.4 oil). Images were analyzed with the Adobe Photoshop software.

2.6. Electron microscopy

For transmission electron microscopy (TEM), bacterial cells producing mGFP were fixed with 4% (v/v) paraformaldehyde (EM grade, Merck) in 0.1 M phosphate buffer (PB) pH = 7.4. Later, samples were rinsed with phosphate buffer, incubated in 20 mM glycine solution to quench the free aldehyde groups and embedded in 12% (w/v) gelatine, cryoprotected in 2.1 M sucrose solution and cryofixed in liquid nitrogen. All sections were cut at −120 °C with a cryoultramicrotome (Leica Ultracut UCT, Vienna) and deposited onto formvar coated Cu/Pd grids. Ultra-thin sections were initially blocked in PBS containing 1% (v/v) BSA, then incubated with a primary polyclonal antibody anti-GFP (sc-8334 Santa Cruz Biotechnology, Inc., 1/50 dilution) for 40 min. After washing in PBS, sections were incubated with gold-labeled protein A (Utrech, 10 nM). Following the final washes with PBS, samples were fixed with 1% glutaraldehyde and washed with distilled water. Samples were finally mounted in methylcellulose-uranyl acetate and visualized in a transmission electron microscope Hitachi H-7000.

Scanning electron microscopy (SEM) of purified IBs was performed by conventional procedures [23] using a Hitachi S-570 microscope (Hitachi LTD Tokyo, Japan).

2.7. Cell culture conditions

Mammalian cell growth was assayed as described [23]. Essentially, convenient amounts of isolated IBs were irradiated with an UV light (253 nm) germicidal lamp for 4 h and added to non-treated 96-well Falcon 3072 tissue-culture polystyrene plates (Becton Dickinson) for overnight incubation at 4 °C. Wells were further washed with PBS and blocked with 3% BSA in PBS for 1 h at 37 °C. Then, 3×10^3 new born hamster kidney (BHK21) cells or 2×10^4 rat pheochromocytoma (PC12) cells were added per well and incubated in Dulbecco's modified Eagle's medium (DMEM) supplemented with non-essential amino acids, fetal calf serum (5%), gentamicin and antimycotics at 37 °C for different times. Cell proliferation was analyzed with the EZ4U kit (Biomedica, GmbH) according to manufacturer instructions, and determined in triplicate in a multilabel reader VICTOR3 V 1420 (Perkin Elmer) at 450 nm.

3. Results

While the size of IBs is clearly influenced by the production time [25, 36], genetic background and culture conditions [24, 25, 37], spherical-like morphologies (with only slight variations tending to ovoid-cylindrical shapes) have been consistently observed irrespective of these parameters (table 1). Such steady IB symmetry can be accounted for by the particular biofabrication process of these particles. *De novo* produced recombinant polypeptide chains interact with each other through stereo-specific hydrophobic contacts [38] that allow the creation of seeding nuclei (usually one or two per cell) [36], on which additional protein molecules or proto-aggregates are progressively deposited [39]. Since polypeptides forming IBs are also steadily removed from these clusters by a combination of chaperones and proteases (the constituents of the cell protein quality control network) [24, 40], the volumetric growth of IBs in biosynthetic competent cells is due to an unbalanced equilibrium between these opposite activities, as the protein deposition rate is faster than protein removal [28]. IB particles are then the result of a continuous reconstruction process occurring at the IB surface level [41] that probably renders their highly regular, spherical-like forms.

In previous studies, we analyzed the size and biological properties of IBs produced by *E. coli* strains with mutations affecting the protein quality control up to 2–3 h after the induction of the recombinant protein production, without detectable variations in their spherical-like morphology [24]. However, with IB formation being a continuous reconstruction process, we speculated that any eventual genetic determination of the IB morphology would be more apparent after longer fabrication times. Therefore, we analyzed the morphology of IBs formed by the model fluorescent protein mGFP 4 h after triggering the recombinant protein synthesis in a wider catalog of bacterial mutants (deficient in the chaperones DnaK,

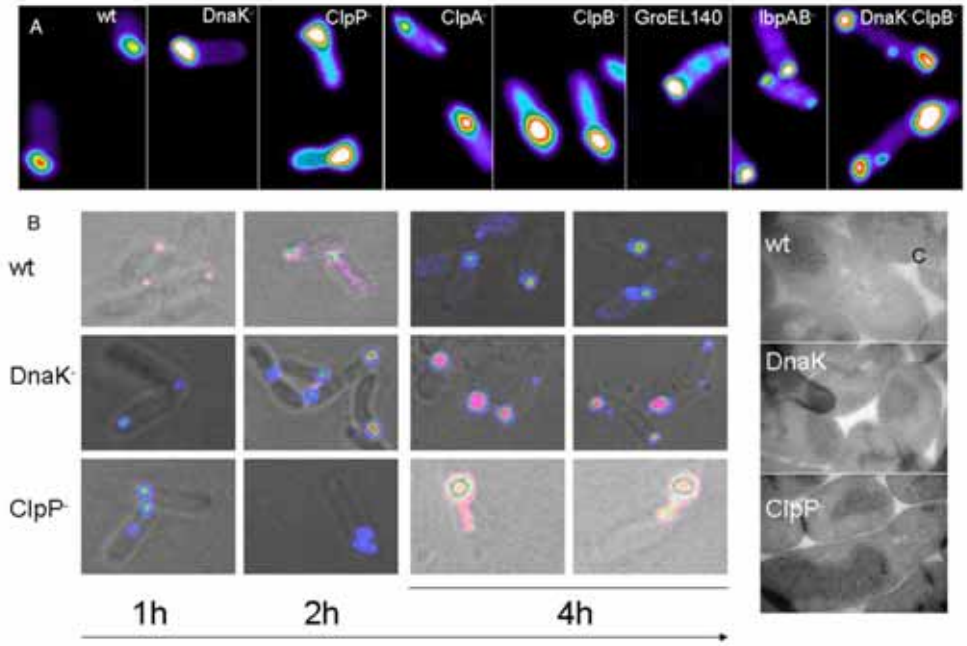

Figure 1. (A) Fluorescence microscopy images of IB-producing bacterial cells after 2 h of fabrication, in which the intensity of green fluorescence is mapped in a color scale from low (purple) to high (white). (B) Confocal sections of selected IB-producing bacterial cells analyzed at different production times, in which the intensity of green fluorescence is mapped from low (purple) to high (white). (C) Immunodetection of mGFP in ultra-thin sections of IB-producing cells 3 h after starting the production process. The relevant phenotypes of the producer bacterial strains are indicated.

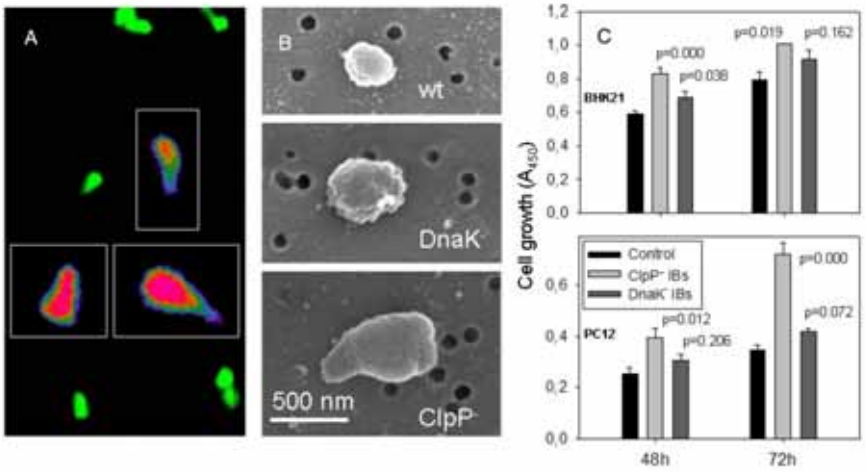

Figure 2. (A) General view of fluorescent IBs isolated from ClpP-deficient cells. Insets: magnifications of randomly selected particles pictured as confocal sections, in which the fluorescence intensity has been mapped from dark (blue) to clear (white) colors. (B) SEM images of morphologically representative IBs isolated from different producing strains. (C) Growth of two different mammalian cell lines monitored by a MTT assay, as stimulated by IB variants or without IBs (control). In all cases, particles were harvested at 4 h of production. An ANOVA test was applied to a pairwise comparison, for each experiment, of MTT values obtained in the presence and in the absence of IBs. The resulting *p* values are indicated.

ClpB, IbpAB and GroEL, the protease ClpP or the ATPase subunit ClpA). The microscopic analysis of the particles inside the cells indicated an unusually diffuse fluorescence in the cytoplasm of a few tested mutants that was much more evident, in terms of regularity, in ClpP$^-$ cells (figure 1(A)). To assess if these images corresponded to morphologically variant IBs, we analyzed confocal sections of ClpP-deficient producing cells, in which budding structures were clearly associated

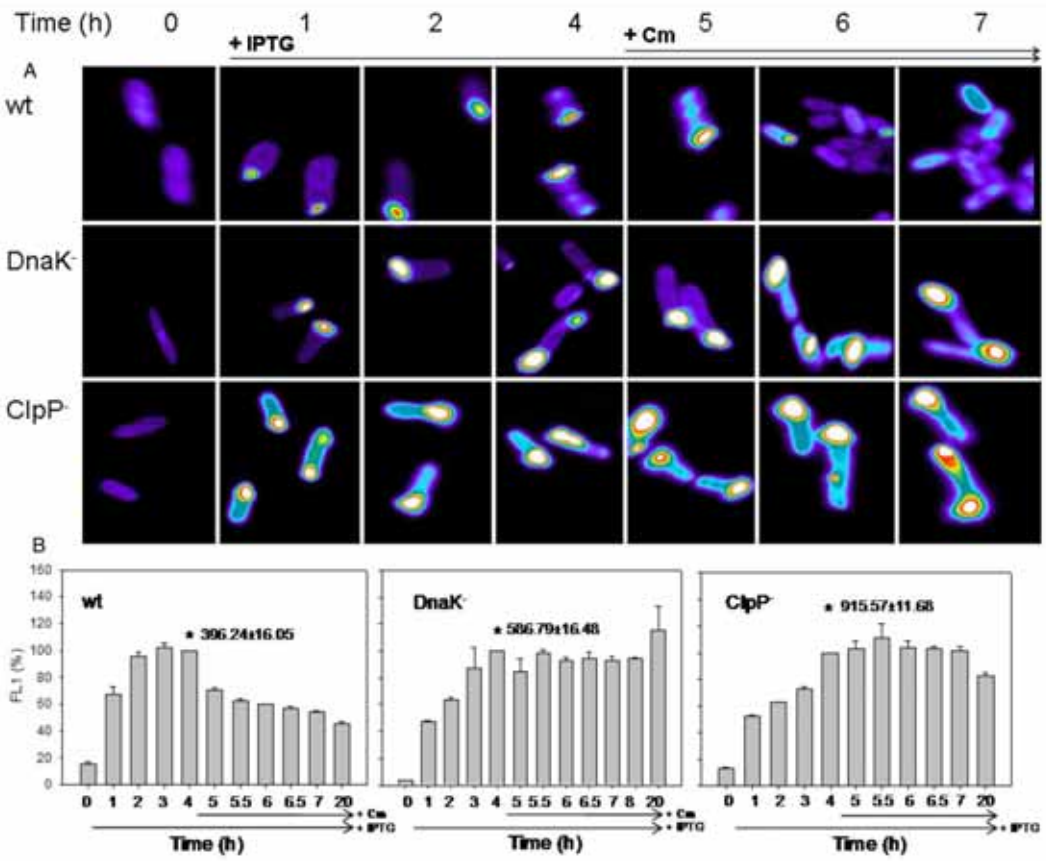

Figure 3. (A) Dynamic fluorescence mapping of intracellular IBs, during their formation in different bacterial strains and when protein synthesis was blocked by the addition of chloramphenicol (Cm). (B) mGFP fluorescence during IB fabrication relative to that observed four hours after its initiation, and during the further arrest of protein synthesis mediated by chloramphenicol (Cm).

with IBs (figure 1(B)). Such morphological variations were also observed by immunoelectron microscopy (figure 1(C)). Furthermore, upon ultrasonic cell disruption and repeated detergent washing, purified ClpP$^-$ IBs were still observed as morphologically abnormal, tear-shaped particles (figures 2(A) and (B)), indicating the mechanical resistance of the budding structures that remained firmly connected to the particle core.

To investigate at what extent variations of the IB morphology could affect their biological properties as biocompatible materials we have comparatively analyzed tear-shaped ClpP$^-$ and spherical DnaK$^-$ IBs in a mammalian cell proliferation test. Mammalian cell growth is highly responsive to micro- and nanostructuration of the substrate [42, 43], and we have previously shown that different surfaces decorated with DnaK$^-$ IBs promote a significant stimulation of mammalian cell growth relative to naked surfaces or those functionalized with vitronectin [23]. In this regard, the effective volume of these two IB variants determined by DLS was very similar, namely 459 and 531 nm [23], which allowed us to discard in advance relevant influences of the particle size itself. As observed, (figure 2(C), top), ClpP$^-$ IBs were slightly better than DnaK$^-$ IBs in stimulating the growth of BHK cells on polystyrene plates, and much more efficient in promoting proliferation of PC12 cells (figure 2(C), bottom), especially when comparing data obtained at 72 h. These adrenal gland cells, tending to grow in floating clusters, probably benefit more than BHK kidney cells, from the improved substrate properties exhibited by ClpP$^-$ IBs.

Since the tear shape of IBs had a significant effect on cell growth stimulation, the morphologic engineering of IBs turns into a highly promising concept regarding fabrication of tailored soft materials for tissue engineering. To better understand the mechanics of the biological regulation of IB fabrication in the bacterial cell cytoplasm, we determined, by means of GFP fluorescence, the kinetics of protein incorporation during IB construction and protein release (upon chloramphenicol-induced arrest of protein synthesis). Interestingly, in both wild type and DnaK-deficient cells most of the fluorescence remained associated with the IBs, while the cytoplasm was poorly fluorescent during protein synthesis and upon its arrest (figure 3(A)). On the contrary, ClpP$^-$ cells steadily show a highly fluorescent cytoplasm since very early fabrication times, indicative of a molecular fabrication process different from that carried out in the

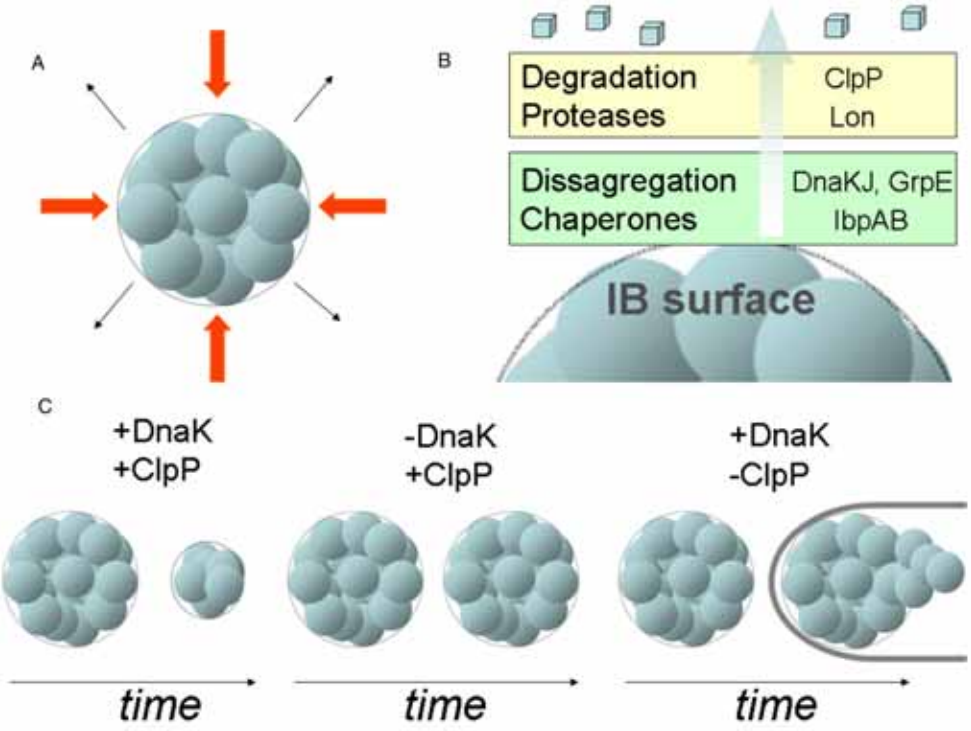

Figure 4. Physiological model of the morphologically aberrant biofabrication of ClpP$^-$ IBs. (A) IBs are generated by simultaneous protein deposition (red arrows) and removal events (black arrows), resulting in a sustained, surface-restricted reconstruction process. In biosynthetically competent cells, the reconstruction process is unbalanced towards protein deposition, thus allowing the volumetric growth of the particles. The spherical shape of IBs results from a homogeneous protein incorporation and removal over their entire surface. (B) Protein removal is mediated by two consecutive and mechanistically connected processes occurring at the IB surface, namely disaggregation and proteolysis. Disaggregation is executed by a set of cooperating chaperones that involve DnaK, DnaJ, GrpE, IbpA and IbpB [40, 58, 59], with DnaK being essential [24]. Proteolysis of disaggregating protein species is majorly mediated by Lon and ClpP proteases [60], in a strictly DnaK-dependent process [24] during which most of the DnaK molecules of the cell are found associated with the IB surface [61]. (C) In the absence of protein synthesis, already formed IBs disintegrate in the presence of DnaK and ClpP, remain stable in the absence of DnaK and are partially reconstructed in a polar manner in the presence of DnaK but in the absence of ClpP.

(This figure is in colour only in the electronic version)

two other genetic backgrounds (figure 3(A)). The monitoring of protein dynamics during IB evolution with and without chloramphenicol (through measuring the GFP fluorescence in isolated IBs) indicates a similar profile of protein incorporation into growing protein particles (figure 3(B)). However, in wild type cells, around 50% of IB protein was removed in the absence of *de novo* protein incorporation (figure 3(B)), in agreement with previous data obtained in different experimental setups [28]. However, in the absence of DnaK, IB-forming proteins were not released from the particles, proving that this chaperone is necessary not only for protein disaggregation at the IB surface but also for the associated proteolytic activity that ensures the further elimination of removed polypeptides. However, in the absence of ClpP there was a significant loss of GFP from IBs, which although more modest than in wild type cells was still significant (figure 3(B)). This fact indicates the occurrence of an aberrant IB morphogenesis in which the disaggregation occurs in the absence of ClpP-mediated proteolysis. This fact is probably responsible for the highly fluorescent cytoplasm (figure 3(A)) and for the polar extension of IBs in the absence of ClpP, which is much more evident at late fabrication times (figure 1), when in discontinuous bacterial cultures, the protein synthesis rate is naturally minimized.

4. Discussion

Mammalian cells feel their nano- and micro-environment through filopodia [44, 45], and differentially respond to specific topographical stimuli [42, 46–48] by triggering the expression of selected gene sets regulating the cell cycle, spreading and differentiation [46]. The comprehension of the fine mechanotransduction signals involved in such processes is expected to permit a rational engineering of cellular environments in improved scaffolds for regenerative medicine [49]. In simple 2D models of surface engineering, both top-down and bottom-up approaches permit a controlled topographical modification [43]. In the first case, the generation of grooves or pits by lithographic methods is highly convenient and flexible for research applications [42],

but on the contrary, limited by the chemical nature of the substrate on which cells are forced to grow. On the other hand, surface decoration with carbon nanotubes [50, 51] and spherical particles made of different materials [52–54], being more independent on the chemical nature and spatial organization of the scaffold, has so far generated less consistent and comparative data regarding the stimulation of cell growth and the triggering of specific cell functions.

In a very recent study [23], we have proposed bacterial IBs as fully biocompatible, protein-based materials for bottom-up nano-environment engineering. These non-enveloped spherical particles, ranging from around 50 to 500 nm in diameter [23, 25, 36], are mainly formed by a single protein species, only contain traces of other cell components [55] and are produced by cost-effective conventional bioprocesses (table 1, and references therein). Here, we have identified a bacterial gene, encoding a main cytosolic protease, whose inactivation results in the formation of tear-shaped IBs at late steps of their fabrication process (figures 1(B), 2(A) and (B)). This indicates a genetic determination of the IB geometry probably related to their continuous reconstruction process [41] (figures 4(A) and (B)). DnaK-mediated protein disassembly in the absence of ClpP seems to promote only a partial release of proteolytically stable polypeptides, that would precipitate again on the IB surface in the form of a conical protrusion (figure 4(C)). Since most of the IBs have a polar situation in the producing bacterial cell (figure 1), due to an energy-dependent mechanism aimed to accumulate aggregated proteins in the bacterial cell poles [56], the cell wall and cell membrane could mechanically orientate the protrusion towards the IB surface that is exposed to the cell cytoplasm (figure 4(C)).

Since the mechanotransduction system of mammalian cells senses and responds to the aberrant ClpP^{-} IB morphology (figure 2(C)), the possibility of a refined genetic control of IB geometry beyond the spherical forms (table 1) could enrich the potential of these protein-based particulate materials in surface decoration for tissue engineering. Further investigation on the catalog of genes controlling the quality control network in *E. coli* should provide additional clues for a tailored control of the IB fabrication process.

Acknowledgments

The authors appreciate the financial support through grants BIO2007-61194 and BFU2010-17450 (MICINN) and 2009SGR-108 (AGAUR). We also acknowledge the support of the CIBER de Bioingeniería, Biomateriales y Nanomedicina (CIBER-BBN), an initiative funded by the VI National R&D&i Plan *2008-2011, Iniciativa Ingenio 2010, Consolider Program, CIBER Actions*and financed by the Instituto de Salud Carlos III with assistance from the *European Regional Development Fund*. The authors also thank Francisco Cortés, from Servei de Cultius Cel·lulars (UAB) for routine maintenance of insect cell cultures, and both Servei de Microscòpia and Servei de Citometria (UAB) for helpful technical assistance. AV was distinguished with an ICREA ACADEMIA award (Catalonia, Spain).

References

[1] Remminghorst U and Rehm B H 2006 Bacterial alginates: from biosynthesis to applications *Biotechnol. Lett.* **28** 1701–12
[2] Chen G Q 2009 A microbial polyhydroxyalkanoates (PHA) based bio-and materials industry *Chem. Soc. Rev.* 2434–46
[3] Wu Q, Wang Y and Chen G Q 2009 Medical application of microbial biopolyesters polyhydroxyalkanoates *Artif. Cells Blood Substit. Immobil. Biotechnol.* **37** 1–12
[4] Edwards K J and Bazylinski D A 2008 Intracellular minerals and metal deposits in prokaryotes *Geobiology* **6** 309–17
[5] Arakaki A, Nakazawa H, Nemoto M, Mori T and Matsunaga T 2008 Formation of magnetite by bacteria and its application *J. R. Soc. Interface* **5** 977–99
[6] Corchero J L and Villaverde A 2009 Biomedical applications of distally controlled magnetic nanoparticles *Trends Biotechnol.* **27** 468–76
[7] Lee C D, Yan Y P, Liang S M and Wang T F 2009 Production of FMDV virus-like particles by a SUMO fusion protein approach in *Escherichia coli J. Biomed. Sci.* **16** 69
[8] Ramqvist T, Andreasson K and Dalianis T 2007 Vaccination, immune and gene therapy based on virus-like particles against viral infections and cancer *Expert Opin Biol. Ther.* **7** 997–1007
[9] Ferrer-Miralles N, Vazquez E and Villaverde A 2008 Membrane-active peptides for non-viral gene therapy: making the safest easier *Trends Biotechnol.* **26** 267–75
[10] Vazquez E, Ferrer-Miralles N and Villaverde A 2008 Peptide-assisted traffic engineering for nonviral gene therapy *Drug Discov. Today* **13** 1067–74
[11] Villaverde A and Carrio M M 2003 Protein aggregation in recombinant bacteria: biological role of inclusion bodies *Biotechnol. Lett.* **25** 1385–95
[12] Baneyx F and Mujacic M 2004 Recombinant protein folding and misfolding in *Escherichia coli Nat. Biotechnol.* **22** 1399–408
[13] Ferrer-Miralles N, Domingo-Espin J, Corchero J L, Vazquez E and Villaverde A 2009 Microbial factories for recombinant pharmaceuticals *Microb. Cell Fact.* **8** 17
[14] Ventura S and Villaverde A 2006 Protein quality in bacterial inclusion bodies *Trends Biotechnol.* **24** 179–85
[15] Gonzalez-Montalban N, Garcia-Fruitos E and Villaverde A 2007 Recombinant protein solubility-does more mean better? *Nat. Biotechnol.* **25** 718–20
[16] Peternel S, Grdadolnik J, Gaberc-Porekar V and Komel R 2008 Engineering inclusion bodies for non denaturing extraction of functional proteins *Microb. Cell Fact.* **7** 34
[17] Martinez-Alonso M, Gonzalez-Montalban N, Garcia-Fruitos E and Villaverde A 2009 Learning about protein solubility from bacterial inclusion bodies *Microb. Cell Fact.* **8** 4
[18] Garcia-Fruitos E *et al* 2005 Aggregation as bacterial inclusion bodies does not imply inactivation of enzymes and fluorescent proteins *Microb. Cell Fact.* **4** 27
[19] Nahalka J, Vikartovska A and Hrabarova E 2008 A crosslinked inclusion body process for sialic acid synthesis *J. Biotechnol.* **134** 146–53
[20] Garcia-Fruitos E, Aris A and Villaverde A 2007 Localization of functional polypeptides in bacterial inclusion bodies *Appl. Environ. Microbiol.* **73** 289–94
[21] Nahalka J 2008 Physiological aggregation of maltodextrin phosphorylase from Pyrococcus furiosus and its application in a process of batch starch degradation to alpha-D:-glucose-1-phosphate *J. Indust. Microbiol. Biotechnol.* **35** 219–23
[22] Nahalka J, Dib I and Nidetzky B 2008 Encapsulation of trigonopsis variabilis D-amino acid oxidase and fast comparison of the operational stabilities of free and immobilized preparations of the enzyme *Biotechnol. Bioeng.* **99** 251–60
[23] Garcia-Fruitos E *et al* 2009 Surface cell growth engineering assisted by a novel bacterial nanomaterial *Adv. Mater.* **21** 4249–53

[24] Garcia-Fruitos E, Martinez-Alonso M, Gonzalez-Montalban N, Valli M, Mattanovich D and Villaverde A 2007 Divergent genetic control of protein solubility and conformational quality in *Escherichia coli J. Mol. Biol.* **374** 195–205

[25] Margreiter G, Messner P, Caldwell K D and Bayer K 2008 Size characterization of inclusion bodies by sedimentation field-flow fractionation *J. Biotechnol.* **138** 67–73

[26] Peternel S, Jevsevar S, Bele M, Gaberc-Porekar V and Menart V 2008 New properties of inclusion bodies with implications for biotechnology *Biotechnol. Appl. Biochem.* **49** 239–46

[27] Bowden G A, Paredes A M and Georgiou G 1991 Structure and morphology of protein inclusion bodies in *Escherichia coli Biotechnology (NY)* **9** 725–730

[28] Carrio M M and Villaverde A 2001 Protein aggregation as bacterial inclusion bodies is reversible *FEBS Lett.* **489** 29–33

[29] Sambrook J, Fritsch E and Maniatis T 1989 *Molecular Cloning: a Laboratory Manual*

[30] Thomas J G and Baneyx F 1998 Roles of the Escherichia coli small heat shock proteins IbpA and IbpB in thermal stress management: comparison with ClpA, ClpB, and HtpG *in vivo J Bacteriol.* **180** 5165–72

[31] Mogk A *et al* 1999 Identification of thermolabile Escherichia coli proteins: prevention and reversion of aggregation by DnaK and ClpB *EMBO J.* **18** 6934–49

[32] Ziemienowicz A, Skowyra D, Zeilstra-Ryalls J, Fayet O, Georgopoulos C and Zylicz M 1993 Both the Escherichia coli chaperone systems, GroEL/GroES and DnaK/DnaJ/GrpE, can reactivate heat-treated RNA polymerase. Different mechanisms for the same activity *J. Biol. Chem.* **268** 25425–31

[33] Sambrook J, Fritsch E and Maniatis T 1989

[34] Feliu J X, Cubarsi R and Villaverde A 1998 Optimized release of recombinant proteins by ultrasonication of *E.coli* cells *Biotechnol. Bioeng.* **58** 536–40

[35] Laemmli U K 1970 Cleavage of structural proteins during the assembly of the head of bacteriophage T4 *Nature* **227** 680–5

[36] Carrio M M, Corchero J L and Villaverde A 1998 Dynamics of *in vivo* protein aggregation: building inclusion bodies in recombinant bacteria *FEMS Microbiol. Lett.* **169** 9–15

[37] Carrio M M and Villaverde A 2003 Role of molecular chaperones in inclusion body formation *FEBS Lett.* **537** 215–21

[38] Speed M A, Wang D I and King J 1996 Specific aggregation of partially folded polypeptide chains: the molecular basis of inclusion body composition *Nat. Biotechnol.* **14** 1283–7

[39] Carrio M, Gonzalez-Montalban N, Vera A, Villaverde A and Ventura S 2005 Amyloid-like properties of bacterial inclusion bodies *J. Mol. Biol.* **347** 1025–37

[40] Weibezahn J, Bukau B and Mogk A 2004 Unscrambling an egg: protein disaggregation by AAA+ proteins *Microb. Cell Fact.* **3** 1

[41] Carrio M M and Villaverde A 2002 Construction and deconstruction of bacterial inclusion bodies *J. Biotechnol.* **96** 3–12

[42] Dalby M J *et al* 2007 The control of human mesenchymal cell differentiation using nanoscale symmetry and disorder *Nat Mater.* **6** 997–1003

[43] Dalby M J 2007 Cellular response to low adhesion nanotopographies *Int. J. Nanomed.* **2** 373–81

[44] Dalby M J, Gadegaard N, Riehle M O, Wilkinson C D and Curtis A S 2004 Investigating filopodia sensing using arrays of defined nano-pits down to 35 nm diameter in size *Int. J. Biochem. Cell Biol.* **36** 2005–15

[45] Dalby M J, Riehle M O, Johnstone H, Affrossman S and Curtis A S 2004 Investigating the limits of filopodial sensing: a brief report using SEM to image the interaction between 10 nm high nano-topography and fibroblast filopodia *Cell Biol. Int.* **28** 229–36

[46] Dalby M J *et al* 2007 Nanomechanotransduction and interphase nuclear organization influence on genomic control *J. Cell Biochem.* **102** 1234–44

[47] Dalby M J 2005 Topographically induced direct cell mechanotransduction *Med. Eng. Phys.* **27** 730–42

[48] Kantawong F, Burchmore R, Gadegaard N, Oreffo R O and Dalby M J 2009 Proteomic analysis of human osteoprogenitor response to disordered nanotopography *J. R. Soc. Interface* **6** 1075–86

[49] Dalby M J 2009 Nanostructured surfaces: cell engineering and cell biology *Nanomedicine* **4** 247–8

[50] Keefer E W, Botterman B R, Romero M I, Rossi A F and Gross G W 2008 Carbon nanotube coating improves neuronal recordings *Nat. Nanotechnol.* **3** 434–9

[51] Jan E and Kotov N A 2007 Successful differentiation of mouse neural stem cells on layer-by-layer assembled single-walled carbon nanotube composite *Nano Lett.* **7** 1123–8

[52] Lipski A M, Pino C J, Haselton F R, Chen I W and Shastri V P 2008 The effect of silica nanoparticle-modified surfaces on cell morphology, cytoskeletal organization and function *Biomaterials* **29** 3836–46

[53] Dulgar-Tulloch A J, Bizios R and Siegel R W 2009 Human mesenchymal stem cell adhesion and proliferation in response to ceramic chemistry and nanoscale topography *J. Biomed. Mater. Res.* A **90** 586–94

[54] Samaroo H D, Lu J and Webster T J 2008 Enhanced endothelial cell density on NiTi surfaces with sub-micron to nanometer roughness *Int. J. Nanomed.* **3** 75–82

[55] Neubauer P, Fahnert B, Lilie h and Villaverde A 2006 Protein inclusion bodies in recombinant bacteria *Inclusions in Prokaryotes* (*Microbiology Monographs*) ed J M Shively (Berlin: Springer) pp 237–92

[56] Rokney A, Shagan M, Kessel M, Smith Y, Rosenshine I and Oppenheim A B 2009 *E. coli* transports aggregated proteins to the poles by a specific and energy-dependent process *J. Mol. Biol.* **392** 589–601

[57] Rinas U, Boone T C and Bailey J E 1993 Characterization of inclusion bodies in recombinant *Escherichia coli* producing high levels of porcine somatotropin *J. Biotechnol.* **28** 313–20

[58] Weibezahn J, Schlieker C, Tessarz P, Mogk A and Bukau B 2005 Novel insights into the mechanism of chaperone-assisted protein disaggregation *Biol. Chem.* **386** 739–44

[59] Mogk A and Bukau B 2004 Molecular chaperones: structure of a protein disaggregase *Curr. Biol.* **14** R78–80

[60] Vera A, Aris A, Carrio M, Gonzalez-Montalban N and Villaverde A 2005 Lon and ClpP proteases participate in the physiological disintegration of bacterial inclusion bodies *J. Biotechnol.* **119** 163–71

[61] Carrio M M and Villaverde A 2005 Localization of chaperones DnaK and GroEL in bacterial inclusion bodies *J. Bacteriol.* **187** 3599–601

Paper 2

Bioadhesiveness and efficient mechanotransduction stimuli synergistically provided by bacterial inclusion bodies as scaffolds for tissue engineering

Joaquin Seras-Franzoso, César Díez-Gil, Esther Vazquez, Elena García-Fruitós, Rafael Cubarsi, Imma Ratera, Jaume Veciana and Antonio Villaverde

Nanomedicine, 7, 2012

Cell adhesion and cell proliferation are crucial events for effective cell substrate colonization and often will determine the successfulness of a biomaterial in the tissue engineering field. This study was aimed to test IB suitability as a tissue engineering biomaterial by evaluating cell response of 4 different cell types, human skin fibroblasts (1BR3.G), new born hamster kidney cells (BHK21), human liver carcinoma cells (HepG2) and rat pheochromocytoma cells (PC12) when cultured on IB-based topographies. Additionally, we wanted to investigate the differential cell response in front of topographies formed by IB fabricated in different genetic backgrounds, since the genetic alteration in the IB deposition process was proved to originate particles with distinct physicochemical properties and morphologies (see annex biomaterials). To produce these topographies IBs formed of VP1GFP in MC4100 and its derivatives DnaK$^-$, ClpA$^-$ and ClpP$^-$ *E. coli* strains were used. Thus, in this work we have provided evidence of the effectiveness of bacterial IBs to promote cell adhesion and cell proliferation. Moreover we have shown that these two activities are not directly connected but act in a synergistic manner favoring cell substrate colonization on IB-based topographies. Besides, we have detected an enhanced phosphorylation of the extracellular signal-regulated protein kinase (ERK), which indicates the activation of a mechanotransduction-mediated stimulation of cell growth. Interestingly, we observed that even IB adhesiveness was evident for the four tested cell lines, the maintained stimulation of cell growth was cell line dependent. Nevertheless, both cell adhesion and proliferation have been shown to be modulated by the distinct IB type forming the surface topography.

RESEARCH ARTICLE

Bioadhesiveness and efficient mechanotransduction stimuli synergistically provided by bacterial inclusion bodies as scaffolds for tissue engineering

Background: Bacterial inclusion bodies (IBs), mechanically stable, submicron protein particles of 50–500 nm dramatically favor mammalian cell spread when used for substrate surface decoration. The mechanisms supporting fast colonization of IB-modified surfaces have not yet been identified. **Results:** This study provides evidence of mechanotransduction-mediated stimulation of mammalian cell proliferation on IB-decorated surfaces, as observed by the enhanced phosphorylation of the signal-regulated protein kinase and by the dramatic emission of filopodia in the presence of IBs. Interestingly, the results also show that IBs are highly bioadhesive materials, and that mammalian cell expansion on IBs is synergistically supported by both enhanced adhesion and mechanical stimulation of cell division. **Discussion:** The extent in which these events influence cell growth depends on the particular cell line response but it is also determined by the genetic background of the IB-producing bacteria, thus opening exciting possibilities for the fine tailoring of protein nanoparticle features that are relevant in tissue engineering.

Original submitted: 07/02/2011; Revised submitted: 07/04/2011

KEYWORDS: adhesion enhanced phosphorylation of the signal-regulated protein kinase filopodia inclusion body proliferation protein material protein nanoparticle

Joaquin Seras-Franzoso[1,2,3], César Díez-Gil[3,4], Esther Vazquez[1,2,3], Elena García–Fruitós[3,1], Rafael Cubarsi[3,5], Imma Ratera[3,4], Jaume Veciana[3,4] & Antonio Villaverde*[1,2,3]

[1]Institute for Biotechnology and Biomedicine, Universitat Autònoma de Barcelona, Bellaterra, 08193 Barcelona, Spain
[2]Department of Genetics and Microbiology, Universitat Autònoma de Barcelona, Bellaterra, 08193 Barcelona, Spain
[3]CIBER de Bioingeniería, Biomateriales y Nanomedicina (CIBER-BBN), Bellaterra, 08193 Barcelona, Spain
[4]Institut de Ciencia de Materials de Barcelona (ICMAB-CSIC) Bellaterra, 08193 Barcelona, Spain
[5]Departament de Matemàtica Aplicada IV, Universitat Politècnica de Catalunya, Jordi Girona 1-3, 08034 Barcelona, Spain
*Author for correspondence
Tel.: +34 935 813 086
antoni.villaverde@uab.cat

Regenerative medicine is clinically focused on the reconstruction of damaged tissues through the controlled cultivation of stem cells on artificial scaffolds, a procedure often approached *ex vivo* followed by implantation into the damaged organ. Efficient cell attachment and colonization of scaffold surfaces are then necessary to promote further differentiation and formation of correct tissue structures. Several protein factors are used for surface functionalization and biologically mediated stimulation of cell migration, proliferation and differentiation, as well as *de novo* vascularization of new tissues. They include EGF [1], FGF-1 [2], FGF-2 [3], osteoprotegerin [4], IGF-1 [5], NGF-β [6–8], VEGF [3], TGF-β [5,9,10] and bone morphogenetic proteins [11], apart from cell adhesion agents such as vitronectin [12], fibronectin [13] and arginine–glycine–aspartic acid peptides [14,15].

On the other hand, engineering the roughness of surfaces where cells are to be attached and proliferate (to provide appropriate mechanical stimuli) is progressively being recognized as a powerful tool to modulate mammalian cell differentiation and proliferation in regenerative medicine [16,17]. Such a bio-inspired approach allows the mimicking of the natural matrix for cell growth, at the size at which mechanical effectors trigger cell responses [18]. In general, mechanical stimulation of cell proliferation has been studied through the lithographical modification of polystyrene or other surfaces (top-down approach) to produce micro- and nano-grooves or pits [19–22]. These topographical elements, sensed by cultured cells, guide cell division and differentiation upon appropriate surface patterning [23–27].

Alternatively, several categories of particulate materials have been explored for the nanomorphological modification of scaffold surfaces (bottom-up approach), including ceramics, polymers and carbon nanotubes [28–31]. Particle-based surface decoration is highly promising since it is less dependent on the chemical nature of the scaffold material in contrast to its lithographical modification. However, the limited control of the nanoscale properties of most of these particles during their fabrication restricts their tailoring, improvement and adaptation to the requirements of the cell mechano-sensing machinery. Recently, we have shown that bacterial inclusion bodies (IBs), pseudoespherical protein clusters spontaneously formed in recombinant bacteria [32,33], can be used as biocompatible materials for surface decoration and stimulation of mammalian cell spread [34]. Since IB formation is multigenically determined through the cell's quality control system [35,36], mechanical [37], morphological [38], structural [39] and biological [40] properties of

10.2217/NNM.11.83 © 2011 Future Medicine Ltd

Nanomedicine (Epub ahead of print)

ISSN 1743-5889

IBs can be adjusted by the genetic manipulation of the producing cells. Interestingly, by using different cell lines and IB variants, we have shown that the IB-mediated cell colonization is supported by two independent but synergistically acting mechanisms, namely enhanced cell adhesion and proliferation. The contribution of bioadhesiveness and IB-mediated mechanotransduction stimulation of cultured cells have been determined, as both are events influenced by the protein packaging style supported by each particular bacterial genetic background. This fact demonstrates not only the plasticity of IBs as protein particles, but also the tunability and adaptability of protein-based bacterial nanomaterials over their already recognized functional properties.

Material & methods

Bacterial production of IBs

IBs were fabricated in *Escherichia coli* MC4100 (wild-type [wt] regarding protein folding and degradation, araD139 Δ[argF-lac] U169 rpsL150 relA1 flbB5301 deoC1 ptsF25 rbsR) [41] and derived mutants in which different genes involved in protein quality control had been knocked down (strain JGT4 deficient in the coprotease ClpA, *clpA::kan*, strain JGT19, deficient in the coprotease ClpP, *clpP::cat*, and strain JGT20, deficient in the chaperone DnaK, *dnak756 thr::Tn10*) [42]. All of these strains produced an aggregation-prone green fluorescent protein (GFP), encoded by plasmid pTVP1GFP, that form fully fluorescent IBs [40]. Details of the bacterial culture and IB purification procedures have been given elsewhere [34]. Once isolated, IBs were resuspended in phosphate-buffered saline (PBS) and their concentration determined by conventional fluorescence microscopy using a counting chamber in a microscope Leica DMRB (Leica Microsystems GmbH, Wetzlar, Germany).

Cell culture & proliferation assay

IBs produced in bacteria during 1, 3 or 4 h, of known concentrations, were sterilized by exposure to a 253 nm UV light germicidal lamp for 3 h. Then, 2.6×10^8 IBs in 0.05 ml were deposited per well on a 96-well nontreated flat bottom polystyrene culture plates (Costar 3370, NY, USA), to reach a density of 8.4×10^8 IBs per cm^2, and they were incubated overnight at 4°C. Wells were washed in PBS, blocked with 3% bovine serum albumin in PBS for 1 h at 37°C and washed again in PBS. Then 3×10^3 cells from new born hamster kidney (BHK21), 2×10^4 cells from rat pheochromocytoma (PC12), 5×10^3 human skin fibroblasts (1BR3.G) and 7×10^3 cells from human liver carcinoma (HepG2) were seeded per well and incubated in DMEM or in minimum essential medium in the case of HepG2 cells. Both media were supplemented with GlutaMAX and 10% fetal bovine serum and plates were incubated at 37°C for different times. Control wells without IBs were equally treated and used for cell culture. The amounts of living cells were determined by the 3-(4,5-dimethylthiazol-2-yl)-2,5-diphenyltetrazolium bromide assay, using the EZ4U kit (Biomedica, GmbH, Vienna, Austria), and data were recorded in the Labsystems iEMS Reader MF (Helsinki, Finland) as described [34]. All the cell culture experiments were carried out in triplicate and comparisons statistically validated through a Student's t-test.

Cell adhesion assay

Ninety six-well nontreated flat bottom polystyrene culture plates, decorated (as described above) with DnaK$^-$ IBs produced for 3 h, were seeded with 1.5×10^4 1BR3.G cells or 2.1×10^4 HepG2 cells and cultured for 24 h at 37°C. The same number of cells were seeded on nondecorated wells as a negative control. Increasing number of washing steps with PBS were carried out on the plates and the amount of retained cells were measured by 3-(4,5-dimethylthiazol-2-yl)-2,5-diphenyltetrazolium bromide assay, using EZ4U kit and recording data in the Labsystems iEMS Reader MF.

Cell viability assay

A total of 1.5×10^5 1BR3.G cells or 2.1×10^5 HepG2 cells were seeded, each on six-well nontreated flat bottom polystyrene culture plates (Nunc, Roskilde, Denmark), previously decorated with DnaK$^-$ IBs produced for 3 h. Cells cultured on naked plates were used as a control. At 24 and 72 h, the culture media was removed, cells were washed in 1 ml of Dulbecco's PBS, and 1 ml of 0.5% trypsin solution was added to each well. After incubation at 37°C (15 min for HepG2 cells and 8 min for 1BR3.G cells), trypsin was neutralized by the addition of 2 ml of culture media. Both the removed culture media as well as the Dulbecco's PBS used for washing were centrifuged at 1400 rpm for 5 min to recover any weakly attached or nonattached cell and include them in the final counting. Cell pellets were resuspended in 1 ml of culture media and cell viability was determined by cell number using hemocytometer counts with trypan blue exclusion staining.

Cell disruption & protein extraction

1BR3.G and HepG2 cells were cultured on six-well nontreated flat bottom polystyrene culture plates (Nunc), prepared as in the 'cell culture and proliferation assay' section. Cells were sampled at selected times, washed with PBS and 100 µl of lysis buffer (50 mM Tris HCl, pH 7.4, 50 mM NaF, 0.27 M sucrose, 1 mM orthovanadate, 10 mM glycerol 3-P, 5 mM NaPyrophosphate, 1% Nonidet P-40, 1% Tween 20, 1 mM ethylenediaminetetraacetic acid, 1 mM ethylene glycol tetraacetic acid and β-mercaptoethanol 0.1%) with protease inhibitor cocktail (Roche Diagnostics GmbH, Mannheim, Germany, ref. 1 836 170) was added. The buffer was added to each well, incubated on ice and mixed by pipetting to facilitate cell disruption. Soluble protein was obtained by centrifugation at 13,200 rpm for 15 min at 4°C and quantified by a Bradford assay as indicated [43].

Determination of IB stability in cell culture

VP1GFP IBs that were aged 3 h and produced in the DnaK$^-$ background, were deposited on six-well nontreated flat bottom polystyrene culture plates (Nunc) at a density of 8.4×10^8 IBs per cm^2. Then, 6×10^4 1BR3.G cells and 1.2×10^5 HepG2 cells were seeded. Control wells consisting of IBs in cell media but without cells were included. IBs were recollected manually at 24, 48 and 72 h by PBS washing and scraping. The resulting suspension was centrifuged for 15 min at 15,000 G and the IBs pellets stored until analysis. IBs were resuspended in 1 ml PBS and fluorescence at 510 nm and their transmittance was recorded with a Cary Eclipse fluorescence spectrophotometer (Variant) by using 450 nm as the excitation wavelength.

Western blot analysis

Equal amounts of total protein, for each cell line and culture time, were loaded in 10% acrylamide sodium dodecyl sulfate polyacrylamide gel electrophoresis gels (enhanced phosphorylation of the signal-regulated protein kinase [ERK], p-ERK and β-actin detection) while VP1GFP IBs from the stability assay were loaded in 7.5% acrylamide sodium dodecyl sulfate polyacrylamide gel electrophoresis gels. Once ran, the gels were transferred to nitrocellulose membranes for western blot analysis. The mouse monoclonal antibodies anti-β-actin, anti-p-ERK (1/2) and anti-GFP (Santa Cruz Biotechnology Inc., CA, USA), as well as the rabbit polyclonal antibody anti-p44/42 Map Kinase (9102) were used for the detection of p-ERK, GFP and ERK, respectively. A goat antimouse and a goat antirabbit, conjugated with the horseradish peroxidase, were used as secondary antibodies (BioRad, CA, USA). ERK, p-ERK and β-actin bands were developed by chemiluminiscence (Pierce Prod #34080, IL, USA) and visualized in a VersaDoc Imaging system (BioRad), while GFP bands were developed by a chromogenic reaction.

Scanning electron microscopy

IBs at the same density as those used for proliferation assays were deposited in a defined area (9.6 cm^2) of a 90-mm polystyrene Petri dish (Sterilin), washed in PBS and blocked with 3% bovine serum albumin as mentioned previously. The IB-decorated area was delimited by previously UV-sterilized silicone. Then, appropriate amounts of PC12 and HepG2 cells were seeded and incubated in their respective optimum media at 37°C for 48 h. Samples were fixed in 2.5% (v/v) glutaraldehyde in phosphate buffer (0.1 M pH 7.4) for 2 h at room temperature, washed and postfixed in 1% (w/v) osmium tetraoxide. After an additional wash, cells were dehydrated by incubation for 15 min in growing ethanol concentrations: 50, 70, 80, 90, 95 and 100% (the step using 100% ethanol was carried out twice). Samples were dried by critical point with CO_2, mounted on scanning electron microscope supports with carbon film and coated with gold. Observation was carried out in an S-570 scanning electron microscope (Hitachi Ltd, Tokyo, Japan) at an accelerating voltage of 15 kV.

IBs size & zeta potential determination by dynamic light scattering

The size and zeta potential of IB variants were determined using a dynamic light scattering instrument (Malvern, Nanosizer Z, Worcestershire, UK) in suspension on PBS buffer (pH 7.4, IB final concentration was 20 µg/ml). In order to facilitate the formation of an appropriate suspension of the liquid, 2 ml of the mixture was sonicated for 1 min. Dynamic light scattering measurements were carried out at 37°C using 1 ml of freshly prepared IB suspension into a disposable plastic cubette. Each IB sample was analyzed by triplicate averaging 30 single measurements.

Mixed thiol self-assembled monolayer preparation

Gold substrates modified with self-assembled monolayers (SAMs) with different degrees of

doi:10.2217/NNM.11.83

hydrophobicity were obtained by the use of different molar ratios of hydrophilic (-OH terminated) and hydrophobic (-CH_3 terminated) alkane thiols, as shown by static contact angle measurements (ranging from 100 to 35°). SAMs of 1-undecenethiol (-CH_3 terminated) and 11-mercapto-1-undecanol (-OH terminated) with different proportions, were prepared by immersion of the freshly cleaned gold substrates in an ethanolic solution of the organic thiols with the appropriate molar ratio for 24 h. Afterwards, substrates were rinsed with clean ethanol and sonicated for 5 min in ethanol to remove the physisorbed molecules. The substrates were then dried under a stream of nitrogen and immediately used to avoid ambient contamination.

Contact angle measurements

The wettability of the SAMs of the mixed thiols before and after being in contact with IBs was determined with an OCA 15+ (Dataphysics, Filderstadt, Germany) contact angle goniometer. Data treatment and angle determination were carried out with the software SCA20 (Dataphysics, Germany). Four sets of static contact angles, at different positions on each sample, were measured.

Coverage of IBs on the mixed SAMs

Freshly prepared mixed monolayers of the thiols were immersed for 2 h into an IB suspension in PBS buffer (IB suspension was sonicated for 5 min prior to the introduction of the substrate). Afterwards, the IB-covered substrates were gently rinsed with Mili-Q water (18.2 mΩ) and dried under a stream of nitrogen. Optical microscope fluorescence images of the deposited IBs were performed using an Olympus Bx51 microscope with an Olympus DP20 camera with a 3-s shutter time and an Olympus U-RFL-T mercury lamp accessory. In order to remove background light a GFP pass filter was used. ImageJ (GNU) software was utilized to perform the particle counting.

Atomic force microscopy

Atomic force microscopy (AFM) images were taken with a commercial AFM (MFP-3D-SA, Asylum Research, CA, USA). Samples were analyzed in tapping mode working at 8 kHz of frequency and in a liquid environment (PBS buffer media pH 7.4) in order to mimic the cytoplasmic environment of the cell. Pyramidal NSC35/AlBS silicon tips (MikroMacsh, CA, USA) having nominal spring constants of 0.28 N/m were used. Sample preparation was carried out by drop casting of an IB suspension in the same PBS buffer (20 µg/ml) over freshly cleaved mica.

Force spectroscopy AFM

AFM indentation measurements were carried out with a commercial AFM (MFP-3D-SA, Asylum Research, CA, USA) equipped with a close loop tracking system and working on liquid environment. Pyramidal NSC35/AlBS silicon tips (MikroMacsh, USA) having nominal spring constants of 0.28 N/m were used. The spectroscopic calibration of the raw cantilever on liquid media (PBS buffer solution pH 7.4) was developed by measuring force versus distance curves, on freshly cleaved mica. Sample preparation was carried out by drop casting an IB suspension in the same PBS buffer (20 µg/ml) over freshly cleaved mica. The force curves, consisting of 2048 data points, were obtained imposing a maximum applied force of 50 nN at a frequency of 8 kHz. AFM mechanical properties data were calculated from force distance curves according to the procedures previously described [44,45]. To achieve spatial resolution of the spectroscopic measurements, dynamic AFM images of the studied IBs were developed prior to and after force versus distance measurements. Therefore, observations allowed us to follow any movement or deformation produced on the sample during the experiment.

Numerical analysis

The correlation r between pairs of variables X and Y in the samples was calculated to determine the strength of their relationship, and the significance of the correlation coefficient was tested against the null hypothesis that there is no relationship between X and Y in the population, p = 0. For that, we used the t-distribution value with n-2 degrees of freedom. For a level of significance ε, generally assumed as 0.01, the probability $P(|t|> t_0) = \varepsilon$ renders the value t_0, such that if t lies below the critical t_0, the null hypothesis of no relationship in the population (p = 0) cannot be rejected. Then the correlation was observed as not significant; otherwise, the significance of the correlation was accepted.

Results

Mammalian cell colonization of IB-decorated surfaces is stimulated by two independent but synergistically acting mechanisms

Two selected mammalian cell lines (HepG2, hepatocytes and 1BR3.G, fibroblasts) were

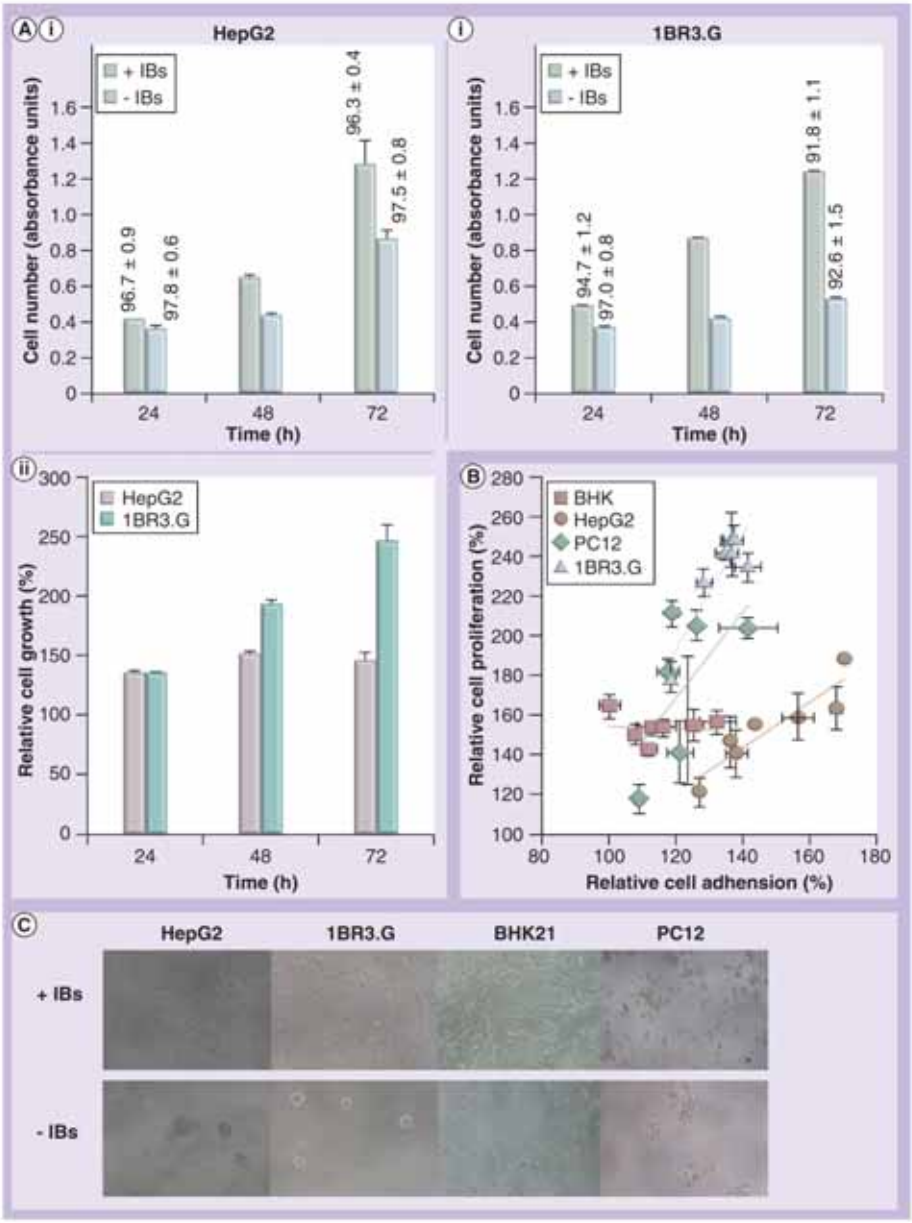

Figure 1. Inclusion bodies-mediated surface colonization by different cell lines. (A, i) Number of living cells, monitored by a 3-(4,5-dimethylthiazol-2-yl)-2,5-diphenyltetrazolium bromide analysis, during prolonged cultivation of two cell lines (HepG2 and 1BR3.G) on flat and IB-decorated polystyrene surfaces. Numbers indicate the percentage of viable cells at 24 and 72 h; **(A, ii)** cell amounts on IB-decorated surfaces relative to those observed on nondecorated surfaces. In all cases IBs produced in DnaK$^-$ bacteria for 3 h were used for decoration. **(B)** Correlation between relative adsorption and proliferation of the four cell lines on IB-decorated surfaces. Data were retrieved from Table 1. **(C)** Micrographs of cultures of HepG2, 1BR3.G, BHK21 and PC12 cells on IB-free and IB-decorated polystyrene surfaces (taken at 48 h).
IB: Inclusion body.

cultured on nontreated polystyrene surfaces upon random decoration with IBs. Both HepG2 and 1BR3.G cells responded positively to surface decoration with IBs (Figure 1A, i) and without any sign of toxicity. However, when plotting cell growth on IB-decorated surfaces relative to that on nondecorated surfaces (in %), two different patterns were clearly observed

doi:10.2217/NNM.11.83

(FIGURE 1A, ii). At 24 h, the number of HepG2 cells on IB-decorated surfaces was significantly higher than in nondecorated flat surfaces, and this difference was maintained at later monitoring times. This indicated an improved attachment of HepG2 cells enhanced by IBs (values at early cultivation times, t_{24}), but a moderate stimulation of proliferation on the modified substrate (late values, t_{72}). By contrast, the relative number of 1BR3.G cells was also initially high, but it further increased with cultivation time (FIGURE 1A, ii), proving that in this case, IBs stimulated not only cell attachment but also promoted a sustained activation of cell division.

The IB-mediated stimulation of cell attachment and proliferation was assessed through the analysis of two additional cell lines (BHK21, fibroblasts and PC12, neuron-like cells) (FIGURE 1C), and by incorporating diverse IB variants produced in different genetic backgrounds (TABLE 1, SUPPLEMENTARY TABLE 1, see online, www.futuremedicine.com/doi/suppl/10.2217/nnm.11.83). The selected mutations had previously shown a dramatic influence on recombinant protein folding and aggregation, which resulted in variations in IB shape and size [34,38], conformational status of the embedded protein [40,46] and several nanomechanical properties of the protein particles [37]. Interestingly, the capabilities of IBs to stimulate cell attachment (t_{24} data, ranging between 117 and 139%, TABLE 1) and proliferation (t_{72} data, between 141 and 229%, TABLE 1), were both evidenced in the four tested cell lines. In general, the bioadhesiveness of ClpP IBs was slightly weaker and those of wt IBs, stronger than the average.

Characterization of IB-mediated cell adhesion

Interestingly, ClpP IBs were inefficient in enhancing the attachment of BHK21 cells (100.3%) but clearly stimulated their proliferation (164.1%), suggesting that both events were mechanistically unconnected. In this line, when the set of t_{72} and t_{24} data from all cell lines was compared, data appeared highly scattered (FIGURE 1B), indicating that IB-mediated stimulation of cell proliferation was not a straightforward consequence of favored cell adhesion. However, significant lineal correlations were uniquely and independently observed for HepG2 ($p = 0.0038$) and 1BR3.G ($p = 0.0085$), the cell lines with the highest affinity for IB-decorated surfaces (see average t_{24} data for these cell lines in TABLE 1). In this regard, strong cell adhesion at early experimental times might represent a catalyst for the stimulation of further division.

To confirm attachment and proliferation as differentially activated by IBs, the cell adhesiveness to IB-decorated surfaces was investigated in HepG2 and 1BR3.G cells in a step washing experiment. The modified surfaces retained a significantly higher number of cells than nude polystyrene surfaces (FIGURE 2A), and HepG2 cells remained more strongly attached to the surface than 1BR3.G cells, in agreement with data shown in TABLE 1.

IB-mediated cell proliferation involves media probing & mechanical signal transduction

On the other hand, we wanted to assess to what extent cell proliferation mediated by IBs

Table 1. Cell number, monitored by 3-(4,5-dimethylthiazol-2-yl)-2,5-diphenyltetrazolium bromide absorbance units, in cultures of four selected cell lines on inclusion body-decorated surfaces relative to nondecorated flat surfaces.

Cell line	Culture time	Observed effect	Genetic background of producing bacteria (%)				Average data (%)
			Wild-type	*ClpA*$^-$	*DnaK*$^-$	*ClpP*$^-$	
1BR3.G	t24	Attachment	137.00	137.03	136.46	118.81	132.32
	t72	Proliferation	248.09	242.51	248.24	178.78	229.41[†]
PC12	t24	Attachment	123.53	121.36	109.09	126.32	120.07
	t72	Proliferation	156.78	141.08	117.92	205.06	154.96[†]
BHK21	t24	Attachment	132.66	112.11	125.62	100.36	117.69
	t72	Proliferation	156.02	142.23	154.71	164.15	154.28[†]
HepG2	t24	Attachment	156.71	138.39	136.4	127.32	139.72
	t72	Proliferation	158.68	140.29	146.54	120.92	141.37[†]
Average data	t24	Attachment	135.75[‡]	127.22[‡]	126.67[‡]	118.17[‡]	
	t72	Proliferation	179.87	166.50	166.85	167.22	

Data are shown at 24 and 72 h. Cell lines are ordered in the table by the average proliferation data (relative cell number at 72 h[†]) and IB variants by the average cell attachment data (relative cell number at 24 h[‡]), from higher to lower. Data derive from IBs produced for 3 h (4 h for ClpP IBs).
IB: Inclusion body.

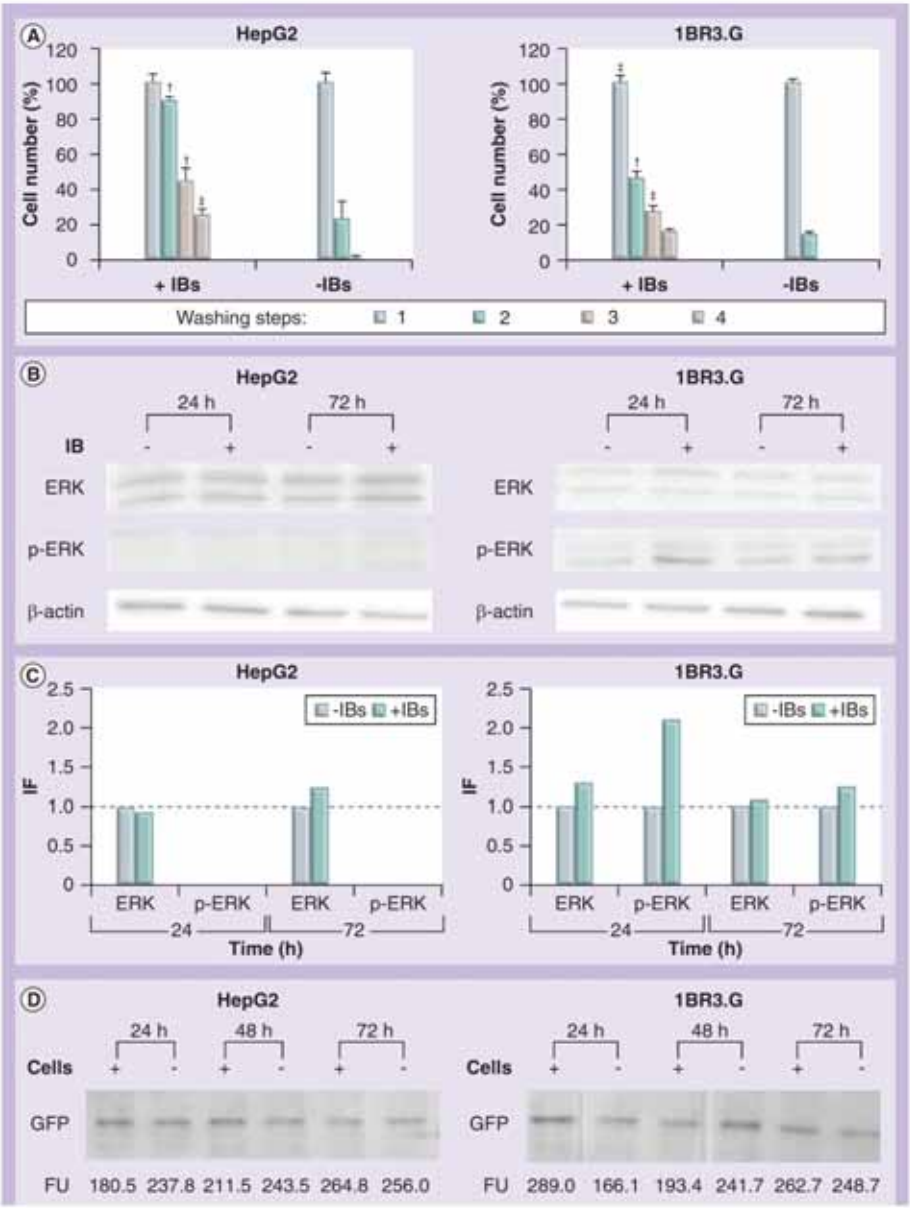

Figure 2. Mechanics of inclusion-body-mediated stimulation of cell spread and surface colonization. (A) HepG2 and 1BR3.G cell retention (monitored by 3-(4,5-dimethylthiazol-2-yl)-2,5-diphenyltetrazolium bromide analysis) in nude polystyrene plates (-) or in plates decorated with IBs (+), during sequential washing steps. Significance of the differences between retention on IB-decorated or nude surfaces is given as: $^{\dagger}0.01 < p \leq 0.05$; $^{\ddagger}p \leq 0.01$. **(B)** ERK, p-ERK and β-actin (as control) immunodetection at 24 and 72 h of HepG2 and 1BR3.G cell culture on IB-decorated and nude polystyrene plates. No significant variations in ERK and β-actin were observed. Samples were obtained from a pool of six independent cultures. **(C)** Representation of ERK expression and activation on IB-decorated surfaces relative to nondecorated plain surfaces. In ERK bars, IF represents the ERK induction fold expression in cells growing on IB-decorated surfaces relative to those growing on nondecorated surfaces, while in p-ERK bars, the activation factor by phosphorylation. Dashed lines indicate no variation. **(D)** Prevalence of IBs on plates during culture of HepG2 and 1BR3.G cells, as monitored by green fluorescence protein immunodetection and determination of green fluorescence emission. IB-decorated plates in absence of cells were used as controls.
ERK: Enhanced phosphorylation of the signal-regulated protein kinase FU: Fluorescence units; GFP: Green fluorescence protein; IB: Inclusion body.

doi:10.2217/NNM.11.83

was triggered by the mechanical stimuli offered by these protein particles. Interestingly, the phosphorylated form of the signal-regulated protein kinase (p-ERK), which transduce extracellular growth stimuli to the nuclei and whose activation is intimately linked to cell proliferation [47,48], was found to be increased in 1BR3.G but not in HepG2 cells (Figure 2B). This is according to the higher division rate of this cell line when comparing with HepG2 (Figure 1A, ii). The cellular amounts of ERK were moderately enhanced in both cell lines, but the low levels of ERK increase prevented us to strongly suggest an IB-promoted stimulation of *ERK* gene expression.

At this point, we wanted to exclude that IBs would have been metabolized by the cells during the experimental time, and to confirm that the observed events were uniquely derived from the mechanical stimuli of IBs as nanostructured, inert materials. In this context, IBs were still present in the cell cultures after 72 h (Figure 2D), indicative of a high stability of these protein particles and of the absence of important indirect effects through the cell's protein metabolism.

To explore how cells growing on IBs might gain information about their modified environment, we investigated their morphology by scanning electron microscope. Observation of HepG2 and PC12 cells revealed a dramatic occurrence of filopodia in IB-stimulated cells, which were essentially absent in cells growing on flat polystyrene surfaces (Figure 3). Interestingly, filopodia and lamelipodia were seen in close contact with IBs (Figure 3, insets and magnifications at the right), indicative not only of fine environmental probing but also proving that IB dimensions are within the cellular sensing range. These observations support filopodia sensing as the key element in the cell growth response to effector topographies as previously proved using nonbiological substrate materials [49,50].

IB variants are differently adhesive & differentially stimulate cell proliferation

In an attempt to identify the features of IBs responsible for adhesion and growth stimulation we firstly explored IB size (Table 2). When plotting the effective diameter of all IB variants versus proliferation, a negative effect was observed in PC12 and HepG2, although data obtained with ClpP IBs (459 nm) were always apart from the general pattern (Figure 4A). As a confirmation that cell attachment and proliferation are independently regulated by IBs, IB diameter did not have any impact on PC12 cell attachment (red circles, Figure 4A).

The unusual biological effects of ClpP IBs (Figure 4A; Table 1) as well as the previously observed unusual tear-like shape of these particles [38] prompted us to explore their mechanical properties. Force spectroscopy AFM depicted the occurrence of four different stiffness populations (Figure 4B & 4C), two of them situated within the range previously observed for ClpA$^-$ IBs (3.33 ± 0.21 and 7.10 ± 0.09 MPa with full

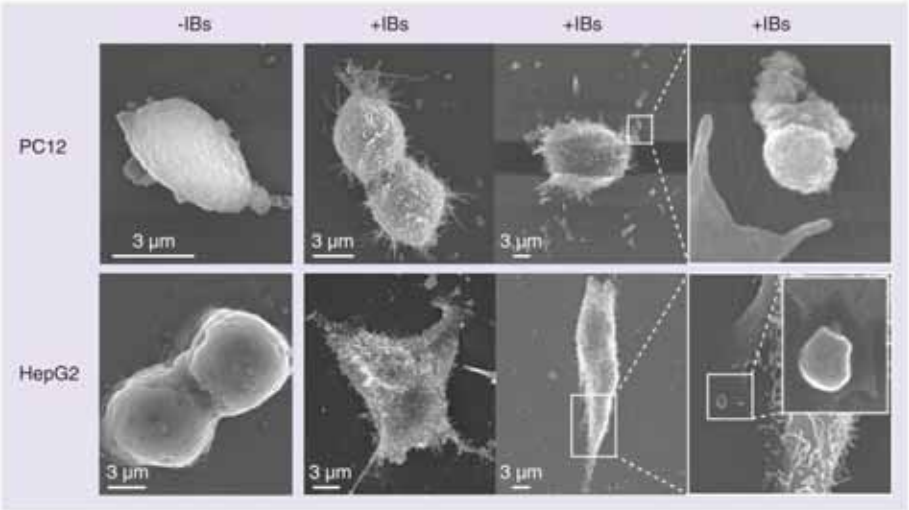

Figure 3. Scanning electron microscope images of PC12 and HepG2 cells cultures for 48 h on flat surfaces and upon decoration with DnaK$^-$ inclusion bodies (aged 3 h), showing the abundance of inclusion body-induced filopodia. Inset frames contain magnified images showing filopodia in contact with surface-attached inclusion bodies.

Table 2. Relevant nanoscale properties of inclusion bodies biofabricated in different bacterial strains during different times.

Phenotype of producing bacteria	Fabrication time (h)	Diameter (nm)	Average stiffness	Maximal stiffness	Morphology	Zeta potential	Contact angle at the maximum coverage
Wild-type	1	120	nd	nd	Spherical	nd	nd
	3	342	3.76	3.73	Spherical	-16.7	4.5
DnaK⁻	1	206	nd	nd	Spherical	nd	nd
	3	531	5.65	7.75	Spherical	-18.2	2.4
ClpA⁻	1	235	nd	nd	Spherical	nd	nd
	3	435	8	10.99	Spherical	-17.8	1.9
ClpP⁻	4	459	7.96 (11.48)	13.45 (22)	Tear-shaped	-26.5	6.5

Data indicated in the parenthesis might eventually be influenced by the analytical procedure and were not used for further correlation analysis. Some of the depicted data relative to wild-type, DnaK⁻ and ClpA⁻ inclusion bodies had been obtained in a previous study [37].
nd: Not determined.

width at half maximum of 2.67 ± 0.59 and 1.05 ± 0.39 MPa, respectively). The other two were at higher Young modulus values (13.45 ± 2.28 and 22.07 ± 0.168 MPa with full width at half maximum of 18.75 ± 2.59 and 1.21 ± 0.468 MPa, respectively). However, Young modulus values obtained by mathematical treatment of the force spectroscopy AFM measurements onto ClpP⁻ IBs indicated the appearance of harder elasticity distributions. The presence of one peak at 22.07 MPa could not be explained just by the modification of the protein stiffness, as it differs by almost 10 MPa from the previous distribution of the same IB material. Therefore, this peak can be assigned to the influence of the substrate on the AFM tip during the force spectroscopy AFM measurement. In order to easily compare the results obtained for all the IBs tested, stiffness histograms obtained for all IBs used in this study are depicted in Figure 4D. This eventual artifact value was not included in further numerical analysis.

On the other hand, ClpP⁻ IBs wettability and coverage dependence indicated that ClpP⁻ IBs do not strongly modify the initial contact angle of the surface (Figure 4E). In addition, the data indicate a broad heterogeneity of ClpP⁻ IBs surface chemistry. Nevertheless, IB surface coverage dependence on the substrate contact angle was also determined. The obtained results (Figure 4F) showed the existence of two maxima of IB coverage (one at 60° and the other one at angles more than 90°) reaching absolute values of 0.007 IB/μm², for surface contact angle of approximately 80°.

Mechanical data of ClpP⁻ IBs and other IB variants were used for a multiple correlation analysis with the relative cell number (at both early and late times), to screen any possible dependence between attachment or proliferation and IB properties (Figure 4G). Interestingly, the average stiffness and contact angle showed very poor influence on cell growth. However, maximal stiffness had important negative effects on cell adhesion and moderate effects on cell proliferation, while zeta potential positively influenced proliferation but also cell adhesion. The diameter of the protein particles negatively modulated both attachment and proliferation in the tested ranges, as discussed previously. The exclusion of ClpP⁻ IB data in the analysis did not dramatically alter the significance of correlations, indicating the absence of relevant methodological deviations in the size determination of these morphologically aberrant particles.

Discussion

Bacterial IBs are pseudo-spherical deposits of insoluble protein commonly occurring in recombinant bacteria [32,51–53], whose formation, observed since early recombinant DNA times [54], has limited the applicability of recombinant proteins in industry and research [55]. IBs are formed when bacteria are forced to express foreign or engineered genes over physiological rates, and important fractions of the newly produced encoded protein do not reach the native conformation. Then, these misfolded polypeptides accumulate through sterospecific crossmolecular contacts [56,57] in a seeding-based style, that results in the formation of protein clusters with amyloid-like architecture [58]. Protein deposition through crosspleated β-sheet-based interactions [33,58,59] confer high mechanical stability to the resulting particles [34], that converts them into intriguing self-organizing biomaterials with appealing tunable properties [35,36,60–62]. Previously, we have shown that deposition of IBs on flat surfaces, in a bottom-up

doi:10.2217/NNM.11.83

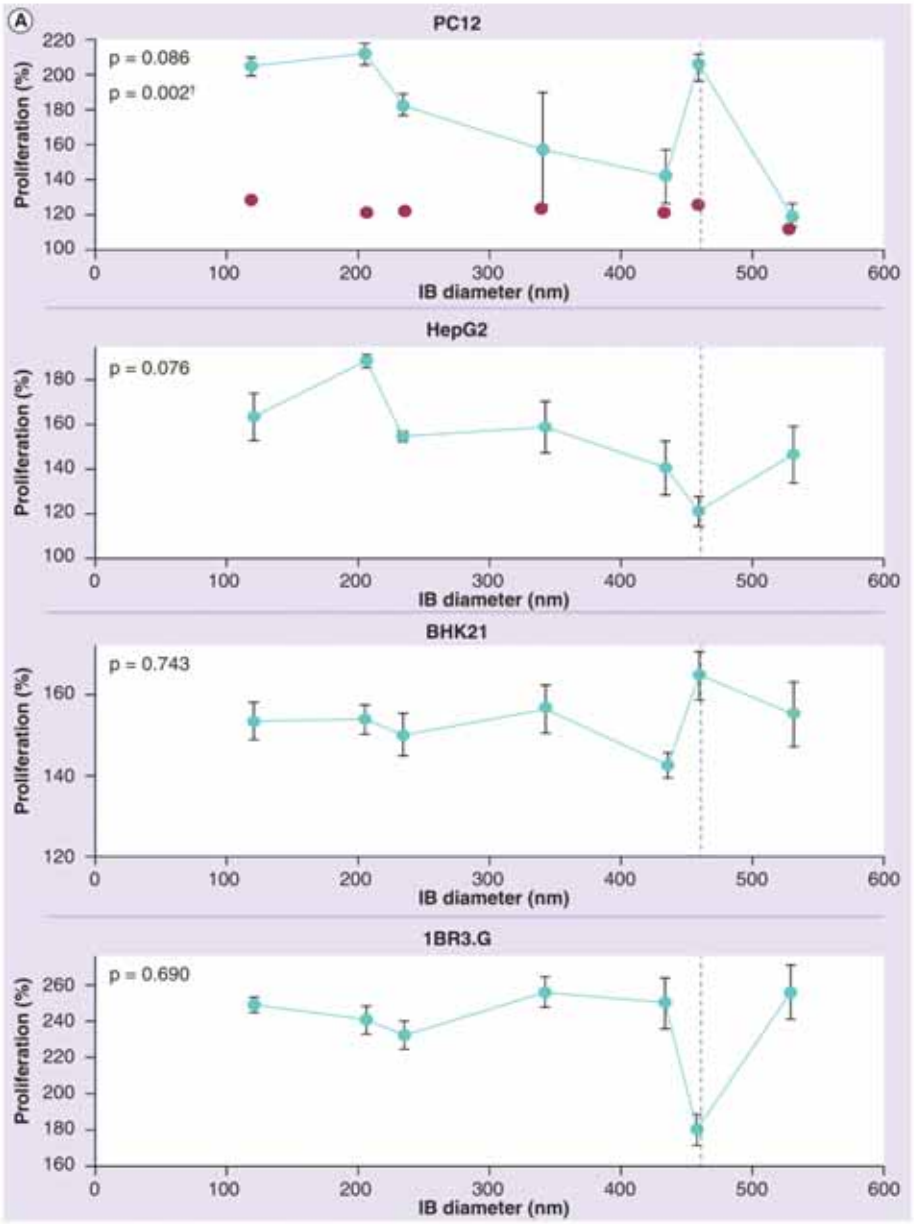

Figure 4. Influence of inclusion body physicochemical properties on cell adhesion and proliferation. (A) Relative proliferation of four cell lines (t_{72}) versus the diameter of IBs used for decoration. Dotted vertical line indicates the data obtained when rowing cells on ClpP$^-$ IBs. The significance (p-value) of linear correlations is indicated in each panel. For PC12, the significance obtained without ClpP$^-$ IB data is also shown (†), as well as the relative cell number at t_{24} (average, as red circles). IB: Inclusion body.

approach to nano- and micro-environment engineering, dramatically favor mammalian cell colonization [34,37,38]. In the present study, we have shown that the stimulation of colonization of IB-decorated surfaces is a combined result of two independent events, namely cell attachment and proliferation, which are triggered differently by IBs (Figures 1 & 2; Table 1). The efficiency of cell attachment was dependent on the IB variant, suggesting a spectrum of adhesiveness exhibited by the protein materials depending on the specific aggregation pattern undergone in each genetic background (for instance, ClpP$^-$ IBs being less adhesive than wt IBs).

Stimulation of cell proliferation by IBs involves the activation of the ERK pathway (Figure 2B), used here as a convenient reporter of cell cycle activation and of transduction of external mechanical stimuli [47,63]. Interestingly, IB-mediated stimulation of cell proliferation is based on the activity of filopodia-like sensing probes (Figure 3), in agreement with previous observations on different materials derived from chemical synthesis [25,49,50,64]. The main properties of bacterial IBs determining the proliferative cell response are size, maximal stiffness and zeta potential (Figure 4). Size discrimination was not unexpected, since in generic terms, the size of nanoparticles seems to be a critical effector in biological interfaces [65]. Interestingly, decreasing the IB diameter from 500 to 200 nm had a positive effect on PC12, and at a lesser extent, on HepG2 division rates, while adsorption of PC12 was completely independent on IB size (Figure 1B). Noteworthy, the size of IBs can be easily regulated by both fabrication time and genetic background of producing bacteria, in a range between approximately 50 and 500 nm [40,34].

Finally, the nanoscale exploration of ClpP IBs has revealed that, apart from their abnormal tear-shaped geometry (Figure 4) [38], other parameters of this material exhibits unusual values (Figure 4; Table 2). Interestingly, the use of ClpP IBs as scaffolds for mammalian cell culture results in anomalous cell proliferation responses (Figure 4A), that maximized growth of PC12 and restricted that of 1BR3.G. The selective modulation of cell attachment and proliferation exhibited by ClpP IBs and, in general, by all IB variants, could be of interest in the enrichment of defined cell types from primary cultures and in the fabrication of hybrid tissues, that is now being achieved by using magnetic force-based tissue engineering [66–71].

Being protein materials, IBs exhibit nanoscale properties in ranges matching those of the natural matrices in which cells grow and differentiate, and differ from those offered by other materials used for substrate decoration, such as ceramic nanoparticles or carbon nanotubes, which in addition, eventually show undesired toxic effects. Finally, protocols to produce bacterial-free IBs on a large scale, whilst keeping the mechanical and biological properties of these particles intact are under continuous development [60,61,72,73], further prompting the consideration of bacterial IBs, as other bacterial products [35,36,62], as a new category of biocompatible and promising self-assembling materials for biomedical applications.

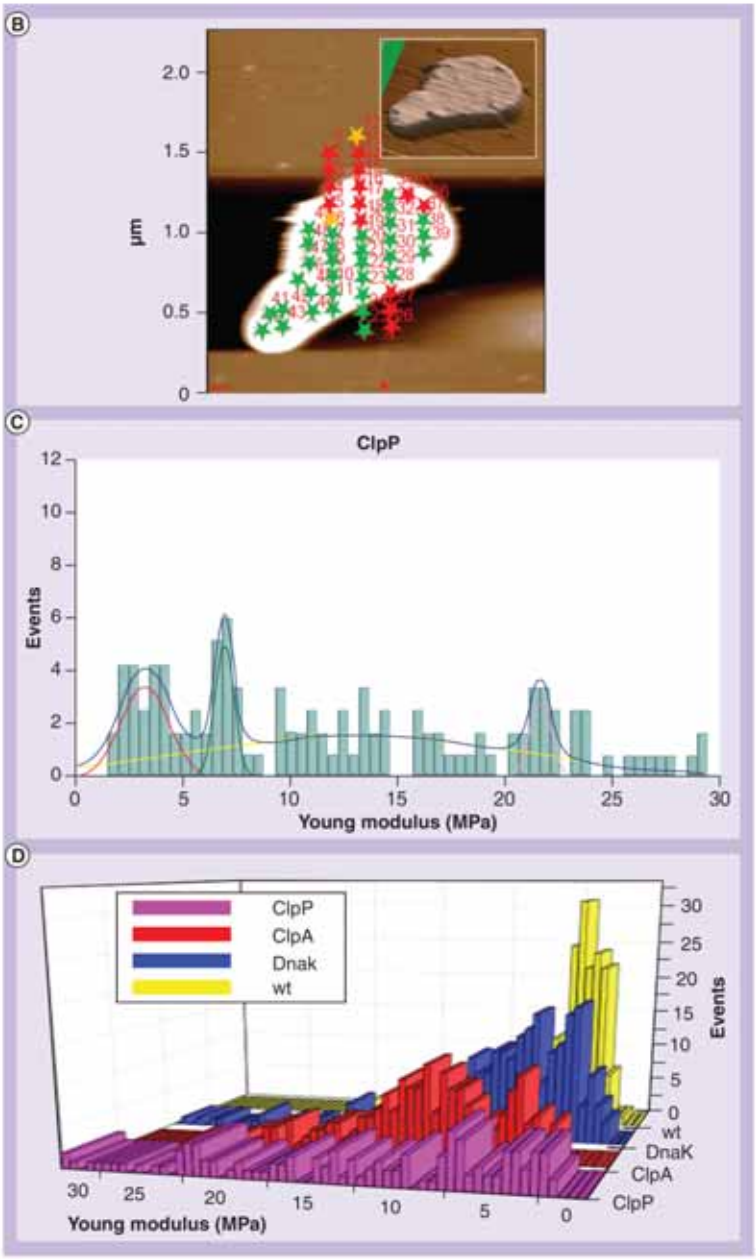

Figure 4 (cont.). (B) Atomic force microscopy image of a ClpP⁻ IB after the indentation procedure. Green crosses represent the force spectroscopical measurements performed on the inclusion body (IB) while the red crosses are ones performed over the clean mica surface. Inset, 3D atomic force microscopy image of a ClpP⁻ IB prior to indentation measurements. **(C)** Histogram representation of the number of events versus Young modulus obtained for IBs produced in ClpP-deficient bacteria, showing four different peaks at 3.33, 7.10 13.45 and 22.07 MPa. **(D)** 3D histogram representation of the number of events versus Young modulus for different IBs produced in bacterial mutants. From softer to stiffer: wt IBs show only one peak at 3.73 MPa; DnaK⁻ IBs show two overlapped Young modulus distributions, which centered at 3.56 and 7.75 MPa; ClpA⁻ IBs show the presence of two different Young modulus distributions, at 5.01 and 10.99 MPa and ClpP⁻ IBs show three different peaks at 3.33, 7.10 and 13.45 MPa.
wt: Wild-type.

doi:10.2217/NNM.11.83

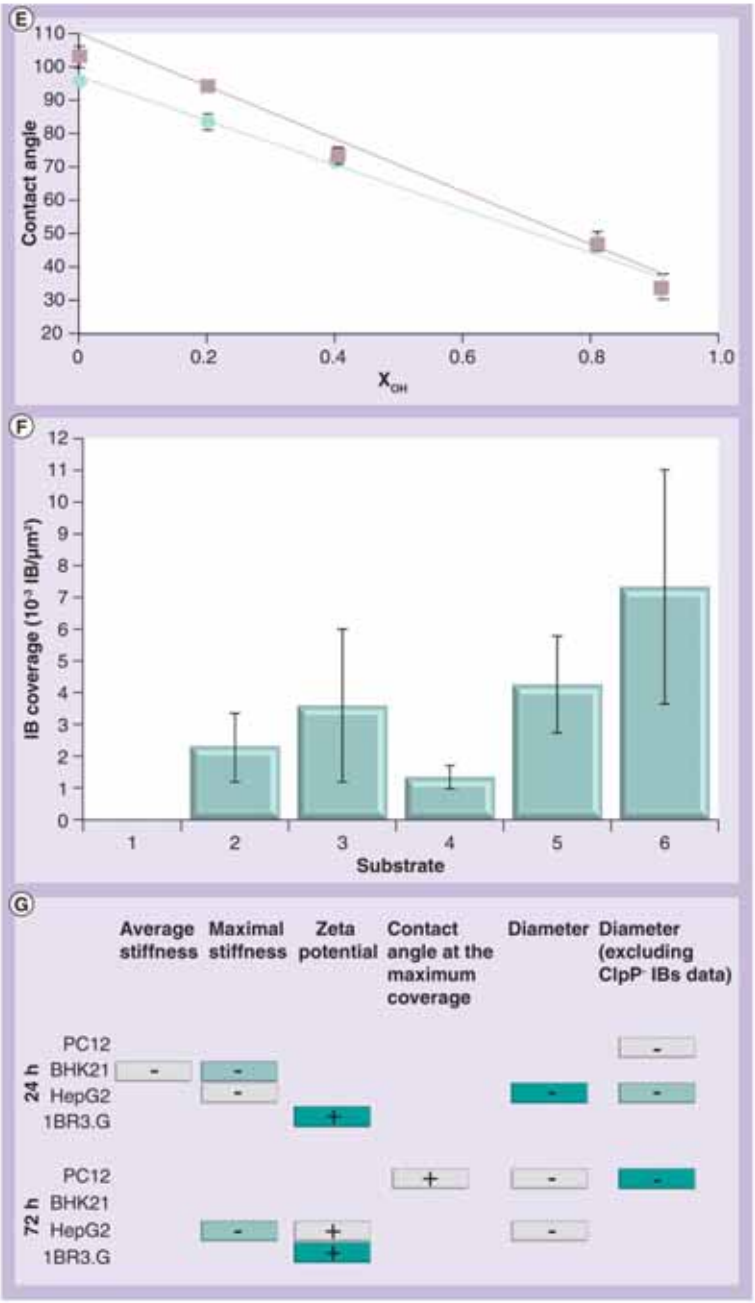

Figure 4 (cont.). (E) Contact angles of the six different functionalized gold surfaces, containing different molar ratio of -OH terminated alkanethiols, gold surfaces before (purple) and after (green) deposition of IBs.
(F) Dependence of the ClpP- IB's coverage on the functionalized gold substrate wettability. Substrate wettability ranging (1) 20–30°, (2) 40–50°, (3) 60–70°, (4) 70–80°, (5) 80–90° and (6) 100–110°. **(G)** Statistical significance (represented in a color intensity scale) of lineal correlations between attachment (t24) or proliferation (t72) data and physicochemical parameters of the IBs used for surface decoration. Because of the aberrant morphology of ClpP- IBs, comparisons were carried out including and excluding ClpP- IBs diameters. Signs within cells indicate the type of influence of the variable parameters on cell adhesion or growth. +: Positive; -: Negative; IB: Inclusion body; XOH: OH terminated alkanethiol.

Conclusion

Randomly deposited bacterial IBs stimulate mammalian cell colonization of flat surfaces by enhancing cell attachment but also through the mechanical stimulation of cell division, being independent but synergistically acting events. The genetic tunability of nanoscale features, exemplified by IBs produced in the absence of protease ClpP, offers an important flexibility for the adaptation of these protein particles to specific conditions in which either adhesion or stimulation of proliferation are especially convenient. The triggering of filopodia-based media sensing and the activation of ERK pathway prove the mechanical nature of the stimuli provided by IBs on mammalian cells. In addition, the bioadhesiveness of IBs firstly identified in this study prompts to further examine this property in the context of the multiple applications of bacterial materials in conventional and innovative medicines.

Future perspective

Biologically produced protein materials have so far been poorly incorporated to nanomedical applications despite their high functional versatility. The characterization of bacterial IBs at the nanoscale and the discovery of their mechanical tunability by genetic approaches, offer a paradigm for further investigation of these and other protein-based materials in biological interfaces. Being biocompatible substrates, with physicochemical features within the mammalian cell sensing range, the potential of IBs in tissue engineering and other biomedical landscapes is expected to provide important insights and novel fields of application.

Acknowledgements

We are indebted to the Cell Culture Unit of the Servei de Cultius Cellulars, Producció d'Anticossos i Citometria (SCAC), and to the Servei de Microscòpia, both at the UAB. The authors thank the Protein Production Platform (CIBER-BBN) for helpful technical assistance and for protein production and purification services (http://bbn.ciber-bbn.es/programas/plataformas/equipamiento). We also appreciate helpful discussions with M Dalby about ERK biology and valuable advice from JM Lizcano and his group. This study has been funded by MICINN (BFU2010-17450, CTQ2006-06333 and CTQ2010-19501), AGAUR (2009SGR-00108 and 2009SGR-00516) and CIBER de Bioingeniería, Biomateriales y Nanomedicina (CIBER-BBN, Spain). CIBER-BBN is an initiative funded by the VI National R&D&i Plan 2008–2011, Iniciativa Ingenio 2010, Consolider Program, CIBER Actions and financed by the Instituto de Salud Carlos III

with assistance from the European Regional Development Fund. Joaquin Seras-Franzoso is recipient of a PIF doctoral fellowship from UAB, and Antonio Villaverde of an ICREA ACADEMIA award.

Financial & competing interests disclosure

A Villaverde, E García-Fruitós, E Vazquez, J Veciana, I Ratera and C Díez-Gil are coinventors of a patent (P200900045) on the use of inclusion bodies as reagents for mammalian cell culture. The authors have no other relevant affiliations or financial involvement with any organization or entity with a financial interest in or financial conflict with the subject matter or materials discussed in the manuscript apart from those disclosed.

No writing assistance was utilized in the production of this manuscript.

Ethical conduct of research

The authors state that they have obtained appropriate institutional review board approval or have followed the principles outlined in the Declaration of Helsinki for all human or animal experimental investigations. In addition, for investigations involving human subjects, informed consent has been obtained from the participants involved.

Executive summary

- Inclusion bodies, used as topographical surface modifiers, differentially stimulate colonization by different cell lines.
- Cell surface colonization mediated by inclusion bodies is based on two independent but synergistic events, namely adhesion and proliferation.
- Different inclusion body nanoscale features, that are relevant to either bioadhesiveness or mechanical stimulation of cell proliferation (especially size and zeta potential), adopt a range of values that depend on the genetic background of the producing bacteria.
- Inclusion bodies are probed by cell filopodia and efficiently activate the ERK mechanotransduction pathway.

References

Papers of special note have been highlighted as:
* of interest
** of considerable interest

1 Marcantonio NA, Boehm CA, Rozic RJ *et al.* The influence of tethered epidermal growth factor on connective tissue progenitor colony formation. *Biomaterials* 30(27), 4629–4638 (2009).

2 Moya ML, Cheng MH, Huang JJ *et al.* The effect of FGF-1 loaded alginate microbeads on neovascularization and adipogenesis in a vascular pedicle model of adipose tissue engineering. *Biomaterials* 31(10), 2816–2826 (2010).

3 Zieris A, Prokoph S, Levental KR *et al.* FGF-2 and VEGF functionalization of starPEG-heparin hydrogels to modulate biomolecular and physical cues of angiogenesis. *Biomaterials* 31(31), 7985–7994 (2010).

4 Doschak MR, Kucharski CM, Wright JE, Zernicke RF, Uludag H. Improved bone delivery of osteoprotegerin by bisphosphonate conjugation in a rat model of osteoarthritis. *Mol. Pharm.* 6(2), 634–640 (2009).

5 Jaklenec A, Hinckfuss A, Bilgen B, Ciombor DM, Aaron R, Mathiowitz E. Sequential release of bioactive IGF-I and TGF-β 1 from PLGA microsphere-based scaffolds. *Biomaterials* 29(10), 1518–1525 (2008).

6 Madduri S, di SP, Papaloizos M, Kalbermatten D, Gander B. Effect of controlled co-delivery of synergistic neurotrophic factors on early nerve regeneration in rats. *Biomaterials* 31(32), 8402–8409 (2010).

7 Bhang SH, Lee TJ, Lim JM *et al.* The effect of the controlled release of nerve growth factor from collagen gel on the efficiency of neural cell culture. *Biomaterials* 30(1), 126–132 (2009).

8 Dodla MC, Bellamkonda RV. Differences between the effect of anisotropic and isotropic laminin and nerve growth factor presenting scaffolds on nerve regeneration across long peripheral nerve gaps. *Biomaterials* 29(1), 33–46 (2008).

9 Wang W, Li B, Yang J *et al.* The restoration of full-thickness cartilage defects with BMSCs and TGF-β 1 loaded PLGA/fibrin gel constructs. *Biomaterials* 31(34), 8964–8973 (2010).

10 Ripamonti U, Klar RM, Renton LF, Ferretti C. Synergistic induction of bone formation by hOP-1, hTGF-β3 and inhibition by zoledronate in macroporous coral-derived hydroxyapatites. *Biomaterials* 31(25), 6400–6410 (2010).

11 Visser R, Arrabal PM, Becerra J, Rinas U, Cifuentes M. The effect of an rhBMP-2 absorbable collagen sponge-targeted system on bone formation *in vivo*. *Biomaterials* 30(11), 2032–2037 (2009).

12 Molnar P, Wang W, Natarajan A, Rumsey JW, Hickman JJ. Photolithographic patterning of C2C12 myotubes using vitronectin as growth substrate in serum-free medium. *Biotechnol. Prog.* 23(1), 265–268 (2007).

13 Petrie TA, Raynor JE, Dumbauld DW *et al.* Multivalent integrin-specific ligands enhance tissue healing and biomaterial integration. Sci. Transl. Med. 2(45), 45ra60 (2010).

14 Zouani OF, Chollet C, Guillotin B, Durrieu MC. Differentiation of pre-osteoblast cells on poly(ethylene terephthalate) grafted with RGD and/or BMPs mimetic peptides. Biomaterials 31(32), 8245–8253 (2010).

15 Hennessy KM, Clem WC, Phipps MC, Sawyer AA, Shaikh FM, Bellis SL. The effect of RGD peptides on osseointegration of hydroxyapatite biomaterials. Biomaterials 29(21), 3075–3083 (2008).

16 Biggs MJ, Richards RG, Dalby MJ. Nanotopographical modification: a regulator of cellular function through focal adhesions. Nanomedicine 6(5), 619–633 (2010).

17 Dalby MJ. Nanostructured surfaces: cell engineering and cell biology. Nanomedicine (Lond.) 4(3), 247–248 (2009).

18 Vagaska B, Bacakova L, Filova E, Balik K. Osteogenic cells on bio-inspired materials for bone tissue engineering. Physiol. Res. 59(3), 309–322 (2010).

19 Zhu B, Zhang Q, Lu Q et al. Nanotopographical guidance of C6 glioma cell alignment and oriented growth. Biomaterials 25(18), 4215–4223 (2004).

20 Walboomers XF, Ginsel LA, Jan sen JA. Early spreading events of fibroblasts on microgrooved substrates. J. Biomed. Mater. Res. 51(3), 529–534 (2000).

21 Walboomers XF, Croes HJ, Ginsel LA, Jansen JA. Growth behavior of fibroblasts on microgrooved polystyrene. Biomaterials 19(20), 1861–1868 (1998).

22 Yoshinari M, Matsuzaka K, Inoue T, Oda Y, Shimono M. Effects of multigrooved surfaces on fibroblast behavior. J. Biomed. Mater. Res. A 65(3), 359–368 (2003).

doi:10.2217/NNM.11.83

23 Kantawong F, Burgess KE, Jayawardena K *et al.* Whole proteome analysis of osteoprogenitor differentiation induced by disordered nanotopography and mediated by ERK signalling. *Biomaterials* 30(27), 4723–4731 (2009).

24 Kantawong F, Burchmore R, Gadegaard N, Oreffo RO, Dalby MJ. Proteomic analysis of human osteoprogenitor response to disordered nanotopography. *J. R. Soc. Interface* 6(40), 1075–1086 (2009).

25 Dalby MJ, Gadegaard N, Tare R *et al.* The control of human mesenchymal cell differentiation using nanoscale symmetry and disorder. *Nat. Mater.* 6(12), 997–1003 (2007).

** **The authors demonstrate the possibility to control stem cell differentiation through the engineering of the substrate nanotopography, and how cells sense and physiologically respond to order and disorder in their environment.**

26 Dalby MJ. Cellular response to low adhesion nanotopographies. *Int. J. Nanomedicine* 2(3), 373–381 (2007).

27 Curtis AS, Dalby M, Gadegaard N. Cell signaling arising from nanotopography: implications for nanomedical devices. *Nanomedicine (Lond.)* 1(1), 67–72 (2006).

28 Keefer EW, Botterman BR, Romero MI, Rossi AF, Gross GW. Carbon nanotube coating improves neuronal recordings. *Nat. Nanotechnol.* 3(7), 434–439 (2008).

* **Substrate coating with nanoparticles is shown to deeply influence electrophysiological neuronal responses, indicating how powerful is the nanotopography of the environment regarding cell behavior.**

29 Samaroo HD, Lu J, Webster TJ. Enhanced endothelial cell density on NiTi surfaces with sub-micron to nanometer roughness. *Int. J. Nanomedicine* 3(1), 75–82 (2008).

30 Ludden MJ, Mulder A, Tampe R, Reinhoudt DN, Huskens J. Molecular printboards as a general platform for protein immobilization: a supramolecular solution to nonspecific adsorption. *Angew. Chem. Int. Ed. Engl.* 46(22), 4104–4107 (2007).

31 Lipski AM, Pino CJ, Haselton FR, Chen IW, Shastri VP. The effect of silica nanoparticle-modified surfaces on cell morphology, cytoskeletal organization and function. *Biomaterials* 29, 3836–3846 (2008).

32 Garcia-Fruitos E, Villaverde A. Friendly production of bacterial inclusion bodies. *Korean J. Chem. Eng.* 27(2), 385–389 (2010).

33 Martinez-Alonso M, Gonzalez-Montalban N, Garcia-Fruitos E, Villaverde A. Learning about protein solubility from bacterial inclusion bodies. *Microb. Cell Fact.* 8(8), 4 (2009).

34 Garcia-Fruitos E, Rodriguez-Carmona E, Diez-Gil C *et al.* Surface cell growth engineering assisted by a novel bacterial nanomaterial. *Adv. Mater.* 21(42), 4249–4253 (2009).

* **The use of bacterial inclusion bodies as nanoparticulate biomaterials in biological interfaces is proposed for the fist time.**

35 Rodriguez-Carmona E , Villaverde A. Nanostructured bacterial materials for innovative medicines. *Trends Microbiol.* 18(9), 423–430 (2010).

36 Villaverde A. Nanotechnology, bionanotechnology and microbial cell factories. *Microb. Cell Fact.* 9, 53 (2010).

37 Diez-Gil C, Krabbenborg S, Garcia-Fruitos E *et al.* The nanoscale properties of bacterial inclusion bodies and their effect on mammalian cell proliferation. *Biomaterials* 31, 5805–5812 (2010).

38 Garcia-Fruitos E, Seras-Franzoso J, Vazquez E, Villaverde A. Tunable geometry of bacterial inclusion bodies as substrate materials for tissue engineering. *Nanotechnology* 21(20), 205101 (2010).

39 Gonzalez-Montalban N, Garcia-Fruitos E, Ventura S, Aris A, Villaverde A. The chaperone DnaK controls the fractioning of functional protein between soluble and insoluble cell fractions in inclusion body-forming cells. *Microb. Cell. Fact.* 5, 26 (2006).

40 Garcia-Fruitos E, Martinez-Alonso M, Gonzalez-Montalban N, Valli M, Mattanovich D, Villaverde A. divergent genetic control of protein solubility and conformational quality in *Escherichia coli*. *J. Mol. Biol.* 374, 195–205 (2007).

41 Sambrook J, Fritsch E, Maniatis T. *Molecular Cloning, A Laboratory Manual*. Cold Spring Harbor Laboratory Press, NY, USA (1989).

42 Thomas JG , Baneyx F. Roles of the *Escherichia coli* small heat shock proteins IbpA and IbpB in thermal stress management: comparison with ClpA, ClpB, and HtpG *in vivo*. *J. Bacteriol.* 180(19), 5165–5172 (1998).

43 Bradford MM. A rapid and sensitive method for the quantitation of microgram quantities of protein utilizing the principle of protein-dye binding. *Anal. Biochem.* 72, 248–254 (1976).

44 Domke J, Radmacher M. Measuring the elastic properties of thin polymer films with the atomic force microscope. *Langmuir* 14(12), 3320–3325 (1998).

45 Parra A, Casero E, Lorenzo E, Pariente F, Vazquez L. Nanomechanical properties of globular proteins: lactate oxidase. *Langmuir* 23(5), 2747–2754 (2007).

46 Martinez-Alonso M, Vera A, Villaverde A. Role of the chaperone DnaK in protein solubility and conformational quality in inclusion body-forming *Escherichia coli* cells. *FEMS Microbiol. Lett.* 273(2), 187–195 (2007).

47 Tsuboi Y, Ichida T, Sugitani S *et al.* Overexpression of extracellular signal-regulated protein kinase and its correlation with proliferation in human hepatocellular carcinoma. *Liver Int.* 24(5), 432–436 (2004).

48 Kiyokawa E, Takai S, Tanaka M *et al.* Overexpression of ERK, an EPH family receptor protein tyrosine kinase, in various human tumors. *Cancer Res.* 54(14), 3645–3650 (1994).

49 Dalby MJ, Gadegaard N, Riehle MO, Wilkinson CD, Curtis AS. Investigating filopodia sensing using arrays of defined nano-pits down to 35 nm diameter in size. *Int. J. Biochem. Cell Biol.* 36(10), 2005–2015 (2004).

50 Dalby MJ, Riehle MO, Johnstone H, Affrossman S, Curtis AS. Investigating the limits of filopodial sensing: a brief report using SEM to image the interaction between 10 nm high nano-topography and fibroblast filopodia. *Cell Biol. Int.* 28(3), 229–236 (2004).

51 Gonzalez-Montalban N, Garcia-Fruitos E, Villaverde A. Recombinant protein solubility-does more mean better? *Nat. Biotechnol.* 25(7), 718–720 (2007).

52 Martinez-Alonso M, Garcia-Fruitos E, Ferrer-Miralles N, Rinas U, Villaverde A. Side effects of chaperone gene co-expression in recombinant protein production. *Microb. Cell. Fact.* 9(1), 64 (2010).

53 Garcia-Fruitos E. Inclusion bodies: a new concept. *Microb. Cell. Fact.* 9(1), 80 (2010).

54 Marston FA. The purification of eukaryotic polypeptides synthesized in *Escherichia coli*. *Biochem. J.* 240(1), 1–12 (1986).

55 Ferrer-Miralles N, Domingo-Espin J, Corchero JL, Vazquez E, Villaverde A. Microbial factories for recombinant pharmaceuticals. *Microb. Cell. Fact.* 8(1), 17 (2009).

56 Speed MA, Wang DI, King J. Specific aggregation of partially folded polypeptide chains: the molecular basis of inclusion body composition. *Nat. Biotechnol.* 14(10), 1283–1287 (1996).

57 Morell M, Bravo R, Espargaro A *et al.* Inclusion bodies: specificity in their aggregation process and amyloid-like structure. *Biochim. Biophys. Acta* 1783(10), 1815–1825 (2008).

58 Carrio M, Gonzalez-Montalban N, Vera A, Villaverde A, Ventura S. Amyloid-like properties of bacterial inclusion bodies. *J. Mol. Biol.* 347(5), 1025–1037 (2005).

59 Ventura S, Villaverde A. Protein quality in bacterial inclusion bodies. *Trends Biotechnol.* 24(4), 179–185 (2006).

60 Peternel S, Komel R. Isolation of biologically active nanomaterial (inclusion bodies) from bacterial cells. *Microb. Cell. Fact.* 9, 66 (2010).

61 Peternel S, Jevsevar S, Bele M, Gaberc-Porekar V, Menart V. New properties of inclusion bodies with implications for biotechnology. *Biotechnol. Appl. Biochem.* 49(Pt 4), 239–246 (2008).

62 Vazquez E , Villaverde A. Engineering building blocks for self-assembling protein nanoparticles. *Microb. Cell. Fact.* 9, 101 (2010).

63 Bastow ER, Lamb KJ, Lewthwaite JC *et al.* Selective activation of the MEK–ERK pathway is regulated by mechanical stimuli in forming joints and promotes pericellular matrix formation. *J. Biol. Chem.* 280(12), 11749–11758 (2005).

64 Biggs MJ, Richards RG, Gadegaard N, Wilkinson CD, Oreffo RO, Dalby MJ. The use of nanoscale topography to modulate the dynamics of adhesion formation in primary osteoblasts and ERK/MAPK signalling in STRO-1+ enriched skeletal stem cells. *Biomaterials* 30(28), 5094–5103 (2009).

65 Jiang W, Kim BY, Rutka JT, Chan WC. Nanoparticle-mediated cellular response is size-dependent. *Nat. Nanotechnol.* 3(3), 145–150 (2008).

* **The relevance of nanoparticle size on the cell physiology is demonstrated during particle/cell interactions.**

66 Corchero JL , Villaverde A. Biomedical applications of distally controlled magnetic nanoparticles. *Trends Biotechnol.* 27(8), 468–476 (2009).

67 Akiyama H, Ito A, Kawabe Y, Kamihira M. Fabrication of complex three-dimensional tissue architectures using a magnetic force-based cell patterning technique. *Biomed. Microdevices* 11(4), 713–721 (2009).

68 Ito A, Akiyama H, Kawabe Y, Kamihira M. Magnetic force-based cell patterning using Arg–Gly–Asp (RGD) peptide-conjugated magnetite cationic liposomes. *J. Biosci. Bioeng.* 104(4), 288–293 (2007).

** **Heterotypic tissue engineering directed by magnetic force is described for the first time, opening a plethora of opportunities to fully-controlled complex tissue construction *in vitro*.**

69 Ito A, Jitsunobu H, Kawabe Y, Kamihira M. Construction of heterotypic cell sheets by magnetic force-based 3-D coculture of HepG2 and NIH3T3 cells. *J. Biosci. Bioeng.* 104(5), 371–378 (2007).

70 Shimizu K, Ito A, Yoshida T, Yamada Y, Ueda M, Honda H. Bone tissue engineering with human mesenchymal stem cell sheets constructed using magnetite nanoparticles and magnetic force. *J. Biomed. Mater. Res B Appl. Biomater.* 82(2), 471–480 (2007).

71 Shimizu K, Ito A, Lee JK *et al.* Construction of multi-layered cardiomyocyte sheets using magnetite nanoparticles and magnetic force. *Biotechnol. Bioeng.* 96(4), 803–809 (2007).

72 Rodriguez-Carmona E, Cano-Garrido O, Seras-Franzoso J, Villaverde A, Garcia-Fruitos E. Isolation of cell-free bacterial inclusion bodies. *Microb. Cell. Fact.* 9(1), 71 (2010).

73 Peternel S, Grdadolnik J, Gaberc-Porekar V, Komel R. Engineering inclusion bodies for non denaturing extraction of functional proteins. *Microb. Cell. Fact.* 7(1), 34 (2008).

doi:10.2217/NNM.11.83

Paper 3

Targeted osteogenesis of mesenchymal stem cells stimulated by nanotopographical decoration of inclusion bodies

Joaquin Seras-Franzoso, P. Monica Tsimbouri, Karl V. Burgess, Ugutz Unzueta, Elena Garcia-Fruitos, Esther Vazquez, Antonio Villaverde and Matthew J. Dalby

Submitted to Biomaterials, 2012

Mesenchymal stem cells (MSCs) have been extensively used in recent tissue engineering applications, due to their capability of self-renewal and differentiation into several cell lineages they represent an important source to obtain considerable amounts of cells, able to differentiate into the damaged tissue cell phenotype for its repair. In this work we have focused in the study on MSC response to poly-ε-caprolactone (PCL)-IB based topographies. We have shown that IBs, being mechanically tunable by the proper choice of the *E. coli* producing strain, can be used to direct MSCs to osteogenic differentiation. Interestingly, we have observed a differential response depending on the type of IB used to fabricate the PCL-IB topography. Thus, VP1GFP IBs produced in $ClpA^-$ *E. coli* strain exhibits a stronger osteogenic stimulation than the others types tested. This fact reinforces the idea of generating IBs with specific mechanical and chemical properties depending on the final application of the biomaterial. Moreover, here we have provided evidence of an increased energy demand by MSCs during their differentiation process to osteoblasts raising metabolomics approach as a good tool to study stem cells activity.

Targeted osteogenesis of mesenchymal stem cells stimulated by nanotopographical decoration of inclusion bodies.

Joaquin Seras-Franzoso[1,2,3], P. Monica Tsimbouri[4], Karl V. Burgess[5], Ugutz Unzueta[1,2,3], Elena Garcia-Fruitos[3,1,2], Esther Vazquez[1,2,3], Antonio Villaverde[1,2,3*] and Matthew J. Dalby[4*]

[1] Institut de Biotecnologia i de Biomedicina, Universitat Autònoma de Barcelona, Bellaterra, 08193 Barcelona, Spain.

[2] Departament de Genètica i de Microbiologia, Universitat Autònoma de Barcelona, Bellaterra, 08193 Barcelona, Spain.

[3] CIBER de Bioingeniería, Biomateriales y Nanomedicina (CIBER-BBN), Spain.

[4] Centre for Cell Engineering, Institute of Molecular, Cell and Systems Biology, College of Medical, Veterinary and Life Sciences, Joseph Black Building, University of Glasgow, Glasgow, G12 8QQ, Scotland, UK.

[5] Glasgow Polyomics Facility, Joseph Black Building, Institute of Biomedical and Life Sciences, University of Glasgow, Glasgow, G12 8QQ, Scotland, UK.

*Corresponding authors:

matthew.dalby@glasgow.ac.uk

antoni.villaverde@uab.cat

Abstract

Bacterial inclusion bodies (IBs) are nanostructured, pseudospherical proteinaceous particles produced in recombinant bacteria resulting from ordered protein aggregation. Being mechanically stable, several physicochemical and biological properties of IBs can be tuned by appropriate selection of the producer strain and of culture conditions. We have previously shown that IBs favour cell adhesion and surface colonization by mammalian cells lines upon decoration on materials surfaces. Here we vary topography, stiffness and wettability using the IBs to decorate polycaprolactone surfaces. We show that these topographies can be used to specifically target osteogenesis from mesenchymal stem cells. Furthermore, we use metabolomics to show that the cells have increased energy demand during this bone-related differentiation.

Introduction.

Cells have been known to respond to topography in terms of adhesion and migration for over 100 years(1, 2). In the 1990's it started to become possible to probe cell interactions at the nanoscale(3) and consequently cell response to all nanoscale-defined features was observed(4). Since then, ability to influence gene expression(5) and even stem cell behaviours has been noted; e.g. mesenchymal and embryonic stem cell differentiation(6-8) and self-renewal(8-10) has been shown with nanotopography.

Much of this work has borrowed on technology derived in microelectronics (e.g. photolithography and electron beam lithography(11, 12)). However, there has been a steady increase in more natural lithographical and patterning approaches to cell guidence(13-17). Another emerging approach is the use of bacterial inclusion bodies (IBs) that are produced in recombinant bacteria via cost-effective procedures and are formed by foreign polypeptides whose overexpression is controlled externally(18). IBs range between around 50 and 1000 nm in diameter, normally they have pseudospherical forms and they are mechanically stable, resisting the harsh physical methods used to break the bacterial cell wall(19). In these particles, amyloid fibrils and properly folded versions of the recombinant protein coexist, which can result in detectable biological activity in the IBs(20). Many nanoscale properties of IBs (eg. size, geometry, stiffness, zeta potential and stickiness) can be tuned by the appropriate selection of the genotype of the producer cell (usually by gene knock-down), and also by

controlling production parameters such as temperature, production time and strength of recombinant gene expression(21). Recently, it has been demonstrated that IBs can be successfully used to generate nanotopographies on polystyrene surfaces able to stimulate cell adhesion and proliferation(22).

In this report, we focus on mesenchymal stem cell (MSC) differentiation on the IB patterned materials. They are self-renewing cells that can form mature cells from bone (osteoblast), cartilage (chondrocyte), fat (adipocyte) and reticular (fibroblast) lineages(23, 24). To survey differentiation we have adopted a metabolomic approach coupled to microscopy to identify adhesion and cytoskeletal changes and quantitative (q)PCR to study phenotypical marker expression at transcriptional level.

Materials and Methods.

Bacterial cell culture and IB production

The *Escherichia coli* strains used in this work for the production of IBs were MC4100 (*araD139* (*argF-lac*) U169 *rpsL150 relA1 flbB5301 deoC1 ptsF25* Rbs^R, Sm^R)(25) as a wild type (wt) strain regarding the protein quality control system and its derivatives JGT4 (*clpA::kan*, Sm^R), JGT19 (*clpP::cat*, Sm^R) and JGT20 (*dnak756 thr::Tn10*, Sm^R, Tc^R)(26). These strains, referred to as MC4100, $ClpA^-$, $ClpP^-$ and $DnaK^-$, were transformed with the pTVP1GFP (Ap^R) which encodes mGFP(27) placed under the control of an IPTG-inducible *trc* promoter.

All bacterial strains were cultured in shaker flasks at 37°C and 250 rpm using LB rich medium supplemented with the corresponding antibiotics, ampicillin (Ap) for plasmid maintenance and streptomycin (Sm) as a strain selection marker. Tetracycline (Tc) was also added in $DnaK^-$ *E. coli* cultures. Bacterial cultures for IB production were started at an optical density at 550nm (OD_{550}) of 0.05 and cultured in the conditions mentioned above till they reach an OD_{550} of 0.5. Then protein expression was induced by the addition of 1 mM IPTG (final concentration) and further incubated for 3 hr under the same conditions.

IB purification

At the desired time, lysozyme and PMSF were added at 1 mg/mL and 0.4 mM respectively, and incubated for 2 hr at 37 °C. After bacterial cell wall digestion, samples

were frozen at -80 °C to disrupt the weakened bacterial cells and release the IBs. Then, IBs were washed in Triton X-100 1% (v/v) for 1 hr at RT and frozen again at -80 °C. An additional washing step was carried out by adding Nonidet P-40 detergent 0.03 % (v/v) and incubating IBs 1 hr at 4°C. Next, samples were treated with DNAse 1 µg/mL in presence of $MgSO_4$ 1mM during 1 hr at 37°C in order to remove contaminant DNA. Finally, bacterial cell growth was tested by plating 100 µL of sample on LB plates and cultured overnight at 37°C. Samples were frozen/thawed till no viable bacteria were observed. All the incubations were done under agitation conditions.

Purified IBs were quantified by Western blot using Quantity One software (Bio-Rad) to analyze band intensity and infer protein concentration from a GFP standard curve.

Surface preparation

Polycaprolactone (PCL) (SIGMA) discs were obtained by melting PCL beads (MW 45000) placed between two glass slides, at 80 °C. Pressure was applied to the upper glass slide till a smooth circular layer (13 mm Ø) was obtained. PCL discs were then sterilised in 70 % ethanol for a minimum of 30 min and washed in 1xPhosphate Buffered Saline (PBS). mGFP IBs from all producing *E. coli* strains were resuspended in PBS and 500 µL of IB suspension at 64 µg/mL was added to 24 well plates where the PCL discs had been previously placed. Plates were incubated overnight at 4°C allowing IB deposition. IB-modified PCL discs were washed with PBS, blocked using a 3 % bovine serum albumin (BSA)/PBS (w/v) solution and washed again in PBS. PCL adhesive controls were obtained by a 30 sec plasma clean treatment of the PCL discs.

Contact angle measurements

Wettability of wild-type (MC4100), $DnaK^-$, $ClpA^-$ and $ClpP^-$ IB-PCL surfaces, as well as planar PCL controls, was determined in an OCA15+ (Dataphysics, Germany) goniometer. Three sets of static contact angles were measured per surface using droplets of ultrapure water (18.2 MΩ·cm) (Millipore). Three replicas of each surface type were measured and significance analysed by t-test.

Mesenchymal stem cell culture

MSCs (Promocell) were routinely maintained in α-MEM supplemented with 10 % fetal bovine serum (FBS) (PAA), 1% (v/v) 200 mM L-glutamine (Gibco), and antibiotics (6.74 U/ml Penicillin-Streptomycin, 0.2 µg/ml Fungizone) (PAA) at 37^{o}C and 5% CO_2 in a humidified incubator. Medium was changed every 3 days. For all the experiments 1x10^{4} cells in passage 2 - 3 were seeded per well on PCL or IB-covered PCL discs.

Immunofluorescence

MSCs cultures growing on IB-PCL and PCL adhesive controls were processed at 24 hr and 96 hr for vinculin immunodetection and 21 days for osteogenic marker detection (osteocalcin (OCN) and osteopontin (OPN)). For staining, they were washed with pre-warmed PBS and fixed in 10 % formaldehyde/PBS (v/v) with 2 % sucrose (w/v), 15 min at 37 °C. Then, cells were permeabilized by the addition of buffer P (10.3 g sucrose, 0.292 g NaCl, 0.06 g $MgCl_2$, 0.476 g HEPES buffer, 0.5 ml Triton-X, in 100 ml PBS, pH 7.2), for 5 min at 4°C. Samples were blocked in 1 % BSA/PBS (w/v) for 5 min at 37 °C and the primary antibody added (in 1 % BSA/PBS (w/v)), 1 hr at 37 °C. Mouse monoclonal antibodies h-vin (vinculin 1:150) (Sigma), anti-OCN (1:50) and anti-OPN (1:50) (Santa Cruz Biotechnology) were used. Also rhodamine-phalloidin, in the case of focal adhesion detection or FITC-phalloidin for OCN and OPN analysis (1:500 in 1 % BSA/PBS (w/v)) (Molecular Probes) were added at this step. After incubation, samples were washed 3 times in 0.5 % Tween 20/PBS (v/v) for 5 min. The secondary biotinylated horse anti-mouse antibody (Vector Laboratories) (1:50 in 1% BSA/PBS (w/v)) was added for 1 hr at 37 °C. Samples were washed 3 times in 0.5 % Tween 20/PBS (v/v) before they were incubated at 4°C for 30 min in Cy3-conjugated streptavidin (Insight Biotechnology, 1:100 in 1 % BSA/PBS (w/v)). The samples were then washed as previously and a drop of Vectashield mountant containing DAPI (Vector labs), for DNA staining of the nucleus, was added. Observation was carried out by fluorescence microscopes Zeiss Axiovert 200 M and Zeiss Axiophot 200 M.

Confocal microscopy

Samples for confocal imaging were processed as described above after 4 days of culture on IB-PCL surfaces. Anti clathrin (Sigma-Aldrich no. C1985) was added as the

primary antibody, diluted 1:50 in 1% BSA/PBS (w/v). These samples were observed in a TCS SP2 confocal laser scanning microscope (Leica Microsystems, Mannheim, Germany) using a Plan-Apochromat 63X 1.4 N.A lens. Up to 20 confocal plans were captured every 0.7 µm along the z-axis in order to perform *in silico* 3D reconstruction. Imaris v 6.3.1 software (Bitplane; Zürich, Switzerland) was then used to process the data and generate the final reconstruction.

Scanning electron microscopy

Purified IBs were resuspended in 1xPBS and deposited on Nucleopore Track-Etch membranes with a pore size of 0.2 µm (Whatman, United Kingdom). Samples were fixed in 2.5 % glutaraldehyde-0.1 M phosphate buffer (v/v) for 2 hr at 4 °C and after appropriate washing dehydrated in an increasing concentration ethanol series (50, 70, 80, 90 and 95 % for 10 min each and twice with 100 % ethanol). After dehydration, CO_2 critical point drying was carried out and samples were mounted on adhesive carbon films. Prior to observation, mounted samples were coated with gold. Samples were examined in a S-570 scanning microscope (Hitachi Ltd., Japan) at an accelerating voltage from 15kV to 20kV.

MSC morphology

MSC morphology analysis was carried out using images from cultures at 24 hr and 96 hr, stained as described above. ImageJ (version 1.34s; Rasband, W.S.,Image J, U.S. National Institutes of Health -http://rsb.info. nih.gov/ij/) was used to select positively stained cells and calculate cell area and cell perimeter. In all the samples a minimum of 50 cells were analyzed. T- test was performed to analyze variances between samples.

RT-qPCR

MSCs cultures at 7 and 14 days of culture on IB-PCL and PCL plasma-cleaned discs were lysed and total RNA was extracted using a Qiagen RNeasy Kit. Samples were treated with DNAse and RNA quantified by nanodrop (Thermo Fisher). Equal amounts of total RNA were then reverse-transcribed using Omniscript RT kit (Qiagen), according to manufacturer´s instructions. Real-time qPCR reaction was performed in order to

determine the expression of the following genes: GapDH, ALCAM, PPARG, SOX9 and OPN (table 1). GapDH was used as constitutive gene, thus the expression of the genes of interest was normalized to GapDH expression value. SYBR green (Applied Biosystems) method was used to measure gene amplification and gene expression was quantified by the comparative analysis of cycle-threshold procedure. Sequences of the primers used in this study were validated by the analysis of the melting curves. Real-time qPCR was performed using the 7500 Real Time PCR system (Applied Biosystems). Gene expression levels were represented as the relative value obtained when comparing IB-PCL samples to PCL plasma cleaned controls. All samples were performed in triplicate and t-test was used to analyze variances between samples.

Metabolomic analysis.

Cell cultures were collected at day 7 and washed in pre warmed 1x PBS. Then, 400 µL of ice-cold extraction solvent (chloroform: methanol: water, 1:3:1) was added and incubated for 1 hr at 4 °C with gentle agitation. Solvent was next transferred to clean sterile eppendorf tubes and centrifuged at 13000G for 5 min at 4°C. After centrifugation supernatants were transferred to new eppendorf tubes and stored at -80 °C till processing by LC-MS. The samples were then used for hydrophilic interaction liquid chromatography-mass spectrometry (UltiMate 3000 RSLC (Thermo Fisher) with a 150 x 4.6 mm ZIC-HILIC column running at 300 µl/min and Orbitrap Exactive (Thermo Fisher) respectively). Total protein content was measured by Nanodrop (Thermo Fisher) and was found identical for all samples, thus no further standardization was required. Raw mass spectrometry data was processed using the standard pipeline, consisting of XCMS(28) (for peak picking), MzMatch(29) (for filtering and grouping) and IDEOM(30) (for further filtering, post-processing and identification). This was followed by core metabolite IDs validation against a panel of unambiguous standards by mass and retention time. Further putative identifications were assigned by mass and predicted retention time(31). Means and standard errors of the mean were generated for all groups of picked peaks. The resulting data was uploaded to Ingenuity pathway analysis software for pathway analysis and Metaboanalyst for heatmap production.

Results.

Inclusion Bodies. A range of IBs were produced using bacterial mutant strains as shown in table 2. The average diameter for the particles used in this study range from 340 nm (wt) to 531nm ($DnaK^-$) being of 435 nm and 459 nm for $ClpA^-$ and $ClpP^-$ variants respectively. A low negatively charged zeta-potential was exhibited by IBs resuspended in PBS indicating a tendency to aggregate with time. Please note that this data is pooled from previous analysis with the same IBs(32, 33).

Surface Topographies. Surfaces were successfully fabricated that were decorated with bacterial IBs (figure 1). Reasonably homogenous IB distribution was observed in the four types of IB-based surfaces despite the appearance of some particle supraggregates; these were more evident when IBs were produced in the wt, MC4100 cells. Measurement of contact angle demonstrated that all surfaces (planar PCL and decorated PCL) were hydrophilic, but that the wt and $ClpP^-$ were most hydrophilic with $ClpA^-$ and $DnaK^-$ strains having similar contact angle to control PCL (figure 2).

Fluorescence & Confocal Microscopy. MSCs on planar control surfaces were well spread with many adhesions and well-organised actin cytoskeleton (figure 3). MSCs on the IB nanotopographies also had large adhesions (apart from wt) and supported more contracted cell morphologies (on wt IBs the cells tended to be more bipolarized, elongate) (figure 3 and supplementary figure 1). An interesting observation was that on $ClpP^-$ the cells appeared to have cleared areas for themselves amongst the topography (arrows in figure 3, also see supplementary figure 2), this was not the case on the other surfaces ($DnaK^-$ showed slight evidence of this).

Confocal comparison of $ClpA^-$ and $ClpP^-$ demonstrates this further (figure 4). On $ClpA^-$ surfaces, the MSCs grew over the IBs (figure 4B) with the proteinacious IB nanoparticles appearing to penetrate the cell membrane with no toxic effect (figure 4A). On $ClpP^-$, however, cells occupied cleared areas (figure 4C-E). There was little evidence of free $ClpP^-$ IBs within the cell cytoplasm suggesting the particles were not internalised (figure 4E). Clathrin staining in the figures supports this as no evidence of strong clathrin tracks, indicative of high levels of endocytosis, were visible for $ClpA^-$ or $ClpP^-$ (figure 4).

QPCR Differentiation Analysis. At transcript level, OPN (bone), SRY (sex determining region Y)-box 9 (SOX9, cartilage), peroxisome proliferator-activated receptor gamma (PPARG) and activated leukocyte cell adhesion molecule (ALCAM, progenitor phenotype) were studied to identify differentiation (or lack of) of the MSCs on the IB nanotopographies.

At day 7 all the test nanotopographies prompted an initial increase in OPN mRNA expression; only ClpA$^-$ supported prolonged expression to 14 days of culture (figure 5A). No significant up-regulations in SOX9 or PPARG transcripts were noted at either time point (figure 5B&C). Finally, For ALCAM no increase in expression was noted suggesting the MSCs on all materials were losing stem cell phenotype at similar rate to MSCs on the control surfaces. The osteospecific differentiations were confirmed by immunofluorescence of OPN and OCN at 21 days of culture (supplementary figure 3).

Metabolite Analysis. Building heatmaps of differentially regulated metabolites (red = up-regulated, green = down-regulated, black = no change to planar control) demonstrates large changes in expression (figure 6). ClpP$^-$ was revealed as most similar to control with a number of down-regulations, but few up-regulations. Wt (MC4100), DnaK$^-$ and ClpA$^-$ showed similar profiles and whilst there were a small number of down regulations, the trend was very much up-regulation.

Studying individual metabolic pathways (please note that we don't provide statistics as the groupings are made from different metabolites with highly varying expression and unless otherwise stated statistics are quoted for the most osteogenic, ClpA$^-$ compared to control), some large changes were noted. Trends for carbohydrate (significantly changed $p<0.05$ are D-sorbitol, 2-hydroxy-3-oxoadipate and D-erythrose important in fructose / mannose metabolism and glyoxylate / dicarboxylate metabolism), nucleotide (almost all metabolites detected as significantly up-regulated (10 of 16) are involved in purine and pyrimidine metabolism) were significantly up-regulated and this group is significant as a whole to $p<0.05$ for all IB nanotopographies), lipid (1 of 3 significantly up-regulated, CDP-ethanolamine involved in glycerophospholipid metabolism) and fatty acid biosynthesis (7 of 19 significantly up-regulated) reflect the general heatmap changes with large up-regulations for wt, DnaK$^-$ and ClpA$^-$ and slightly lower up-regulations for ClpP$^-$ (figure 7).

Some key pathways, however, e.g. amino acyl t-RNA biosynthesis and amino acid metabolism were unchanged overall compared to control (figure 8). However, probing amino acid metabolism further for the most osteogenic material, ClpA$^-$, it was seen that within these key metabolic pathways, some amino acids were up-regulated and others down-regulated producing the overall neutral result. Figure 8 shows a KEGG (Kyoto Encyclopedia of Genes and Genomes) map for amino-acyl tRNA biosynthesis of the amino acids and noted on it are up-regulations in glutamine, serine, valine, leucine, proline, phenylalanine and tyrosine and down-regulations in asparganine, glycine, methionine, arginine, histidine and tryprophan tRNA complexing for protein synthesis. Note that the KEGG map for arginine and proline is shown in supplementary figure 4 to further exemplify how breakdown of 'unchanged' metabolic pathways can reveal large changes.

Discussion.

Our data shows that IB nanotopographies have large effect on MSC spreading, metabolism and differentiation. The MSCs on the nanotopographies tend to form large adhesions and have contractile morphologies. They also tend to specifically target osteogenesis; this was most notable for ClpA$^-$ IBs. These results are in agreement with current theory that large adhesions(34-36) and high levels of intracellular tension mediated by myosin/actin contraction(37, 38) are required for osteogenic differentiation.

Metabolite analysis may prove to be particularly powerful for stem cell experiments as they have a low basal metabolism. In their niche, stem cells are metabolomically quiet with stocks of unsaturated metabolites and this may be speculated to allow for self-renewal and growth without differentiation and provide metabolite chemical plasticity (in terms of redox) in response to regenerative cues(9, 39, 40).

That stem cells activate their metabolism in response to differentiation allows us another way to view their activity. Here, on the IB nanotopographies, a general trend of metabolic up-regulation was noted, especially on the most osteogenic, ClpA$^-$, surface. Responses in carbohydrate and fatty acid (energy), nucleotide (DNA/RNA synthesis, cell signalling, energy storage in respiration e.g. ATP) and lipid metabolism (energy, cell structure) suggest increased energy demand on the MSCs as they activate to become

osteoblasts. The differential amino-acid-related regulations may be due to the different proteins used by different lineages. That individual amino acid tRNA pathways were altered, but overall there was no change from control demonstrates that there can be need to dissect 'omics' pathways with appropriate analysis, e.g. Pathos, before simply considering there to be no changes.

It has previously been shown that IB nanotopographies can increase adhesion and growth of a range of fastidious mammalian cells(33, 41) mediated by ERK signalling(22) (as has been noted on other nanotopographies(36, 42)). In this report we demonstrate that MSC differentiation can be targeted to bone formation and that this happens through metabolomic signalling events with osteogenesis producing a high-metabolic demand on the MSCs and hence driving energy-related pathways.

It is interesting to note from this new study that some IBs work better as functional topographies for osteogenesis than others. ClpA$^-$ IB surfaces performed best in terms of osteogenesis and this is sensible in terms of the IBs' high elastic modulus, bimodal 5.01/10.99 MPa compared to wt 3.73 MPa (stiffness has been demonstrated to be key to osteogenesis(43)). However, the ClpA$^-$ contact angle was one of the highest (i.e. most hydrophobic) with no difference from planar PCL. Theoretically, it could be postulated that ClpP$^-$ IBs should have been the most osteogenic as they can achieve the highest stiffnesses (up to ~ 13.5 MPa) and they have the lowest contact angle (~ 27^o, significantly lower than planar PCL). However, the IBs did not appear firmly fixed to the surface. As the ClpP$^-$ particles were not seen to be internalised and were not bunched around the cells (as if they had been pushed together) we assume they were removed into suspension in the cell media. It can thus be speculated that their bioactivity was limited due to the number of particles left in contact with the cells (i.e. number of particles available to influence the cells) stressing the importance not only of the features of the particles *per se*, but also their ability to effectively coat the surface of the biomaterial. In this case, the difference in hydrophilicity between ClpP$^-$ IBs topographies and PCL controls is postulated to prevent the formation of stable IB-surface interactions.

Conclusions.

We have shown that IBs can work as functional nanotopographies supporting MSC growth and differentiation. Furthermore, we have used the surfaces to illustrate that

osteogenesis places high-energy demand on the cells compared to the assumed default fibrogenesis on the planar controls. This adds to the evidence that osteogenesis is a highly active process requiring adhesion, high levels of cytoskeletal contraction and raised signalling in pathways such as ERK. The study further delineates metabolomics as a good way of dissecting MSC behaviour on biomaterials.

Acknowledgements.

We thank BBSRC grant BB/G008868/1 and MICINN BFU2010-17450 grant for funding the biological elements of this work, and also the support from CIBER de Bioingeniería, Biomateriales y Nanomedicina, Spain. We also thank Carol-Anne Smith for technical support at the University of Glasgow and Servei de Microscòpia (UAB) and Protein Production Platform (CIBER-BBN - UAB) for helpful technical assistance at the Universitat Autònoma de Barcelona We thank European Molecular Biology Organization for awarding JSF with a short term fellowship to carry out this project ASTF 359.00-2011. JSF it is also recipient of a PIF doctoral fellowship from UAB EGF is supported by the Programa Personal de Técnico de Apoyo (Modalidad Infraestructuras científico-tecnológicas, MICINN). AV has been distinguished with an ICREA Academia award.

Figure Legends.

Figure 1. On top, fluorescence micrographs of IB-based topographies used in this study. IB coverage is highly homogenous despite the appearance of some particle clusters. superaggregation is clearer in wt IB type. Below, SEM images of isolated IB illustrating their morphology and fine structure (note the IBs are not on planar PCL, but on a support membrane used just for morphology SEM). $ClpP^-$ IBs show a significantly different "tear-shape" morphology compared to the other more spherical IB types. $ClpA^-$ $ClpP^-$, $DnaK^-$, and wt correspond to the IB variant used to generate each surface.

Figure 2. Contact angle measurements for planar PCL and IB decorated surfaces. All samples were hydrophilic, with $ClpP^-$ and wt having the lowest contact angles. N=3, *=$p<0.05$ by t-test.

Figure 3. Focal adhesion staining. Control cells were well spread with numerous focal adhesions. On $ClpA^-$, $ClpP^-$ and $DnaK^-$ IBs cells had large focal adhesions and contractile morphologies. Cultured on wt IBs, MSCs adopted bipolarised, fibroblastic morphologies with smaller adhesions. It was noteworthy that MSCs on $ClpP^-$ were situated within 'cleared' areas.

Figure 4. Cytoskeletal confocal microscopy showing differences between MSCs on $ClpA^-$ and $ClpP^-$. On $ClpA^-$, the MSCs grew on top of the IBs (A&B) and it could be seen that the IBs appeared to be able to be transmembranous (A), appearing fixed to the surface but inside the plasma membrane. On ClpP, however, cells occupied clear areas with little evidence of particle internalisation (C-E). Red = clathrin, green = IBs, blue = nucleus.

Figure 5. QPCR data for MSC differentiation. (A) OPN (osteogenesis), all the nanotopographies induced OPN expression at day 7, but only $ClpA^-$ maintained expression to day 14. There were no significant changes in SOX9 and PPARG suggesting no adipose or chondrogenic differentiation (B&C). For ALCAM there was no change to control, suggesting that the cells were differentiating at a similar rate to those on control (likely progression to fibroblasts). It was notable that wt had reduced ALCAM expression at day 7, tied into the morphological observations in figure 2, this could

suggest rapid fibrogenesis as no other differentiation markers were flagged. Results = mean±SD, n=3, *=p<0.05, **=p<0.01 by ANOVA. Red = actin, green = IBs, blue = nucleus.

Figure 6. Heatmap of metabolomic data (red = up-regulation, green = down-regulation). MSCs on $ClpP^-$ showed mainly down-regulation compared to cells on control whereas cells on $ClpA^-$, $DnaK^-$ and wt showed mainly up-regulation. This upwards trend was most prominent on $ClpA^-$.

Figure 7. Metabolomic groupings for amino acyl tRNA biosynthesis, amino acid, carbohydrate, nucleotide, lipid and fatty acid metabolisms. Largest changes in all nanotopographies compared to control were in carbohydrate and nucleotide biosynthesis related to cell energy. Results = mean, n=3.

Figure 8. Amino acyl tRNA KEGG pathway for $ClpA^-$ with regulations illustrated through PATHOS bioinformatic software (Blue = up-regulation, yellow = no change and red = down-regulation compared to MSCs on planar control). Within this metabolic pathway, shown overall as similar to control, it can be seen that there was a complex balance of up and down-regulations for different amino acids.

Table 1. qPCR primer details for SYBR green analysis.

Table 2. Description of IBs used in this study. Through use of mutants, control of size, stiffness, shape and zeta potential can be controlled(22, 33).

Figure 1

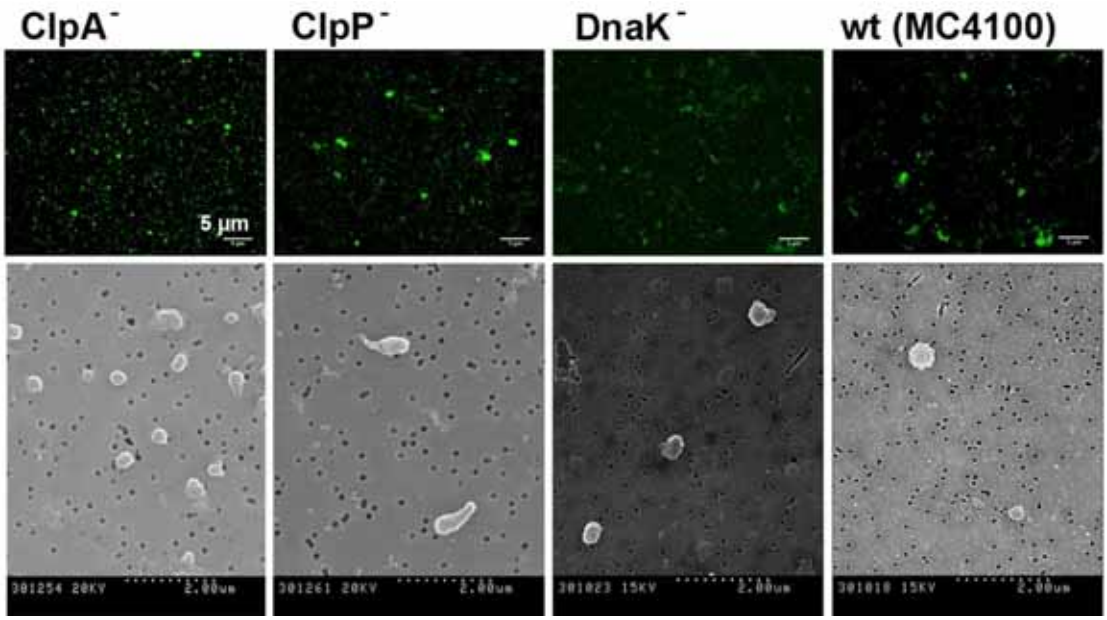

Figure 2

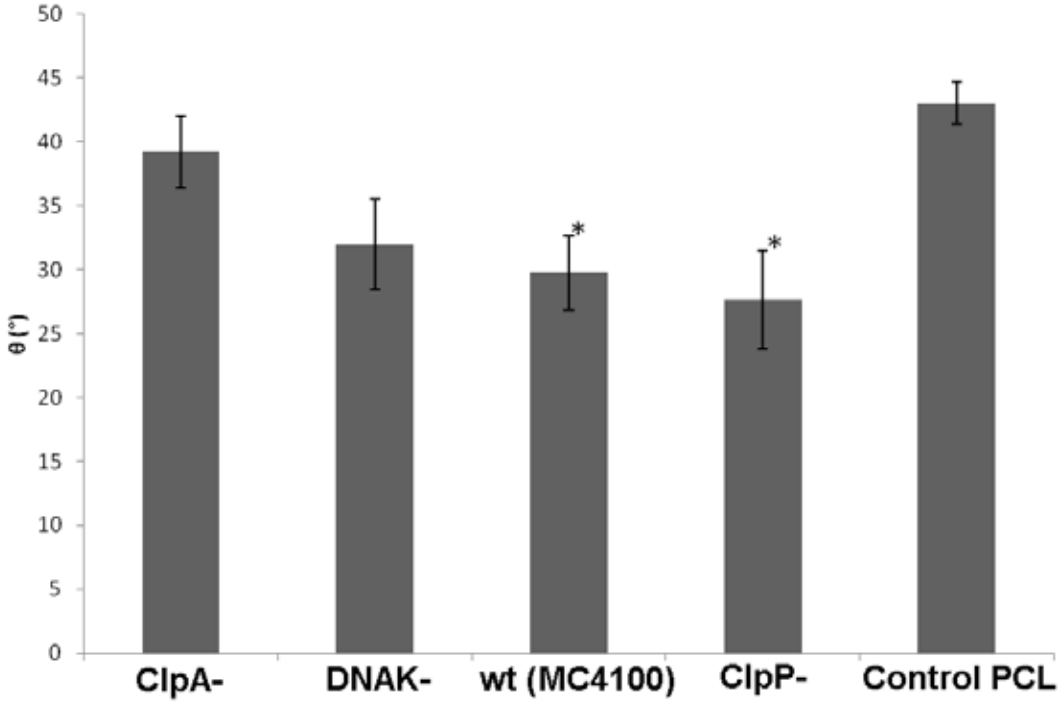

Figure 3

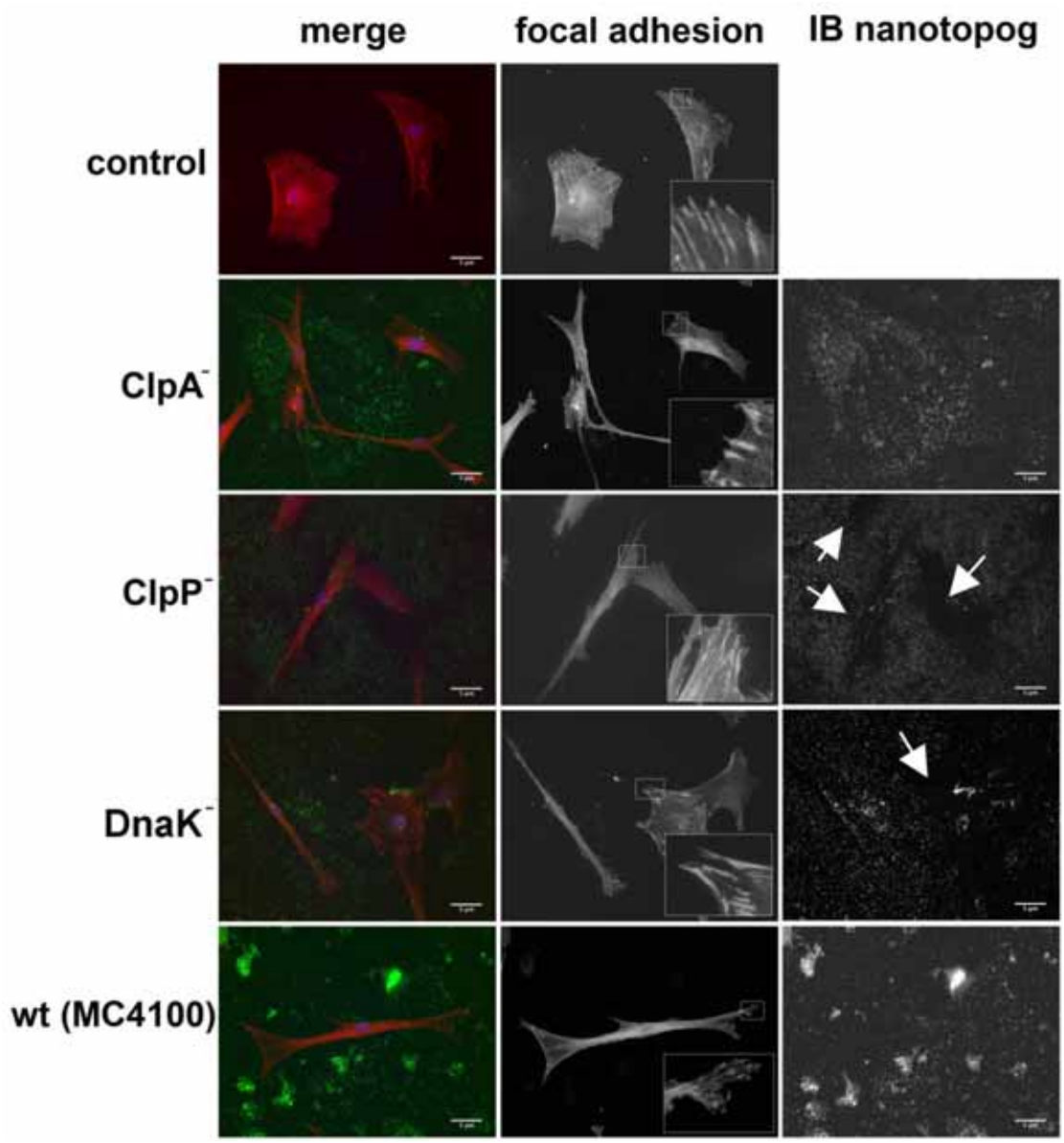
merge
focal adhesion
IB nanotopog
control
ClpA-
ClpP-
DnaK-
wt (MC4100)

Figure 4

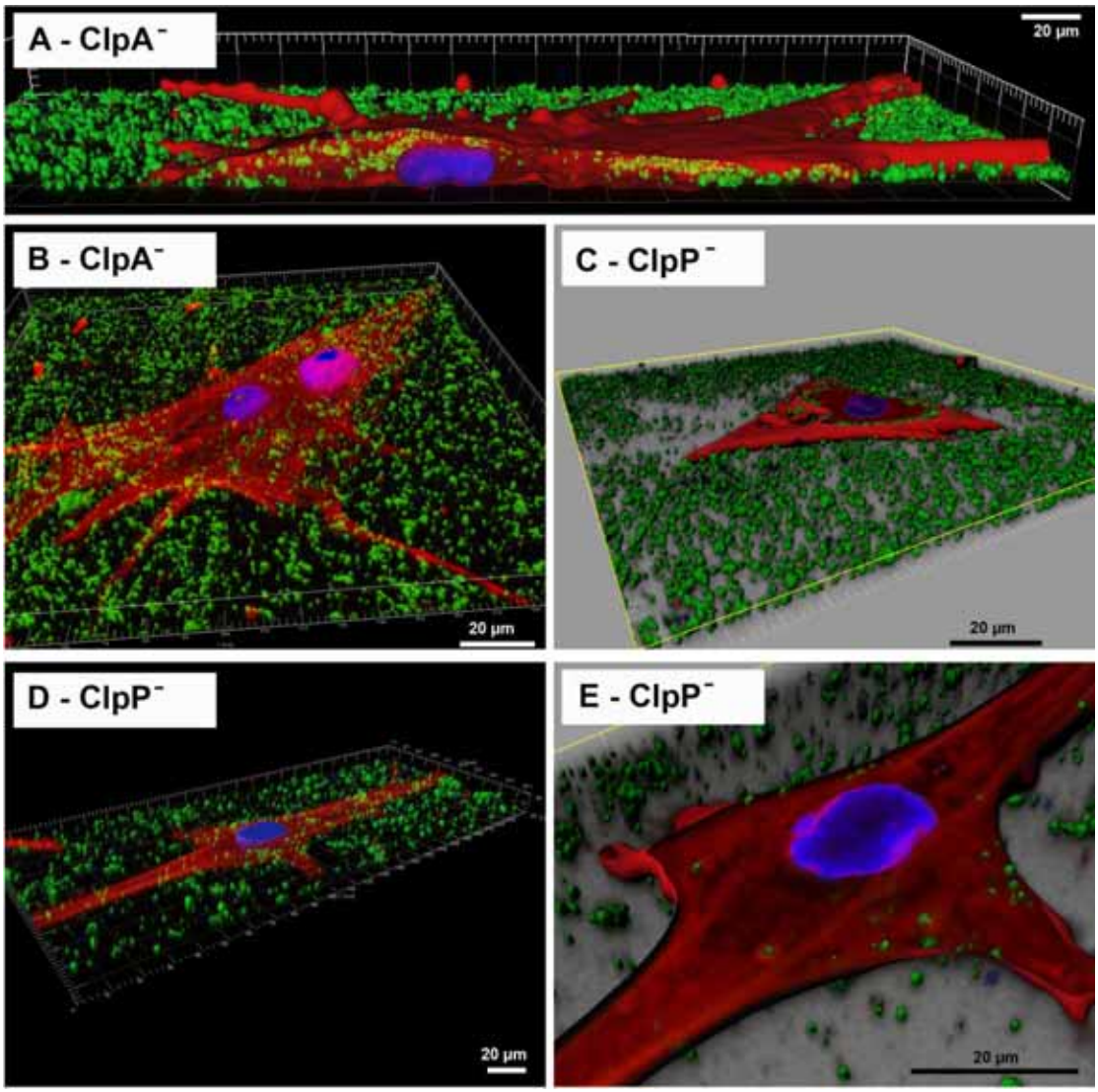

Figure 5

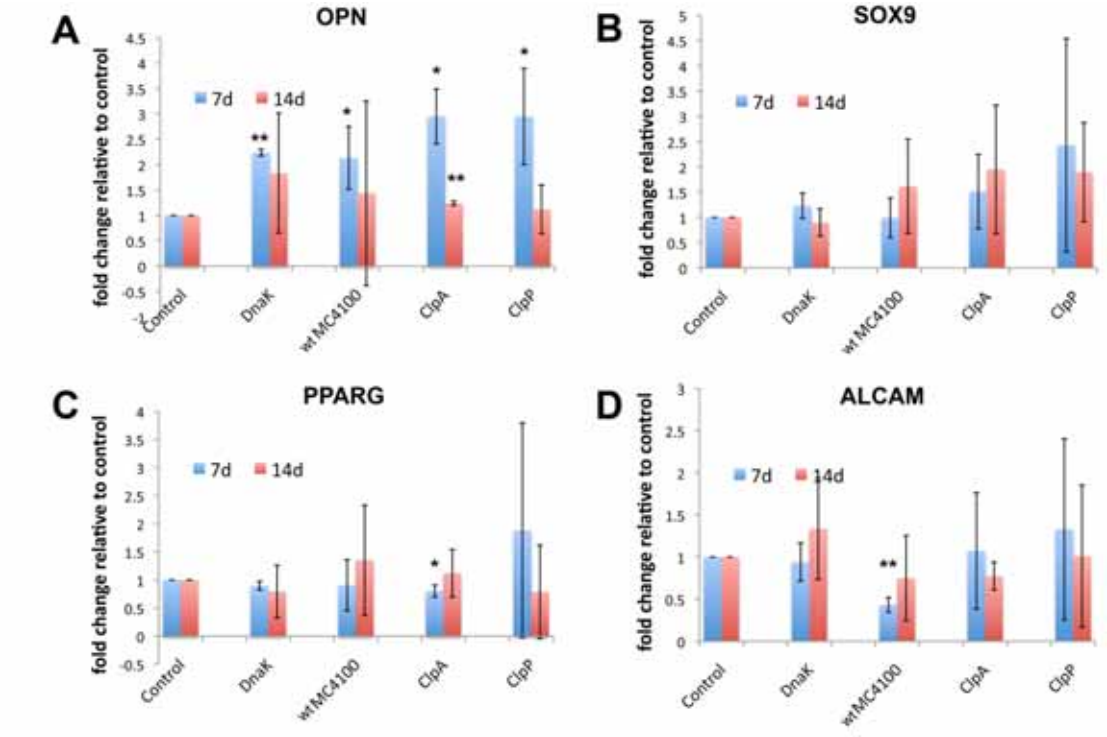

Figure 6

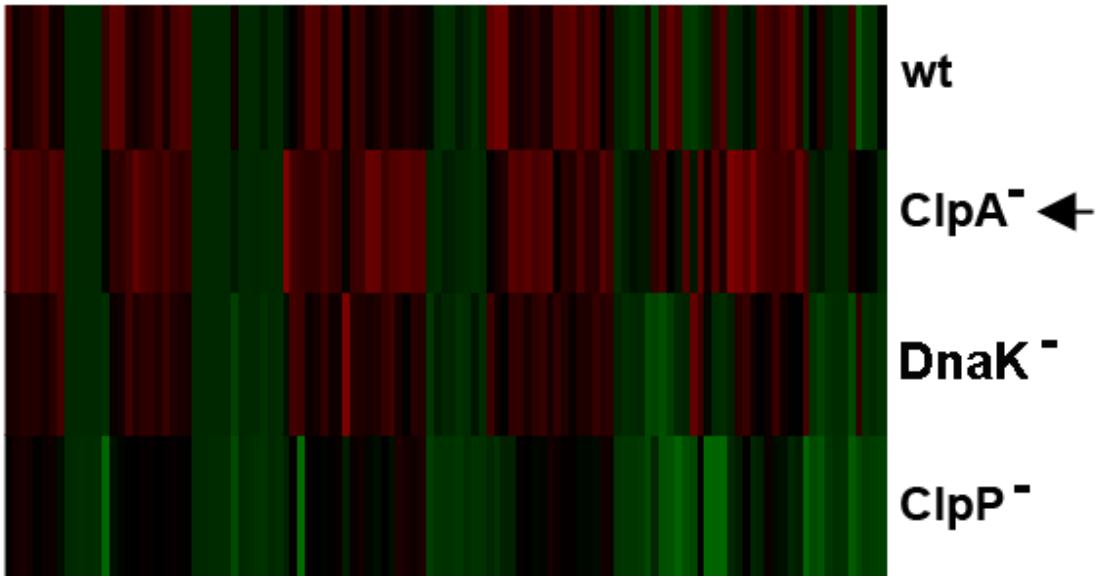

Figure 7

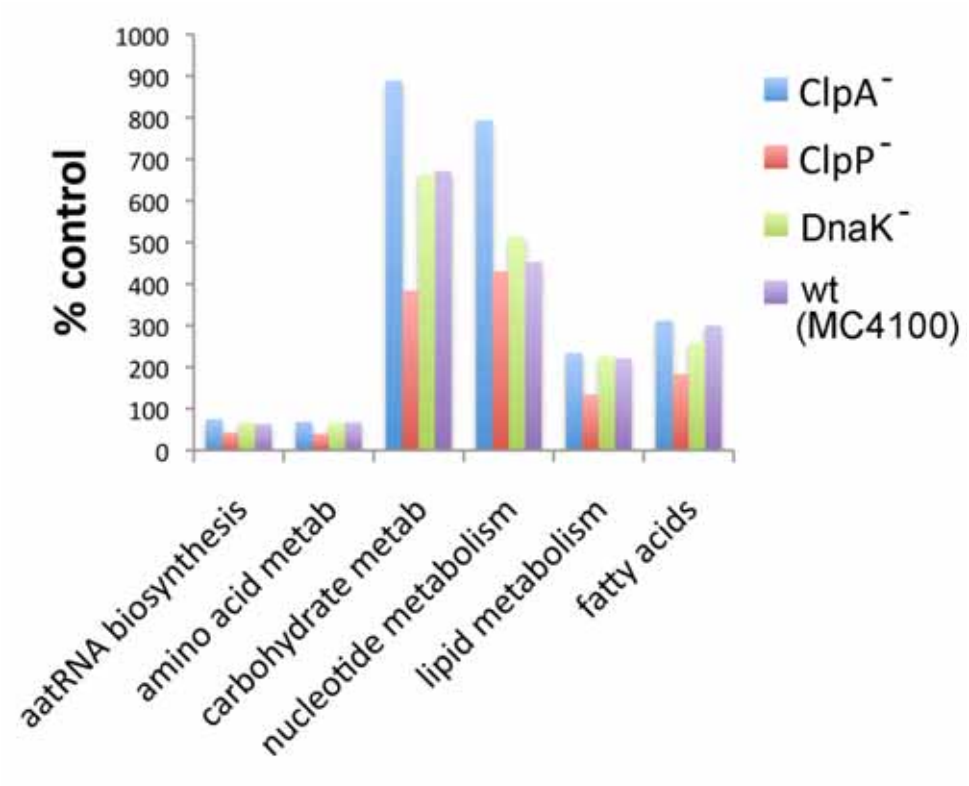
% control
1000
900
800
700
600
500
400
300
200
100
0
ClpA⁻
ClpP⁻
DnaK⁻
wt (MC4100)
aatRNA biosynthesis
amino acid metab
carbohydrate metab
nucleotide metabolism
lipid metabolism
fatty acids

Figure 8

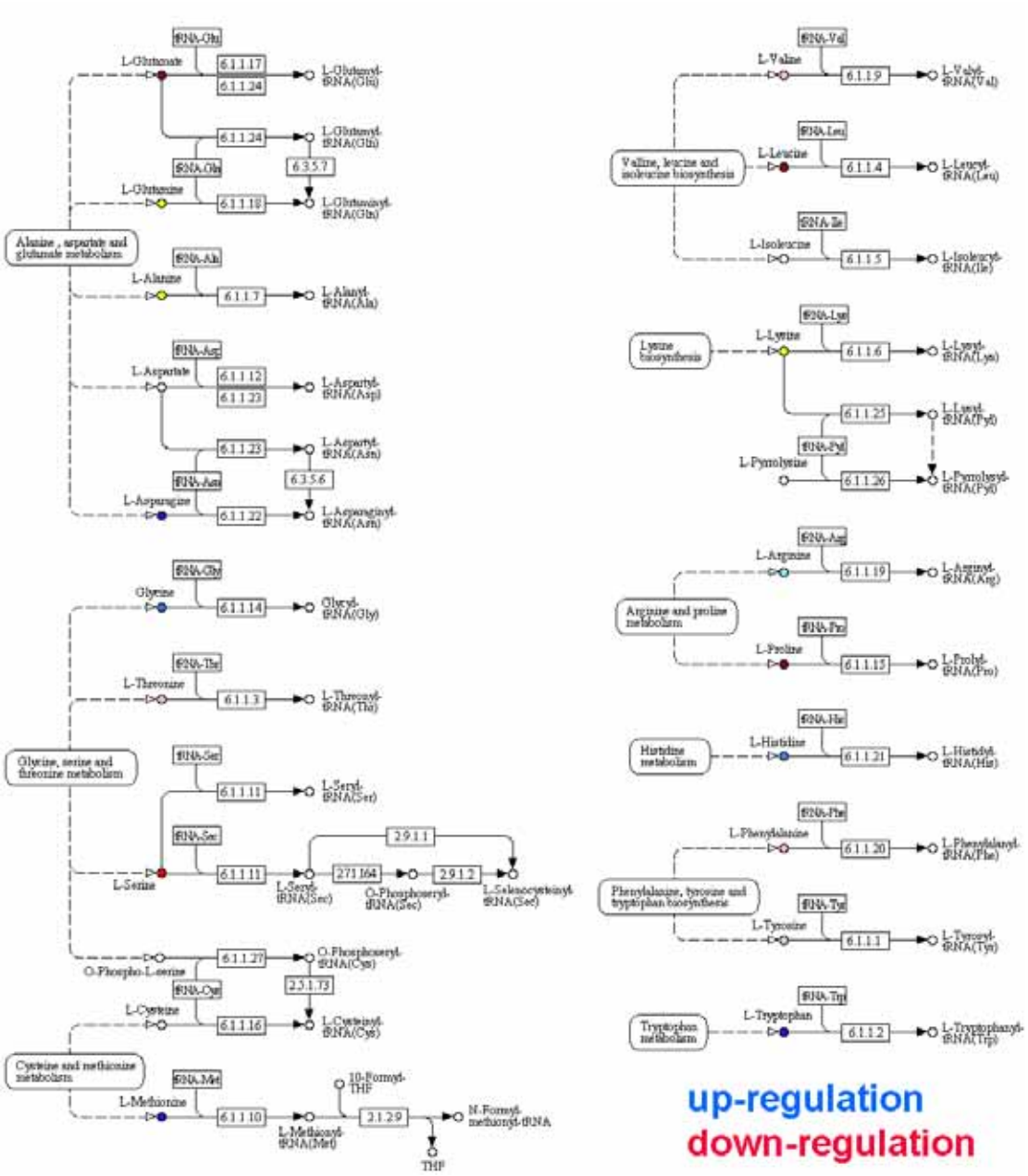
Alanine, aspartate and glutamate metabolism
Glycine, serine and threonine metabolism
Cysteine and methionine metabolism
Valine, leucine and isoleucine biosynthesis
Lysine biosynthesis
Arginine and proline metabolism
Histidine metabolism
Phenylalanine, tyrosine and tryptophan biosynthesis
Tryptophan metabolism
up-regulation
down-regulation

Table 1

Gene	Forward Primer	Reverse Primer
ALCAM	ACGATGAGGCAGACGAGATAAGT	CAGCAAGGAGGAGACCAACAAC
SOX9	AGACAGCCCCCTATCGACTT	CGGCAGGTACTGGTCAAACT
PPARG	TGTGAAGCCCATTGAAGACA	CTGCAGTAGCTGCACGTGTT
OPN	AGCTGGATGACCAGAGTGCT	TGAAATTCATGGCTGTGGAA
GapDH	GTCAGTGGTGGACCTGACCT	ACCTGGTGCTCAGTGTAGCC

Table 2

IB relevant properties regarding the genetic background of the fabricating strain				
Phenotype	Diameter (nm)	Stiffness populations (MPa)	Morphology	Z-potential (mV)
Wild-type	342	3.73	Spherical	-16.7
DnaK^{-}	531	3.56 / 7.75	Spherical	-18.2
ClpA^{-}	435	5.01 /10.99	Spherical	-17.8
ClpP^{-}	459	3.33 /7.10/13.45	Tear-Shaped	-26.5

Supplementary Data

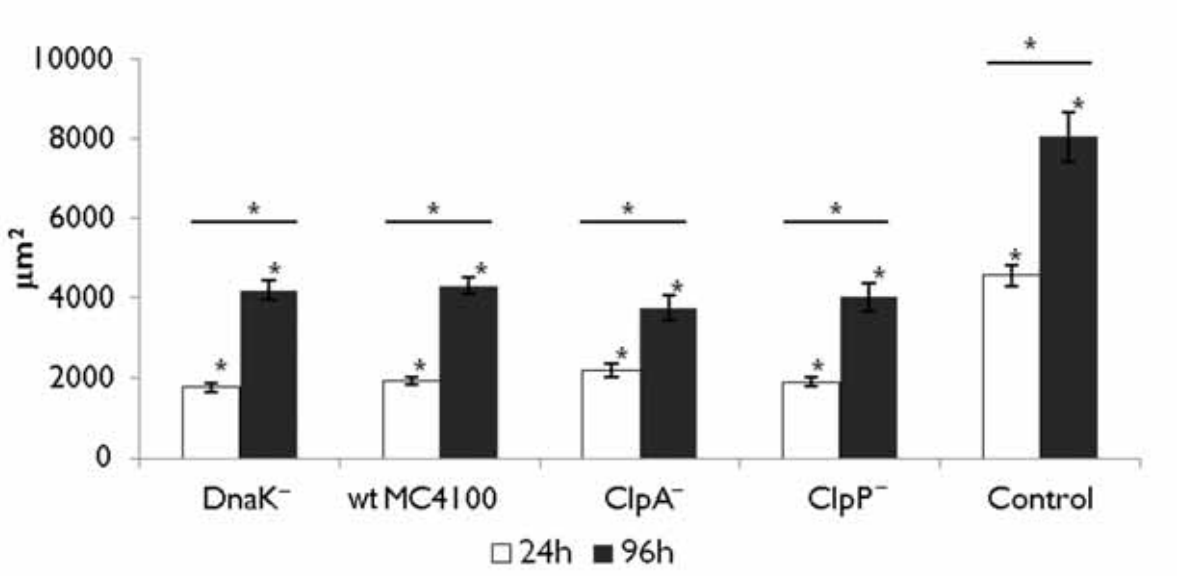

Supplementary figure 1. MSC areas measured in ImageJ showing that cells on the nanotopographies tended to be smaller than on planar control.

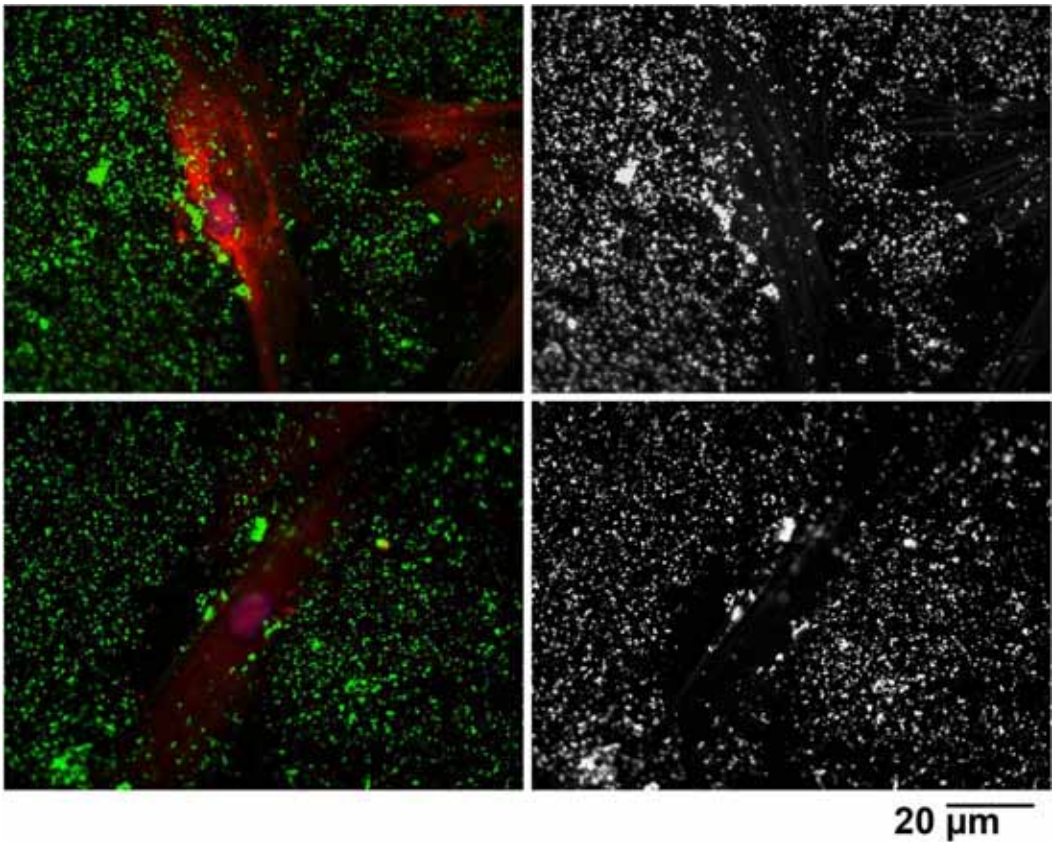

Supplementary figure 2. Further illustration of cells clearing areas on the ClpP$^-$ surfaces. (Red – Osteocalcin, green – ClpP$^-$ and actin, blue = nucleus).

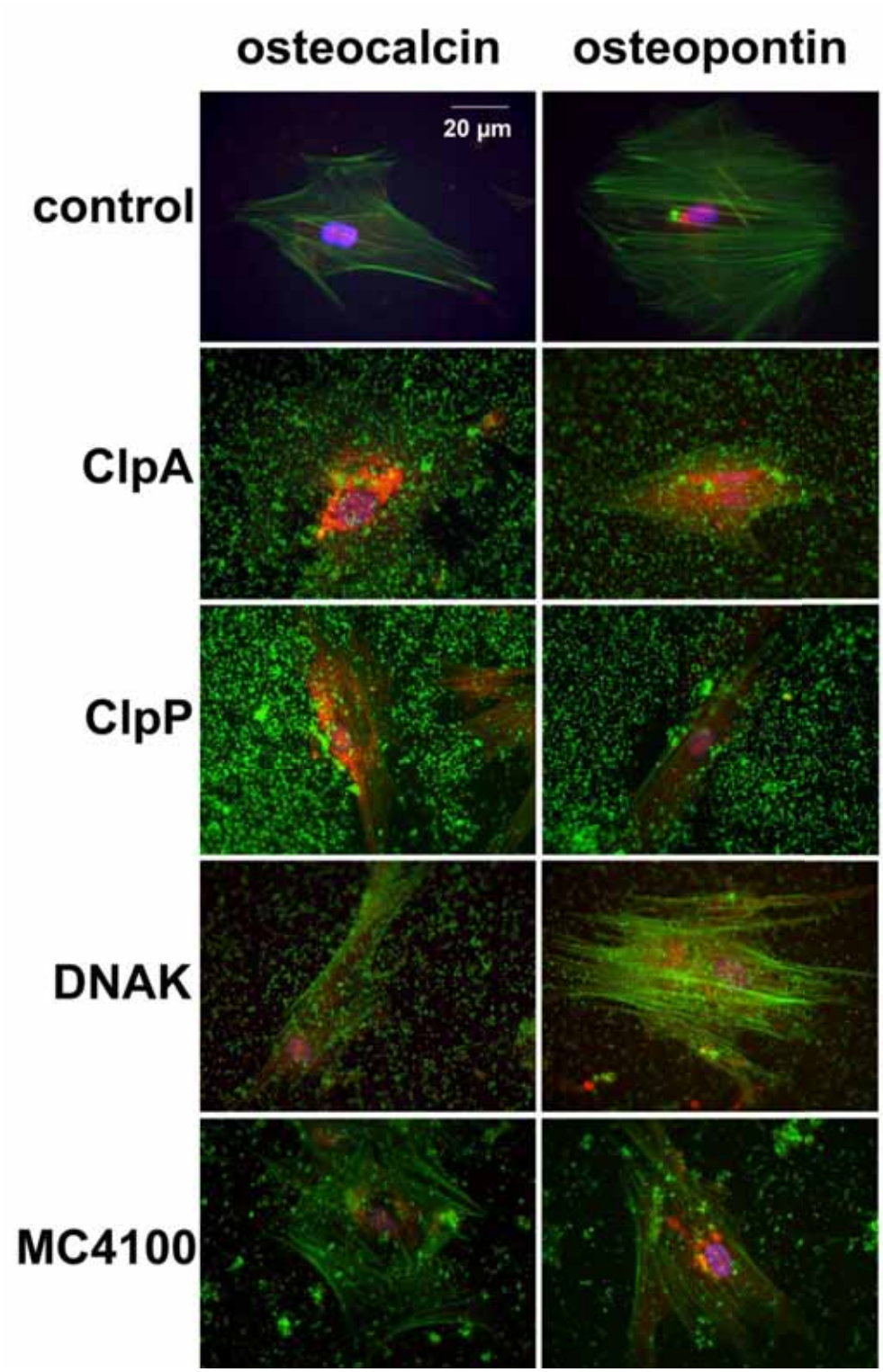

Supplementary figure 3. Osteocalcin and osteopontin staining after 21 days of culture. Cells on planar control, DnaK$^-$, ClpP$^-$ and MC4100 (wt) had little expression of the osteoblast markers. However, MSCs on ClpA$^-$ formed multicell aggregates and expressed intense foci of the marker proteins. (Red – clathrin, green – ClpP$^-$ and actin, blue = nucleus).

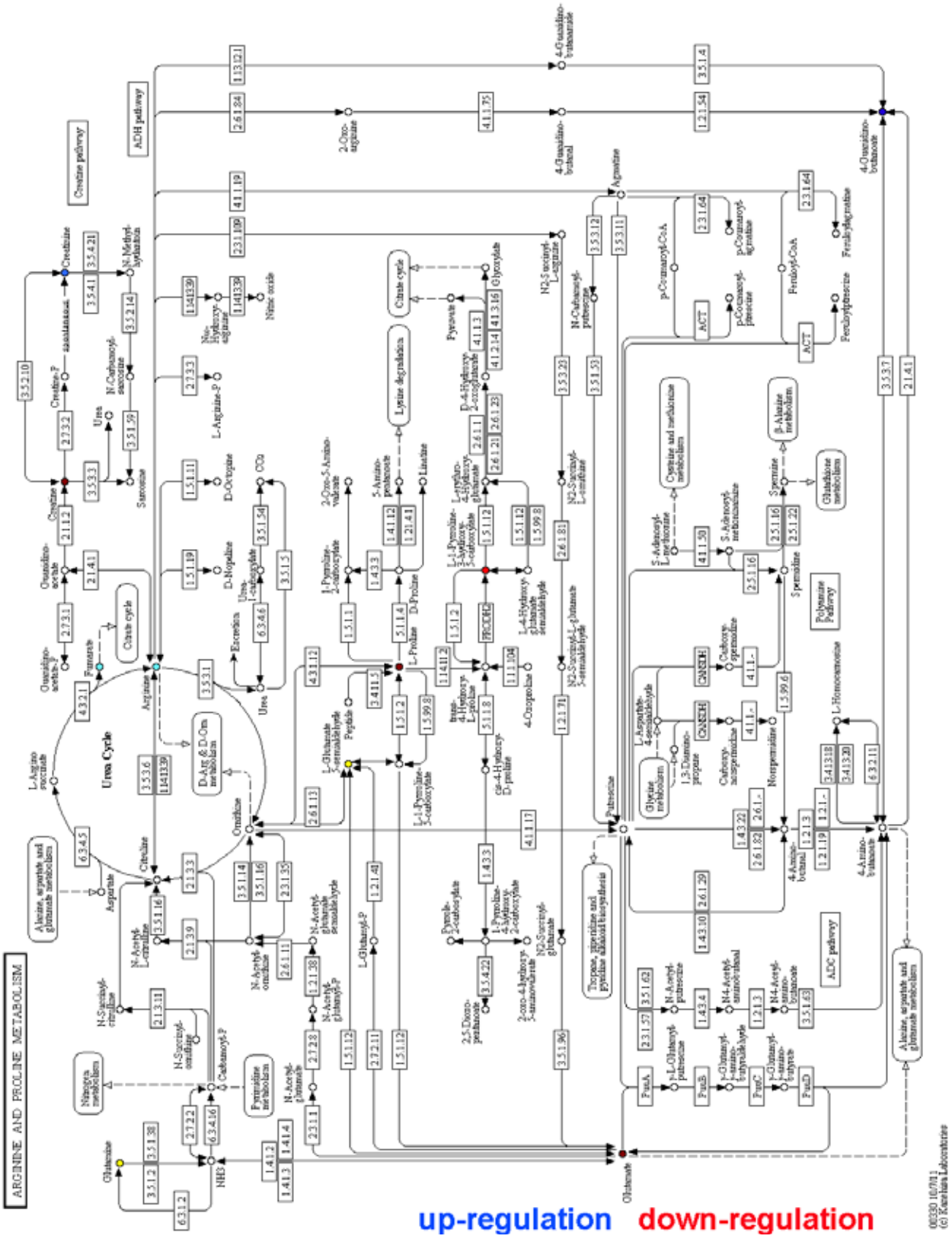

Supplementary figure 4. KEGG pathways with up-and down-regulations noted (using Pathos) for argenine and proline metabolism for MSCs cultured on ClpA^{-} vs control. Blue = up-regulation, yellow = no change, red = down-regulation.

Supplementary table 1. Quantitative metabolite data.

Name	Map	Pathway	ClpA⁻	ClpP⁻	DnaK⁻	Wt MC4100
		Alanine and aspartate metabolism__Cysteine metabolism__Taurine and hypotaurine metabolism__Selenoamino acid metabolism__D-Alanine				
	Amino Acid	metabolism__Carbon fixation__Reductive				
L-Alanine	Metabolism	carboxylate cycle (CO2 fixation)	0.3	0.1	0.2	0.2
		Alanine and aspartate metabolism__Tetracycline				
	Amino Acid	biosynthesis__Cyanoamino acid				
L-Asparagine	Metabolism	metabolism__Nitrogen metabolism	0.1	0.0	0.1	0.1
	Amino Acid	Arginine and proline				
L-Proline	Metabolism	metabolism__Novobiocin biosynthesis	0.6	0.4	0.5	0.8
		Arginine and proline metabolism__Glutamate metabolism__Histidine metabolism__D-Glutamine and D-glutamate metabolism__Glutathione metabolism_Butanoate metabolism_C5-Branched dibasic acid				
	Amino Acid	metabolism_Porphyrin and chlorophyll				
L-Glutamate	Metabolism	metabolism_Nitrogen metabolism	0.0	0.0	0.0	0.0
		Arginine and proline metabolism__Clavulanic acid				
	Amino Acid	biosynthesis__D-Arginine and D-ornithine				
L-Arginine	Metabolism	metabolism	0.0	0.0	0.0	0.1
		Glutamate metabolism__Purine metabolism__Pyrimidine metabolism__D-Glutamine and D-glutamate				
	Amino Acid					
L-Glutamine	Metabolism	metabolism__Nitrogen metabolism	0.8	0.5	0.7	1.0
		Glycine, serine and threonine metabolism__Methionine metabolism__Cysteine metabolism__Cyanoamino acid metabolism__Sphingolipid				
	Amino Acid	metabolism__Methane				
L-Serine	Metabolism	metabolism__Sulfur metabolism	0.1	0.1	0.1	0.1
		Glycine, serine and threonine metabolism__Valine, leucine and				
	Amino Acid	isoleucine biosynthesis__Porphyrin and				
L-Threonine	Metabolism	chlorophyll metabolism	0.1	0.0	0.3	0.1
L-Histidine	Amino Acid	Histidine metabolism__beta-Alanine	3.6	2.2	3.2	2.7

	Metabolism	metabolism				
		Lysine biosynthesis__Lysine				
	Amino Acid	degradation__Biotin				
L-Lysine	Metabolism	metabolism__Alkaloid biosynthesis II	1.4	0.8	1.5	1.1
	Amino Acid					
L-Carnitine	Metabolism	Lysine degradation	4.4	2.2	3.9	3.0
	Amino Acid					
L-Methionine	Metabolism	Methionine metabolism	0.4	0.2	0.3	0.5
		Phenylalanine				
		metabolism__Phenylalanine, tyrosine and				
		tryptophan				
	Amino Acid	biosynthesis__Phenylpropanoid				
L-Phenylalanine	Metabolism	biosynthesis__Alkaloid biosynthesis II	0.0	0.0	0.0	0.0
		Tryptophan metabolism__Phenylalanine,				
		tyrosine and tryptophan				
	Amino Acid	biosynthesis__Indole and ipecac alkaloid				
L-Tryptophan	Metabolism	biosynthesis	0.7	0.5	0.5	0.9
		Valine, leucine and isoleucine				
		degradation__Valine, leucine and				
		isoleucine biosynthesis__Penicillin and				
		cephalosporin biosynthesis__Propanoate				
	Amino Acid	metabolism__Pantothenate and CoA				
L-Valine	Metabolism	biosynthesis	0.0	0.0	0.0	0.0
		Valine, leucine and isoleucine				
	Amino Acid	degradation__Valine, leucine and				
L-Leucine	Metabolism	isoleucine biosynthesis	0.0	0.0	0.0	0.0
		Tyrosine metabolism__Phenylalanine,				
		tyrosine and tryptophan				
		biosynthesis__Novobiocin				
		biosynthesis__Thiamine				
	Amino Acid	metabolism__Phenylpropanoid				
L-Tyrosine	Metabolism	biosynthesis__Alkaloid biosynthesis I	0.2	0.2	0.3	0.2
		Alanine and aspartate				
		metabolism__Cysteine				
		metabolism__Taurine and hypotaurine				
		metabolism__Selenoamino acid				
		metabolism__D-Alanine				
	Amino Acid	metabolism__Carbon fixation__Reductive				
L-Alanine	Metabolism	carboxylate cycle (CO2 fixation)	0.3	0.1	0.2	0.2
		Alanine and aspartate				
		metabolism__Tetracycline				
	Amino Acid	biosynthesis__Cyanoamino acid				
L-Asparagine	Metabolism	metabolism__Nitrogen metabolism	0.1	0.0	0.1	0.1
	Amino Acid					
O-Acetylcarnitine	Metabolism	Alanine and aspartate metabolism	0.1	0.0	0.1	0.1
Creatinine	Amino Acid	Arginine and proline metabolism	0.3	0.2	0.2	0.3

	Metabolism					
	Amino Acid	Arginine and proline				
L-Proline	Metabolism	metabolism__Novobiocin biosynthesis	0.6	0.4	0.5	0.8
		Arginine and proline metabolism__Glutamate metabolism__Histidine metabolism__D-Glutamine and D-glutamate metabolism__Glutathione metabolism_Butanoate metabolism_C5-Branched dibasic acid				
	Amino Acid	metabolism_Porphyrin and chlorophyll				
L-Glutamate	Metabolism	metabolism_Nitrogen metabolism	0.0	0.0	0.0	0.0
		Arginine and proline metabolism__Clavulanic acid				
	Amino Acid	biosynthesis__D-Arginine and D-ornithine				
L-Arginine	Metabolism	metabolism	0.0	0.0	0.0	0.1
	Amino Acid					
L-Cystine	Metabolism	Cysteine metabolism	0.9	0.6	0.7	1.3
		Glutamate metabolism__Purine metabolism__Pyrimidine metabolism__D-Glutamine and D-glutamate				
	Amino Acid					
L-Glutamine	Metabolism	metabolism__Nitrogen metabolism	0.8	0.5	0.7	1.0
	Amino Acid	Glutamate metabolism__Cysteine				
Glutathione	Metabolism	metabolism__Glutathione metabolism	1.2	0.7	0.7	1.1
		Glycine, serine and threonine				
	Amino Acid	metabolism__Glycerophospholipid				
Choline	Metabolism	metabolism	0.1	0.1	0.1	0.2
		Glycine, serine and threonine metabolism__Methionine metabolism__Cysteine metabolism__Cyanoamino acid metabolism__Sphingolipid				
	Amino Acid	metabolism__Methane				
L-Serine	Metabolism	metabolism__Sulfur metabolism	0.1	0.1	0.1	0.1
		Glycine, serine and threonine metabolism__Valine, leucine and				
	Amino Acid	isoleucine biosynthesis__Porphyrin and				
L-Threonine	Metabolism	chlorophyll metabolism	0.1	0.0	0.3	0.1
		Glycine, serine and threonine				
	Amino Acid	metabolism__Glycerophospholipid				
Ethanolamine phosphate	Metabolism	metabolism__Sphingolipid metabolism	14.4	9.0	8.7	9.3
	Amino Acid	Histidine metabolism__beta-Alanine				
L-Histidine	Metabolism	metabolism	3.6	2.2	3.2	2.7
		Lysine biosynthesis__Lysine				
	Amino Acid	degradation__Biotin				
L-Lysine	Metabolism	metabolism__Alkaloid biosynthesis II	1.4	0.8	1.5	1.1
4-	Amino Acid	Lysine degradation	46.7	30.1	34.1	28.8

Trimethylammoniobutanoate	Metabolism					
	Amino Acid					
L-Carnitine	Metabolism	Lysine degradation	4.4	2.2	3.9	3.0
	Amino Acid					
L-Methionine	Metabolism	Methionine metabolism	0.4	0.2	0.3	0.5
		Phenylalanine metabolism__Phenylalanine, tyrosine and tryptophan				
	Amino Acid	biosynthesis__Phenylpropanoid				
L-Phenylalanine	Metabolism	biosynthesis__Alkaloid biosynthesis II	0.0	0.0	0.0	0.0
		Tryptophan metabolism__Phenylalanine, tyrosine and tryptophan				
	Amino Acid	biosynthesis__Indole and ipecac alkaloid				
L-Tryptophan	Metabolism	biosynthesis	0.7	0.5	0.5	0.9
		Valine, leucine and isoleucine degradation__Valine, leucine and isoleucine biosynthesis__Penicillin and cephalosporin biosynthesis__Propanoate				
	Amino Acid	metabolism__Pantothenate and CoA				
L-Valine	Metabolism	biosynthesis	0.0	0.0	0.0	0.0
		Valine, leucine and isoleucine				
	Amino Acid	degradation__Valine, leucine and				
L-Leucine	Metabolism	isoleucine biosynthesis	0.0	0.0	0.0	0.0
		Alanine and aspartate metabolism__Arginine and proline metabolism__Glycine, serine and threonine metabolism__Lysine biosynthesis__Arginine and proline metabolism__Histidine metabolism__beta-Alanine				
	Amino Acid	metabolism__Cyanoamino acid				
L-Aspartate	Metabolism	metabolism__Carbon fixation	0.3	0.2	0.3	0.2
L-1-Pyrroline-3-hydroxy-5-	Amino Acid					
carboxylate	Metabolism	Arginine and proline metabolism	0.1	0.1	0.1	0.2
	Amino Acid					
L-Glutamate 5-semialdehyde	Metabolism	Arginine and proline metabolism	0.5	0.4	0.4	0.8
		Bile acid biosynthesis__Purine metabolism__Glycine, serine and threonine metabolism__Lysine degradation__Cyanoamino acid metabolism__Glutathione metabolism__Methane metabolism__Thiamine				
	Amino Acid	metabolism__Porphyrin and chlorophyll				
Glycine	Metabolism	metabolism__Nitrogen metabolism	1.6	1.0	1.6	2.3
	Amino Acid	Glycine, serine and threonine				
Creatine	Metabolism	metabolism__Arginine and proline	0.2	0.1	0.1	0.1

		metabolism				
	Amino Acid					
Urocanate	Metabolism	Histidine metabolism	0.4	0.6	0.5	0.3
	Amino Acid					
N6,N6,N6-Trimethyl-L-lysine	Metabolism	Lysine degradation	4.7	3.3	4.8	5.9
1-Aminocyclopropane-1-	Amino Acid	Methionine metabolism__Propanoate				
carboxylate	Metabolism	metabolism	8.0	1.5	8.4	6.9
	Amino Acid					
Sulfoacetate	Metabolism	Taurine and hypotaurine metabolism	27.0	12.0	116.1	28.5
		Tyrosine metabolism__Phenylalanine, tyrosine and tryptophan biosynthesis__Novobiocin biosynthesis__Thiamine				
	Amino Acid	metabolism__Phenylpropanoid				
L-Tyrosine	Metabolism	biosynthesis__Alkaloid biosynthesis I	0.2	0.2	0.3	0.2
[FA hydroxy,oxo(7:0/2:0)] 4-						
hydroxy-2-oxo-Heptanedioic	Amino Acid					
acid	Metabolism	Tyrosine metabolism	28.3	19.0	17.9	17.0
	Amino Acid					
(3R)-beta-Leucine	Metabolism	Valine, leucine and isoleucine degradation	0.1	0.1	0.1	0.2
	Amino Acid					
4-Guanidinobutanoate	Metabolism	Arginine and proline metabolism	59.1	33.3	57.7	60.7
Methylimidazole	Amino Acid					
acetaldehyde	Metabolism	Histidine metabolism	1.1	0.7	0.8	0.9
	Amino Acid					
N6-Acetyl-L-lysine	Metabolism	Lysine degradation	0.9	0.7	1.2	0.7
		Valine, leucine and isoleucine				
(S)-3-Methyl-2-oxopentanoic	Amino Acid	degradation__Valine, leucine and				
acid	Metabolism	isoleucine biosynthesis	62.1	35.0	60.6	47.2
		Citrate cycle (TCA cycle)__Oxidative phosphorylation__Arginine and proline metabolism__Glutamate metabolism__Alanine and aspartate metabolism__Arginine and proline				
	Carbohydrate	metabolism__Tyrosine				
Fumarate	Metabolism	metabolism__Phenylalanine metabolism	0.4	0.2	0.4	0.3
		Citrate cycle (TCA cycle)__Oxidative phosphorylation__Glutamate metabolism__Alanine and aspartate metabolism__Tyrosine metabolism__Phenylalanine metabolism__gamma-Hexachlorocyclohexane				
	Carbohydrate	degradation__Glyoxylate and				
Succinate	Metabolism	dicarboxylate metabolism	1.0	0.6	0.7	1.1
D-Sorbitol	Carbohydrate	Fructose and mannose	38.7	15.0	26.3	26.7

	Metabolism Carbohydrate	metabolism__Galactose metabolism				
2-Hydroxy-3-oxoadipate	Metabolism Carbohydrate	Glyoxylate and dicarboxylate metabolism	16.1	8.0	13.2	13.6
D-Erythrose	Metabolism Carbohydrate	0	2.7	1.4	2.3	2.1
2-Acetolactate	Metabolism	Butanoate metabolism__Pantothenate and CoA biosynthesis	3.0	1.5	3.4	2.9
myo-Inositol	Carbohydrate Metabolism	Inositol metabolism__Galactose metabolism__Ascorbate and aldarate metabolism__Streptomycin biosynthesis__Inositol phosphate metabolism	0.3	0.2	0.2	0.4
Allantoin	Nucleotide Metabolism	0	0.8	0.5	0.7	1.1
Hypoxanthine	Nucleotide Metabolism	Purine metabolism	52.9	28.2	42.9	37.5
Xanthine	Nucleotide Metabolism	Purine metabolism__Caffeine metabolism	300.4	170.3	216.3	177.3
Inosine	Nucleotide Metabolism	Purine metabolism	1.6	1.3	1.5	1.0
Guanosine	Nucleotide Metabolism	Purine metabolism	2.8	1.9	2.5	1.7
Cytosine	Nucleotide Metabolism	Pyrimidine metabolism	572.2	344.1	362.9	322.6
Cytidine	Nucleotide Metabolism	Pyrimidine metabolism	3.1	1.4	1.8	2.4
Urate	Nucleotide Metabolism	Purine metabolism	110.1	38.3	57.3	49.7
Deoxyguanosine	Nucleotide Metabolism	Purine metabolism	51.6	21.1	31.4	31.1
Orotate(Fragment)	Nucleotide Metabolism	Pyrimidine metabolism	141.7	60.8	82.2	73.6
Thymidine	Nucleotide Metabolism	Pyrimidine metabolism	1.2	1.4	1.4	1.8
Uridine	Nucleotide Metabolism	Pyrimidine metabolism	1.5	0.9	0.9	0.9
5-Amino-4-imidazole carboxylate	Nucleotide Metabolism	Purine metabolism	13.7	10.6	11.7	13.4
5-Amino-4-imidazole carboxylate	Nucleotide Metabolism	Purine metabolism	0.8	0.4	0.6	0.7
Deoxyinosine	Nucleotide Metabolism	Purine metabolism	14.7	7.1	9.2	10.2
Deoxycytidine	Nucleotide Metabolism	Pyrimidine metabolism	1.1	0.6	0.8	0.7
Taurine	Lipid Metabolism	Bile acid biosynthesis__Taurine and	0.6	0.3	0.4	0.4

		hypotaurine metabolism					
2-C-Methyl-D-erythritol 4-phosphate	Lipid Metabolism	Biosynthesis of steroids		0.0	0.0	0.0	0.0
CDP-ethanolamine	Lipid Metabolism	Glycerophospholipid metabolism		6.4	3.7	6.4	6.3
3-Hydroxydodecanedioicacid	Lipids: Fatty Acyls		0	2.2	1.2	1.6	2.7
[FA amino(20:4/4:2)] N-(5Z,8Z,11Z,14Z-eicosatetraenoyl)-L-gamma-amino butyric acid	Lipids: Fatty Acyls	Amino Fatty Acids		0.3	0.2	0.2	0.2
Docosahexaenoicacid	Lipids: Fatty Acyls	Biosynthesis of unsaturated fatty acids		0.7	0.5	1.4	0.5
[FA hydroxy(9:0)] 2-hydroxy-nonanoic acid	Lipids: Fatty Acyls	Fatty Acids and Conjugates		276.2	175.2	217.2	350.9
[FA (18:1)] 9Z-octadecenamide	Lipids: Fatty Acyls	Fatty amides		0.0	0.0	0.1	0.1
Traumatic acid	Lipids: Fatty Acyls	alpha-Linolenic acid metabolism		0.0	0.0	0.0	0.0
[FA amino(20:4/4:2)] N-(5Z,8Z,11Z,14Z-eicosatetraenoyl)-L-gamma-amino butyric acid	Lipids: Fatty Acyls	Amino Fatty Acids		0.1	0.1	0.1	0.2
[FA amino(20:4/4:2)] N-(5Z,8Z,11Z,14Z-eicosatetraenoyl)-L-gamma-amino butyric acid	Lipids: Fatty Acyls	Amino Fatty Acids		0.0	0.0	0.0	0.0
10,16-Dihydroxyhexadecanoic acid	Lipids: Fatty Acyls	cutin biosynthesis		267.9	145.6	235.5	183.0
[FA trihydroxy(2:0)] 9S,11,15S-trihydroxy-2,3-dinor-thromboxa-5Z,13E-dien-1-oic acid	Lipids: Fatty Acyls	Eicosanoids		0.0	0.0	0.0	0.0
2-Oxooctadecanoic acid	Lipids: Fatty Acyls	Fatty Acids and Conjugates		0.9	0.5	0.8	0.7
[FA hydroxy(18:0)] 2S-hydroxy-octadecanoic acid	Lipids: Fatty Acyls	Fatty Acids and Conjugates		30.4	16.5	24.1	21.2
[FA hydroxy(18:1)] 9,10-dihydroxy-12Z-octadecenoic acid	Lipids: Fatty Acyls	Fatty Acids and Conjugates		2.1	1.3	1.5	2.2
[FA hydroxy(18:0)] 9,10-dihydroxy-octadecanoic acid	Lipids: Fatty Acyls	Fatty Acids and Conjugates		6.0	3.7	5.0	4.2
[FA (20:0/2:0)] Eicosanedioic acid	Lipids: Fatty Acyls	Fatty Acids and Conjugates		4.7	2.4	4.7	3.2
[FA methyl(5:1/5:2/8:0)] methyl 8-[3,5-epidioxy-2-(3-hydroperoxy-1-pentenyl)-cyclopentyl]-octanoate	Lipids: Fatty Acyls	Fatty Acids and Conjugates		1.2	0.7	0.9	1.1
[FA (18:1)] 9Z-octadecenamide	Lipids: Fatty Acyls	Fatty amides		0.4	0.2	0.3	0.3
[FA (20:4)] 5Z,8Z,11Z,14Z-	Lipids: Fatty Acyls	Fatty amides		0.3	0.2	0.3	0.2

eicosatetraenoyl amine [FA methyl,hydroxy,ethyl(20:4)] N-(1-methyl-2-hydroxy-2-phenyl-ethyl)-5Z,8Z,11Z,14Z-eicosatetraenoyl amine	Lipids: Fatty Acyls	Fatty amides	0.2	0.2	0.3	0.3
[PC (16:0)] 1-hexadecanoyl-sn-glycero-3-phosphocholine	Lipids: Glycerophospholipids	Glycerophosphocholines	53.2	33.6	39.3	38.0
[PC (18:0)] 1-octadecanoyl-sn-glycero-3-phosphocholine	Lipids: Glycerophospholipids	Glycerophosphocholines	9.8	5.2	8.4	8.0
[PS (18:0/19:0)] 1-octadecanoyl-2-nonadecanoyl-sn-glycero-3-phosphoserine	Lipids: Glycerophospholipids	Glycerophosphoserines	438.7	303.1	348.3	329.7
[PR] 3beta-(3-methyl-butanoyloxy)-villanovane-13alpha,17-diol	Lipids: Prenols	Isoprenoids	45.7	28.8	35.0	30.3
[SP (17:0)] heptadecasphinganine	Lipids: Sphingolipids	Sphingoid bases	15.0	9.5	10.1	9.6
Nicotinamide	Metabolism of Cofactors and Vitamins	Nicotinate and nicotinamide metabolism	44.3	28.2	39.9	33.6
1-Methylnicotinamide	Metabolism of Cofactors and Vitamins	Nicotinate and nicotinamide metabolism	0.1	0.1	0.1	0.1
4-Hydroxybenzoate	Metabolism of Cofactors and Vitamins	Ubiquinone biosynthesis__Phenylalanine metabolism__Benzoate degradation via hydroxylation__Bisphenol A degradation__Toluene and xylene degradation__2,4-Dichlorobenzoate degradation__Benzoate degradation via CoA ligation	0.4	0.2	0.3	0.2
6-Hydroxynicotinate	Metabolism of Cofactors and Vitamins	Nicotinate and nicotinamide metabolism	2.1	1.0	1.4	1.1
4-Methyl-5-(2-phosphoethyl)-thiazole	Metabolism of Cofactors and Vitamins	Thiamine metabolism	6.5	4.1	4.8	3.4

References

1.Harrison R. On the Stereotropism of Embryonic Cells. Science. 1911;34(870):279-81.

2.Curtis ASG, Varde M. Control of Cell Behaviour: Topological Factors. J Nat Cancer Res Inst. 1964;33:15-26.

3.Clark P, Connolly P, Curtis AS, Dow JA, Wilkinson CD. Cell guidance by ultrafine topography in vitro. J Cell Sci. 1991 May;99 (Pt 1):73-7.

4.Dalby MJ, Riehle MO, Johnstone H, Affrossman S, Curtis AS. In vitro reaction of endothelial cells to polymer demixed nanotopography. Biomaterials. 2002 Jul;23(14):2945-54.

5.Dalby MJ, Yarwood SJ, Riehle MO, Johnstone HJH, Affrossman S, Curtis ASG. Increasing Fibroblast Response to Materials Using Nanotopography: Morphological and Genetic Measurements of Cell Response to 13-nm-High Polymer Demixed Islands. Experimental Cell Research. 2002;276(1):1-9.

6.Dalby MJ, Gadegaard N, Tare R, Andar A, Riehle MO, Herzyk P, et al. The control of human mesenchymal cell differentiation using nanoscale symmetry and disorder. Nat Mater. 2007;6(12):997-1003.

7.Yim EK, Pang SW, Leong KW. Synthetic nanostructures inducing differentiation of human mesenchymal stem cells into neuronal lineage. Exp Cell Res. 2007 May 15;313(9):1820-9.

8.Chen W, Villa-Diaz LG, Sun Y, Weng S, Kim JK, Lam RH, et al. Nanotopography influences adhesion, spreading, and self-renewal of human embryonic stem cells. ACS Nano. 2012 May 22;6(5):4094-103.

9. McMurray RJ, Gadegaard N, Tsimbouri PM, Burgess KV, McNamara LE, Tare R, et al. Nanoscale surfaces for the long-term maintenance of mesenchymal stem cell phenotype and multipotency. Nat Mater. 2011;10(8):637-44.

10.Ji L, LaPointe VL, Evans ND, Stevens MM. Changes in embryonic stem cell colony morphology and early differentiation markers driven by colloidal crystal topographical cues. Eur Cell Mater. 2012;23:135-46.

11.Wilkinson CDW, Riehle M, Wood M, Gallagher J, Curtis ASG. The Use of Materials Patterned on a Nano- and Micro- Metric Scale in Cellular Engineering. Materials Science and Engineering. 2002;19:263-9.

12.Gadegaard N, Thoms S, MacIntyre DS, McGhee K, Gallagher J, Casey B, et al. Arrays of Nano-Dots for Cellular Engineering. Microelectronic Engineering. 2003;67-68:162-8.

13.Andersson AS, Backhed F, von Euler A, Richter-Dahlfors A, Sutherland D, Kasemo B. Nanoscale features influence epithelial cell morphology and cytokine production. Biomaterials. 2003 Sep;24(20):3427-36.

14.Andersson AS, Brink J, Lidberg U, Sutherland DS. Influence of Systematically Varied nanoscale Topography on the Morhphology of Epithelial Cells. IEEE Transactions on Nanobioscience. 2003;2(2):49-57.

15.Dalby MJ, McCloy D, Robertson M, Agheli H, Sutherland D, Affrossman S, et al. Osteoprogenitor response to semi-ordered and random nanotopographies. Biomaterials. 2006 May;27(15):2980-7.
16.Zhang L, Webster TJ. Decreased lung carcinoma cell functions on select polymer nanometer surface features. J Biomed Mater Res A. 2012 Jan;100(1):94-102.
17.Maclaine SE, Gadhari N, Pugin R, Meek RM, Liley M, Dalby MJ. Optimizing the osteogenicity of nanotopography using block co-polymer phase separation fabrication techniques. J Orthop Res. 2012 Jan 31.
18.Villaverde A, Carrio MM. Protein aggregation in recombinant bacteria: biological role of inclusion bodies. Biotechnol Lett. 2003 Sep;25(17):1385-95.
19.Garcia-Fruitos E, Rodriguez-Carmona E, Diez-Gil C, Ferraz RM, Vazquez E, Corchero JL, et al. Surface cell growth engineering assisted by a novel bacterial nanomaterial. Advanced Materials. 2009;21(42):4292-53.
20.Ventura S, Villaverde A. Protein quality in bacterial inclusion bodies. Trends Biotechnol. 2006 Apr;24(4):179-85.
21.Garcia-Fruitos E, Vazquez E, Diez-Gil C, Corchero JL, Seras-Franzoso J, Ratera I, et al. Bacterial inclusion bodies: making gold from waste. Trends Biotechnol. 2012 Feb;30(2):65-70.
22.Seras-Franzoso J, Diez-Gil C, Vazquez E, Garcia-Fruitos E, Cubarsi R, Ratera I, et al. Bioadhesiveness and efficient mechanotransduction stimuli synergistically provided by bacterial inclusion bodies as scaffolds for tissue engineering. Nanomedicine (Lond). 2012 Jan;7(1):79-93.
23.Mirmalek-Sani SH, Tare RS, Morgan SM, Roach HI, Wilson DI, Hanley NA, et al. Characterization and multipotentiality of human fetal femur-derived cells: implications for skeletal tissue regeneration. Stem Cells. 2006 Apr;24(4):1042-53.
24.Tare RS, Babister JC, Kanczler J, Oreffo RO. Skeletal stem cells: phenotype, biology and environmental niches informing tissue regeneration. Molecular and cellular endocrinology. 2008 Jun 25;288(1-2):11-21.
25.Sambrook J, Fritsch E, Maniatis T. Molecular cloning, a laboratorty manual. Cold Spring Harbor, NY: Cold Spring Harbor Laboratory Press; 1998.
26.Thomas JG, Baneyx F. Roles of the Escherichia coli small heat shock proteins IbpA and IbpB in thermal stress management: comparison with ClpA, ClpB, and HtpG In vivo. J Bacteriol. 1998 Oct;180(19):5165-72.
27.Carrio M, Gonzalez-Montalban N, Vera A, Villaverde A, Ventura S. Amyloid-like properties of bacterial inclusion bodies. J Mol Biol. 2005 Apr 15;347(5):1025-37.
28.Smith CA, Want EJ, O'Maille G, Abagyan R, Siuzdak G. XCMS: processing mass spectrometry data for metabolite profiling using nonlinear peak alignment, matching, and identification. Anal Chem. 2006 Feb 1;78(3):779-87.
29.Scheltema RA, Jankevics A, Jansen RC, Swertz MA, Breitling R. PeakML/mzMatch: a file format, Java library, R library, and tool-chain for mass spectrometry data analysis. Anal Chem. 2011 Apr 1;83(7):2786-93.

30.Creek DJ, Jankevics A, Burgess KE, Breitling R, Barrett MP. IDEOM: an Excel interface for analysis of LC-MS-based metabolomics data. Bioinformatics. 2012 Apr 1;28(7):1048-9.
31.Creek DJ, Jankevics A, Breitling R, Watson DG, Barrett MP, Burgess KE. Toward global metabolomics analysis with hydrophilic interaction liquid chromatography-mass spectrometry: improved metabolite identification by retention time prediction. Anal Chem. 2011 Nov 15;83(22):8703-10.
32.Vazquez E, Corchero JL, Burgueno JF, Seras-Franzoso J, Kosoy A, Bosser R, et al. Functional inclusion bodies produced in bacteria as naturally occurring nanopills for advanced cell therapies. Adv Mater. 2012 Apr 3;24(13):1742-7.
33.Diez-Gil C, Krabbenborg S, Garcia-Fruitos E, Vazquez E, Rodriguez-Carmona E, Ratera I, et al. The nanoscale properties of bacterial inclusion bodies and their effect on mammalian cell proliferation. Biomaterials. 2010 Aug;31(22):5805-12.
34.Biggs MJ, Richards RG, Gadegaard N, Wilkinson CD, Dalby MJ. Regulation of implant surface cell adhesion: characterization and quantification of S-phase primary osteoblast adhesions on biomimetic nanoscale substrates. J Orthop Res. 2007 Feb;25(2):273-82.
35.Biggs MJ, Richards RG, McFarlane S, Wilkinson CD, Oreffo RO, Dalby MJ. Adhesion formation of primary human osteoblasts and the functional response of mesenchymal stem cells to 330nm deep microgrooves. J R Soc Interface. 2008 Mar 18.
36.Biggs MJ, Richards RG, Gadegaard N, Wilkinson CD, Oreffo RO, Dalby MJ. The use of nanoscale topography to modulate the dynamics of adhesion formation in primary osteoblasts and ERK/MAPK signalling in STRO-1+ enriched skeletal stem cells. Biomaterials. 2009 Oct;30(28):5094-103.
37.McBeath R, Pirone DM, Nelson CM, Bhadriraju K, Chen CS. Cell shape, cytoskeletal tension, and RhoA regulate stem cell lineage commitment. Dev Cell. 2004 Apr;6(4):483-95.
38.Kilian KA, Bugarija B, Lahn BT, Mrksich M. Geometric cues for directing the differentiation of mesenchymal stem cells. Proc Natl Acad Sci U S A. 2010 Mar 16;107(11):4872-7.
39.Yanes O, Clark J, Wong DM, Patti GJ, Sanchez-Ruiz A, Benton HP, et al. Metabolic oxidation regulates embryonic stem cell differentiation. Nat Chem Biol. 2010 Jun;6(6):411-7.
40.Reyes JM, Fermanian S, Yang F, Zhou SY, Herretes S, Murphy DB, et al. Metabolic changes in mesenchymal stem cells in osteogenic medium measured by autofluorescence spectroscopy. Stem Cells. 2006 May;24(5):1213-7.
41.Garcia-Fruitos E, Seras-Franzoso J, Vazquez E, Villaverde A. Tunable geometry of bacterial inclusion bodies as substrate materials for tissue engineering. Nanotechnology. 2010 May 21;21(20):205101.
42.Kantawong F, Burgess KE, Jayawardena K, Hart A, Burchmore RJ, Gadegaard N, et al. Whole proteome analysis of osteoprogenitor differentiation induced by disordered nanotopography and mediated by ERK signalling. Biomaterials. 2009 Jun 26.

43.Engler AJ, Sen S, Sweeney HL, Discher DE. Matrix elasticity directs stem cell lineage specification. Cell. 2006 Aug 25;126(4):677-89.

Paper 4

A nanostructured bacterial bio-scaffold for the sustained bottom-up delivery of protein drugs

Joaquin Seras-Franzoso, Karl Peebo, José Luis Corchero, Monica P. Tsimbouri, Ugutz Unzueta, Ursula Rinas, Matthew J. Dalby, Esther Vazquez, Elena García-Fruitós and Antonio Villaverde

Submitted to Nanomedicine, 2012

Bacterial IBs have been proved to mechanically stimulate cell adhesion, cell proliferation and cell differentiation when cultured on IB-based topographies. These particles have also been observed to retain biologically active or partially active protein. Moreover, these "active building blocks" are capable of being released from the IB supramolecular structure to carry out their function (see annex nanopills). In this study we have explored the possibility of combining the appealing mechanical effect of the IB-based nanotopographies with the biological activity of proteins with a therapeutic interest. In this regard, we have proved that IBs forming nanostructured topographies on a cell culture surface can penetrate the membrane of the on growing cells providing bioavailability of the IB forming protein. Specifically, we have tested the activity of two different bio-active IB-based topographies (Bio-scaffolds) formed by either Hsp70 protein or the hFGF-2 growth factor. In both cases the protein forming the IB was able to develop its therapeutic effect, rescuing cells in chemically induced apoptotic cultures (Hsp70 bio-scaffolds) or stimulating cell growth in cultures under serum starvation conditions (hFGF-2 bio-scaffolds). These results prompt to the generation of bio active scaffolds able to provide multiple stimuli to achieve a highly efficient cell response. This approach could prove specially useful in tissue engineering applications in which the scaffolds should mimic the complex natural environment of the damaged tissue cells.

A nanostructured bacterial bio-scaffold for the sustained bottom-up delivery of protein drugs

Joaquin Seras-Franzoso [1, 2, 3], Karl Peebo [1, 4], José Luis Corchero [3, 1, 2], Monica P. Tsimbouri [5], Ugutz Unzueta [1, 2, 3], Ursula Rinas [6, 7], Matthew J. Dalby [5], Esther Vazquez [1, 2, 3], Elena García-Fruitós [3, 1, 2], Antonio Villaverde [1, 2, 3, *]

[1] *Institut de Biotecnologia i de Biomedicina, Universitat Autònoma de Barcelona, Bellaterra, 08193 Barcelona, Spain*

[2] *Department de Genètica i de Microbiologia, Universitat Autònoma de Barcelona, Bellaterra, 08193 Barcelona, Spain*

[3] *CIBER en Bioingeniería, Biomateriales y Nanomedicina (CIBER-BBN), Bellaterra, 08193 Barcelona, Spain*

[4] *Competence Centre of Food and Fermentation Technologies, Akadeemia tee 15b, 12618 Tallinn, Estonia*

[5] *Centre for Cell Engineering, University of Glasgow, College of Medical, Veterinary & Life Sciences, Glasgow, G12 8QQ, Scotland*

[6] *Institute of Technical Chemistry-Life Science, Leibniz University of Hannover, D-30167 Hannover, Germany*

[7] *Helmholtz Centre for Infection Research, Inhoffenstraße 7, D-38124 Braunschweig, Germany*

*Corresponding author: Antoni Villaverde. Phone +34 935813086; Fax +34 935812011; E-mail antoni.villaverde@uab.cat

Keywords: Scaffolds; drug-delivery; building blocks; biomaterials; tissue engineering

ABSTRACT

Bacterial inclusion bodies (IBs) are protein-based, amyloid nanomaterials that mechanically stimulate mammalian cell proliferation upon surface decoration. Using fluorescent proteins, we have here demonstrated significant membrane penetration of surface-attached IBs and a corresponding intracellular bioavailability of the protein material. When IBs are formed by protein drugs, such as the intracellular acting human chaperone Hsp70 or the extracellular/intracellular acting human basic fibroblast growth factor (FGF-2), IB components intervene on top-growing cells, namely by rescuing them from chemically-induced apoptosis or by stimulating cell division under serum starvation, respectively. Protein release from IBs seems to mechanistically mimic the sustained secretion of protein hormones from amyloid-like secretory granules in higher organisms. Therefore, we propose bacterial IBs as bio-mimetic nanostructured scaffolds (Bio-scaffolds) suitable for tissue engineering that, while acting as adhesive materials, partially disintegrate for the slow release of their biologically active building blocks. The bottom-up delivery of protein drugs mediated by Bio-scaffolds offers a highly promising emerging platform in regenerative medicine.

Introduction

In tissue engineering, cell colonization of bioinert substrates can be enhanced by functionalizing them to produce desired bioactivity with chemistry (motifs and proteins such as RGD peptides, vitronectin or mussel proteins) [1,2,3], topography to influence e.g. stem cell behaviours (through lithographic procedures or by decoration with particulate materials) [4] or by the external supply of growth factors, including epidermal growth factor [5], fibroblast growth factors [6], osteoprotegerin [7], insulin like growth factor I [8], nerve growth factor β [9,10,11] and vascular endothelial growth factor [6], among others. These three strategies (all targeted to influence cell adhesion and subsequent growth and differentiation) should be combined to synergistically exploit control of cell behaviors for regenerative therapies.

In this context, bacterial inclusion bodies (IBs) are proteinaceous and regular-shaped nanoparticles usually ranging between around 50 and 500 nm in diameter, that are produced in bacteria by the deposition of recombinant proteins when synthesized at non-physiological high rates [12]. Essentially, any protein species can be produced in bacteria as IBs [13], and IB formation can be favored by the fusion of peptidic aggregation tags [14,15]. In these protein clusters, amyloid-like cross-beta sheet-based molecular architecture coexists with native-like conformations of the forming recombinant protein [15,16]. Being mechanically stable, biocompatible and many of their biomechanical properties tunable by genetic approaches [17], we have previously demonstrated that as nanostructured materials, IBs are suitable for bottom-up surface modification in tissue engineering [18,19,20]. This is simultaneously achieved by the natural adhesiveness of IBs, that promotes strong cell attachment, combined with pERK-mediated stimulation of cell division through topographical modification, subsequent cell-sensing and mechanotransduction events [21]. The properties of IBs as self-organizing microbial materials have been extensively discussed elsewhere [22,23,24,25,17,26,27,28]. Since they contain important amounts of functional proteins [29,30,17] and in addition, show an unexpected cell membrane penetrability [31,32], IBs rapidly enter into exposed mammalian cells and release significant amounts of the forming protein, namely, its natural building block. Acting as nano-sized pills (Nanopills), IBs formed by a therapeutic protein significantly restore viability of exposed mammalian cells when challenged with

different types of stresses [31,32]. Therefore, we wondered to which extent, surface-attached IBs used for decoration in tissue engineering could also deliver active components to the top-growing cells, permitting the use of these nanoparticles as fully bio-functional scaffolds. Following this reasoning, we provide here evidences of bacterial IBs as nanostructured bio-adhesive and bio-functional scaffolds that, when formed by protein drugs, promote, in such immobilized form, the bottom-up intracellular (or extracellular) delivery of the drug in a biologically usable way. This seems to mimic the natural release of peptidic hormones from amyloid protein repositories (secretory granules) recently disclosed in higher organisms as a basic functional mechanism of the endocrine system [33,34,35]. The concept of a protein-based nanostructured material formed by releasable bio-active components (Bio-Scaffold), which additionally promotes cell adhesion and mechanical stimulation of division, opens intriguing possibilities for the development of drug-releasing substrates in which all the mechanical and biological stimuli required for tissue regeneration could be simultaneously achieved with the use of such a single multifunctional material.

Material and methods

Bacterial cells and plasmids

A His-tagged version of the human chaperone Hsp70 and the human basic fibroblast growth factor (FGF-2, 155 amino acid isoform, 18 kDa) were produced as IBs in *Escherichia coli* BL21(DE3), transformed with the commercial expression vector EX-R0068-B01 (OmicsLink ORF Expression Clone, from GeneCopoeia) and the vector pET29c(+)-hFGF-2 [36], respectively. VP1GFP and VP1LAC IBs were produced in the *Escherichia coli* K-12 derivative MC4100 [*araD139 (argF-lac)U169 rpsL150 relA1 flbB5301 deoC1 ptsF25 rbsR Str*^{r}] transformed with either pTVP1GFP or pTVP1LAC [32]. In these GFP and β-galactosidase fusions, the foot-and-mouth disease virus VP1 capsid protein acts as a protein aggregation tag.

IB production and purification

Bacterial cells were cultured in shaker flasks with LB medium supplemented with the required antibiotics at 37 °C and 250 rpm, until the culture optical density at 550 nm reached 0.5. Then, recombinant protein production and IB formation were induced by the addition of isopropyl-D-thiogalactoside (IPTG), at a final concentration of 1 mM. Hsp70 IBs were produced during 5 h at 37 °C, FGF-2 IBs during 3 h at 25 °C, and VP1GFP and VP1LAC IBs during 3 h at 37 ºC (in all cases at 250 rpm). All IBs were purified as described [37] with the exception of FGF-2, for which sonication steps were replaced by cell freeze/thaw cycles to prevent inactivation. After purification IBs were treated for 3 h with an antibiotic mixture containing tetracycline (0.5 mg/mL), kanamycin (2 mg/mL), chloramphenicol (0.8 mg/mL) and streptomycin (1.2 mg/mL), at 37 °C and under agitation. IB proteins were quantified by western blot using the Quantity One software (Biorad), by inferring the amount of protein from standard curves with known amounts of each protein.

Preparation of Bio-Scaffolds with different IB species

Different amounts of Hsp70 IBs diluted in PBS were added to polystyrene 24-well plates (Nunclon^{TM}) ranging from 0.36 to 3.6 μg of Hsp70 protein per well. Hsp70 IBs binding was allowed to occur overnight at 4 °C, and after that, supernatants containing

non-bound IBs were carefully recovered. Such supernatants were used to estimate the amount of aggregated protein effectively attached to the wells by SDS-PAGE and further western blot, using original IB samples as references. Protein amounts in each sample were densitometrically determined using Quantity One software (Biorad) and percentages of effectively bound protein calculated by comparing the amounts of recovered protein to the initial quantity of IBs added.

FGF-2 IBs were resuspended in PBS and different amounts (ranging from 0.02 to 20 μg of FGF-2 protein per well) were added to polystyrene non-treated 96-well plates (Costar®). Then, plates were incubated overnight at 4 °C, supernatants were removed and plates were washed twice with PBS. Surface decoration with VP1GFP and VP1LAC IBs was done following the same procedures. All assays were performed in triplicate and variance between samples determined by a t-test.

Cell culture

HL-60 cells (acute promielocytic leukaemia, ATCC no. CCL-240) were routinely cultured in suspension in RPMI 1640 medium plus 10 % (v/v) fetal bovine serum (FBS), at 37 °C and 5 % CO_2 in a humidified incubator. NIH-3T3 cells (mouse embryo fibroblasts) were routinely cultured in DMEM supplemented with 2 mM L-glutamine and 10 % FBS (v/v) at 37°C and 10 % CO_2 in a humidified incubator. For starvation experiments the medium was switched 24 h prior to the addition of IBs or soluble FGF-2 with a low serum DMEM containing 1 % FBS (v/v). Human mesenchymal stem cells (hMSCs, from Promocell) were routinely cultured in α-MEM supplemented with 10 % FBS (v/v), 1 % (v/v) 200 mM L-glutamine, and antibiotics (6.74 U/ml Penicillin-Streptomycin, 0.2 μg/ml Fungizone) at 37°C and 5 % CO_2 in a humidified incubator. Medium was changed every 3 days. Cells used in this work were at passage 2-3. HeLa cells (human cervical adenocarcinoma, ATCC no. CCL-2) were cultured in α-MEM supplemented with 10% FBS (v/v) and 2 mM L-glutamine at 37°C and 5 % CO_2 in a humidified incubator. Newborn hamster kidney (BHK) cells (kindly supplied by Prof. E. Domingo) were regularly cultured in DMEM supplemented with 10 % FBS (v/v) and 2 mM L-glutamine at 37 °C and 10 % CO_2 in a humidified incubator.

Apoptosis Assay

Cell apoptosis was induced by exposure of HL-60 cells to 15. 6 µM cisplatinum and determined by flow cytometry analysis of the cells stained with Annexin V-FITC57, by using an Annexin V-FITC Apoptosis Detection Kit (Roche). The anti-apoptotic effect of Hsp70 IBs was alternatively determined with Hsp70 Nanopills (that is, IBs added to previously seeded cells) and also when using Hsp70 scaffolds (IBs used to decorate the well surface before cell seeding). To check the effect of Hsp70 Nanopills, exponentially growing HL-60 cells were adjusted to 3×10^5 cells/ml and seeded in 24-well plates with 1 ml/well. Then, 40 µL of different IBs dilutions, (9 ng/µL and 90 ng/µL), were added to each well, simultaneously with cisplatinum to induce apoptosis. To determine the antiapoptotic effect of scaffold IBs, cells were seeded in previously IBs-decorated wells (as described before), and then cisplatinum added to induce apoptosis. In both strategies, cells were subjected to staining with Annexin V-FITC and propidium iodide after 24 h as detailed by the manufacturer. The amount of apoptotic cells was analyzed with a FACSCalibur flow cytometer (BD Biosciences, San José, CA). All the cell culture experiments were carried out in triplicate and variances analyzed by a t-test.

Determination of FGF-2 biological activity

Biological activity of FGF-2 was tested by measuring cell proliferation of NIH-3T3 fibroblast cells in presence of FGF-2 IBs compared to cell growth in absence of these particles. For that, 4 x 10^3 NIH-3T3 cells were seeded either in IB-modified polystyrene plates (as described above) or in regular 96-well culture plates (BD Falcon ™) followed by the addition of FGF-2 IBs 5 min later. The amounts FGF-2 IBs added to the culture medium as Nanopills were the same as those used for Bio-Scaffold preparations. The estimation of cell proliferation was determined after 48 h of cultivation at 37 °C and 10 % CO_2 in a humidified incubator by the 3- (4,5-dimethylthiazol-2-yl) -2,5-diphenyltetrazolium bromide assay, using the EZ4U kit (Biomedica, GmbH, Vienna, Austria) following manufacturer´s intructions. Data were recorded in a Victor3V 1420 (Perkin Elmer™) reader as described [18]. All the cell culture experiments were carried out in triplicate and variances analyzed by a t-test.

Clathrin immunostaining and confocal imaging

32 µg of VP1GFP IBs resuspended in PBS were deposited on smooth polycaprolactone (PCL) discs of 13 mm diameter that were incubated overnight at 4 °C. The decorated disks were then washed in PBS and blocked by adding a 3 % BSA/PBS (w/v) solution, for 1 h at 37 °C. Finally discs were washed in PBS. MSCs cultured for 4 days on IB-decorated PCL discs were fixed with PBS supplemented with 10 % formaldehyde (v/v) and 2 % sucrose (w/v) for 15 min at 37°C. A permeabilizing solution consisting in 10.3 g sucrose, 0.292 g NaCl, 0.06 g MgCl2, 0.476 g HEPES, 0.5 ml Triton X-100, in 100 ml PBS, pH 7.2, was then added and incubated at 4°C for 5 min. Cells were blocked in 1 % BSA/PBS (w/v) solution for 5 min at 37°C and anti-clathrin antibody (Sigma-Aldrich no. C1985) was added, diluted 1:50 in 1% BSA/PBS (w/v). After 1 h at 37°C the first antibody was removed and samples were washed 3 times in 0.5 % Tween 20/PBS (v/v) (PBST) for 5 min at room temperature. Then, a biotinylated horse anti-mouse antibody (Vector Laboratories) was added as diluted 1:50 in 1 % BSA/PBS (w/v) and incubated for 1 h at 37 °C. After convenient washing steps with (PBS-T) samples were incubated for 30 min at 4 °C in a 1:100 dilution of Cy3-conjugated streptavidin (Insight Biotechnology) in PBS-BSA. Finally, samples were washed again in PBS-T and mounted for confocal microscopy observation in Vecta shield with DAPI fluorescence medium (Vector Laboratories). Samples were examined with a TCS SP2 confocal laser scanning microscope (Leica Microsystems, Mannheim, Germany) using a Plan-Apochromat 63X 1.4 N.A lens. For 3D reconstruction, stacks of 20 sections taken every 0.7 µm along the z axis were captured. These data were then processed using the Imaris v 6.3.1 software (Bitplane; Zürich, Switzerland) to generate 3D reconstructions.

Confocal images of hMSC cultured for 4 days on VP1GFP IB-based scaffolds (obtained as described above) were processed with ImageJ software to analyze IB area and fluorescence intensity. IBs situated out of cell reach and IBs placed below cells were processed. Any particle with an area value higher than 1.5 μm^2 was considered to be IBs superaggregates and was excluded from the analysis.

Quantitative analysis of IB protein internalization

Fluorescence in HeLa cells was analyzed after treatment with trypsin under two alternative conditions. A *"Harsh"* treatment consisted in adding 1 mg/mL trypsin (final

concentration), in HBSS and incubating the cells for 15 min at 37°C in a humidified incubator at 5 % CO_2. A *"Mild"* treatment used 0.5 mg/ml trypsin (final concentration) in HBSS for 1 minute at 37°C in a humidified incubator at 5% CO_2. After trypsin treatment cells were processed on a FACSCanto system (Becton Dickinson), using a 15 W air-cooled argon-ion laser at 488 nm. Fluorescence emission was measured with a 530/30 nm band pass filter.

Cell attachment assay

The ability of IB-based surfaces to retain BHK cells was determined by measuring the amount of cells after an increasing number of washings steps in PBS as described elsewhere [21].

Scanning electron microscopy

IBs were deposited on Nuclepore® Track-Etched polycarbonate membranes with a pore size of 0.2 µm (Whatman Ltd., United Kingdom). After that, samples were fixed in 2.5 % (v/v) glutaraldehyde in 0.1 M phosphate buffer (pH 7.4), washed 4 times (10 min each wash) in 0.1 M phosphate buffer, washed in water and dehydrated in an ascending ethanol series (50, 70, 80, 90, and 95 % for 10 min each and twice with 100% ethanol). Samples were further dried by CO_2 critical point procedure. All samples were mounted on adhesive carbon films and then coated with gold. Images were taken with an EVO® MA 10 scanning electron microscope (Zeiss) at an accelerating voltage of 20 kV and an EDS Oxford INCA detector.

Results

We have recently shown that bacterial IBs are able to cross the cell plasma membrane with no signs of toxicity when added in suspension to cell cultures [32]. Excitingly, as the IBs are formed by releasable functional proteins [38,39], these nanoparticles show great potential in cell therapy (in form of Nanopills), acting extracellularly but also in both the cytoplasmic and nuclear compartments. Thus, this report moves to investigate the nature of the interaction between cell membranes and IBs when these particles remain attached to a 2D surface when used as bottom-up topographical modifiers in cell culture [21]. To explore this issue, we analyzed by confocal microscopy cell cultures (mesenchymal stem cells as a typical cell type used by tissue engineers) growing on surfaces decorated with fluorescent IBs (formed by the fluorescent protein VP1GFP). As previously shown [18], mammalian cells flattered and grew on IB-decorated polystyrene plates in absence of toxicity (Figure 1a). In confocal cell sections scanning for the endocytosis marker clathrin, we clearly identified surface-attached IBs showing partial penetration into the cells cultured on top of the nanotopographies (Figure 1 b, c). Higher magnification of the sections clearly showed that many immobilized IBs emerged through the cell membrane without clathrin coating (Figure 1 d), some even contacting the nucleus (e.g. Figure 1 c, vertical arrow). Detached IBs could also be observed as fully internalized in clathrin-coated vesicles (yellow merging in e.g. Figure 1 c, horizontal arrow) but this was a rare event and most of IBs remained fully linked to the surface during the progression of the cell culture. To quantitatively determine the number of cells that internalized IB material from the decorated surface, we analyzed the percentage of fluorescent cells after *mild* or *harsh* trypsin treatments. In the last case, in which externally linked protein is fully removed by the protease [40], around 20 % of cells were observed to be fluorescent by flow cytometry (Figure 1 e).

The bottom-up penetration of surface-linked IBs and the intracellular availability of the IB material led us to explore the potential biological effects of IBs, when formed by protein drugs, on the top growing cells [17]. Specifically, we considered if the protein scaffold could release sufficient protein for clear physiological effects, as the integrity of bacterial IBs seemed unchanged at least during 4 days of culture (Figure 1). For that, we

prepared Hsp70 IBs (and latter FGF-2 IBs, Figure 2), which have recently been observed as having an anti-apoptotic effect when administered as Nanopills [32]. For a comparative analysis of Hsp70 administered as Nanopills (top-down) or as a scaffold (bottom-up), we first determined the efficiency of the surface coating with Hsp70 Nanopills. An almost linear dependence between the amounts of added IB protein and the final amount of IB protein retained after the final washing steps was observed with approx. 60% of the initial protein retained in the IB protein range tested (Figure 3 a). This relation was considered for further comparison. The anti-apoptotic effect of Hsp70 on the model HL-60 cells challenged with cisplatinum was determined when administered as both Nanopills or topographically as a biofunctional scaffold. It was seen (Figure 3 b) that Hsp70 Nanopills indeed rescued cell viability as expected [32], thus providing control to our experiment. In a new observation, it was also seen that the topographical Hsp70 scaffold also rescued cells from apoptosis. Cell viability on the Hsp70 nanotopography was significantly higher than in absence of IBs (C bars), or when the surface had been functionalized with non-functional IB controls (made from VP1LAC, denoted as IR, irrelevant). These data confirmed the concept of functional scaffolds based on bacterial IBs and formed by a releasable, bioavailable form of protein drugs.

The more moderate effect of the Hsp70 nanotopographical scaffold compared to that of Hsp70 Nanopills could be due to the fact that the model cells used in this assay normally grow in suspension. Rather than forming strong cell adhesions, they rather simply sediment to the bottom when seeded in polystyrene plates. In this situation, the intimate contact presumed to occur between cell membranes and adsorbed IBs will be reduced. Therefore, we decided to move to another IB model of immediate applicability in biomaterials and tissue engineering coupled to using anchorage-dependant fibroblasts (NIH3T3 – form large cell adhesions) for further analysis. IBs formed by the basic fibroblast growth factor (FGF-2) were produced in *E. coli* (Figure 2) and their biological activity compared when administered, again, in the forms of Nanopills or as a topographical substrate. To first assess the biological activity of FGF-2 IBs they were added as Nanopills under serum deprivation conditions. As observed (Figure 4 a), FGF-2 IBs and soluble FGF-2 (but not non-functional IR IBs) were able to stimulate cell proliferation. Furthermore, FGF-2 IBs presented as a nanotopography also stimulated

cell proliferation at levels over those promoted by non-functional IB controls (Figure 4 b) and more efficiently than when presented as Nanopills, proving a synergistic action (physical and biological) of the bio-functional FGF-2 scaffolds. This was not due to any IB-linked toxicity event as soluble FGF-2 added to cells growing on IB-formed scaffold by an non-functional (IR) protein was also able to stimulate cell proliferation (Figure 4 c). Interestingly, all the IBs tested in this study, both biologically active (formed by Hsp70 and FGF-2) and those formed by inert (IR) proteins increased base-line cell adhesivity to the substrates upon which they were fixed and thus it is conceivable that nanotopographical biomaterial structures that can control one cellular facet (adhesion) or multiple cell activities (e.g. adhesion and proliferation) could be fabricated (Figure 4 d). In agreement, the fluorescence emission of VP1GFP IBs observed down cultured cells 4 days after seeding was significantly reduced when compared to the emission of cell free, substrate adsorbed IBs, although the average IB volume was poorly affected (Figure 5 a). This is indicative of protein release without strong implications in the global morphology of the material. Therefore, this strongly supports the concept of that the bioactive scaffolds formed by Hsp70 and especially by FGF-2 effectively combined positive physical and biological stimuli, indeed acting as Bio-Scaffolds.

Discussion

Biomaterial scaffolds generated for regenerative medicine should ideally mimic the intricate milieu of natural stimuli (mechanical and biological) to favour cell adhesion, migration, positioning, differentiation and proliferation in unnatural environments. So far, this is being achieved through the generation of biocompatible substrates and matrices acting as mechanical effectors, the use of cell attachment peptides or bioadhesive materials and by the external supply of cell growth factors that potentiate cell differentiation, growth or colonization of material surfaces. Hybrid scaffolds combining synthetic and natural materials should synergistically provide mechanical support and biological stimuli and are a matter of rapidly growing importance in the context of their regenerative potential. In addition, scaffolds loaded with releasable growth factors, again targeting regeneration, are under continuous development. In this context, polyurethane-fibrin complexes [41], electrospun fibers loaded with growth factor-encoding expressible DNA [42], TGF-β-loaded fibrin scaffolds [43], PDGF-loaded electrospun PLGA/PEG-PLA composite [44] and FGF-1-loaded PEGDA hydrogels [45] are a few recent among the wide spectrum of examples illustrating these approaches.

Since the discovery of bacterial IBs formed by biologically active proteins [30,16,38,29], these protein particles have been initially explored as functional materials in biocatalysis [46] and nanomedicine [17,25,24]. The development of improved protocols to separate fully functional IBs from potentially toxic bacterial remains [37,27] has permitted to use IBs in intimate contact with mammalian cells as bioadhesive scaffolds for cell culture [21]. However, we note that to achieve the ideals of third-generation biomaterials, that deliver reproducible molecular control of cells [47], we need to move beyond cell adhesion *per se* and into targeted control of desired cell functions to achieve sophisticated tissue regeneration.

IBs are self-organizing protein particles [22] produced by cost-effective bioprocesses that show high porosity and mechanical stability [18]. Here we demonstrate that when IBs formed by bioactive building blocks (protein drugs) are used as biofunctional scaffolds in cell culture, sufficient amounts of the protein drug are released outside or even inside

the cell to allow significant physiological impact. In particular, the nuclear acting chaperone Hsp70 and the 155 amino acid (18 kD) form of FGF-2, when exposed to cells as stable IB scaffolds, reach their target sites to rescue cell viability under pro-apoptotic or serum-starvation conditions respectively. The 155 amino acid form of FGF-2 (the low molecular weight isoform [48]) can act both extracellularly by binding its receptor for conventional cascade signaling but it can be also translocated into the nucleus [49], were in association with CK2, stimulates cell proliferation in a direct mitogenic activity [50]. These biological effects promoted by the bio-active IB scaffold (Bio-Scaffold) demonstrate bioavailability of the IB components outside the cultured cells but also in the cytoplasm and nucleus. The release of IB components occurs without significant changes in the IB morphology, remaining stable at least up to 94 h (Figure 1), time enough to deliver the drug-based effector to impact on cell behavior (Figure 3 and 4). How the protein building blocks are organized in the IB material to allow drug release whilst maintaining mechanical stability remains an unsolved question, but it might represent a parallel mechanism to that supporting protein hormone secretion from almyloid granules in endocrine glands of higher organism [33,35]. Al least 30 protein hormones are stored in amyloid fibrils forming tight granular particles, from which functional building blocks (the protein monomers) are steadily released during secretion [34]. Although the generic interest of amyloids as bionanomaterials is rapidly increasing [51,24], the inner structure of this material supporting protein release properties remains unsolved. For bacterial IBs we hypothesize that protein particles are formed by a limited amount of amyloidal fibrils acting as tensor agents, creating a cotton-like matrix [28] filled by functional proteins in native or native-like conformations (Figure 5 b). These fibrils have been indeed indentified as minor IB components that remain after extensive digestion with proteinase K [52], while native-like architecture seems to be a common trait in IB, as supported by both structural [53,54,55,56] and bio-activity analyses [38,57,30]. Such loosely linked proteins are expected to be releasable under appropriate physiological conditions [39,58] (Figure 5), while the amyloidal scaffold would remain unchanged. Eventually, misfolded protein species could be refolded once delivered into the cell cytoplasm (Figure 5 b, inset). This model would be in full agreement with experimental findings suggesting that fiber-based scaffolds are supportive of the IB architecture [52,59,28,60] with the coexistence of amyloid-like and properly folded protein

species in the IB clusters [16]. This concept is also supported by the loss of VP1GFP IB fluorescence without significant alterations of IB volume, as experimentally demonstrated here (Figure 5 a). Further dissection of the fine IB molecular architecture (in progress) should permit us to expand the fields of application of these promising protein nanoparticles in nanomedicine and material sciences. However, irrespective of other potential applications of IBs, we show here that they are excellent bio-active materials formed by releasable and bioavailable components able to target desired cell functions (Bio-Scaffolds). This means that the IB decorated surfaces go beyond merely promoting adhesion to inert surfaces but that they fit the requirements of third generation biomaterials.

Conclusions

We have demonstrated that bacterial IBs can act as bioactive scaffolds (Bio-Scaffolds), accelerating surface colonization and cell proliferation by a combination of adhesion and subsequent biological stimuli. This occurs when the building blocks of the IB material are protein drugs, with effects on the biology of the top-growing cells. At least a significant fraction of the IB material in the form of active protein species is made available to cells, and due to an unexpected ability of (even immobilized) IBs to penetrate the cell membrane it is also available inside of the cells without toxicity. The design and fabrication of nanostructured, protein-only biomaterials in form of bacterial IBs, with partial degradation properties, offers a spectrum of possibilities for the use of growth factors, mimicking the natural hormone release properties of the endocrine system. In this context, a combination of physical and biological stimuli are offered by the use of a single material species produced by cost-effective bioprocess with tunable potential, without the need of external addition of soluble cell effectors. Work in our laboratories continues to explore their potential for utility in tissue engineering because of their excellent regenerative potential.

Future perspective

Amyloids are being considered as intriguing functional materials, some of them, in nature, acting as slow secretory agents in the endocrine system. Bacterial inclusion

bodies are nanoscale amyloid particles produced by cost effective processes whose bio-physical properties (including the protein species that form them), can be easily tailored. When used to decorate substrates for topographical modification they penetrate top-growing mammalian cells and deliver their functional building blocks for a biological impact. This fact opens a wide spectrum of possibilities for the controlled release of selected protein drugs, growth factors and hormones. Tunable bacterial amyloids can be then envisaged as promising platforms in tissue engineering and regenerative medicine to provide both physical and mechanical stimuli to target cells under pre-defined profiles.

Executive summary

Inclusion bodies formed by different proteins mechanically stimulate mammalian cell attachment and proliferation when used as topographies.

Surface–attached bacterial inclusion bodies penetrated cultured mammalian cells, resulting embedded in the plasma membrane, without any sing of toxicity.

A fraction of the polypeptides forming inclusion bodies are released from these nanoparticles and become biologically available to top-growing cells.

When inclusion bodies are formed by protein drugs, a biological effect on the cultured cells is evidenced, as a result of the functionality of the released protein monomers.

The partial protein release of building blocks from inclusion bodies occurs without significant los of their volume, the particles keeping their scaffolding potential during the slow disintegration.

Bacterial inclusion bodies formed by protein drugs act as robust bio-active scaffolds, that being fully tunable by genetic and process engineering, mimicking natural slow protein delivery systems based on amyloidal protein granules.

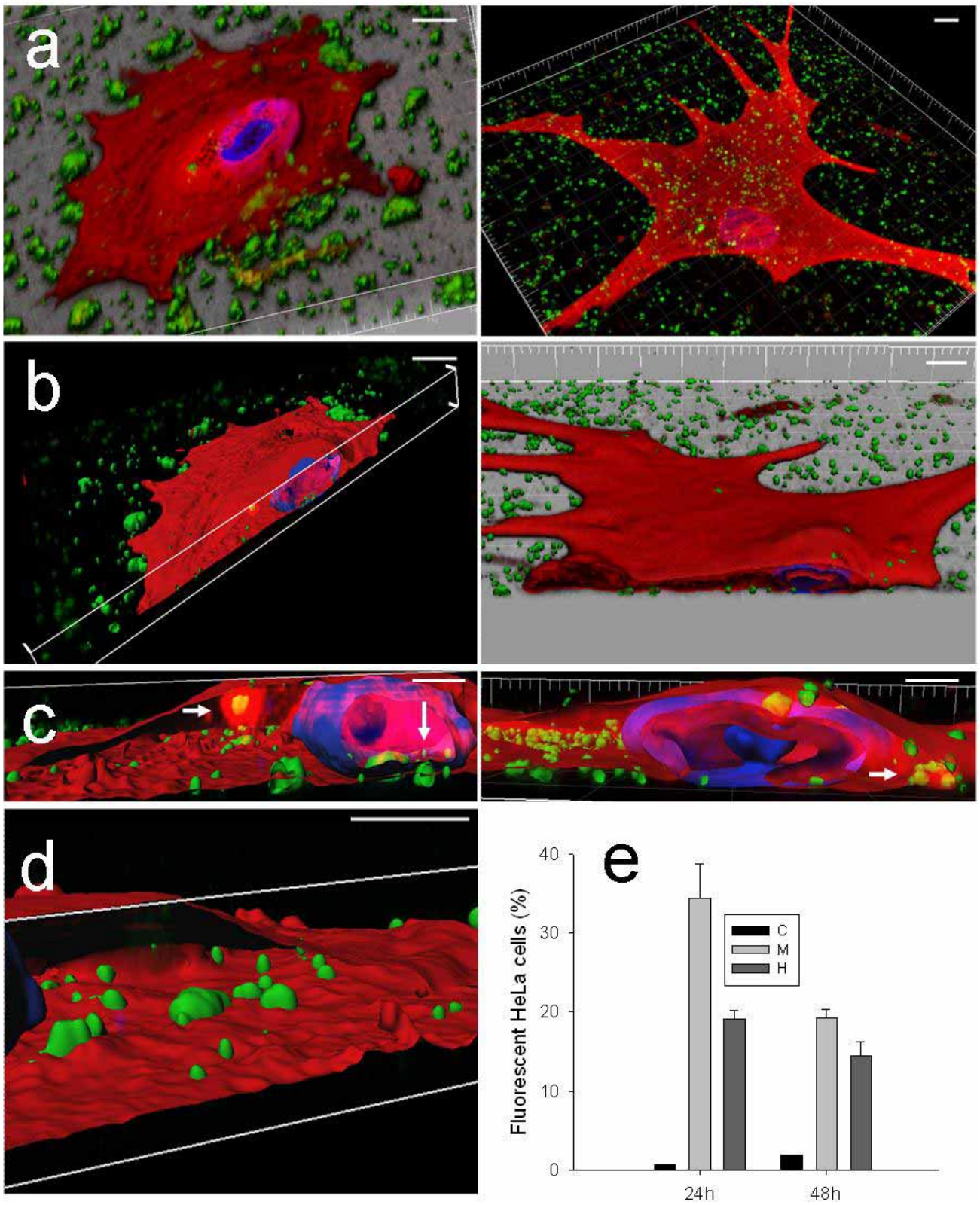

Figure 1. A. 3D-confocal analysis of hMSC cells growing for 96 h on IB-decorated PCL discs. Clathrin is labelled in red, the cell nucleus in blue and IBs, formed by VP1GFP, are naturally green. Two different cells are dissected in either left or right columns. **B**. Cell

sections at different angles showing green fluorescence emitted by surface attached IBs, emerging through the clathrin layer. **C**. Magnification of the same cells from a slightly different angle showing intracellular IBs embedded in the clathrin layer. A few detached IBs were seen to be internalized in clathrin-coated vesicles (yellow signal, indicated by horizontal arrows), while some surface attached IBs appear inside or practically inside the cell nucleus (vertical arrow). **D.** A detail of IBs embedded in the intracellular clathrin of the cell analyzed in the left column observed from the cytoplasmic side**.** 10 µm scale bars are showed as white sticks. **E**. Percentage of fluorescent HeLa cells, cultured at different times on IB scaffolds, after a *mild* (M) or *harsh* (H) trypsin treatment. C indicates control cells grown on IB-free equivalent surfaces.

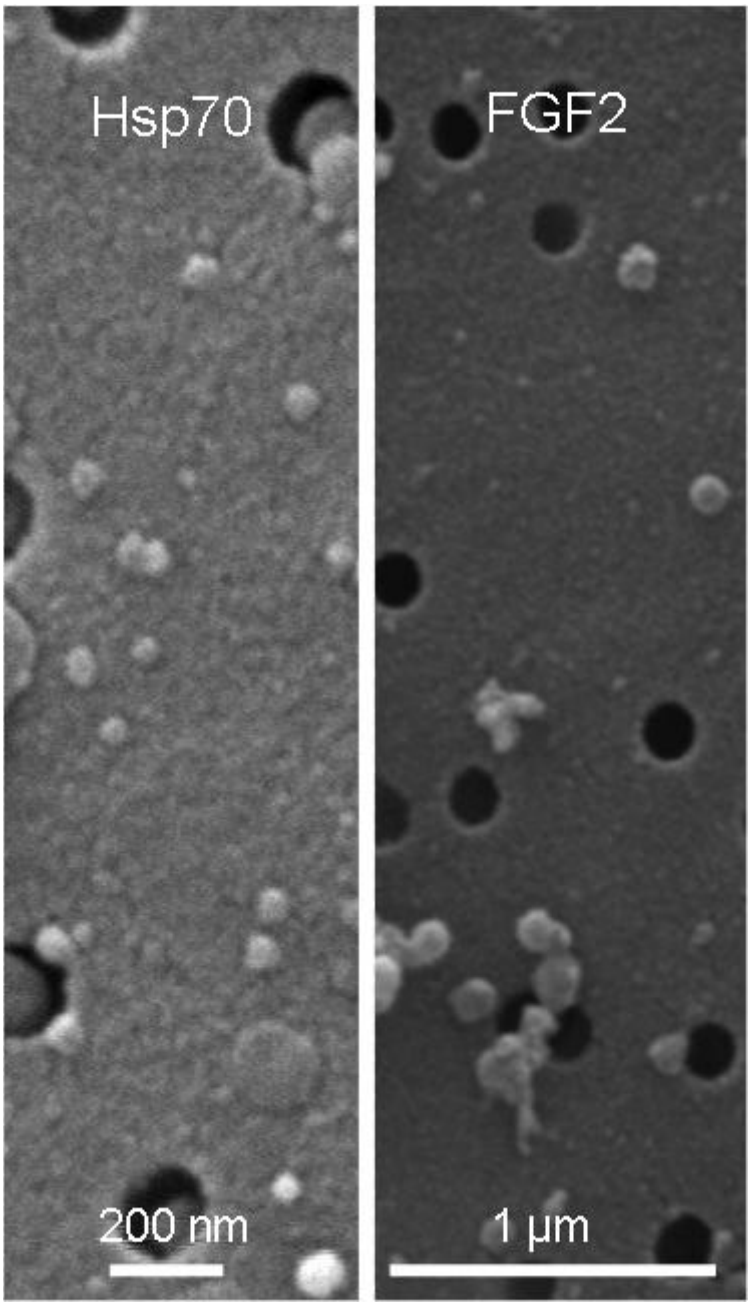

Figure 2. SEM images of isolated Hsp70 IBs (of around 50 nm in diameter) and FGF-2 IBs (of around 100 nm in diameter).

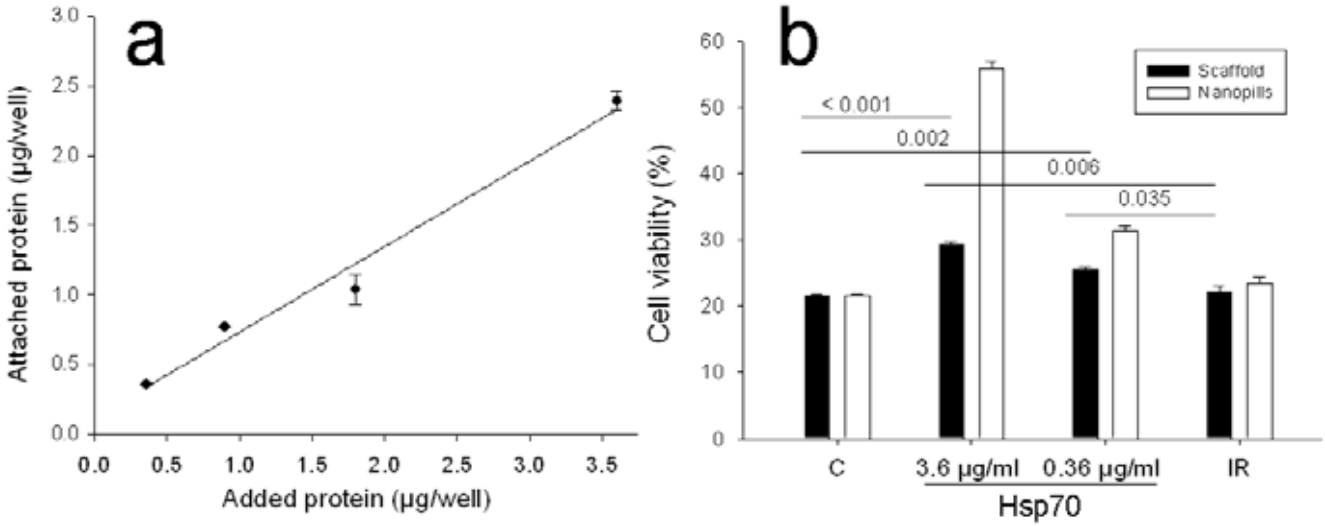

Figure 3. A. Linear range relationship between starting IB protein amount (as Hsp70 IBs) at the start and the end of IB adsorption protocol on polystyrene 24-well plates (y = 0.6136x + 0.1187; r = 0.9897; *p* = 0.0103). B. HL-60 cell viability upon exposure to cisplatinum (C) for 24 hours (non treated cells were used as a reference and were given 100 % viability), and challenged with cisplatinum but either treated with Hsp70 Nanopills (white bars) or growing on the equivalent amount of Hsp70 topographical scaffold (black bars). Non-functional (or irrelevant, IBs) were formed by protein VP1LAC and used at 3.6 µg/ml. The significance (*p* values) of cell viability in the presence of Hsp70 scaffold when compared to the controls (C and IR) is shown. Differences of viability between Nanopill-treated and untreated cells were always significant ($p<0.004$). Differences between C and IR pairs were not significant ($p=0.502$ for the IB scaffold and $p=0.163$ for Nanopills).

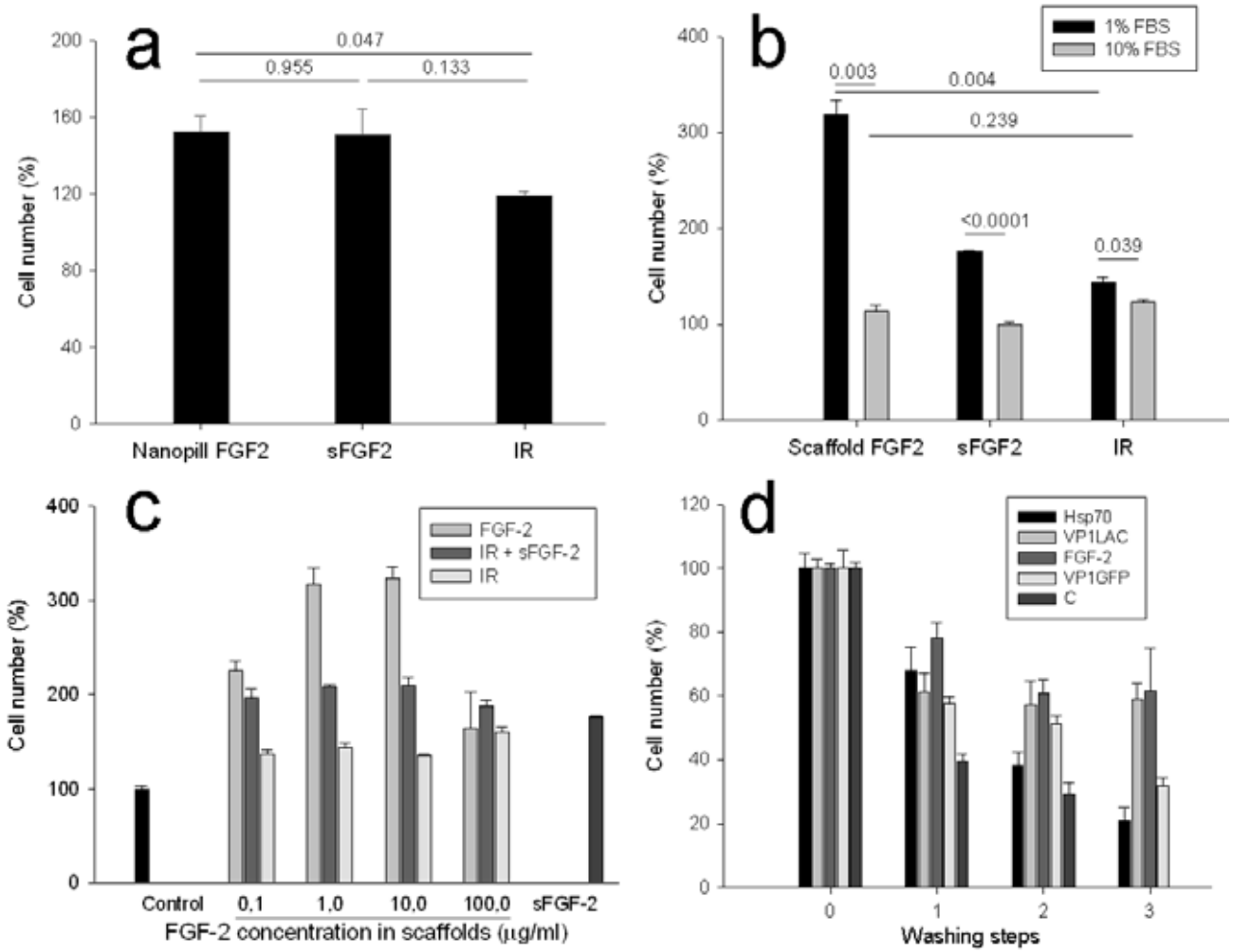

Figure 4. A. Recovery of cell viability by exposure to FGF-2 Nanopills under serum starvation (1 % fetal serum). The control (not shown, 100 %) corresponds to non-treated cells growing under the same conditions. sFGF-2 indicates the soluble version of the growth factor (10 ng/ml) and IR, irrelevant IBs formed by VP1GFP. Levels of significance between relevant pair-wise comparisons (through *p* values) are shown. B. Rescue of cell viability by FGF-2 scaffolds in presence of fetal serum (10 %) and under serum starvation (1 %). C. Dose-dependent rescue of cell viability under serum starvation promoted by FGF-2 scaffolds, compared to cell growth on IR IBs and on IR IBs with the supplementary addition of soluble FGF-2 (10 ng/ml). D. Cell attachment analysed through sequential washing steps on polystyrene surfaces decorated with different types of bacterial IBs as scaffolds. C indicates data from control cell cultures growing on IB-free surfaces.

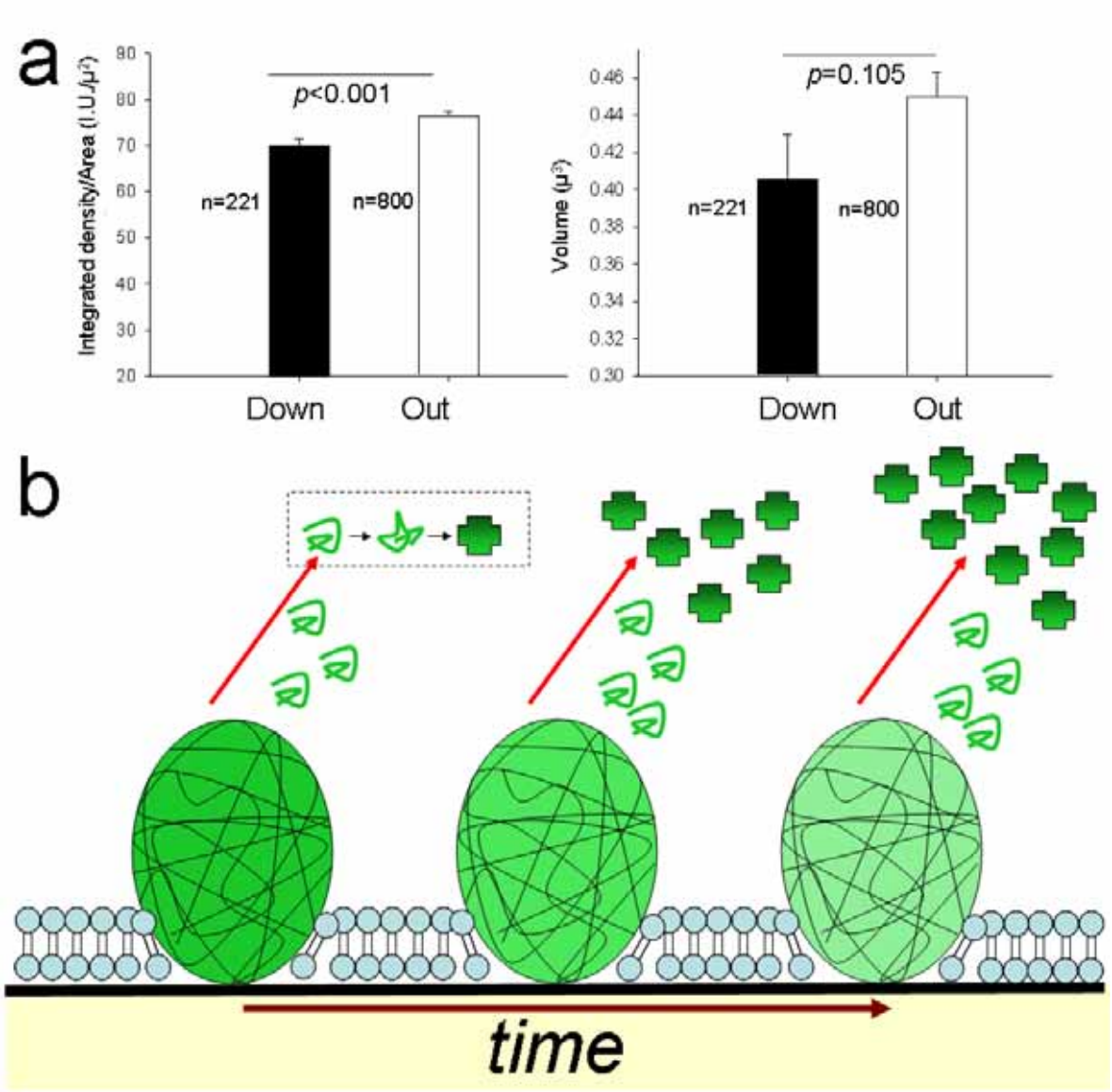

Figure 5. A. Integrated density of fluorescent emission (intensity units, I.U.), corrected per area, in 2D maximum intensity confocal images (obtained by the sum of fluorescence intensity from every confocal plane) of IBs adsorbed to PCL surfaces, and observed to be down or out cultured hMSC cells, 4 days after cell seeding. The estimated IB volume is also represented in both cases. B. A model of IB scaffolds for tissue engineering in which the IB architecture and mechanical properties are sustained by amyloidal forms of the protein drug (black lines). The cotton-like architecture [28] that these fibers create is filled in with active forms of the drug, with a native or native-like secondary structure (green material). Part of these protein forms can be released inside (and also outside) the cells cultured on top due to the high penetrability of bacterial IBs into mammalian cell membranes. This is conducive to biological effects associated with

the bottom-up drug delivery, which occurs during a slow disintegration of IB without destruction of its scaffold structure. Native-like but partially misfolded protein species (green lines) could be refolded inside the cell (inset) into a fully active form of the drug (crosses). Alternatively, IB protein could also act on the extracellular cell side. Protein release from IBs could be similar to that proposed for amyloids in mammalian secretory glands [(34)].

Disclosure

AV, EGF and EV are co-inventors of a patent (P200900045) on the use of IBs as reagents for mammalian cell culture.

Acknowledgments: We are indebted to the Cell Culture Unit of the Servei de Cultius Cel·lulars, Producció d'Anticossos i Citometria (SCAC), and Servei de Microscòpia, both at the UAB. We are also indebted to the Protein Production Platform (CIBER-BBN - UAB) for its helpful technical assistance (http://bbn.ciber-bbn.es/programas/plataformas/equipamiento). This study has been funded by MINECO (BFU2010-17450,), AGAUR (2009SGR-00108) and CIBER de Bioingeniería, Biomateriales y Nanomedicina (CIBER-BBN, Spain). CIBER-BBN is an initiative funded by the VI National R&D&i Plan *2008-2011*, Iniciativa Ingenio 2010, Consolider Program, CIBER Actions and financed by the Instituto de Salud Carlos III with assistance from the European Regional Development Fund. EGF is supported by the Programa Personal de Técnico de Apoyo (Modalidad Infraestructuras científico-tecnológicas, MICINN). JSF is recipient of a PIF doctoral fellowship from UAB, KP of an Erasmus placement scholarship and AV of an ICREA ACADEMIA award.

Reference List

1. Molnar P, Wang W, Natarajan A, Rumsey JW, Hickman JJ: Photolithographic patterning of C2C12 myotubes using vitronectin as growth substrate in serum-free medium. *Biotechnol.Prog.* 23(1), 265-268 (2007).

2. Cha HJ, Hwang DS, Lim S: Development of bioadhesives from marine mussels. *Biotechnol J.* 3(5), 631-638 (2008).

3. Hennessy KM, Clem WC, Phipps MC, Sawyer AA, Shaikh FM, Bellis SL: The effect of RGD peptides on osseointegration of hydroxyapatite biomaterials. *Biomaterials* 29(21), 3075-3083 (2008).

4. McMurray RJ, Gadegaard N, Tsimbouri PM *et al:* Nanoscale surfaces for the long-term maintenance of mesenchymal stem cell phenotype and multipotency. *Nat.Mater.* 10(8), 637-644 (2011).

5. Marcantonio NA, Boehm CA, Rozic RJ *et al:* The influence of tethered epidermal growth factor on connective tissue progenitor colony formation. *Biomaterials* 30(27), 4629-4638 (2009).

6. Zieris A, Prokoph S, Levental KR *et al:* FGF-2 and VEGF functionalization of starPEG-heparin hydrogels to modulate biomolecular and physical cues of angiogenesis. *Biomaterials* 31(31), 7985-7994 (2010).

7. Doschak MR, Kucharski CM, Wright JE, Zernicke RF, Uludag H: Improved bone delivery of osteoprotegerin by bisphosphonate conjugation in a rat model of osteoarthritis. *Mol.Pharm.* 6(2), 634-640 (2009).

8. Jaklenec A, Hinckfuss A, Bilgen B, Ciombor DM, Aaron R, Mathiowitz E: Sequential release of bioactive IGF-I and TGF-beta 1 from PLGA microsphere-based scaffolds. *Biomaterials* 29(10), 1518-1525 (2008).

9. Madduri S, di SP, Papaloizos M, Kalbermatten D, Gander B: Effect of controlled co-delivery of synergistic neurotrophic factors on early nerve regeneration in rats. *Biomaterials* 31(32), 8402-8409 (2010).

10. Bhang SH, Lee TJ, Lim JM *et al:* The effect of the controlled release of nerve growth factor from collagen gel on the efficiency of neural cell culture. *Biomaterials* 30(1), 126-132 (2009).

11. Dodla MC , Bellamkonda RV: Differences between the effect of anisotropic and isotropic laminin and nerve growth factor presenting scaffolds on nerve regeneration across long peripheral nerve gaps. *Biomaterials* 29(1), 33-46 (2008).

12. Villaverde A , Carrio MM: Protein aggregation in recombinant bacteria: biological role of inclusion bodies. *Biotechnol.Lett.* 25(17), 1385-1395 (2003).

13. Garcia-Fruitos E: Inclusion bodies: a new concept. *Microb.Cell Fact.* 9(1), 80- (2010).

14. Wu W, Xing L, Zhou B, Lin Z: Active protein aggregates induced by terminally attached self-assembling peptide ELK16 in Escherichia coli. *Microb.Cell Fact.* 10(1), 9- (2011).

15. Zhou B, Xing L, Wu W, Zhang XE, Lin Z: Small surfactant-like peptides can drive soluble proteins into active aggregates. *Microb.Cell Fact.* 11(1), 10- (2012).

16. Ventura S , Villaverde A: Protein quality in bacterial inclusion bodies. *Trends Biotechnol.* 24(4), 179-185 (2006).

17. Garcia-Fruitos E, Vazquez E, ez-Gil C *et al:* Bacterial inclusion bodies: making gold from waste. *Trends Biotechnol* 30(2), 65-70 (2012).

18. García-Fruitós E, Rodríguez-Carmona E, Díez-Gil C *et al:* Surface Cell Growth Engineering Assisted by a Novel Bacterial Nanomaterial. *Advanced Materials* 21, 4249-4253 (2009).

19. Garcia-Fruitos E, Seras-Franzoso J, Vazquez E, Villaverde A: Tunable geometry of bacterial inclusion bodies as substrate materials for tissue engineering. *Nanotechnology.* 21(20), 205101- (2010).

20. Diez-Gil C, Krabbenborg S, Garcia-Fruitos E *et al:* The nanoscale properties of bacterial inclusion bodies and their effect on mammalian cell proliferation. *Biomaterials* 31, 5805-5812 (2010).

21. Seras-Franzoso J, ez-Gil C, Vazquez E *et al:* Bioadhesiveness and efficient mechanotransduction stimuli synergistically provided by bacterial inclusion bodies as scaffolds for tissue engineering. *Nanomedicine (Lond)* 7(1), 79-93 (2012).

22. Vazquez E , Villaverde A: Engineering building blocks for self-assembling protein nanoparticles. *Microb.Cell Fact.* 9, 101- (2010).

23. Vazquez E, Corchero JL, Villaverde A: Post-production protein stability: trouble beyond the cell factory. *Microb.Cell Fact.* 10(1), 60- (2011).

24. Villaverde A: Nanotechnology, bionanotechnology and microbial cell factories. *Microb.Cell Fact.* 9, 53- (2010).

25. Rodriguez-Carmona E , Villaverde A: Nanostructured bacterial materials for innovative medicines. *Trends Microbiol.* 18(9), 423-430 (2010).

26. Mitraki A: Protein aggregation from inclusion bodies to amyloid and biomaterials. *Adv.Protein Chem.Struct.Biol.* 79, 89-125 (2010).

27. Peternel S , Komel R: Isolation of biologically active nanomaterial (inclusion bodies) from bacterial cells. *Microb.Cell Fact.* 9, 66- (2010).

28. Peternel S , Komel R: Active Protein Aggregates Produced in Escherichia coli. *Int.J.Mol.Sci.* 12(11), 8275-8287 (2011).

29. Gonzalez-Montalban N, Garcia-Fruitos E, Villaverde A: Recombinant protein solubility-does more mean better? *Nat.Biotechnol.* 25(7), 718-720 (2007).

30. Garcia-Fruitos E, Gonzalez-Montalban N, Morell M *et al:* Aggregation as bacterial inclusion bodies does not imply inactivation of enzymes and fluorescent proteins. *Microb.Cell Fact.* 4, 27- (2005).

31. García-Fruitós E, Vazquez E, Corchero JL, and Villaverde A. **Use of inclusion bodies as therapeutic agents**.IB2010/001330(WO2010131117A1) (2010)

32. Vazquez E, Corchero JL, Burgueno JF *et al:* Functional Inclusion Bodies Produced in Bacteria as Naturally Occurring Nanopills for Advanced Cell Therapies. *Adv.Mater.* 24(13), 1742-1747 (2012).

33. Maji SK, Perrin MH, Sawaya MR *et al:* Functional amyloids as natural storage of peptide hormones in pituitary secretory granules. *Science* 325(5938), 328-332 (2009).

34. Badtke MP, Hammer ND, Chapman MR: Functional amyloids signal their arrival. *Sci.Signal.* 2(80), e43- (2009).

35. Maji SK, Schubert D, Rivier C, Lee S, Rivier JE, Riek R: Amyloid as a depot for the formulation of long-acting drugs. *PLoS Biol.* 6(2), e17- (2008).

36. Hoffmann F, van den Heuvel J, Zidek N, Rinas U: Minimizing inclusion body formation during recombinant protein production in *Escherichia coli* at bench and pilot plant scale. *Enzyme Microb.Technol.* 34, 235-241 (2004).

37. Rodriguez-Carmona E, Cano-Garrido O, Seras-Franzoso J, Villaverde A, Garcia-Fruitos E: Isolation of cell-free bacterial inclusion bodies. *Microb.Cell Fact.* 9(1), 71- (2010).

38. Garcia-Fruitos E, Aris A, Villaverde A: Localization of functional polypeptides in bacterial inclusion bodies. *Appl.Environ.Microbiol.* 73(1), 289-294 (2007).

39. Peternel S, Grdadolnik J, Gaberc-Porekar V, Komel R: Engineering inclusion bodies for non denaturing extraction of functional proteins. *Microb.Cell Fact.* 7(1), 34- (2008).

40. Richard JP, Melikov K, Vives E *et al:* Cell-penetrating peptides. A reevaluation of the mechanism of cellular uptake. *J.Biol.Chem.* 278(1), 585-590 (2003).

41. Lisi A, Briganti E, Ledda M *et al:* A combined synthetic-fibrin scaffold supports growth and cardiomyogenic commitment of human placental derived stem cells. *PLoS One* 7(4), e34284- (2012).

42. He S, Xia T, Wang H, Wei L, Luo X, Li X: Multiple release of polyplexes of plasmids VEGF and bFGF from electrospun fibrous scaffolds towards regeneration of mature blood vessels. *Acta Biomater.* (2012).

43. Diederichs S, Baral K, Tanner M, Richter W: Interplay between local versus soluble TGF-beta and fibrin scaffolds: role of cells and impact on human mesenchymal stem cell chondrogenesis. *Tissue Eng Part A* (2012).

44. Zhao X , Hadjiargyrou M: Induction of cell migration in vitro by an electrospun PDGF-BB/PLGA/PEG-PLA nanofibrous scaffold. *J.Biomed.Nanotechnol.* 7(6), 823-829 (2011).

45. Sokic S , Papavasiliou G: FGF-1 and proteolytically mediated cleavage site presentation influence three-dimensional fibroblast invasion in biomimetic PEGDA hydrogels. *Acta Biomater.* (2012).

46. Garcia-Fruitos E , Villaverde A: Friendly production of bacterial inclusion bodies. *Korean J.Chem.Eng.* 27(2), 385-389 (2010).

47. Hench LL , Polak JM: Third-generation biomedical materials. *Science* 295(5557), 1014-1017 (2002).

48. Seghezzi G, Patel S, Ren CJ *et al:* Fibroblast growth factor-2 (FGF-2) induces vascular endothelial growth factor (VEGF) expression in the endothelial cells of forming capillaries: an autocrine mechanism contributing to angiogenesis. *J.Cell Biol.* 141(7), 1659-1673 (1998).

49. Amalric F, Baldin V, Bosc-Bierne I *et al:* Nuclear translocation of basic fibroblast growth factor. *Ann.N.Y.Acad.Sci.* 638, 127-138 (1991).

50. Bailly K, Soulet F, Leroy D, Amalric F, Bouche G: Uncoupling of cell proliferation and differentiation activities of basic fibroblast growth factor. *FASEB J.* 14(2), 333-344 (2000).

51. Cherny I , Gazit E: Amyloids: not only pathological agents but also ordered nanomaterials. *Angew.Chem.Int.Ed Engl.* 47(22), 4062-4069 (2008).

52. Morell M, Bravo R, Espargaro A *et al:* Inclusion bodies: specificity in their aggregation process and amyloid-like structure. *Biochim.Biophys.Acta* 1783(10), 1815-1825 (2008).

53. Oberg K, Chrunyk BA, Wetzel R, Fink AL: Nativelike secondary structure in interleukin-1 beta inclusion bodies by attenuated total reflectance FTIR. *Biochemistry* 33(9), 2628-2634 (1994).

54. Gonzalez-Montalban N, Natalello A, Garcia-Fruitos E, Villaverde A, Doglia SM: In situ protein folding and activation in bacterial inclusion bodies. *Biotechnol.Bioeng.* 100(4), 797-802 (2008).

55. Ami D, Natalello A, Taylor G, Tonon G, Maria DS: Structural analysis of protein inclusion bodies by Fourier transform infrared microspectroscopy. *Biochim.Biophys.Acta* 1764(4), 793-799 (2006).

56. Ami D, Natalello A, Gatti-Lafranconi P, Lotti M, Doglia SM: Kinetics of inclusion body formation studied in intact cells by FT-IR spectroscopy. *FEBS Lett.* 579(16), 3433-3436 (2005).

57. Garcia-Fruitos E, Martinez-Alonso M, Gonzalez-Montalban N, Valli M, Mattanovich D, Villaverde A: Divergent Genetic Control of Protein Solubility and Conformational Quality in *Escherichia coli*. *J.Mol.Biol.* 374, 195-205 (2007).

58. Upadhyay AK, Murmu A, Singh A, Panda AK: Kinetics of inclusion body formation and its correlation with the characteristics of protein aggregates in Escherichia coli. *PLoS One* 7(3), e33951- (2012).

59. Carrio M, Gonzalez-Montalban N, Vera A, Villaverde A, Ventura S: Amyloid-like properties of bacterial inclusion bodies. *J.Mol.Biol.* 347(5), 1025-1037 (2005).

60. de Groot NS, Sabate R, Ventura S: Amyloids in bacterial inclusion bodies. *Trends Biochem.Sci.* 34(8), 408-416 (2009).

32: ** of considerable interest. The release of protein drugs from inclusion bodies in suspension is demonstrated in several model proteins.
33: ** of considerable interest. The authors demonstrate than more than 30 natural hormones in higher organisms are delivered from amyloidal repositories.
53: * of interest. Native-like secondary structure is clearly observed in inclusion bodies formed by protein drugs (with potential therapeutic application).
59: * of interest. The amyloid architecture of bacterial inclusion bodies is solved by a combination of structural analyses.

Discussion

1. IBs as tunable biomaterial for tissue engineering

Tissue engineering is a promising field in regenerative medicine since it could represent a promise in the treatment of many diseases and injuries, in which damaged tissue compromise the health of the patients. In this regard, it is important to note that tissue engineering success will depend, in a high degree, on the development of suitable scaffolds for sustaining cell growth but also for actively directing cell response at a molecular level in terms of cell adhesion, proliferation and differentiation. Thus, biomaterials used to build scaffolds for tissue engineering applications should not only being able to integrate themselves with the tissue surroundings, exhibiting biocompatibility, similar mechanical features and degradation rates than the targeted tissue, but also they should be able to be sensed by the cells and interact with them in order to achieve the desired cell responses in a tightly controlled manner (third generation of biomaterials)[144, 145]. In order to obtain better materials for tissue engineering, the study of the surface topography has been proved crucial. Scaffolds should mimic the environmental conditions of the targeted tissue cells trying to provide a similar range of stimuli, mechanical and biochemical, than those found in their natural niche[146]. In this regard, simple studies on 2D nanotopographies have been proved extremely powerful to investigate the influence of mechanical nanocues in cell response. Particularly, lithographic methods have been largely employed for generating controlled nanotopographies providing consistent results[118]. However, this technique is quite limited by the chemical nature of the material to modify. On the other hand, deposition of nanoparticles to fabricate nano-topographical modified surfaces is more independent of the material chemical composition but, so far, has provided less consistent data.

Recently, a study carried out by García-Fruitós and co-workers proposed bacterial IBs as a protein-based material for surface nano-topographical modification by a simple particle deposition procedure[73]. Bacterial IBs are protein nano-sized particles generated during recombinant protein production processes. These protein clusters can be obtained by cost-effective biofabrication procedures and their protein composition analysis indicates that the recombinant protein represents up to 95% of the total protein content[56, 147]. In addition, they have been shown to provide positive stimuli when used

to generate random topographies in cell culture surfaces. However, very little has been explored about mechanical and chemical properties of bacterial IBs. Nevertheless, the plasticity of the IB formation suggested by the structural diversity of IB forming proteins as well as the evidence that properties such as IB size are influenced by production time[148], genetic background and culture conditions[32, 149] prompted us to hypothesize the possible formation of structurally distinct aggregates, showing different patterns of protein self-organization within the particle.

In this regard, we have identified an important *E. coli* cytosolic protease (ClpP) which inactivation has a clear incidence in the IB deposition pattern, as shown by the aberrant ((unusual) final morphology of the aggregate. This fact indicates a genetic control of the IB shape. Thus, IBs produced in *E. coli* ClpP$^-$ strains exhibit a tear-shaped morphology **(see figure 2, results, paper 1**), contrarily to what has been observed for most of the IBs so far described, which usually present a spherical, or in a minor extent ovoid-cylindrical morphologies. IB shape regularity can be explained by the nature of protein deposition in recombinant bacteria, in which the balance between deposited protein and protein removed from the IB surface, by a network of chaperones and proteases, determine the volumetric growth of the aggregate[32, 150]. Therefore, IB formation can be understood as the result of a destruction/reconstruction process occurring at the surface level of the aggregate suprastructure likely rendering their common spherical morphology[49].

In this scenario, the ClpP$^-$ bacterial cell environment would alter the mentioned balance. Thus, a part of the DnaK-mediated released polypeptides, prone to be proteolysed by ClpP, would aggregate again on the IB surface, generating a polar protrusion on the protein cluster. The unidirectional growth observed for ClpP$^-$ IB is probably due to the polar situation of the aggregate within the bacteria. It has been described that *E. coli* accumulates aggregated protein in the cell poles by an energy-dependent manner[151]. Therefore, the own bacterial cell wall could be acting as a steric impediment forcing the deposition of the unproteolysed polypeptides toward the inner site of the cell (**see figure 4C, results, paper 1**).

Interestingly we observed a significant difference when comparing proliferation of BHK (baby hamster kidney) and PC12 (rat adrenal pheochromocytoma) cells, cultured on two different types of IB-based nano-topographies, which were fabricated with

VP1GFP IB in either tear-shaped (ClpP$^-$) or spherical (DnaK$^-$) form. Cells cultured on ClpP$^-$ IBs showed faster proliferation than the ones cultured on spherical IBs. This fact was clearer for PC12 cells probably due to the low adhesion capability exhibited by this cell line, by which any improvement on the cell-substrate interaction would have a higher incidence. These data suggests that mammalian cells are able to sense and respond to distinct IB geometry opening the possibility of enriching IBs capability as biomaterial by producing genetically tailored particles.

According to this data, our group, in collaboration with Prof. Jaume Veciana´s team, from the department of molecular nanosciences and organic materials in the material science institute of Barcelona, further investigated IB structural tunability by analyzing several properties such as size, stiffness, zeta-potential, morphology and wettability in four different types of IBs. *E. coli* MC4100 (wt) strain and its defective mutants DnaK$^-$, ClpA$^-$ and ClpP$^-$ were used to produce IBs formed by the VP1GFP model protein. These strains have respective mutations inactivating key genes in the protein quality control network. As we previously speculated, the absence of these modulators, devoted to control protein quality and therefore intervening in protein deposition as IBs, significantly altered the aggregation pattern originating IBs with distinct structural properties (**see table 3**). Interestingly, besides the differences observed in the studied parameters' values, a general transition from monomodal to bimodal distributions was also observed for some properties such as stiffness or wettability, in IBs produced by DnaK$^-$ and ClpA$^-$ mutant strains, or to trimodal in the case of ClpP$^-$ IBs stiffness. These data reflect more than one population of structurally distinct IBs that can be formed during the same biofabrication process, adding a new degree of complexity to the produced particles. Thus, this study provides new insights to IB tailoring by demonstrating that IBs not only can be optimized regarding the content of biologically active protein, but also that their mechanical features at the nanoscale level can be genetically determined. Tissue engineering could take advantage of this mechanically tunable material since the different IB structures could lead to the modulation of the mechanotransductive cell response.

IB relevant properties regarding the genetic background of the fabricating strain.					
Phenotype	**Diameter (nm)**	**Stiffness populations (MPa)**	**Morphology**	**Z-potential (mV)**	**Contact angle at Maximum IB Coverage**
Wild-type	342	3,73	Spherical	-16,7	80°
DnaK$^-$	531	3,56 / 7,75	Spherical	-18,2	75°/>90°
ClpA$^-$	435	5,01 /10,99	Spherical	-17,8	60°/ >90°
ClpP$^-$	459	3,33/7,10/13,45	Tear-shaped	-26,5	60°/ >90°

Table 3. IB nanoscale properties. Values separated by bars indicate that more than one value was obtained for the same IB sample, suggesting the co-existence of different IB populations within the same biofabrication process**.**

2. IB-mediated cell growth mechanisms

Bacterial IBs have been successfully used to engineer micro- and nano-environment on cell culture surfaces. This results in a dramatic enhancement of substrate colonization[73]. by a mechanism not yet elucidated. In this regard, some studies performed on inert polymeric nanotopographies, generated by lithographic approaches, demonstrated the incidence of mechanical environmental stimulation[152], suggesting that an analogous mechanism could be acting for the cells cultured on IB-based topographies. In order to work out the mechanism by which IBs trigger cell colonization upon surface decoration, a battery of different cell types, each one with their own features and requirements, were analyzed when cultured on four structurally distinct IB-based topographies. Thus, despite that absolute cell number was higher for all the cell lines tested on every IB-based topography compared to nude polystyrene controls, two clear tendencies were observed when analyzing the relative cell numbers at the three different culture times (namely 24h, 48h and 72h). This allowed us to identify two differential behaviors exemplified by HepG2 and 1BR3.G cell lines (**see figure 1, results, paper 2**). On one hand an increase of the relative cell number at early culture times (24h) for both cell types was observed, suggesting a primary positive effect probably due to an enhanced cell adhesion. On the other hand, while the relative cell number is maintained nearly constant in the HepG2 case at the three tested times, an active induction of cell proliferation is observed for 1BR3.G cells, denoted by higher relative cell numbers at long cell culture times than at early cell cultures. This cell behavior leads us to speculate with a dual effect of IB-based topographies, namely bioadhesiveness and mechanical stimulation of cell proliferation. To further explore mechanical stimulation of cell proliferation, activation of ERK pathway was analyzed. In this regard, ERK has been proved a convenient reporter of cell growth activation by mechanical stimuli in independent studies [153, 154].. Accordingly with the previous results (**see figure 1, results, paper 2**) ERK in its active phosphorylated form was clearly detected for 1BR3.G cells growing on IBs while non-significant amounts were observed in the case of HepG2 cells. Additionally, bioadhesiveness of IB-based topographies was stronger for HepG2 cells than the one observed for 1BR3.G (**see figure 2, results, paper 2**).

All these data corroborates the dual effect provided by IB-based topographies, improving cell adhesion compared to cells cultured on polystyrene nude surfaces and actively stimulating cell growth via mechanotransductive events (**see figure 7**).

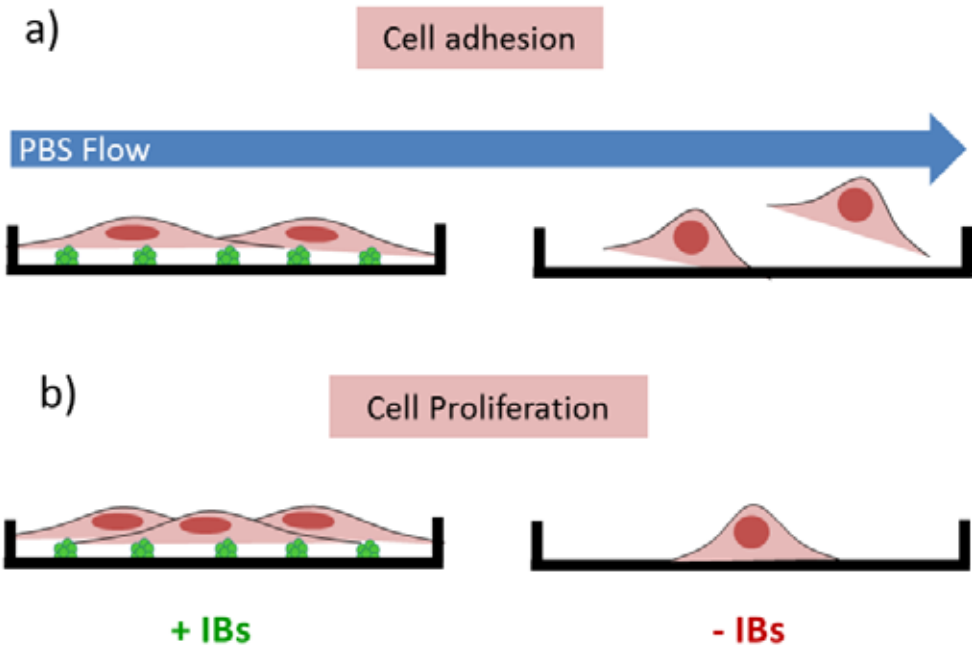

Figure 7 Representation of the dual effect provided by IB-based topographies being a) cell adhesion and b) cell proliferation responses

In this regard, as expected, global cell response is highly dependent on the nature of the tested cell line but interestingly it can also be modulated by the IB structural properties. Thus, the main physico-chemical properties influencing cell response in IB-based topographies are size, maximal stiffness and zeta potential. Therefore, in theory it would be possible to fabricate IB with physicochemical properties on demand depending on the final application of the biomaterial and the cell type requirements. However, despite the identification of some important features with incidence in cell surface colonization, IB tunability still presents major inconvenients since genetically determined IB biofabrication supposes a whole structural modification of the protein cluster that may alter at the same time several relevant particle features in an undesired manner. Thus, in order to overcome this limitation in the potential use of bacterial IBs, it would be highly advisable to generate in a near future a structural IB database, broad enough to screen in every application which structurally distinct IB join the best combination of properties to carry out each specific function. Alternatively, it would also be interesting

to explore chemical modifications to specifically modulate the desired particle feature. In addition, a deeper analysis of these results also raises bioadhesiveness as a characteristic feature of IB as biomaterial, since higher relative cell numbers are observed at early culture times in the four tested cell lines when cultured on IB-based topographies. On the contrary, those topographies are only able to actively enhance cell division rates depending on the specific cell line, as it has been observed by activated ERK detection.

From a tissue engineering point of view, IB protein biomaterials are able to generate topographies presenting physicochemical properties in the same range than the one found in natural tissue environments, probably better than other particulate materials explored for surface engineering such as ceramics or carbon nanotubes. In addition, the selective modulation of the two described independent effects exhibited by the different IB variants, and especially by $ClpP^-$ IBs, could be interesting in order to enrich primary cell cultures with defined cell types. Nevertheless, in general terms IB-based topographies have been shown to effectively increase cell surface colonization by enhancement of cell adhesion or the synergistic action of IBs bioadhesiveness and mechanotransduction-mediated cell growth activation. Therefore, IBs are a promising self-assembled protein material for tissue engineering.

3. MSCs response to IB-based topographies

Stem cells exhibit very promising properties in regenerative medicine such as their self-renewal capacity and their ability to generate multiple cell lineages. Therefore, important efforts have been carried out in order to influence stem cell gene expression and subsequently, cell response, with the aim of directing differentiation of these cells to specific cell types able to restore tissue or organ functionality. In this regard, many researchers have developed well defined nanotopographies to control cell response. For instance mesenchymal[155] and embryonic stem cells[156] have been shown to be affected in their self-renewal capacity and differentiation processes when cultured on nanotopographical modified environments. However, these studies have been often limited by the technical procedure used to obtain the 2D nanotopographies, being material dependent lithographic methods the most used. Thus, bacterial IBs could become a good alternative to generate nanotopographies able to direct stem cell response. IBs have been proved mechanically stable protein particles ranging from around 50 nm to 1000 nm in diameter. Additionally, their nanoscale properties have been shown tunable by the selection of the proper genetic background of the producing bacteria and by the modulation of production process variables such as temperature or expression time.

In this report we have explored the effect of IB nanotopographies, patterned on PCL, on MSCs response. MSCs are able to generate several cell lineages such as osteoblast, chondrocytes and adipocytes[84] while PCL is a degradable polymer extensively used to generate scaffolds for tissue engineering[157]. In this regard, our study has been focused in adding IB-based random surface nanostructure to the PCL in order to stimulate MSC differentiation. In this regard, other studies, show that MSC osteogenesis can occur in response to disordered nanotopographies fabricated by lithographical procedures[117].

IB-PCL topographies provide significant stimuli to MSCs in terms of cell spreading, metabolic activity and differentiation. These cells, when cultured on IBs, tend to establish large focal adhesions. Focal adhesions (FA) are protein complexes that connect the extracellular environment with the cell cytoskeleton providing cell anchorage to the

substrate, as well as a signaling platform from the extracellular matrix to inner cell. These structures have been shown to trigger non-receptor tyrosine kinases signaling pathways that regulate transcription factor activity being ERK signaling cascade one of them[158]. Thus, formation of focal adhesions is crucial for physical stimuli transduction and mechanotransduction-mediated MSC differentiation[159, 160] (**see figure 8**). Induction of osteogenesis by IB-based topographies was further observed by the detection of osteoespecific transcriptional markers such as Osteopontin. Significant up-regulations, relative to planar PCL controls, of this marker were observed for the four IB-based topographies tested at seven days of MSC cultures. The osteogenic capacity was additionally assessed by the immunodetection at 21 days of cell culture of the protein marker Osteopontin and Osteocalcin.

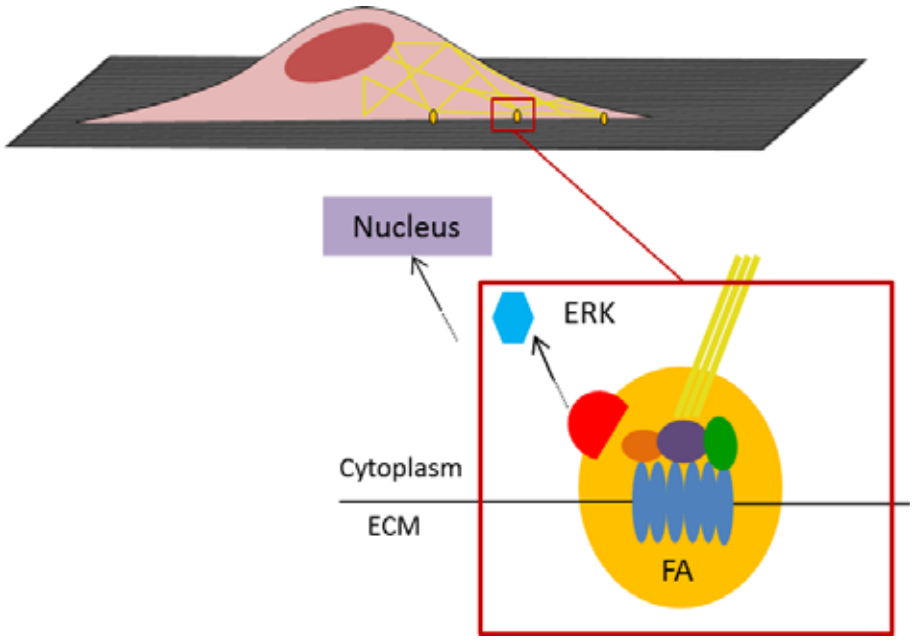

Figure 8 Simplified scheme of mechanotransduction signaling mediated by non-receptor tyrosine kinases.

Besides, activation of stem cell metabolism in response to differentiation has been also described[161] and it can represent a promising tool for stem cell response analysis, since these cells exhibit a low basal metabolism. In this regard, a general metabolic up-regulation was observed on the IB-based topographies. Interestingly, the metabolomics profiles obtained for carbohydrate, nucleotide and lipid metabolisms suggest an increased energy demand on the MSCs cultured on IB indicating a higher requirement of these cells to carry out the differentiation process. Moreover, despite

the overall aminoacid metabolic pathway remained unchanged, a deeper dissection of the data revealed differential up and down regulations of specific amino acids, probably due to the distinct proteins expressed by different lineages.

Finally, it is important to note that some IBs types performed better in terms of osteogenic induction, being ClpA$^-$ the genetic background providing the most osteogeneic IBs. These results are in agreement with previous studies in which structurally distinct IB induced differential cell responses depending on the tested cell type (**see results, paper 2**). In addition it has been proved that substrate stiffness play an important role in osteogenesis[162]. Thus, it would be expected that IBs with the highest elastic young modulus stimulate the strongest MSCs differentiation to osteoblasts. Although ClpA$^-$ IBs show higher stiffness than wt and DnaK$^-$ IBs, we would expect ClpP$^-$ to have the bigger influence in MSC differentiation. Nevertheless, ClpP$^-$ IBs were not observed to be firmly attached to the PCL as it can be observed by the absence of this type of IBs present under the cells (**see figure 4, results, paper 3**). Since there is no clear evidence of ClpP$^-$ IBs in the cell cytoplasm or partially internalized, contrarily to what is observed in the ClpA$^-$ IBs-based topographies and the particles have not been bunched around the cells it is plausible to think that a low adhesion of these particles to PCL has prompted their release to the cell media during the MSC spreading and therefore the low incidence of ClpP$^-$ IBs on ostegenesis would probably due to a reduced number of particles in contact with the cells. This fact could be easily overcome by immobilizing the particles to the substrate by for instance adding an elastomer such as poly(dimethylsiloxane) (PDMS), classically used in micro contact printing approaches acting as a sticky layer[163].

4. IB topographies as protein drug delivery platforms

Regenerative medicine and specifically tissue engineering applications have been benefited of the development in nanotopographical surface modulation to control cellular response[164]. Nevertheless, although physic stimuli have been shown crucial, cells in their natural niches are also exposed to biochemical signaling. In this regard, substrate functionalization or external supply of bioactive proteins, have been explored. Some examples are the use of epidermal growth factor (EGF)[128], fibroblast growth factor (FGF)[130], vascular endothelial growth factor (VEGF)[130], osteopotegerin[165], insulin like growth factor I (IGF)[166] and nerve growth factor β (NGF)[167] among others, in cell cultures to direct cell behavior. All these bioactive proteins have been shown to influence cell response in terms of cell growth and/or differentiation, key events in tissue engineering applications. Thus, the combined action of topographical modification and controlled delivery of bioactive protein would be a powerful tool in the regenerative medicine field.

In this context, bacterial IBs are protein aggregates in which amyloid like structure coexists with globular protein in several folding states. These nanoparticles have also been shown to retain a certain degree of biological activity, being the quality protein conformation of the forming polypeptides easily modulated by controlling parameters such as process variables like temperature or the genetic background of the producing strain. Moreover, our group has recently proved that IBs, fabricated with therapeutic proteins, when added in challenged cultures can rescue stressed cells by providing enough amount of bioactive protein to restore their functionality. In particular, four different proteins with distinct therapeutic activities, the enzymes dihydrofolate reductase and catalase, the chaperone Hsp70 and the leukemia inhibitory factor were fabricated as IB and tested in differently injured cultures. Moreover, also IB's tolerance was evaluated via oral administration of these nanopills in mice, observing no evidence of any toxic effect. Thus, IBs formed by therapeutic protein can be engineered as protein nanopills able to provide a steady availability of the active therapeutic agent (**see annex 4**). Very recently, another example of IBs used as carriers of bioactive protein was provided by Liovic and co-workers. Accordingly to our results they fabricated Keratin 14-formed IBs able to provide their bioactive forming protein to

epithelial cells[168]. All these data, coupled to the amyloidal properties of bacterial IBs suggested a similar mechanism than the natural delivery system observed for peptide hormones from amyloid reservoirs (secretory granules), with a slow release purpose in the endocrine system[14, 169].

In this work, we have proved that IB-based topographies formed by protein with potential therapeutic effects provide the bioactive forming protein (building blocks) in enough amounts to influence the cell response. Interestingly, we observed a high degree of IB cell penetrability without compromising the nanotopography integrity. This fact could explain protein bioavailability, particularly relevant in Hsp70 IB-based topographies since this protein function is carried out in the cell cytosol and nucleus[170]. Nevertheless, when comparing the effect of these IB between substrate delivery and by nanopills cell media supplement, we observed a clear higher effect on the second strategy. This fact it is probably due to the low adhesion capability of the model cell type used (HL60 cell line) in this experiment. Since these cells usually grow in suspension and are unable to spread, the cell-substrate contact is limiting the number of particles in contact with the cells and therefore the forming protein bioavailability. In addition, it is important to note that the amount of effectively attached IBs onto the plate surface is lower than the quantity of protein added to generate the IB-based topography (around 60% of the initial protein is retained). The rest is removed with the washing steps present in the fabrication procedure.

In order to corroborate these results, hFGF-2 IB based topographies were tested and compared to its nanopill strategy counterpart. In this regard, hFGF-2 has been shown to stimulate cell proliferation in starved NIH3T3 fibroblast cultures, among many other functions[171]. Noteworthy, unlike HL60 cells, NIH3T3 fibroblasts tend to strongly adhere to the cell culture surface exhibiting good levels of cell spreading. Sensibly with our previous hypothesis, we observed a higher extent of cell proliferation in serum-starved cells, cultured on hFGF-2 IB-based topographies. In this case, IB availability shouldn't be impaired by a low cell membrane-surface contact. Moreover the extra difference observed is probably due to a dual effect of the hFGF-2 IB based topographies, combining mechanical stimuli with the biological activity of the hFGF-2 protein. Interestingly, nanotopographies formed of both hFGF-2 and Hsp70 showed a

higher bioadhesiveness reinforcing the hypothesis of combined cell stimulation by both physical and biochemical cues.

The mechanism by which IBs release their building blocks is not fully understood. However, we have observed that IBs can provide bioactive polypeptides without compromising the mechanical integrity of the aggregates (**see figure 5, results, paper 4**). In addition, some studies have suggested a "cotton like" structure of bacterial IBs in which loosely linked building blocks would be expected to be released under physiological conditions[172]. On the other hand, the presence of amyloid fibrils has been extensively observed in this kind of aggregates. In this regard, an interesting study performed by Maji and co-workers showed how amyloids, produced from analogs of the gonadotropin-releasing hormone, were able to develop a sustained release of the peptide drug from the termini of the fibril. Moreover, the released peptides were found to be fully active upon their release[173]. All these data led us to hypothesize, based on the previously described cotton like architecture, an IB structure in which amyloid fibrils act as tensor agents devoted to preserve mechanical stability of the particle but also providing a scaffold where the globular protein could be trapped. Thus, other IB building blocks loosely attached could be released without compromising the structural integrity of the particle. In addition, a possible release from the termini of the amyloidal fibrils cannot be disregarded although given their relatively low presence it would probably suppose a secondary delivery pathway.

The possibility of generating scaffolds able to provide multifaceted stimuli combining adhesion, mechanical modulation and biochemical control of cell response could be the solution to fulfill third generation ideal biomaterials, being the control of the cell response at a molecular level a crucial function of them. In this regard, hybrid scaffolds, combining synthetic and natural materials are under constant investigation, as well as scaffolds with controlled release properties to deliver bioactive agents. All these studies provide an ever increasing spectrum of sophisticated materials very promising for tissue engineering applications. In this regard, IBs have been shown to be able to generate nanotopographies, increasing cell adhesion as well as providing mechanical stimuli in order to induce cell growth or control cell differentiation, additionally to their previously described utility as immobilized biocatalyzers (**see annex 5)**. In this study, we

prove how these topographies could incorporate an additional level of complexity and cellular response control, by the delivery of biochemical regulators. Therefore bacterial IB cell substrate coatings could be considered as a third generation biomaterial even if further research should be necessary for the clinical application of tissue engineering devices based on IB technology.

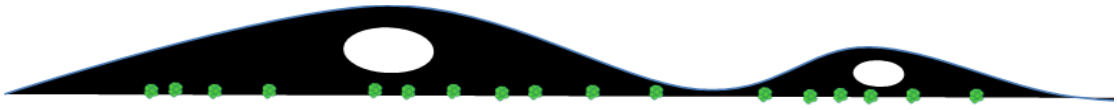

Conclusions

1. *E. coli* ClpP$^-$ strain is able to generate tear-shaped IBs, clearly distinct form the classical spherical-like geometries generally observed for these particles. In addition, we have provided evidence of altered physicochemical properties such as size, stiffness, z-potential and hydrophobicity in other *E. coli* strains defective for key regulators of the protein quality machinery such as ClpA and DnaK, when comparing with those observed in the wild type strain. Therefore, IBs are tunable in terms of morphology and physicochemical properties since these features are genetically determined.

2. Four mammalian cell lines used in this study have shown higher adhesion on IB-based topographies compared to those seeded on nude polystyrene surfaces. This fact indicates IB bioadhesiveness as an intrinsic feature of these nanoparticles that favor cell attachment when they are used for surface decoration.

3. Additionally, IB-based topographies have been shown to actively stimulate cell growth in two of the tested cell lines. It has been proved, by the analysis of the active form of the ERK protein, that such stimulation of cell division is related to a mechanical sensing of the IB-topography that triggers the signaling mechanotransductive cascade.

4. Both cell adhesion and stimulation of cell proliferation can be modulated by producing the nano-topography with physicochemically distinct IBs. Nevertheless, as expected, distinct cell lines respond in a different way to the IB-based topography being necessary to consider cell type requirements in order to direct the desired cell response.

5. IB-based topographies can stimulate osteogenesis in mesenchymal stem cells. In addition, the degree of stimulation have been shown to be linked to the physicochemical properties of the nanotopography-forming particles, being those based on ClpA$^-$ IBs the strongest inducer of the osteogenic response.

6. IB-guided MSC differentiation is an energetically demanding process that can be analyzed by metabolomic approaches.

7. IB-based topographies fabricated with proteins with therapeutic interest are able to rescue challenged cell cultures, improving cell viability in chemically induced apoptotic cells in the case of Hsp70 IBs, or stimulating cell growth under starvation conditions in the case of FGF-2 IBs. In this case the rescue was carried out by two simultaneous mechanisms: the stimulus to growth due to topography and the physiological effect of the therapeutic protein released from IBs

8. The intracellular activity of Hsp70 combined with the high degree of cell membrane penetrability of IB-based topographies prompt us to suggest bacterial IBs as a drug delivery system based in the sustained release of the IB active building blocks (the forming functional protein) into the growing cell.

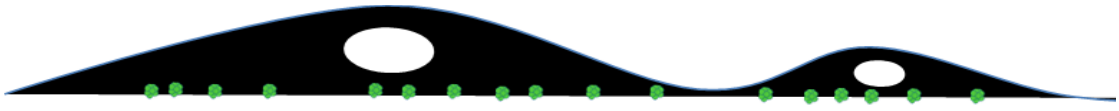

Annex

Annex 1

Disulfide Bond Formation and Activation of *Escherichia coli* β-Galactosidase under Oxidizing Conditions

Joaquin Seras-Franzoso, Roman Affentranger, Mario Ferrer-Navarro, Xavier Daura, Antonio Villaverde and Elena García-Fruitós

Applied and Environmental Microbiology, Vol 78, 2012

Applied and Environmental Microbiology

Disulfide Bond Formation and Activation of Escherichia coli β-Galactosidase under Oxidizing Conditions

Joaquin Seras-Franzoso, Roman Affentranger, Mario Ferrer-Navarro, Xavier Daura, Antonio Villaverde and Elena García-Fruitós

***Appl. Environ. Microbiol.* 2012, 78(7):2376. DOI: 10.1128/AEM.06923-11.**
Published Ahead of Print 27 January 2012.

AEM
Journals.ASM.org

Disulfide Bond Formation and Activation of *Escherichia coli* β-Galactosidase under Oxidizing Conditions

Joaquin Seras-Franzoso,[a,b,c] Roman Affentranger,[a]* Mario Ferrer-Navarro,[a] Xavier Daura,[a,d] Antonio Villaverde,[a,b,c] and Elena García-Fruitós[a,c]

Institut de Biotecnologia i de Biomedicina, Universitat Autònoma de Barcelona, Bellaterra (Cerdanyola del Vallès), Barcelona, Spain[a]; Departament de Genètica i de Microbiologia, Universitat Autònoma de Barcelona, Bellaterra (Cerdanyola del Vallès), Barcelona, Spain[b]; CIBER de Bioingeniería, Biomateriales y Nanomedicina (CIBER-BBN)[c]‡; and Institució Catalana de Recerca i Estudis Avançats (ICREA), Barcelona, Spain[d]

***Escherichia coli* β-galactosidase is probably the most widely used reporter enzyme in molecular biology, cell biology, and biotechnology because of the easy detection of its activity. Its large size and tetrameric structure make this bacterial protein an interesting model for crystallographic studies and atomic mapping. In the present study, we investigate a version of *Escherichia coli* β-galactosidase produced under oxidizing conditions, in the cytoplasm of an Origami strain. Our data prove the activation of this microbial enzyme under oxidizing conditions and clearly show the occurrence of a disulfide bond in the β-galactosidase structure. Additionally, the formation of this disulfide bond is supported by the analysis of a homology model of the protein that indicates that two cysteines located in the vicinity of the catalytic center are sufficiently close for disulfide bond formation.**

Since the inception of recombinant DNA technology, a large number of proteins of economic and therapeutic interest have been produced using *Escherichia coli* as a cell factory. The conformational quality of the proteins expressed is controlled by a complex network of chaperones and proteases, and in fact, this parameter determines the potential biotechnological use of the product obtained (31, 35, 50, 52).

Nowadays, the wide spectrum of cloning and gene expression vectors and mutant strains, and the knowledge of bacterial metabolism, allows the expression of an enormous range of proteins, whether prokaryotic or eukaryotic. Specifically, genetically modified *E. coli* strains have contributed significantly to the expression of soluble recombinant proteins, proving that the genetic background is extremely important for recombinant protein expression (29, 49, 50, 53). In this context, since prokaryotes have a reducing cytoplasm and since proteins that require disulfide bond formation to reach their functional conformation cannot be active under these conditions (9), many strategies have been developed for the production in *E. coli* of proteins containing disulfide bonds in their stable native structure (7). It has been reported that a considerable number of factors are involved in the thiol-disulfide balance in the *E. coli* cytoplasm (37); the thioredoxin system (which consists of thioredoxin reductase [encoded by *trxB*] and thioredoxin [*trxA*]) and the glutaredoxin system (which consists of glutaredoxin reductase [*gor*], glutathione [*gshA*, *gshB*], and three glutaredoxins [*grxA*, *grxB*, *grxC*]) are the main pathways (32, 37). One of the most common approaches that allow the folding of proteins requiring the formation of disulfide bridges is the use of the Origami strain. Origami (*gor trxB* mutant) is a double mutant strain in which the thioredoxin/glutaredoxin reductase pathway is knocked out, resulting in an oxidizing cytoplasm, compatible with the folding of proteins whose structure and function depend on the correct formation of cysteine-cysteine bridges (7). Besides the use of the Origami strain as a host cell, other strategies are also used to promote the production of proteins with disulfide bonds in bacteria. Since the periplasm is an oxidizing compartment, the export of proteins from the cytoplasm to the periplasm is a widely used alternative (23, 31). In many cases, however, this strategy results in a lower protein yield than that obtained by expression in the cytoplasm. It has also been shown that, in addition to producing the protein in an Origami strain or in the periplasm to allow the formation of disulfide bonds (27), the fusion of solubilizing carriers (e.g., Sumo) to the desired protein can improve the quality of the expressed protein (53). Another frequently used method is the coexpression of chaperones/foldases during the production process (44).

Disulfide bond formation is, in many cases, essential for the production of functional proteins (5, 9, 38, 47) and, in other situations, for the improvement of folding and therefore for enhancement of the activity of the desired protein (1). Although disulfide bonds are rarely formed in bacterial cytoplasmic proteins, there are some surprising exceptions to this general rule (1, 18, 28, 51). In this context, some studies performed by our group (unpublished data) and data published by others (39, 46) seem to suggest that thiols inactivate *E. coli* β-galactosidase. It is noteworthy that all the known structures of β-galactosidase have been solved in the presence of the reducing agent dithiothreitol (DTT) (19–21), and the activity and structure of β-galactosidase have never been explored under oxidizing conditions. *E. coli* β-galactosidase (EC 3.2.1.23) forms a tetramer and has been one of the most widely used reporter enzymes for many applications, such as analysis of the regulation of gene expression, characterization of protein function/structure, and analysis of target gene expression (6, 48). On the other hand, bacterial β-galac-

Received 20 September 2011 **Accepted** 11 January 2012
Published ahead of print 27 January 2012
Address correspondence to Elena García-Fruitós, efruitos@ciber-bbn.es.
* Present address: R&D, Douglas Connect, Zeiningen, Switzerland.
‡For this virtual institution, see http://www.ciber-bbn.es.

doi:10.1128/AEM.06923-11

tosidases also have enormous potential in the food industry (14, 16). Moreover, β-galactosidase can hydrolyze not only lactose, resulting in glucose and galactose, but also other substrates, yielding colored products, thus making the enzyme a suitable reporter for the applications mentioned. Considering the enormous potential of β-galactosidase and the possible effects of redox conditions on protein functionality, we decided to investigate whether a suitable genetic background might improve its folding. In this study, we measured the activities of a recombinant *E. coli* β-galactosidase (rβ-galactosidase) in two *E. coli* strains: a wild-type and an Origami strain. A recombinant green fluorescent protein (rGFP), which does not form any disulfide bond, was used as a control in all the experiments performed. Our data show that the specific enzymatic activity of β-galactosidase is unexpectedly improved under oxidizing conditions and strongly support the idea that cysteines 500 and 536 of *E. coli* β-galactosidase form a disulfide bond *in vivo* when produced in the Origami strain.

MATERIALS AND METHODS

Strains and plasmids. The *Escherichia coli* strains used in this work were the K-12 derivatives MC4100 [*araD139* Δ(*argF-lac*)*U169 rpsL150 relA1 flbB5301 deoC1 ptsF25 rbsR* Str^r] (43), Origami 2 [Δ(*ara-leu*)*7697* Δ*lacX74* Δ*phoA PvuII phoR araD139 ahpC galE galK rpsL* F′[*lac*$^+$ *lacI*^{q} *pro*] (DE3) *gor522*::Tn*10 trxB* Str^r Tet^r] (bioNova Cientifica s.l.), and XL10-Gold {Tet^r Δ(*mcrA*)*183* Δ(*mcrCB-hsdSMR-mrr*)*173 endA1 supE44 thi-1 recA1 gyrA96 relA1 lac* Hte F′[*proAB lacI*^{q}ZΔM15 Tn*10*(Tet^r) Kan^r]] (Stratagene).

The plasmids used were pTVP1LAC (Ap^r) and pTVP1GFP (Ap^r) (10), encoding rβ-galactosidase and rGFP, respectively, fused to the foot-and-mouth disease virus VP1 capsid protein. The expression of recombinant genes in both plasmids is under the control of an isopropyl-β-D-thiogalactoside (IPTG)-inducible *trc* promoter.

Culture conditions, cell disruption, and cell fractionation. Protein was produced in shake flask bacterial cultures growing at 37°C and 250 rpm in rich LB medium (43) with the required antibiotics. Once the absorbance at 550 nm reached 0.5, gene expression was induced by addition of 1 mM IPTG. Cell samples were collected 2 h later for further analysis. Data were obtained from three or more independent experiments and were submitted to a *t* test analysis.

Protein fractionation. Cells from 2-ml culture samples were collected by low-speed centrifugation at 4°C (15 min at 15,000 × *g*) and were resuspended in 500 μl phosphate-buffered saline (PBS) buffer with protease inhibitor cocktail (reference no. 1,836,170; Roche). These samples were disrupted with a MagNA Lyser instrument (Roche) for 20 s at 3,000 rpm. After centrifugation at 4°C for 15 min at 15,000 × *g*, the supernatants were collected and were used directly for analysis of the soluble protein.

Determination of fluorescence and specific fluorescence. Fluorescence was measured in a Cary Eclipse fluorescence spectrophotometer (Varian) at 510 nm by using an excitation wavelength of 450 nm. Fluorescence measurements were carried out in triplicate and were corrected by either biomass or amounts of rGFP (determined as described below).

Determination of enzymatic activity and specific enzymatic activity. β-Galactosidase activity was determined in PBS through a variant of Miller's protocol (33) by monitoring the colorimetric signal produced by *ortho*-nitrophenyl-β-galactoside (ONPG) degradation at 420 nm. To determine the presence of disulfide bonds, a β-galactosidase enzymatic assay was performed with increasing concentrations of DTT (10 mM and 20 mM) and in the absence of reducing agents. The results presented are averages for at least three independent experiments. Activity values are corrected by either biomass or amounts of rβ-galactosidase protein (determined as described below).

Quantitative protein analysis. Samples were diluted in denaturing buffer (26) at appropriate ratios. After the soluble fraction was boiled for 15 min and the total fraction for 30 min, samples were loaded onto denaturing gels for Western blot determination, using as primary antibodies a polyclonal serum against GFP (Santa Cruz Biotechnology) or a polyclonal serum against β-galactosidase (MP Biomedicals, Inc.), depending on the protein to be analyzed. The secondary antibody was always an anti-rabbit antibody (Bio-Rad). Once the blots were dried, they were scanned at high resolution, and bands were quantified with Quantity One software (Bio-Rad), using known concentrations of commercial GFP or β-galactosidase as controls. Protein concentrations were used to calculate specific activity or fluorescence.

Native gels. To determine disulfide bond formation, rβ-galactosidase (135-kDa) samples in either 0.25 M Tris-HCl–87% glycerol–6 mg bromophenol blue and distilled water or a 20 mM DTT buffer (25) were incubated at 37°C for 15 min and were loaded onto a nondenaturing 6% polyacrylamide gel for Western blot determination as described above. Three replicas were loaded onto each gel (25), and samples A and B were run in the same gel under the same exact conditions. As a reference (C+), we used a commercial *E. coli* beta-galactosidase with a molecular mass of 116 kDa.

Modeling. Homology models of the β-galactosidase used in this work were constructed using MODELLER 9v2 software (42). As a template structure, we used the coordinates of the *E. coli* β-galactosidase with entry 1JYV (19) in the Brookhaven Protein Data Bank (PDB). In what follows, we adhere to the numbering of residues corresponding to the sequence deposited for 1JYV. Alignment of the 1,011 residues (R13 to K1023) covered by 1JYV to the sequence of the protein used in this work results in 983 (97.2%) identical residues. We computed 50 different homology models of the reduced β-galactosidase using a very thorough VTFM (variable target function method with conjugate gradient) schedule and very thorough molecular dynamics refinement (molecular dynamics with simulated annealing). The following settings of MODELLER's automodel class were used: library schedule, autosched. slow; max_var_iterations, 300; md_level, refine_very.slow; repeat_optimization, 5; max_molpdf, 1e6. The resulting models were ranked using the discrete optimized protein energy (DOPE) potential (45).

The part of the β-galactosidase sequence covered by the alignment with 1JYV contains 15 cysteine residues. Generating the distance matrix of all pairs of cysteine sulfur atoms, we identified two pairs separated by a distance of <1 nm: C500-C536 (0.52 nm) and C389-C402 (0.68 nm). To evaluate the structural changes involved in, and possibly necessary for, disulfide bond formation, we generated 50 homology models incorporating either the disulfide bond C500-C536 alone or both C500-C536 and C389-C402 simultaneously. In both cases, the same settings were used as in the calculation of the homology models of the reduced form of the protein. Again, the resulting models were scored using the DOPE potential.

β-Galactosidase mutagenesis. A single mutation in C500 of rβ-galactosidase was carried out by inverse PCR producing a single nucleotide replacement (Cys to Ala). The PCR primers used were CCACCGATATT ATTGCCCCGATGTACGCGC (forward) and GCGCGTACATCGGGG CAATAATATCGGTGG (reverse) (underlining indicates nucleotides that change Cys to Ala).

The PCR product was then treated with DpnI for 2 h at 37°C to remove parental DNA and was transformed into *E. coli* XL10-Gold cells. Positive clones were selected by sequencing and were transformed to the *E. coli* MC4100 and Origami strains for further analysis.

Chemical modification of β-galactosidase. β-Galactosidase was reduced by adding 2 μl of a 44 mM DTT solution to 2 μl of a solution containing 4 μg of β-galactosidase. Reduction was performed for 1 h at 37°C. β-Galactosidase was oxidized using 4 mM H_2O_2 at room temperature as follows: 2 μl of 8 mM H_2O_2 (in 100 mM NH_4HCO_3) was added to a 2-μl solution containing 4 μg of β-galactosidase. For β-galactosidase carboxamidomethylation, three different samples were treated with iodoacetamide (IAA): β-galactosidase in Milli-Q water, β-galactosidase treated with DTT, and β-galactosidase treated with H_2O_2. Two microli-

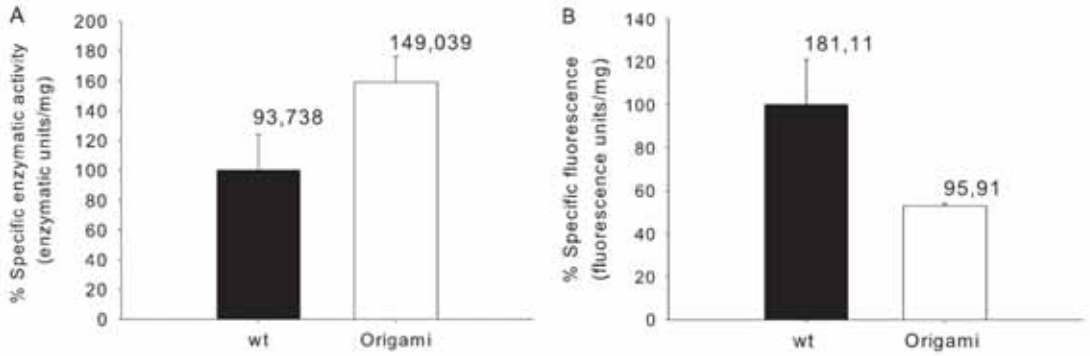

FIG 1 Specific biological activity (measured by either absorbance or fluorescence). The specific activities of rβ-galactosidase (A) and rGFP (B) produced in both the wild-type (wt [MC4100]) and Origami *E. coli* strains were determined. The absolute values for biological activity are given above the bars. The *P* values, obtained by a *t* test, are 0.184 (A) and 0.060 (B).

ters of each sample was incubated with iodoacetamide at a final concentration of 100 mM in 50 mM NH_4HCO_3.

Proteolytic degradations of β-galactosidase and its carboxamidomethylated derivatives were carried out in 50 mM NH_4HCO_3, pH 8. Trypsin (Promega, Madison, WI) was added to a final enzyme-to-substrate ratio of 1:50. Digestions were performed for 3 h at 37°C. The reactions were terminated by adding trifluoroacetic acid (TFA) to a final concentration of 0.2%.

MS analysis. For matrix-assisted laser desorption ionization (MALDI) analysis, 1 μl of sample was mixed with the same volume of a saturated solution of α-cyano-4-hydroxy-*trans*-cinnamic acid matrix (0.3 mg/ml in H_2O–acetonitrile–TFA at 6:3:1), and the mixture was spotted onto a MALDI target plate (Bruker Daltonics, Bremen, Germany). The drop was air dried at room temperature. MALDI mass spectra were recorded in the positive-ion mode on an Ultraflex Extreme time-of-flight instrument (Bruker Daltonics, Bremen, Germany). Ion acceleration was set to 25 kV. All mass spectra were externally calibrated using a standard peptide mixture containing angiotensin II (1,046.54), angiotensin I (1,296.68), substance P (1,347.74), bombesin (1,619.82), rennin substrate (1,758.93), adrenocorticotropic hormone fragment residues 1–17 (2,093.09), adrenocorticotropic hormone fragment residues 18–39 (2,465.20), and somatostatin 28 (3,147.47). Calibration was considered good when a value below 1 ppm was obtained. The spectra were processed using Flex Analysis software, version 2.2 (Bruker Daltonics). The SNAP algorithm included in the software was used to select the monoisotopic peaks from the isotopic distributions observed. For peptide mass fingerprinting (PMF) analysis, the MASCOT search engine (Matrix Science, London, United Kingdom) was used with the following parameters: one missed cleavage permission, 50-ppm measurement tolerance, and at least four matching peptide masses. Positive identifications were accepted with *P* values lower than 0.05. In the searches, methionine residues modified to methionine sulfoxide were allowed, and cysteine residues were allowed to be reduced and alkylated by iodoacetamide to carboxyamidomethyl cysteine wherever necessary. For tandem mass spectrometry (MS-MS) analysis, the same equipment was used. For database searches, the MASCOT search engine was also used with 50 ppm of error in MS and 0.3 Da in MS-MS. Modification of methionine sulfoxide and carboxyamidomethyl cysteine was also allowed in the searches.

RESULTS

Although both Reithel and coworkers and Shifrin and collaborators reported that β-galactosidase is rapidly inactivated in the presence of thiols (39, 46), the possible presence of a disulfide bond in the enzyme structure had never been explored in detail before.

Therefore, in this study, we have analyzed the effect of the oxidizing/reducing background on the structure and functionality of *E. coli* β-galactosidase by measuring the specific activity of the enzyme under both conditions, when expressed in an Origami strain and in a wild-type strain (Fig. 1A). Interestingly, rβ-galactosidase exhibited higher specific activity in the Origami strain than in the wild-type strain (Fig. 1A), showing that the mutations in thioredoxin reductase and glutaredoxin reductase clearly have a positive effect on its activity. On the other hand, when determining the specific fluorescence of rGFP, used as a control, we observed that the protein produced in the *E. coli* wild-type strain showed a higher specific fluorescence than that produced in the Origami strain (Fig. 1B). This observation indicates that the increase in the specific activity of protein is not a general event that takes place in the Origami cytoplasm but a specific fact related to the redox environment.

Analyzing the amount of soluble protein produced under each condition, we observed that larger amounts of both rGFP (Fig. 2B) and rβ-galactosidase (Fig. 2A) are produced in the Origami strain than in the wild-type strain (Fig. 2B). Therefore, the expression of this bacterial β-galactosidase in an oxidizing environment resulted not only in higher specific activity (Fig. 1A) but also in a higher soluble protein yield (Fig. 2A). Additionally, although the soluble protein yield improves when the Origami strain is used, the total-protein yield obtained is lower (7.28 $\pm$ 1.28 ng/μl) than that in the wild-type strain (21.77 $\pm$ 4.17 μg/μl), indicating that the degree of aggregation of rβ-galactosidase is much higher under reducing conditions. Thus, we can conclude that by using oxidizing conditions, it is also possible to enhance solubility, avoiding, at least partially, the formation of protein aggregates known as inclusion bodies (10).

Since the data presented here indicate that an oxidizing background favors *E. coli* β-galactosidase activity and productivity and that this could be related to the formation of a disulfide bond, we decided to study the possible presence of one or more cysteine-cysteine bridges in rβ-galactosidase when expressed in the Origami strain. For that purpose, native polyacrylamide gels under reducing and nonreducing conditions were analyzed in order to determine, by an alternative method, the eventual formation of disulfide bonds in rβ-galactosidase. Proteins containing cysteine-cysteine bridges (oxidized form) migrate faster on a nondenatur-

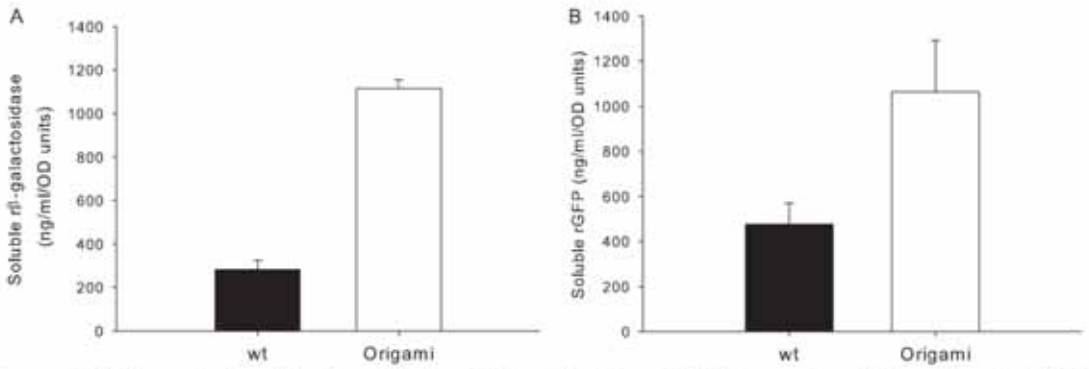

FIG 2 Amounts of soluble protein observed by Western blotting. rβ-Galactosidase (A) and rGFP (B) were produced in the wild-type (wt [MC4100]) and Origami strains. The *P* values, obtained by a *t* test, are 0.056 (A) and 0.076 (B).

ing gel than proteins in the reduced form (8, 9, 36), due to decreases in hydrodynamic volume and flexibility (24). Then, as presumed (8, 36), and considering that protein migration on native gels depends not only on the molecular weight but also on the conformation of the protein, in the absence of a reducing agent, the mobility of the reduced protein was clearly lower than that of the protein produced in the Origami strain (Fig. 3A). Thus, the results obtained prove that the redox environment during protein expression can modify the protein conformation, presumably by the formation of the target disulfide bond.

Interestingly, the differences observed in protein mobility between the two strains strongly decreased in the presence of DTT (Fig. 3B). Therefore, since the difference observed in protein migration is due to a modification of production parameters, but not of the protein amino acid sequence, all these data fit with the possible presence of a disulfide bond in the β-galactosidase structure.

To additionally confirm better protein folding in Origami cells, we monitored the enzymatic activity of the enzyme with and without DTT. We evaluated the enzymatic activity of rβ-galactosidase at different DTT concentrations, ranging from 0 to 20 mM. In Fig. 4 we show that, as previously reported, in the absence of DTT, *E. coli* rβ-galactosidase produced in the Origami strain exhibited higher activity than that produced in the wild-type strain. Moreover, our results also show that rβ-galactosidase activity was significantly reduced in the presence of increasing concentrations of DTT and that this reduction was more progressive in the Origami than in the wild-type strain (Fig. 4). Catalytic activity decreased in both cases in the presence of increasing concentrations of DTT, reaching the same specific activity value at 20 mM DTT (Fig. 4). Although this reduction was more marked in the Origami strain, wild-type β-galactosidase is also affected by the presence of this reducing agent. This could indicate that even in a reducing environment, such as *E. coli* cytoplasm, a fraction of the enzyme produced forms disulfide bonds, as has been reported for other proteins (1, 18, 28, 51) and as might also occur with the natural β-galactosidase protein.

To further investigate the possible formation of disulfide bonds in *E. coli* β-galactosidase, we modeled this protein under oxidizing and reducing conditions. As expected from the very large number of identical residues between the rβ-galactosidase used in this work and the sequence covered by PDB entry 1JYV (19), the homology models computed for the reduced form and 1JYV are structurally nearly identical (Fig. 5A). Interestingly, incorporation of a disulfide bond between cysteines 500 and 536 does not require large conformational changes. In fact, both in the model of the reduced form and in 1JYV, with a simple rotation

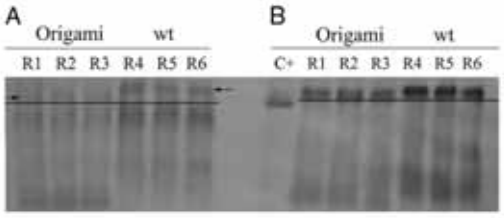

FIG 3 Nondenaturing polyacrylamide electrophoresis gel of rβ-galactosidase produced in the wild-type (wt [MC4100]) and Origami strains. Gels were analyzed in the absence (A) or presence (B) of the reducing agent DTT. R1, R2, and R3 correspond to three Origami replicas, while R4, R5, and R6 correspond to three replicas from the wild-type strain. C+ corresponds to a commercial *E. coli* β-galactosidase. Arrows indicate the positions of the electrophoretic bands.

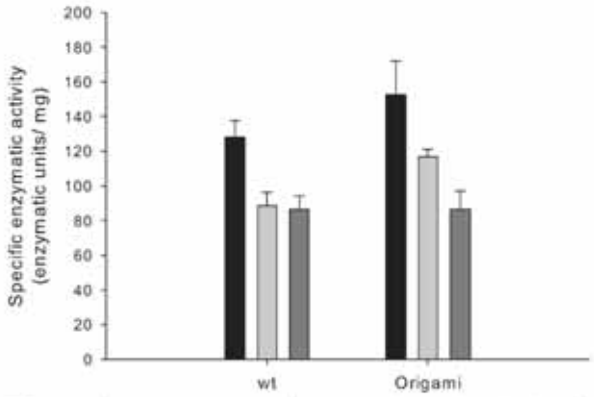

FIG 4 Specific enzymatic activities of rβ-galactosidase produced in the wild-type (wt [MC4100]) and Origami strains. Specific activity was determined without DTT (filled bars) and with increasing concentrations of DTT: 10 mM (light shaded bars) and 20 mM (dark shaded bars). The *P* values, obtained by a *t* test, are 0.028 for the wt strain and 0.043 for the Origami strain.

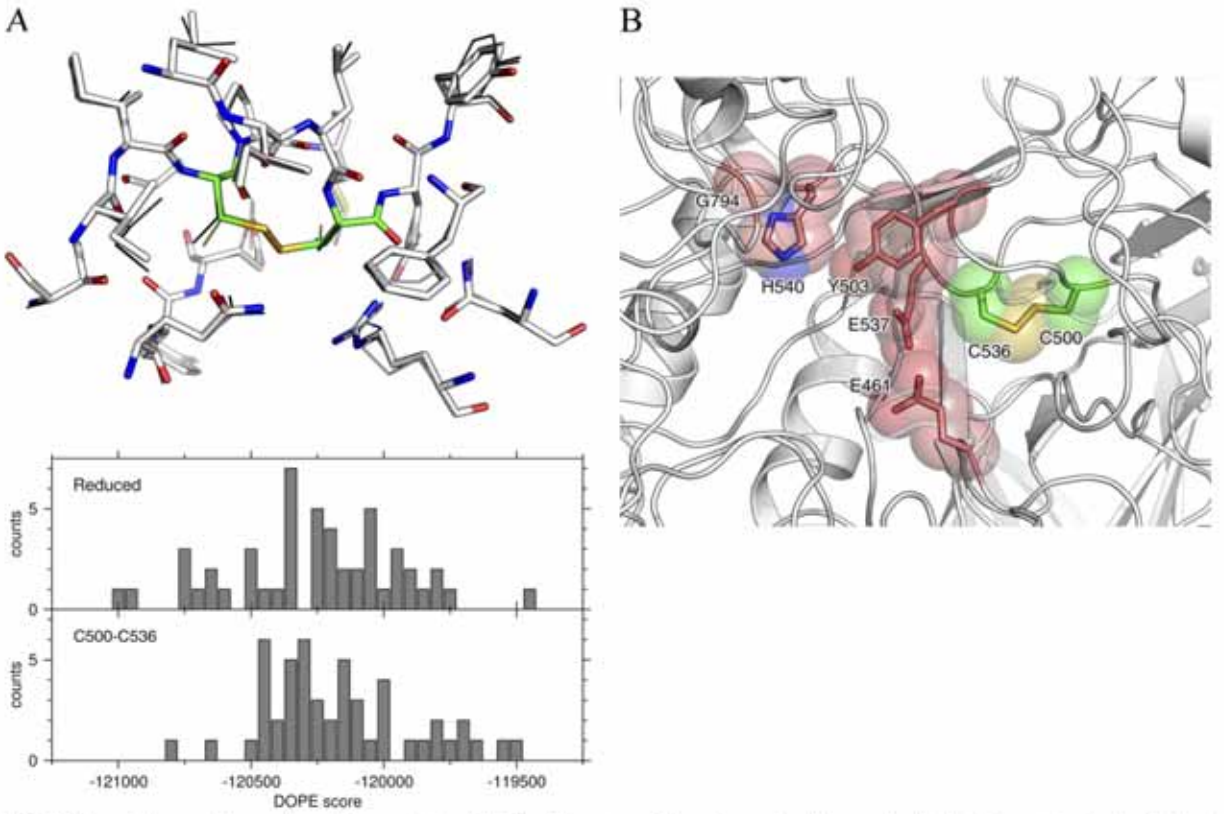

FIG 5 β-Galactosidase modeling under oxidizing conditions. (A) (Top) Illustration of the conformational changes involved in the formation of a disulfide bond between cysteines C500 and C536. Represented are the residues with a minimum distance of <0.5 nm from the two cysteines. The carbon atoms of C500 and C536 are shown in green, and those of all other residues are displayed in white. Oxygen, nitrogen, and sulfur atoms are colored red, blue, and yellow, respectively. Thick sticks represent the best model (according to its DOPE potential) with the disulfide bond formed; thin sticks represent the best model of the reduced form. The template structure (PDB entry 1JYV) is drawn with black lines. (Bottom) Histograms of the DOPE scores of the 50 models obtained for reduced β-galactosidase and of the 50 models obtained with the disulfide bond between C500 and C536. (B) Illustration of the close proximity between the C500-C536 disulfide bond and the active-site residues (E461, Y503, E537, H540, G794). The β-galactosidase backbone is drawn as a white cartoon representation. The side chains of the two cysteine residues involved in the disulfide bond (green) and of the active-site residues (light red) are shown as solid sticks surrounded by semitransparent spheres. Oxygen, nitrogen, and sulfur atoms are colored red, blue, and yellow, respectively.

around the side chain (C-C_{α}-C_{β}-S) dihedral angle of the cysteine residues in question, the two sulfur atoms can easily be brought within bonding distance. The atomic packing in the surrounding region is even low enough to allow such a position without atomic overlaps. Therefore, not surprisingly, the quality of the models (according to the DOPE potential) with a disulfide bond connecting residues 500 and 536 cannot be distinguished from that of the models of the reduced form of the protein (Fig. 5A).

The situation is different for the second disulfide bond whose formation was explored (C389-C402). Although the two sulfur atoms are only slightly farther apart in the reduced models than those for the C500-C536 pair (0.68 nm in the former; 0.52 nm in the latter), disulfide bond formation is more difficult, because the two residues are already oriented toward each other. Thus, it can be anticipated that the disulfide bond between C389 and C402 cannot be formed without distorting the backbone conformation at least locally. Indeed, defining a standard disulfide bond (with a bond length of 0.2 nm) between the two sulfur atoms for the modeling procedure was not sufficient to bring them closer than 0.24 nm (results not shown). While this does not exclude the possibility of disulfide bond formation between C389 and C402, it indicates that a disulfide bond would not be formed as easily as between C500 and C536.

These modeling calculations strongly suggest that at least the disulfide bond between cysteines 500 and 536 could be formed in a nonreducing environment. That the presence of this disulfide bond might affect the activity of β-galactosidase is indicated by its proximity to the catalytic center of the enzyme (Fig. 5B). C536 is adjacent to glutamate 537, and C500 is very close in sequence to tyrosine 503. The rigidity of this part of the active site brought about by the formation of the disulfide bond might increase the activity of the protein, in accordance with the experimental data obtained (Fig. 1A). Indeed, rigidity appears to be an evolutionarily favored characteristic of enzymatic active sites, since active sites have been shown to be significantly more rigid than other protein regions (3, 55). In this case, E537 acts as the nucleophile of the hydrolysis reaction catalyzed by β-galactosidase (11, 54), while Y503 plays the role of an acid catalyst for the cleavage of the covalent bond between E537 and galactose (34, 40, 41). These two catalytic residues act cooperatively on the same step of the hydro-

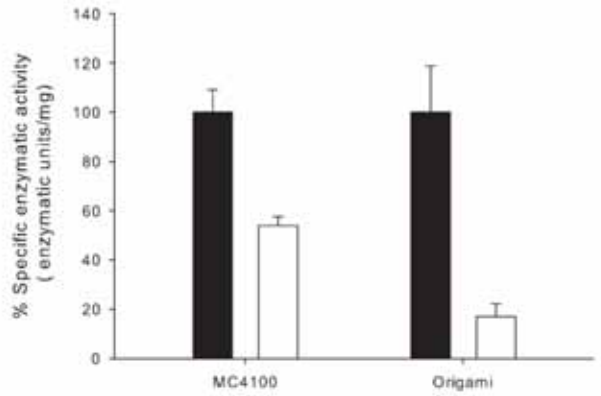

FIG 6 Specific activities of rβ-galactosidase (filled bars) and rβ-galactosidase C500A (open bars). rβ-Galactosidase activities (expressed as the percentage of β-galactosidase activity in rβ-galactosidase C500A with respect to the activity of wild-type rβ-galactosidase) were determined in both the wild-type (wt [MC4100]) and Origami *E. coli* strains. The *P* values, obtained by a *t* test, are 0.086 for the wt and 0.040 for the Origami strain.

lysis reaction (41), and rigidification of their relative positions by a disulfide bond could explain the increased activity of the protein when expressed under oxidizing conditions.

Since the results obtained seem to indicate that cysteines 500 and 536 play a key role in the formation of a disulfide bond, and since it is widely accepted that the mutation of one of the two cysteines is sufficient to determine the formation of a disulfide bond (13), C500 was changed to Ala. The results show that the specific activity values observed for the mutated rβ-galactosidase are lower than those observed for the wild-type enzyme (Fig. 6). Interestingly, we observed that this decrease is particularly marked in the Origami strain (around 85%). Thus, all these data, in agreement with all the previous results, strongly support the involvement of C500 and C536 in the formation of a disulfide bond. It should be noted that involvement of this cysteine in a disulfide bond other than that proposed is unlikely without a large rearrangement of the monomeric protein structure.

Furthermore, in order to finally confirm the presence of a disulfide bond between C500 and C536, a method based on mass spectrometry was used (2). To obtain the peptide maps, β-galactosidase in Milli-Q water, DTT-reduced β-galactosidase, and H_2O_2-oxidized β-galactosidase were carboxamidomethylated and were subsequently cleaved proteolytically with trypsin. The resulting peptide mixtures were analyzed by MALDI-MS peptide mapping. Trypsin cleavage yielded a pattern of 55 different peptides. Both cysteine residues 500 and 536 were found completely alkylated in the reduced sample as well as in β-galactosidase in Milli-Q water (Fig. 7). This indicated that these two cysteine residues are not involved in the formation of a disulfide bridge under these conditions. In order to assign these ion signals unequivocally, their MS-MS spectra were obtained (Fig. 7). MALDI-MS peptide mapping after tryptic digestion of the oxidized β-galactosidase and the oxidized and alkylated β-galactosidase showed the presence of almost all individual peptides except for the two ion signals containing residues C500 (*m/z*, 3,127.51 Da) and C536 (*m/z*, 3,188.671 Da) (Fig. 8A). The absence of these signals indicates that these two cysteines are linked with a disulfide bridge under these conditions. Furthermore, an ion signal of 6,234.546 Da was detected (Fig. 8B) and was assigned as a disulfide-bonded dipeptide containing the peptides 447-SVDPSR PVQYEGGGADTTATDIICPMYAR-505 and 523-WLSLPGETR PLILCEYAHAMGNSLGGFAK-551, where the two methionine residues have undergone oxidation.

DISCUSSION

Since it is widely accepted that the formation of cysteine-cysteine bridges is favored under oxidizing conditions, disulfide bonds of recombinant proteins usually cannot be formed in the reducing cytoplasm of bacteria. Thus, *E. coli* mutant strains lacking the main components of the redox pathway are widely used in order to produce heterologous proteins that require a proper oxidation status of cysteine residues to attain their native structures. In fact, the oxidation of cysteines in the *E. coli* cytoplasm is highly disfavored, due not only to the low redox potential but also to the absence of enzymes that catalyze protein thiol oxidation in the cytoplasm (4). In this context, it is generally accepted that the double mutant TrxB$^-$ Gor$^-$ strain (Origami), which has an intracellular environment shifted toward a more oxidative state, is the most useful cell factory for the production of proteins that contain disulfide bonds (22) and a good tool for understanding the role of disulfide bond formation in recombinant proteins.

On the other hand, β-galactosidase is a tetrameric bacterial protein of four identical subunits essentially composed of α-helices (17) that has been used as a reporter for many years. In this study, we report for the first time that the *E. coli* β-galactosidase enzyme forms a disulfide bond when produced in an oxidizing background, such as the cytoplasmic environment provided by the *E. coli* Origami strain. In this context, our model suggests not only that a disulfide bond is formed but also that it is located close to the catalytic center. Our results prove that β-galactosidase produced in the Origami strain shows the highest specific activity, suggesting that the absence of thioredoxin reductase and glutaredoxin reductase clearly improves the microbial enzyme activity. In a previous study, Derman and Beckwith (8) used a TrxB$^-$ mutant strain to produce β-galactosidase, observing a decrease in the enzymatic activity of this strain compared to that of the control. This behavior could be explained by considering that it is not clear that proteins containing disulfide bonds are successfully produced in a TrxB$^-$ strain. The cytoplasm of this strain is at least partially reducing due to the presence of the still-functional glutathione reductase (15), which has overlapping functions with thioredoxin reductase in preventing disulfide bond formation (1). Therefore, our data also confirm, as reported in the literature, that the formation of disulfide bonds is more favorable in the cytoplasm of a TrxB$^-$ Gor$^-$ mutant strain than in that of a TrxB$^-$ mutant strain (4).

Although solubility has been taken universally as an indicator of protein conformational quality, it has been proposed recently that specific activity, and not solubility, should be used as a marker of protein quality (12). It has also been shown recently that conditions that enhance protein quality often reduce the final amounts of protein produced (12, 30). The comparative analysis performed in this study, surprisingly, shows that conformational quality and solubility are improved simultaneously when *E. coli* rβ-galactosidase is expressed in the Origami strain. In contrast to that observation, it has been reported that both parameters cannot be improved simultaneously for proteins that do not need post-translational modifications (30), such as disulfide bond forma-

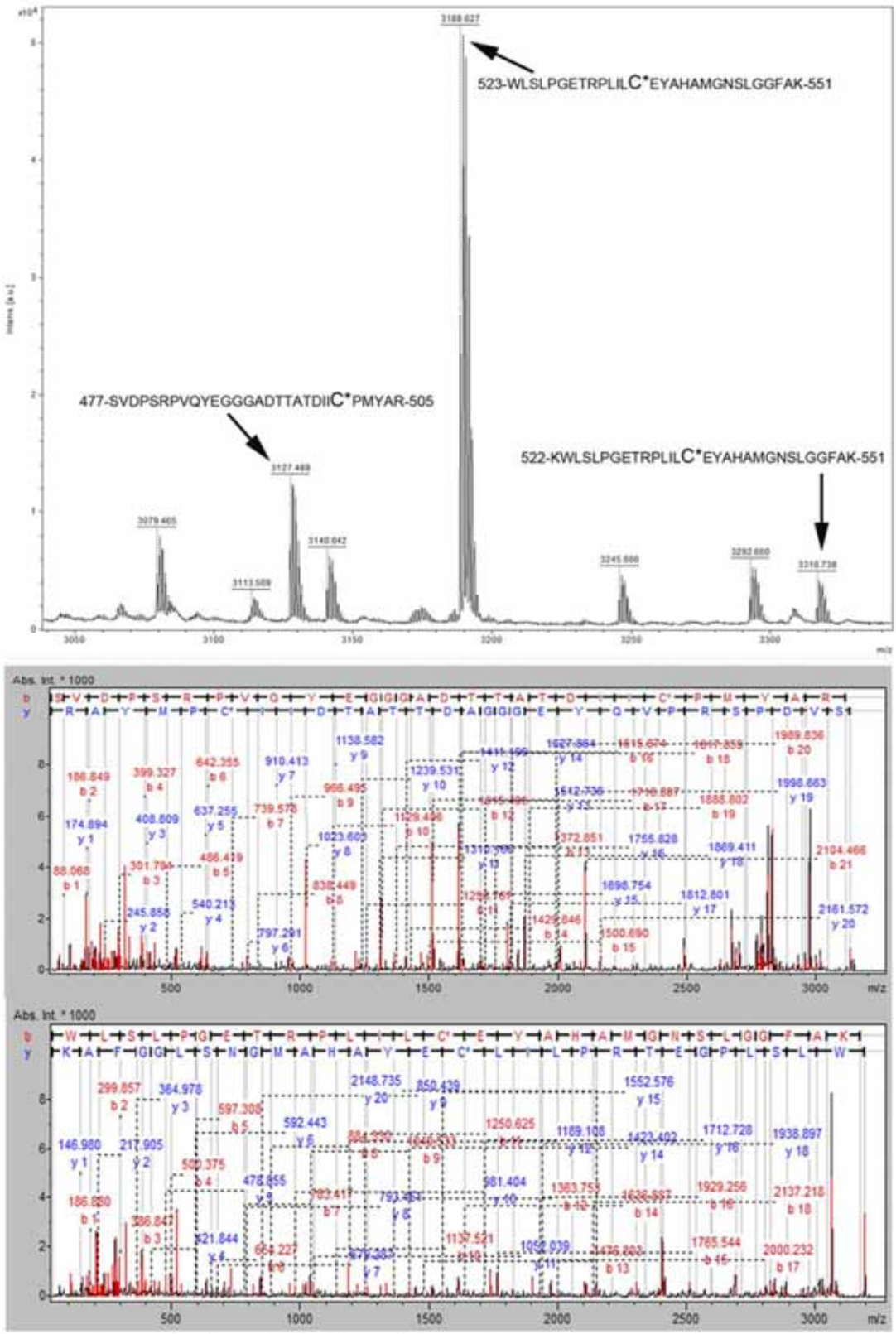

FIG 7 (Top spectrum) Treatment of β-galactosidase with iodoacetamide. Peaks containing C500 (*m/z*, 3,127.489) and C536 (*m/z*, 3,188.627 and 3,316.738) are indicated. (Central and bottom spectra) MS-MS for the 3,127.489-Da (central) and 3,188.627-Da (bottom) peaks.

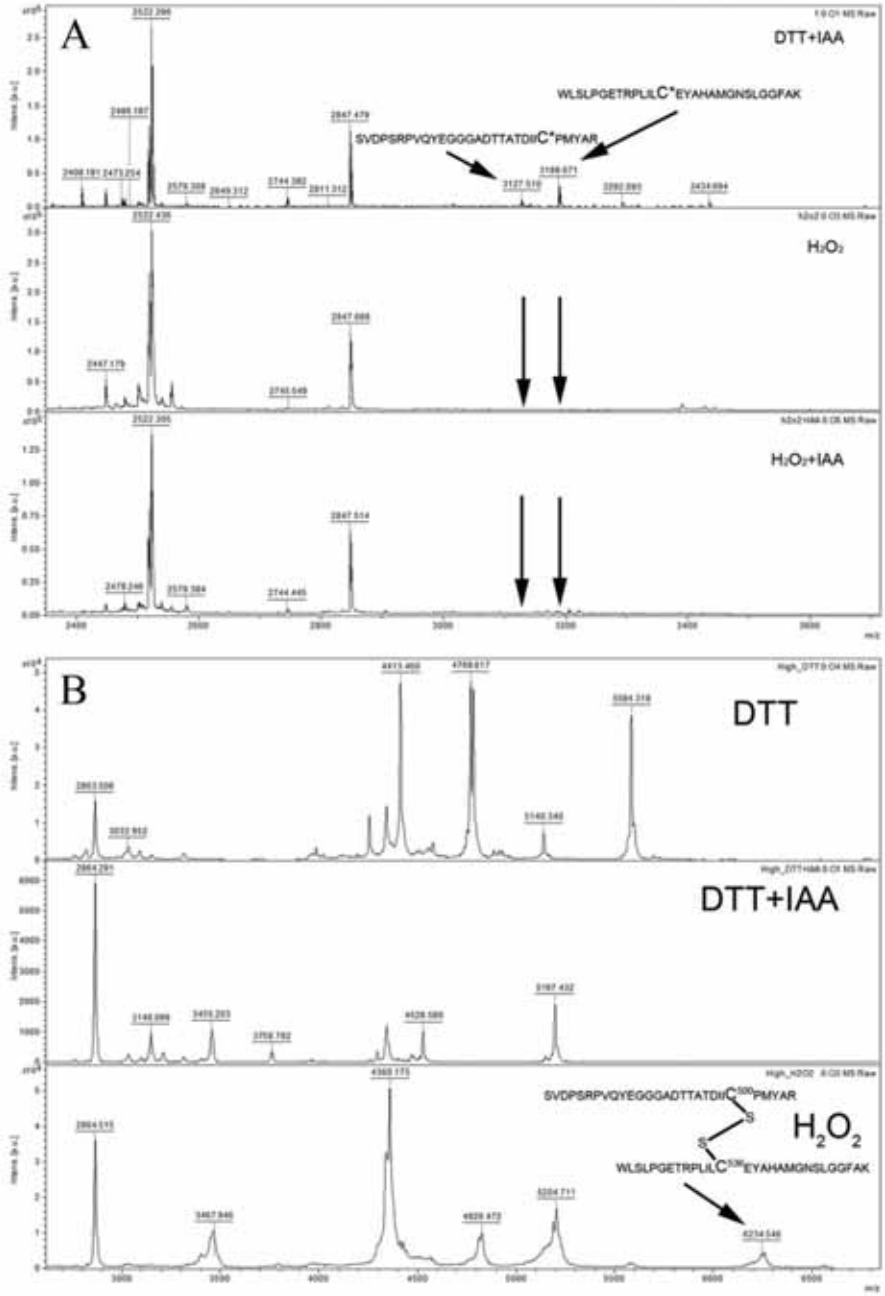

FIG 8 (A) Details of the spectra obtained for different β-galactosidase treatments. (Top spectrum) β-Galactosidase treated with DTT and IAA. The carboxamidomethylated peptides containing C500 and C536 can be observed. (Central spectrum) β-Galactosidase treated with H_2O_2. Under oxidizing conditions, the peaks containing C500 and C536 are not observed. (Bottom spectrum) β-Galactosidase treated with H_2O_2 and IAA. Under oxidizing conditions, alkylation of C500 and C536 does not take place. (B) Details of spectra obtained for different β-galactosidase treatments. After treatment with DTT alone or DTT plus IAA (top and central spectra, respectively), the peptide containing the disulfide bridge formed by C500 and C536 is not detected, but it appears in the H_2O_2-treated sample (bottom spectrum).

tion. Thus, our results show that in those proteins that can reach a more stable conformation under specific conditions, such as an oxidizing background, both properties can be improved simultaneously.

To sum up, in this study we demonstrate, for the first time, an enhancement of rβ-galactosidase activity when the enzyme is produced in an oxidizing environment and, consequently, the formation of a disulfide bond in *E. coli* β-galactosidase under these con-

ditions. Our experimental data—supported and rationalized by modeling calculations—show not only that the oxidative environment in the *E. coli* cytoplasm provided by the Origami strain promotes disulfide bond formation in rβ-galactosidase but also that this phenomenon tends to enhance the biological activity of rβ-galactosidase. Moreover, our data also suggest that, although the formation of disulfide bonds is not favored under reducing conditions, a small percentage of the natural β-galactosidase produced in a reducing *E. coli* cytoplasm could form a C500-C536 disulfide bond, as occurs with other proteins (1, 18, 28, 51). This event would be compatible with the protein function, since we have observed that, although β-galactosidase shows higher specific activity under oxidizing conditions, it can also carry out its function under natural reducing conditions.

ACKNOWLEDGMENTS

We are indebted to Agnes Ullmann for helpful comments and to Ursula Rinas for critical reading of the manuscript.

This work was supported by BFU2010-17450, EUI2008-03610, and IT2009-0021 (MICINN), by 2009SGR-108 (AGAUR), and by the Centro de Investigación Biomédica en Red en Bioingeniería, Biomateriales y Nanomedicina (CIBER-BBN), Barcelona, Spain. CIBER-BBN is an initiative funded by the VI National R&D&i Plan 2008–2011, Iniciativa Ingenio 2010, Consolider Program, CIBER Actions, and financed by the Instituto de Salud Carlos III with assistance from the European Regional Development Fund. We are indebted to the Protein Production Platform (CIBER-BBN) for helpful technical assistance and for protein production and purification services (http://bbn.ciber-bbn.es/programas/plataformas/equipamiento). J.S.-F. is the recipient of a fellowship from the Departament de Genètica i de Microbiologia, Universitat Autònoma de Barcelona, Barcelona, Spain. A.V. has been distinguished by ICREA (Generalitat de Catalunya) through an ICREA ACADEMIA award, and E.G.-F. is supported by the Programa Personal de Técnico de Apoyo (Modalidad Infraestructuras Científco-Tecnológicas, MICINN).

REFERENCES

1. **Aslund F, Zheng M, Beckwith J, Storz G.** 1999. Regulation of the OxyR transcription factor by hydrogen peroxide and the cellular thiol-disulfide status. Proc. Natl. Acad. Sci. U. S. A. **96**:6161–6165.
2. **Barbirz S, Jakob U, Glocker MO.** 2000. Mass spectrometry unravels disulfide bond formation as the mechanism that activates a molecular chaperone. J. Biol. Chem. **275**:18759–18766.
3. **Bartlett GJ, Porter CT, Borkakoti N, Thornton JM.** 2002. Analysis of catalytic residues in enzyme active sites. J. Mol. Biol. **324**:105–121.
4. **Bessette PH, Aslund F, Beckwith J, Georgiou G.** 1999. Efficient folding of proteins with multiple disulfide bonds in the *Escherichia coli* cytoplasm. Proc. Natl. Acad. Sci. U. S. A. **96**:13703–13708.
5. **Cassland P, Larsson S, Nilvebrant NO, Jonsson LJ.** 2004. Heterologous expression of barley and wheat oxalate oxidase in an *E. coli trxB gor* double mutant. J. Biotechnol. **109**:53–62.
6. **Craven GR, Steers EJ, Anfinsen CB.** 1965. Purification, composition, and molecular weight of beta-galactosidase of *Escherichia coli* K12. J. Biol. Chem. **240**:2468–2477.
7. **de Marco A.** 2009. Strategies for successful recombinant expression of disulfide bond-dependent proteins in *Escherichia coli*. Microb. Cell Fact. **8**:26.
8. **Derman AI, Beckwith J.** 1991. *Escherichia coli* alkaline phosphatase fails to acquire disulfide bonds when retained in the cytoplasm. J. Bacteriol. **173**:7719–7722.
9. **Derman AI, Prinz WA, Belin D, Beckwith J.** 1993. Mutations that allow disulfide bond formation in the cytoplasm of *Escherichia coli*. Science **262**:1744–1747.
10. **Garcia-Fruitos E, et al.** 2005. Aggregation as bacterial inclusion bodies does not imply inactivation of enzymes and fluorescent proteins. Microb. Cell Fact. **4**:27.
11. **Gebler JC, Aebersold R, Withers SG.** 1992. Glu-537, not Glu-461, is the nucleophile in the active site of (*lac Z*) beta-galactosidase from *Escherichia coli*. J. Biol. Chem. **267**:11126–11130.
12. **Gonzalez-Montalban N, Garcia-Fruitos E, Villaverde A.** 2007. Recombinant protein solubility—does more mean better? Nat. Biotechnol. **25**:718–720.
13. **Guilhot C, Jander G, Martin NL, Beckwith J.** 1995. Evidence that the pathway of disulfide bond formation in *Escherichia coli* involves interactions between the cysteines of DsbB and DsbA. Proc. Natl. Acad. Sci. U. S. A. **92**:9895–9899.
14. **Halbmayr EG, et al.** 2008. High-level expression of recombinant beta-galactosidases in *Lactobacillus plantarum* and *Lactobacillus sakei* using a Sakacin P-based expression system. J. Agric. Food Chem. **56**:4710–4719.
15. **Hu X, et al.** 2007. Optimisation of production of a domoic acid-binding scFv antibody fragment in *Escherichia coli* using molecular chaperones and functional immobilisation on a mesoporous silicate support. Protein Expr. Purif. **52**:194–201.
16. **Ibrahim SA, et al.** 2010. Enhancement of alpha- and beta-galactosidase activity in *Lactobacillus reuteri* by different metal ions. Biol. Trace Elem. Res. **136**:106–116.
17. **Jacobson RH, Zhang XJ, DuBose RF, Matthews BW.** 1994. Three-dimensional structure of beta-galactosidase from *E. coli*. Nature **369**:761–766.
18. **Jakob U, Muse W, Eser M, Bardwell JC.** 1999. Chaperone activity with a redox switch. Cell **96**:341–352.
19. **Juers DH, et al.** 2001. A structural view of the action of *Escherichia coli* (*lacZ*) beta-galactosidase. Biochemistry **40**:14781–14794.
20. **Juers DH, et al.** 2000. High resolution refinement of beta-galactosidase in a new crystal form reveals multiple metal-binding sites and provides a structural basis for alpha-complementation. Protein Sci. **9**:1685–1699.
21. **Juers DH, et al.** 2009. Direct and indirect roles of His-418 in metal binding and in the activity of beta-galactosidase (*E. coli*). Protein Sci. **18**:1281–1292.
22. **Jurado P, de Lorenzo V, Fernandez LA.** 2006. Thioredoxin fusions increase folding of single chain Fv antibodies in the cytoplasm of *Escherichia coli*: evidence that chaperone activity is the prime effect of thioredoxin. J. Mol. Biol. **357**:49–61.
23. **Kadokura H, Katzen F, Beckwith J.** 2003. Protein disulfide bond formation in prokaryotes. Annu. Rev. Biochem. **72**:111–135.
24. **Kang JG, et al.** 1999. RsrA, an anti-sigma factor regulated by redox change. EMBO J. **18**:4292–4298.
25. **Kim J, Robinson AS.** 2006. Dissociation of intermolecular disulfide bonds in P22 tailspike protein intermediates in the presence of SDS. Protein Sci. **15**:1791–1793.
26. **Laemmli UK.** 1970. Cleavage of structural proteins during the assembly of the head of bacteriophage T4. Nature **227**:680–685.
27. **Le HV, Trotta PP.** 1991. Purification of secreted recombinant proteins from *Escherichia coli*. Bioprocess Technol. **12**:163–181.
28. **Locker JK, Griffiths G.** 1999. An unconventional role for cytoplasmic disulfide bonds in vaccinia virus proteins. J. Cell Biol. **144**:267–279.
29. **Makino T, Skretas G, Georgiou G.** 2011. Strain engineering for improved expression of recombinant proteins in bacteria. Microb. Cell Fact. **10**:32.
30. **Martínez-Alonso M, Garcia-Fruitos E, Villaverde A.** 2008. Yield, solubility and conformational quality of soluble proteins are not simultaneously favored in recombinant *Escherichia coli*. Biotechnol. Bioeng. **101**:1353–1358.
31. **Martínez-Alonso M, Garcia-Fruitos E, Ferrer N, Rinas U, Villaverde A.** 2010. Side effects of chaperone gene co-expression in recombinant protein production. Microb. Cell Fact. **9**:64.
32. **Messens J, Collet JF.** 2006. Pathways of disulfide bond formation in *Escherichia coli*. Int. J. Biochem. Cell Biol. **38**:1050–1062.
33. **Miller JH.** 1972. Experiments in molecular genetics. Cold Spring Harbor Laboratory, Cold Spring Harbor, NY.
34. **Penner RM, Roth NJ, Rob B, Lay H, Huber RE.** 1999. Tyr-503 of beta-galactosidase (*Escherichia coli*) plays an important role in degalactosylation. Biochem. Cell Biol. **77**:229–236.
35. **Platas Rodriguez-Carmona GE, Garcia-Fruitós E, Cano-Garrido O, Villaverde A.** 2011. Co-production of GroELS discriminates between intrinsic and thermally-induced recombinant protein aggregation during substrate quality control. Microb. Cell Fact. **10**:79.
36. **Pollitt S, Zalkin H.** 1983. Role of primary structure and disulfide bond formation in beta-lactamase secretion. J. Bacteriol. **153**:27–32.
37. **Prinz WA, Aslund F, Holmgren A, Beckwith J.** 1997. The role of the thioredoxin and glutaredoxin pathways in reducing protein disulfide bonds in the *Escherichia coli* cytoplasm. J. Biol. Chem. **272**:15661–15667.

38. **Proba K, Ge L, Pluckthun A.** 1995. Functional antibody single-chain fragments from the cytoplasm of *Escherichia coli*: influence of thioredoxin reductase (TrxB). Gene **159**:203–207.
39. **Reithel FJ, Newton RM, Eagleson M.** 1966. Effects of thiols on *Escherichia coli* beta-galactosidases. Nature **210**:1265.
40. **Ring M, Huber RE.** 1990. Multiple replacements establish the importance of tyrosine-503 in beta-galactosidase (*Escherichia coli*). Arch. Biochem. Biophys. **283**:342–350.
41. **Roth NJ, Penner RM, Huber RE.** 2003. Beta-galactosidases (*Escherichia coli*) with double substitutions show that Tyr-503 acts independently of Glu-461 but cooperatively with Glu-537. J. Protein Chem. **22**:663–668.
42. **Sali A, Blundell TL.** 1993. Comparative protein modelling by satisfaction of spatial restraints. J. Mol. Biol. **234**:779–815.
43. **Sambrook J, Fritsch EF, Maniatis T.** 1989. Molecular cloning: a laboratory manual, 2nd ed. Cold Spring Harbor Laboratory Press, Cold Spring Harbor, NY.
44. **Schneider EL, Thomas JG, Bassuk JA, Sage EH, Baneyx F.** 1997. Manipulating the aggregation and oxidation of human SPARC in the cytoplasm of *Escherichia coli*. Nat. Biotechnol. **15**:581–585.
45. **Shen MY, Sali A.** 2006. Statistical potential for assessment and prediction of protein structures. Protein Sci. **15**:2507–2524.
46. **Shifrin S, Grochowski BJ, Luborsky SW.** 1970. Dissociation of beta-galactosidase by thiols. Nature **227**:608–609.
47. **Shimizu TH, et al.** 2005. Expression, purification, and crystallization of endopolygalacturonase from a pathogenic fungus, *Stereum purpureum*, in *Escherichia coli*. Protein Expr. Purif. **44**:130–135.
48. **Silhavy TJ, Beckwith J.** 1985. Use of *lac* fusions for the study of biological problems. Microbiol. Rev. **49**:398–418.
49. **Sorensen HP, Mortensen KK.** 2005. Advanced genetic strategies for recombinant protein expression in *Escherichia coli*. J. Biotechnol. **115**:113–128.
50. **Sorensen HP, Mortensen KK.** 2005. Soluble expression of recombinant proteins in the cytoplasm of *Escherichia coli*. Microb. Cell Fact. **4**:1.
51. **Stewart EJ, Aslund F, Beckwith J.** 1998. Disulfide bond formation in the *Escherichia coli* cytoplasm: an in vivo role reversal for the thioredoxins. EMBO J. **17**:5543–5550.
52. **Terpe K.** 2006. Overview of bacterial expression systems for heterologous protein production: from molecular and biochemical fundamentals to commercial systems. Appl. Microbiol. Biotechnol. **72**:211–222.
53. **Ye T, Lin Z, Lei H.** 2008. High-level expression and characterization of an anti-VEGF165 single-chain variable fragment (scFv) by small ubiquitin-related modifier fusion in *Escherichia coli*. Appl. Microbiol. Biotechnol. **81**:311–317.
54. **Yuan J, Martinez-Bilbao M, Huber RE.** 1994. Substitutions for Glu-537 of beta-galactosidase from *Escherichia coli* cause large decreases in catalytic activity. Biochem. J. **299**(Pt 2):527–531.
55. **Yuan Z, Zhao J, Wang ZX.** 2003. Flexibility analysis of enzyme active sites by crystallographic temperature factors. Protein Eng. **16**:109–114.

Annex 2

The nanoscale properties of bacterial inclusion bodies and their effect on mammalian cell proliferation

César Díez-Gil, Sven Krabbenborg , Elena García-Fruitós, Esther Vazquez, Escarlata Rodríguez-Carmona, Imma Ratera, Nora Ventosa, Joaquin Seras-Franzoso, Olivia Cano-Garrido, Neus Ferrer-Miralles, Antonio Villaverde, Jaume Veciana

Biomaterials, Vol 31, 2010

Biomaterials 31 (2010) 5805–5812

Contents lists available at ScienceDirect

Biomaterials

journal homepage: www.elsevier.com/locate/biomaterials

The nanoscale properties of bacterial inclusion bodies and their effect on mammalian cell proliferation

César Díez-Gil [a,b], Sven Krabbenborg [a], Elena García-Fruitós [b,c], Esther Vazquez [b,c,d], Escarlata Rodríguez-Carmona [b,c], Imma Ratera [a,b], Nora Ventosa [a,b], Joaquin Seras-Franzoso [b,c,d], Olivia Cano-Garrido [b,c], Neus Ferrer-Miralles [b,c,d], Antonio Villaverde [b,c,d,*], Jaume Veciana [a,b,*]

[a] Departament de Nanociència Molecular i Materials Orgànics. Institut de Ciència de Materials de Barcelona (ICMAB-CSIC), Bellaterra, 08193 Barcelona, Spain
[b] Networking Research Centre on Bioengineering, Biomaterials and Nanomedicine, CIBER-BBN, 08193 Barcelona, Spain
[c] Institut de Biotecnologia i de Biomedicina, Universitat Autònoma de Barcelona, Bellaterra, 08193 Barcelona, Spain
[d] Department of Genetics and Microbiology, Universitat Autònoma de Barcelona, Bellaterra, 08193 Barcelona, Spain

ARTICLE INFO

Article history:
Received 23 February 2010
Accepted 4 April 2010
Available online 8 May 2010

Keywords:
Inclusion bodies
Cell growth
Nanoparticles
Stiffness
Wettability
Tissue engineering

ABSTRACT

The chemical and mechanical properties of bacterial inclusion bodies, produced in different *Escherichia coli* genetic backgrounds, have been characterized at the nanoscale level. In regard to wild type, DnaK⁻ and ClpA⁻ strains produce inclusion bodies with distinguishable wettability, stiffness and stiffness distribution within the proteinaceous particle. Furthermore it was possible to observe how cultured mammalian cells respond differentially to inclusion body variants when used as particulate materials to engineer the nanoscale topography, proving that the actual range of referred mechanical properties is sensed and discriminated by biological systems.

The data provide evidence of the mechanistic activity of the cellular quality control network and the regulation of the stereospecific packaging of partially folded protein species in bacteria. This inclusion body nanoscale profiling offers possibilities for their fine genetic tuning and the resulting macroscopic effects when applied in biological interfaces.

1. Introduction

Inclusion bodies are non-enveloped and mechanically stable nanoparticulate entities mainly constituted by proteins, which are generated in vivo during the production and further deposition of a wide catalogue of recombinant polypeptides [1]. Early after the implementation of recombinant DNA technologies in both pharma and biotech industries, the formation of inclusion bodies has been observed as a major obstacle in protein production processes [1,2], as important amounts of target polypeptides commonly precipitate as such water-insoluble protein clusters. For long, inclusion bodies have been seen as undesirable by-products to be discarded for further application, as believed to be formed by misfolded, nonfunctional polypeptides escaping the cell's quality control machinery [2]. However, a dramatic turn in the understanding of the bacterial control of protein aggregation at the cell systems level has recently shown inclusion bodies as formed by properly folded, functional species [3] that are not excluded from cell surveillance regarding their conformational quality [4,5]. This has prompted the straightforward use of inclusion bodies formed by enzymes in different kind of catalytic processes [6]. In addition, inclusion bodies have shown to possess an unexpected amyloid-based molecular architecture structurally comparable to that observed in eukaryotic amyloids [7].

At a nanoscale level, inclusion bodies are pseudo-spherical, quite pure proteinaceous particles ranging from around 50–500 nm [8]. Their mechanical stability is high enough to preserve the integrity and morphology upon mechanical, chemical and enzymatic cell disruption (or combined treatments) and upon long term storage under different conditions, including lyophilisation [9]. Being the size of inclusion bodies within the range of mammalian cell micro- and nano-environment topology influencing mammalian cell proliferation, random surface decoration and patterning with inclusion bodies has a significant and positive impact on cell growth, making them promising biomaterials for tissue engineering [9]. Despite their enormous potential as non-cytotoxic nanomaterials producible by cost effective, scalable procedures, the chemical and mechanical properties of inclusion

* Corresponding authors. Networking Research Centre on Bioengineering, Biomaterials and Nanomedicine, CIBER-BBN, 08193 Barcelona, Spain. Tel.: +34 935801853; fax: +34 935805729.
E-mail addresses: Antoni.Villaverde@uab.cat (A. Villaverde), vecianaj@icmab.es (J. Veciana).

0142-9612/$ – see front matter © 2010 Elsevier Ltd. All rights reserved.
doi:10.1016/j.biomaterials.2010.04.008

bodies remain essentially unexplored. In this regard, only some bibliographic references to their density [10], hydratation level [11] and pH responsiveness [12] are available. For that, we have here approached the physicochemical characterization of *Escherichia coli* inclusion body materials regarding surface chemistry and nanoscale mechanical properties, such as stiffness or hydrophobicity, which might be critical in inclusion body–cell interactions.

2. Materials and methods

2.1. Materials

All materials used are displayed on the Supplementary information.

2.2. Methods

2.2.1. IB's size and Z potential determination by dynamic light scattering (DLS)

The particle sizes and Z potential of IB were determined in a dynamic light scattering (DLS) device (Malvern Nanosizer Z), in suspension on PBS buffer (pH = 7.4, IB final concentration was 20 μg/mL). To facilitate the dispersion on the liquid, 2 mL of the mixture were sonicated for 1 min. DLS measurements were carried out at 37 °C using 1 mL of freshly prepared IBs suspension into a disposable plastic cubette. Each IBs sample was analyzed by triplicate averaging thirty single measurements.

2.2.2. Mixed thiol self assembled monolayer preparation

Different molar ratios of hydrophilic (−OH terminated) and hydrophobic ($-CH_3$ terminated) alkanethiols were used to obtain mixed self assembled monolayers (SAMs) with different degree of hydrophobicity, as shown by static contact angle measurements (Table S1). SAMs with different proportions of 1-undecenethiol ($-CH_3$ terminated) and 11- mercapto-1-undecanol (−OH terminated) were prepared by immersion of the freshly cleaned gold substrates in an ethanolic solution of the organic thiols with the appropriate molar ratio for 24 h. Thus, substrates were rinsed with clean ethanol and sonicated for 5 min in ethanol to remove the physisorbed molecules. Afterwards the substrates were dried under a stream of N_2 and immediately used (see SI).

2.2.3. Contact angle measurements

Wettability of the self assembled monolayer of the mixed thiols before and after being in contact with IBs was determined with an OCA 15+ (Dataphysics, Germany) contact angle goniometer. Data treatment and angle determination were carried out with the software SCA20 (Dataphysics, Germany). Four sets of static contact angles, at different positions on each sample, were measured (see SI).

2.2.4. Coverage of IBs on the mixed SAMs

Freshly prepared mixed monolayers of the thiols were immersed for 2 h into an IB suspension in PBS buffer (IB suspension was sonicated for 5 min prior to the introduction of the substrate). Afterwards, the IBs' covered substrates were gently rinsed with MiliQ water (18.2 MΩ) and dried under a stream of N_2.

Optical fluorescence microscope images of the deposited IBs were performed using an OLYMPUS Bx51 microscope with an OLYMPUS DP20 camera with 3 s shutter time, and an OLYMPUS U-RFL-T mercury lamp accessory. In order to remove background light a GFP pass filter was used. ImageJ (GNU) software was utilized to perform the particle counting.

2.2.5. Atomic force microscopy (AFM)

2.2.5.1. AFM imaging. Atomic force microscopy (AFM) images were taken with a commercial AFM (MFP-3D-SA, Asylum Research, Santa Barbara, USA). Samples were analyzed in dynamic mode working at 8 kHz of frequency and in a liquid environment (PBS buffer media pH = 7.4) in order to mimic the cytoplasmic environment of the cell. Pyramidal NSC35/AlBS silicon tips (Mikromash, USA) having nominal spring constants of 0.28 N/m were used. Sample preparation was done by drop casting of an IBs suspension in the same PBS buffer (20 μg/mL) over freshly cleaved mica.

2.2.5.2. AFM force spectroscopy. AFM indentation measurements were done with a commercial AFM (MFP-3D-SA, Asylum Research, Santa Barbara, USA) equipped with a close loop tracking system and working on liquid environment. Pyramidal NSC35/AlBS silicon tips (Mikromash, USA) having nominal spring constants of 0.28 N/m were used. The spectroscopic calibration of the raw cantilever on liquid media (PBS buffer solution pH = 7.4) was developed by measuring force vs. distance curves, on freshly cleaved mica. Sample preparation was done by drop casting of an IB suspension in the same PBS buffer (20 μg/mL) over freshly cleaved mica. The force curves, consisting of 2048 data points were obtained imposing a maximum applied force of 50 nN at a frequency of 8 kHz. AFM mechanical properties data were calculated from force distance curves according to the procedures described in [13,14] (see SI).

In order to achieve spatial resolution of the spectroscopical measurements, dynamic AFM images of the studied IBs were developed prior and after force vs. distance measurements. Therefore observations allowed us to follow any movement or deformation produced on the sample during the experiment.

2.2.6. Cell proliferation assay

IBs produced and purified from different bacterial strains were sterilized by exposure to a 253 nm UV light germicidal lamp for 4 h. The IBs were resuspended in PBS, and 2.65×10^8 IBs (particles) were added per well to coat untreated Costar 3370 plates, which were left overnight at 4 °C. Wells were washed in PBS and blocked with 3% BSA in PBS for 1 h at 37 °C. Afterwards, 3×10^3 newborn hamster kidney (BHK) cells or 2×10^4 rat pheochromocytoma (PC12) cells were added per well and incubated in Dulbecco's Modified Eagle's Medium (DMEM) supplemented with nonessential amino acids and fetal calf serum (5%), at 37 °C for different times. Blank wells underwent exactly the same treatment as described but without IBs. After incubation, cell proliferation was determined using the EZ4U kit (Biomedica GmbH) following the manufacturer's instructions, and analyzed in the multilabel reader iEMS MF (Labsystems, Helsinki, Finland). The reading absorbances were 450 nm and 620 nm as reference, and the values were standardized with respect to medium-containing wells. A pre-test to select incubation time before saturation was carried out with the kit reagents. All assays were done in triplicate. Data were expressed as the mean ± standard error of the mean (SEM) of the values obtained per condition and evaluated statistically by a *T*-test analysis. Cultured cell pictures under different conditions were taken with a Nikon Eclipse TS100 inverted microscope by using NIS-Elements F 3.00 imaging software.

3. Results

Recent studies on the functionality and applications of IBs have shown their enormous potential, not only from the industrial catalysis point of view, but also in the field of biomaterials [9]. In this regard, IB-decorated or IB-patterned surfaces provide an appropriate topological environment for mammalian cell proliferation [9]. Nevertheless, despite their promising properties as non-cytotoxic and particulate materials, very little is still known about their chemical and physical nanoscale properties [5,15] and how their rational modification at this scale may influence their macroscopic impact on living cells in IB-cell interfaces.

To deeper explore these issues, we have characterized IBs produced in a conventional K-12 wild type (wt) *E. coli* strain, and in derived genetic backgrounds showing deficiencies in the protein quality control network, that is known to regulate, at the systems level, not only protein folding but also aggregation. For that, we have chosen two paradigm mutations affecting different arms of the quality control system, resulting in deficiencies of either DnaK (the main cytosolic chaperone and negative regulator of the heat shock system) or ClpA (foldase and ATPase of the protease ClpP). In these mutants, IBs are distinguishable from those produced in wt cells, in size and biological activity of the embedded proteins [16]. Therefore, we presumed that surface chemistry and mechanical properties of IBs might be eventually affected in these strains.

3.1. Study of the hydrophilic/hydrophobic nature of the IB

Model surfaces with known physicochemical properties have been widely employed for studying not only material surface properties but also complex events such as protein adsorption or cellular responses. Previous studies have already shown how of different surface chemical properties entail variations on the macroscopic behavior of a biomaterial [17], being those related with changes on the chemical charge or material wettability among the most influencing [18,19].

In order to study the wettability properties of IB variants (namely those produced in $DnaK^-$ or $ClpA^-$ mutants vs wt strain), six SAMs on gold substrates were obtained by functionalizing them with different molar ratios (X) of −OH terminated (hydrophilic) and $-CH_3$ terminated (hydrophobic) alkanethiols. As a result, an array of modified gold surfaces bearing controlled contact angles,

ranging from 110 to 20°, were fabricated (see Materials and methods section).

Subsequently, the arrays were immersed in suspensions (20 μg/mL) of IB variants for 2 h and contact angle and IB coverage of the different functionalized gold substrates (X_{OH}) were determined before and after IB deposition. While prior to IB deposition, an increase of 10% in the concentration of the hydroxyl terminated thiol with respect to the $-CH_3$ terminated ones, implied a decrease of 6 ± 1° on the contact angle of the functionalized surface, the measurements performed after the deposition of IBs presented a much smaller reduction (Fig. 1, left). This fact was more intense for $DnaK^-$ and $ClpA^-$ IBs where the decrement was 2.4 ± 0.8 and 1.9 ± 0.5° (Fig. 1b, c left) respectively, than for wt IBs where the diminution was of 4.5 ± 0.8° (Fig. 1a, left). Thus, the presence of IBs on the functional surface, buffers the change of wettability of the substrate at different extent.

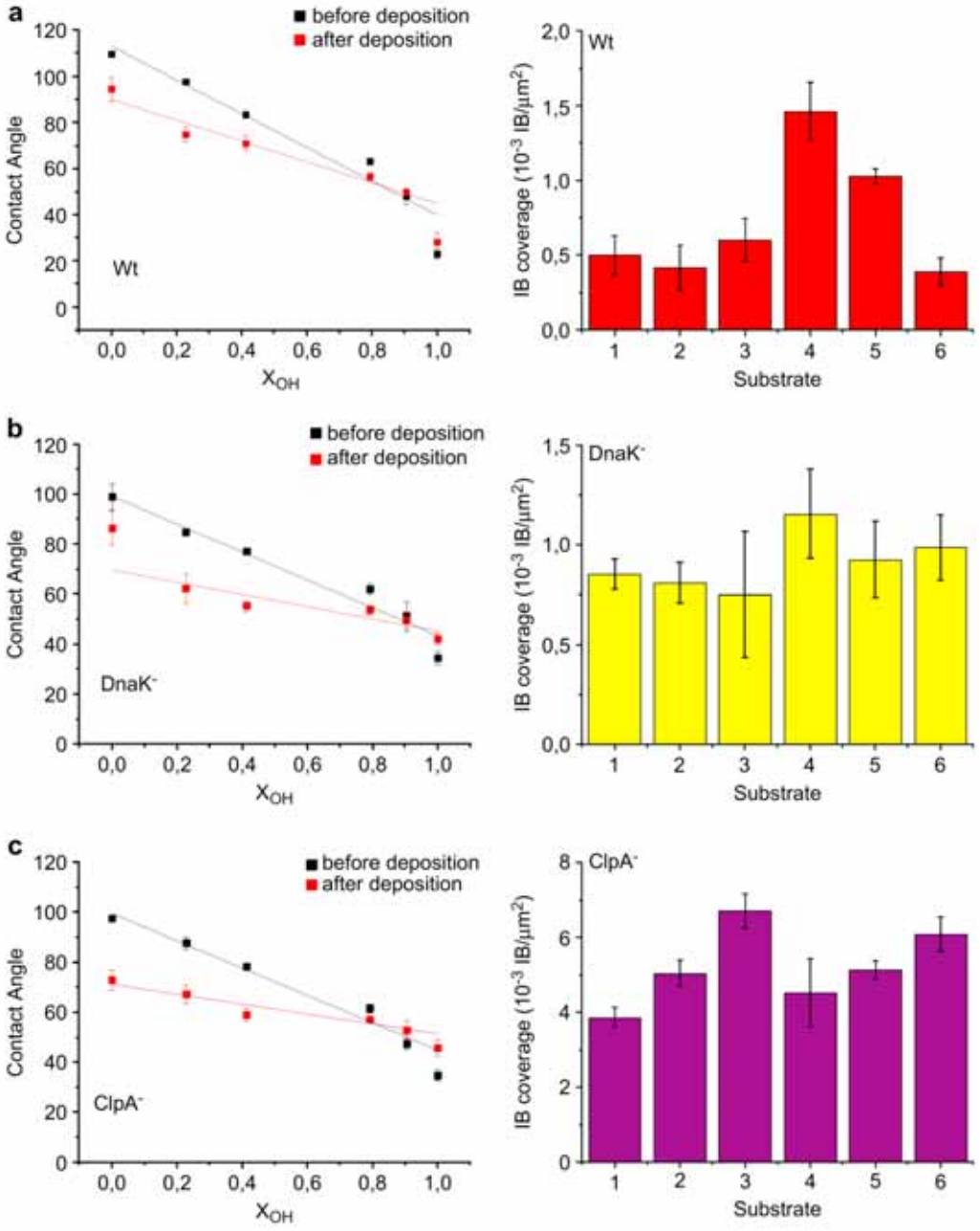

Fig. 1. Left: Contact angles of the 6 different functionalized, containing different molar ratio of −OH terminated (X_{OH}) alkanethiols, gold surfaces before and after deposition of IBs. Right: Dependence of the IB's coverage on the functionalized gold substrate wettability a) Wt, b) $DnaK^-$, c) $ClpA^-$. Substrate wettability ranging from 20 to 30° (1), 40–50° (2), 60–70° (3), 70–80° (4), 80–90° (5) and 100–110° (6).

IB surface coverage dependence with the substrate contact angle was also determined by measuring the density of aggregates per μm^2 using a optical fluorescence microscope. Results obtained for wt IBs (Fig. 1a, right) showed the existence of a maximum of IB coverage reaching absolute values of 0.0015 IB/μm^2, corresponding to a functionalized gold surface contact angle of approximately 80°. Therefore, it is possible to establish a preference of these materials to join slightly hydrophobic surfaces. On the other hand, data obtained from DnaK$^-$ and ClpA$^-$ IBs (Fig. 1b, c right, respectively) exhibited significantly different tendencies. In both cases, the maximum of interaction was slightly shifted to lower contact angles (75 and 60°, respectively) and a gradual increase of the covering of IBs on the modified surfaces at high contact angles (>90°) could also be observed, pointing to the existence of more amphiphilic behaviors of the DnaK$^-$ and ClpA$^-$ IB surfaces. Thus, it is possible to observe how, by changing the IB variant, the substrate contact angle coverage dependence varies from monomodal, with a single maximum at 80° (wt), to bimodal, with two peaks, one at lower angles (75° and 60°) and the other one at higher values (>90°), for DnaK$^-$ and ClpA$^-$ respectively, indicating the existence of two different wettability populations. However, looking at the absolute IBs adsorption values, DnaK$^-$ IBs showed extreme similarity to those obtained with wt IBs, reaching a maximum coverage of 0.0012 IB/μm^2, while ClpA$^-$ IBs depict coverage levels up to 5 times higher (0.007 IB/μm^2). This fact is of extreme importance, as an increase on the IBs density entails the subsequent increase of roughness of the treated surface, usually related to cell proliferation properties modification [20]. Therefore, it was possible to establish that the wettability of the IB surfaces is dependent of the genetic background where they were produced, and that the modification of this parameter has important effects on the interaction of IBs with the media.

3.2. Size determination of IBs

Even though the chemical nature of the surface of a material is extremely important, physical features, such as size or mechanical behavior, might also influence their macroscopic properties. Particle size distribution and Z potential of freshly prepared IBs in aqueous suspension were determined by dynamic light scattering, revealing no significant differences between IBs variants in agreement with previous screenings. Observed particle size ranged from 502 nm for DnaK$^-$ IBs to 580 nm for ClpA$^-$ IBs, while the low Z potential values obtained (see Fig. S1) depict the tendency of all the measured IBs to aggregate with time (Z potential values obtained are lower of |30| mV).

In order to study the influence of a solid interface on the particle size, IBs were imaged by AFM in liquid (PBS buffer solution), once deposited over freshly cleaved mica. Average dimensions obtained from these images show no significant deviation from DLS data previously obtained in PBS. This allowed discarding any strong deformation of the protein aggregates during the adsorption process, which might eventually alter the material properties.

3.3. Nanomechanical properties of IBs determined by AFM

It is known that the mechanical properties of a substrate biomaterial are critically affecting relevant features of mammalian cells growing on it, such as cell morphology [21,22], proliferation [21,22], motility [23] and differentiation [22,24]. During the last decade, AFM has proved its value not only for imaging biological samples [25,26], but also for probing inherent properties of biological structures, like local interaction forces, mechanical properties or dynamics in natural (physiological) environments [27].

To determine how the different genetics of IB bioproduction affects their elasticity, force spectroscopic AFM was employed. This technique consists of an AFM tip which is pressed into the elastic object with a defined force (F), producing the subsequent indentation (δ) at the nanoscale. Spectroscopical measurements were performed in liquid media (PBS buffer pH 7.4) in order to preserve the natural state of the protein aggregates and to mimic the natural cell environment. From the obtained F vs. δ data plot, and using the Hertz model [28–33] (see SI), it was possible to fit the experimental data with the behavior expected for conical (equation (1)) and spherical (equation (2)) indenters, obtaining the Young modulus of the sample. In Fig. 2, an example of the experimental data, together with the subsequent fittings for conical and spherical indenters, is shown. In our case, from the two plausible geometries the one associated with a spherical tip presented the higher agreement, and this compatibility of the experimental data with the model was

$$F = \left[\frac{2E^* \tan\alpha}{\pi(1-\nu^2)}\right]\delta^2 \ (1) \qquad F = \left[\frac{2E^* R^{1/2}}{3(1-\nu^2)}\right]\delta^{2/3} \ (2)$$

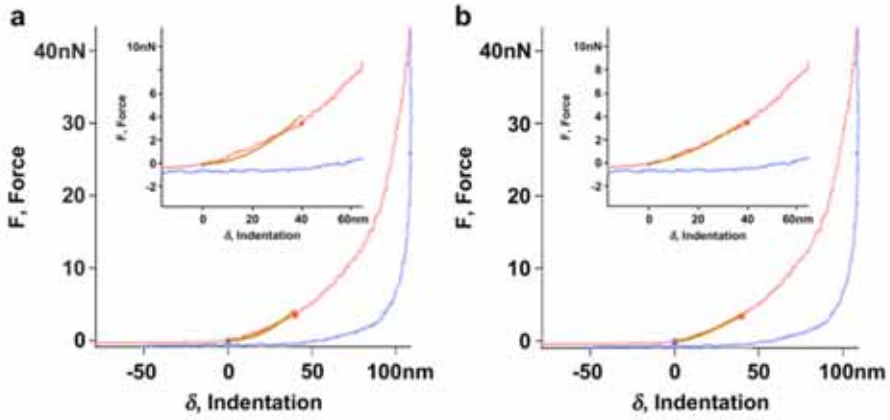

Fig. 2. Conical (a) and spherical (b) fitting of a selected approaching curve measurement over a selected IB. In red is represented the curve resulting from the approaching and indentation of the tip on the IB. In blue is represented the releasing curve generated while moving the AFM tip to its initial position.

verified for the most part of the experimental curves. In order to avoid substrate influence only the first 40 nm of indentation was taken to further analysis.

Statistical studies, presented in Fig. 3, have been obtained after analyzing more than 200 force curves for each aggregate on 7 different IBs obtained in each one of the three different bacterial strains, resulting on different Young modulus distributions according to the IB origin. Stiffness data obtained for wt IBs, represented on Fig. 3a, depicted a monomodal elasticity distribution with a main peak value of 3.73 ± 0.05 MPa and an fwhm (full width at half maximum) of 2.9 ± 0.05 MPa. On the other hand, for DnaK$^-$ and ClpA$^-$ IBs results indicated the presence of two elasticity populations. In the case of DnaK$^-$ IBs (Fig. 3b), the peak at lower strength values was situated at 3.56 ± 0.56 MPa with an fwhm of 3.6 ± 0.48 MPa matching the one obtained for wt particles. However the second population, shifted to harder areas, was placed at 7.75 ± 0.99 MPa with a broader shape of 5.8 ± 0.37 MPa at its fwhm. For ClpA$^-$ IBs (Fig. 3c), the peak distribution was shifted, for both populations, to harder areas with mean peak values of 5.01 ± 0.25 and 10.99 ± 0.30 MPa and fwhm of 3.2 ± 0.28 and 6.6 ± 0.25 MPa, respectively.

These data are in agreement with the results obtained by contact angle measurements, indicating the appearance of two differentiated populations with different wettability and stiffness, in the case of IBs produced in specific phenotypes (DnaK$^-$ and ClpA$^-$), while only one was observed for wt IBs.

3.4. Nanomechanical mapping of the IBs by AFM

AFM spectroscopy might be a destructive technique depending on the sample hardness and the applied force. AFM images of selected IBs, before and after the spectroscopical measurements produced no serious deformation on the IB, which kept its initial shape and structure (see Fig. S2). Therefore, and by the use of an AFM equipped with a closed loop tracking system (see Materials and method), it was possible to obtain the spatial distribution of the elasticity regimes over the different IBs and to develop stiffness maps (Fig. 4), where each force (F) vs. indentation (δ) measurement was spatially localised over the target IB. Fig. 4a shows how the Young modulus was homogeneously spread over the wt IBs, with mean values of 3.6 ± 0.56 MPa. In DnaK$^-$ and ClpA$^-$ IBs two elasticity populations were observed, as entailed in Fig. 4, with the harder areas segregated and localised on the centre of the DnaK$^-$ IBs and on the right side of ClpA$^-$ particles. The above data indicated that, the genetics of IB fabrication, determines the coexistence of more rigid structures and softer ones, and that they seem to be localised on determined areas of individual IB. This fact confirmed the existence of structural diversity inside the protein aggregates. Therefore, it is possible to affirm that the use of modified bacteria for IB production might imply a significant change on their mechanical properties.

3.5. 2D cell proliferation assays

To determine if the alterations in the nanoscale properties observed among variant IBs could be sensed by biological systems, we comparatively explored the abilities of these particulate materials to promote proliferation of mammalian cells, upon decoration of 2D surfaces. In a previous study [14], we have demonstrated that IBs (produced in a DnaK$^-$ strain), when deposited on polystyrene plates, modify the nanoscale topology in a way that stimulated cell proliferation. Therefore, IBs produced in either wt bacteria or in DnaK$^-$ and ClpA$^-$ backgrounds were comparatively tested in a cell culture assay. Interestingly, the proliferation of baby hamster kidney (BHK) cells was favored by all IB variants although at different extents (Fig. 5a). In particular, at 72h after the initiation of the culture the cell density in plates decorated with wt and DnaK$^-$ IBs was about twice than in plates without IBs. While both types of IBs rendered cell density values statistically indistinguishable ($p = 0.538$), ClpA$^-$ IBs dramatically enhanced cell density over the values achieved by other IB variants, although at levels still out the significance level ($p = 0.162$ when comparing with DnaK$^-$ IBs; $p = 0.203$ when comparing with wt IBs). To confirm the differential properties of ClpA$^-$ IBs in stimulating cell proliferation we

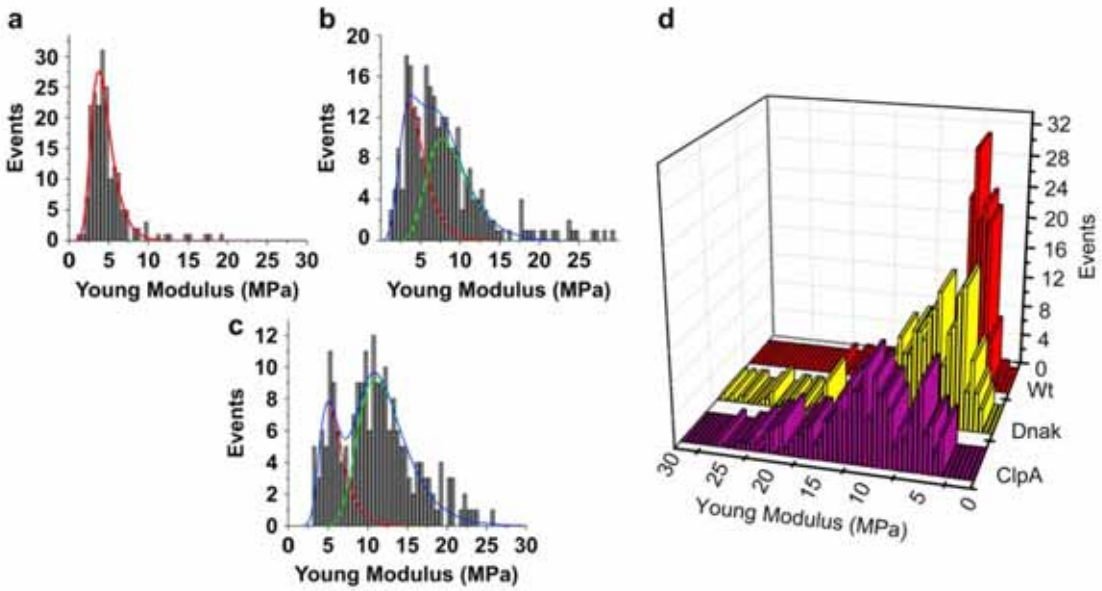

Fig. 3. Histogram representation of the number of events vs. Young modulus for IBs produced in bacterial mutants. a) Wt IBs showing only one peak at 3.73 MPa; b) DnaK$^-$ IBs show two overlapped Young modulus distributions which centered at 3.56 and 7.75 MPa; c) ClpA$^-$ IB show the presence of two different young modulus distributions, at 5.01 and 10.99 MPa; d) 3D representation of the later histograms.

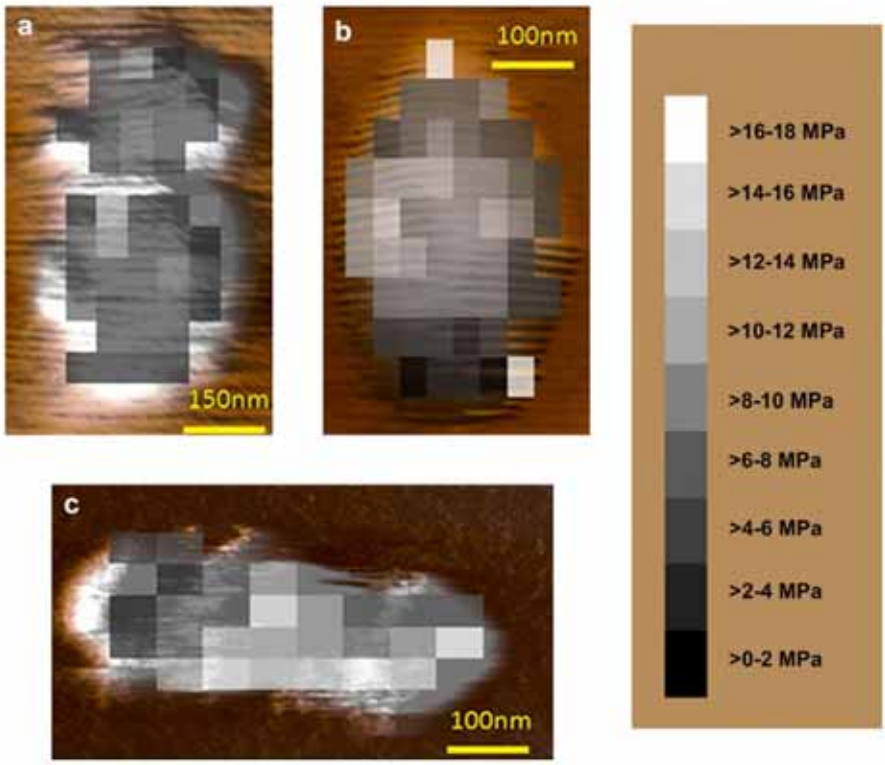

Fig. 4. 2D software developed reconstruction of the elasticity maps of selected IBs from the three genetic backgrounds. a) wt IBs, b) DnaK$^-$ IBs, c) ClpA$^-$ IBs. Observations infer the existence of a homogeneously spread distribution of Young modulus values over the wt IBs. On the other hand, maps obtained for DnaK$^-$ and ClpA$^-$ IBs indicate the existence of two elasticity populations, with the harder areas segregated and localised on the centre of the DnaK$^-$ IBs and on the right side of ClpA$^-$ particles.

extended the study to rat pheochromocytoma (PC12) cells, that tend to grow as floating clusters rather than as firmly attached monolayers. In this model, ClpA$^-$ IBs enhanced cell proliferation over DnaK$^-$ IBs in a still more evident way (Fig. 5b; $p = 0.004$). This confirms that these particles display improved nanoscale properties regarding tissue engineering-oriented topographical modification and that cell proliferation responds to the stiffness increase of the surface decorating material. The progressive temporal increase in the differences in MTT assays promoted by the IB variants indicates that they act stimulating cell proliferation rather than cell adhesion. Interestingly, the similarity between the macroscopic eco of DnaK$^-$ IBs and wt IBs in IB-cell interfaces and the divergent behavior of ClpA$^-$ IBs is highly coincident with the profile of the nanomechanical properties (including wettability and

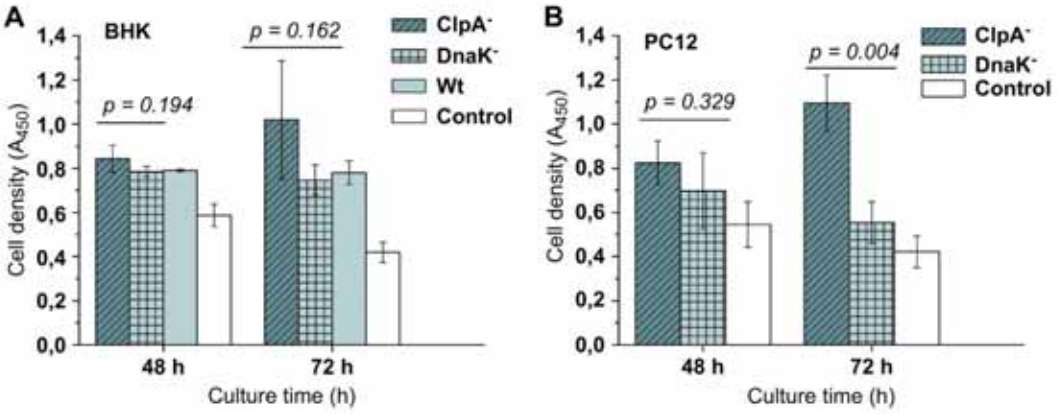

Fig. 5. Cell proliferation determined by a conventional MTT assay monitored in polystyrene plates. Plates were untreated (control) or decorated with 2.65×10^8 IBs per well of different IB variants. The analysis was done in triplicate using BHK (A) and PC12 (B) cell lines. Differences of cell density between IB-decorated wells and IB-free wells (control) were always significant ($p < 0.006$, not shown) in all the experiments. As an exception, growth of PC12 cells on DnaK$^-$ IBs was stimulated over the control in the limits of statistic significance ($p = 0.132$ at 48 h and $p^{\sim} < 0.047$ at 72 h). The significance as p values of the differences between growth on ClpA$^-$ and DnaK$^-$ IBs are depicted over the corresponding bars.

stiffness) exhibited by the IB variants, again very proximal when comparing IBs produced by wt and DnaK$^-$ cells.

4. Discussion

IBs are formed in recombinant bacteria submitted to conformation stress [9], and are now seen as extremely dynamic protein clusters [34] that contain an important extent of polypeptides with native-like secondary structure and are biologically active [5]. At least a significant fraction of polypeptides embedded in IBs are functional [5]. How functional species can coexist with the amyloid-like pattern (governed by cross molecular beta-sheet interactions) is still unsolved. However, the influence of environmental conditions on the folding state of IB proteins [3,35] indicates an important degree of molecular flexibility. In addition, being the IB protein quality tightly surveyed by the quality control system [4] is not unexpected that functional modifications in the bacterial folding machinery would result in IBs with altered physical properties, as protein folding and degradation, but also protein deposition as IBs and removal from these particles would be mechanistically affected. However, the mechanical properties of IBs at the nanoscale have never been explored as these protein clusters have not attracted any interest as biomaterials, although in a different context, they have been recently observed as intriguing catalizers when formed by enzymes [4,6]. Recent experiments strongly supporting the biocompatibility of IBs as nanoparticulate materials [6] has pushed for a fine characterization and eventual tuning of the biophysical properties that might be relevant to biomedical applications, such as the bottom-up topographic surface modification in tissue engineering [9]. In this context, GFP-containing IBs have been fabricated in bacteria deficient in either DnaK or ClpA, in the hope to identify significant modifications in their properties as particulate nanomaterials. DnaK is the main cytosolic chaperone of *E. coli*, that being a negative regulator of the heat shock system [9] and a potent proteolytic stimulator [36] also show folding, holding and disaggregase activities [16]. ClpA is the ATPase subunit of ClpP and possesses intriguing foldase-like properties [37]. GFP IBs produced in these specific backgrounds are more fluorescent than wt IBs [16], indicating at least conformational variations in the aggregated protein regarding to IBs formed by a fully functional quality control. While IBs produced in wild type *E. coli* depict a maximum coverage at slightly hydrophobic surfaces and a monomodal stiffness profile, those developed either in the DnaK$^-$ or ClpA$^-$ derived background show a disrupted wettability pattern (Fig. 1 right) where the coverage maximum is splitted in two and shifted to higher and lower wettability regions. Furthermore, although its coverage and subsequently the substrate roughness of DnaK$^-$ IBs is similar to those of wt derivates, they manifest an enhanced (but not statistically significant) tendency to favour mammalian cell growth (Fig. 5) in cell proliferation assays if compared to wt ones. This could be related to the enhanced values of the IB stiffness map suggesting a dual protein population, that might increase the cell responsiveness to the altered topography. The absence of the chaperone DnaK, that in IB-forming cells mainly transfers polypeptides to the ClpP and Lon proteases for digestion [16] on the surface of IBs [16], results in IBs, which contain a more heterogenous protein population regarding functionality and conformation status than wt IBs [38]. Interestingly, the absence of the ATPase ClpA, that mediates protein translocation to its cognate protease ClpP [39,40], results not only in a higher coverage and therefore, a rougher system but also in an even more stiff IBs in which the dual stiffness mapping is even more evident than in DnaK$^-$ cells (Fig. 4). In this case, the impact on biological systems is dramatic, proving that the extent of the genetically determined mechanical variations of IBs is within the range of the functional capacity of the cells sensory elements that respond more actively to harder IBs.

Those results are in agreement with previous Fourier transformed infrared spectroscopy analyses (FTIR) of DnaK$^-$ and ClpA$^-$ IBs, in which a downshift in the β-sheet peaks (at 1627 and 1693 cm^{-1}) was observed [41], indicating a more compact and therefore stiffer cross-β-sheet architecture than in wt IBs. In addition, recombinant proteins are stabilized in these backgrounds as a result of a global inhibition of the proteolytic activity of the quality control machinery [16], leading to the incorporation of otherwise degraded protein species into IBs. This dual deposition could be linked to the heterogeneous stiffness maps obtained for DnaK$^-$ and ClpA$^-$ IBs, and indicates that the conformational status of the aggregated polypeptides determines the consistence of the protein clusters at the nanoscale level.

As well as other biomaterials used for cell proliferation, such as polymers or hydrogels, IBs have probed their efficiency as grow vector. However, while regularly used non-biologic materials require the use of complicated or expensive production techniques of even some chemical compounds that may affect the target cells, IBs are naturally produced, highly flexible and non-toxic biomaterials which can be easily produced by bacteria on multigram scale. Furthermore, whereas traditional materials properties are, usually, hard to be modified, IBs properties can be easily tuned just by changing its genetic background. IBs can, therefore, be considered as multifunctional tunable biomaterials able to selectively modify cell proliferation when used to decorate a solid substrate.

5. Conclusions

The conformation status of recombinant proteins in *E. coli*, as regulated by the proteins quality control, defines the nanoscale physicochemical properties of inclusion bodies. Such proteinaceous particulate biomaterial exhibit a range of wettability and stiffness when obtained in wild type, DnaK$^-$ and ClpA$^-$ strains, associated to the style of protein packaging occurring in absence of each of these elements of the heat shock machinery. The inhibition of proteolysis allowing the deposition of otherwise degraded protein species and the associated condensation of the inclusion body cross-β-sheet architecture in DnaK$^-$ and ClpA$^-$ backgrounds can account from the up shift of particle stiffness from around 2 up to 16 MPa. Interestingly, when using inclusion bodies for bottom-up surface decoration in tissue engineering, such range of mechanical properties is sensed by cultured mammalian cells, resulting in a dramatic stimulation of cell proliferation, which increases with the stiffness of the substrate material. Since bacterial inclusion bodies are fully compatible nanomaterials that can be obtained at large scale by cost-effective procedures, their physiological modification during biofabrication in selected genetic backgrounds can be observed as an intriguing possibility to generate improved versions tailored for specific biological interfaces. The tuning opportunities offered through adjusting the quality control, so much explored for recombinant protein solubility issues, definitively expands the spectrum of biomedical applications of this novel bacterial nanomaterial.

Acknowledgments

The authors appreciate the financial support through MEC (BIO2007-61194, BFU2010-17450, and CTQ2006-06333) and AGAUR (2009SGR-108 and 2009SGR-00516) grants and from the CIBER de Bioingeniería, Biomateriales y Nanomedicina (CIBER-BBN, promoted by ISCIII), Spain. AV was distinguished by ICREA (Generalitat de Catalunya) with an ICREA ACADEMIA award. Supporting Information is available online from Wiley InterScience or from the

authors. We recognize the technical support from Dr. G. Oncins (Nanometric Techniques unit, Scientific-Technical Services of the University of Barcelona).

Appendix. Supporting information

Supporting information associated with this article can be found, in the online version, at doi:10.1016/j.biomaterials.2010.04.008.

Appendix

Figures with essential colour discrimination. Certain figures in this article, in particular Fig. 4, are difficult to interpret in black and white. The full colour images can be found in the on-line version, at doi:10.1016/j.biomaterials.2010.04.008.

References

[1] Marston FA. The purification of eukaryotic polypeptides synthesized in *Escherichia coli*. Biochem J 1986;240(1):1–12.
[2] Baneyx F, Mujacic M. Recombinant protein folding and misfolding in *Escherichia coli*. Nat Biotechnol 2004;22(11):1399–408.
[3] Garcia-Fruitos E, Gonzalez-Montalban N, Morell M, Vera A, Ferraz R, Aris A, et al. Aggregation as bacterial inclusion bodies does not imply inactivation of enzymes and fluorescent proteins. Microb Cell Fact 2005;4(1):27.
[4] Gonzalez-Montalban N, Garcia-Fruitos E, Villaverde A. Recombinant protein solubility-does more mean better? Nat Biotechnol 2007;25(7):718–20.
[5] Ventura S, Villaverde A. Protein quality in bacterial inclusion bodies. Trends Biotechnol 2006;24(4):179–85.
[6] Martínez-Alonso M, Gonzalez-Montalban N, Garcia-Fruitos E, Villaverde A. Learning about protein solubility from bacterial inclusion bodies. Microb Cell Fact 2009;8(1):4.
[7] deGroot NS, Sabate R, Ventura S. Amyloids in bacterial inclusion bodies. Trends Biochem Sci 2009;34(8):408–16.
[8] Margreiter G, Messner P, Caldwell KD, Bayer K. Size characterization of inclusion bodies by sedimentation field-flow fractionation. J Biotechnol 2008;138(3–4):67–73.
[9] García-Fruitós E, Rodríguez-Carmona E, Díez-Gil C, Ferraz RM, Vázquez E, Corchero JL, et al. Surface cell growth engineering assisted by a novel bacterial nanomaterial. Adv Mater 2009;21(42):4249–53.
[10] Bowden GA, Paredes AM, Georgiou G. Structure and morphology of protein inclusion bodies in *Escherichia coli*. *Biotechnology* (N.Y.). 1991;725–30.
[11] Foguel D, Silva JL. New insights into the mechanisms of protein misfolding and aggregation in amyloidogenic diseases derived from pressure studies. Biochemistry 2004;43(36):11361–70.
[12] Peternel S, JevŠevar S, Bele M, Gaberc-Porekar V, Menart V. New properties of inclusion bodies with implications for biotechnology. Biotechnol Appl Biochem 2008;49(4):239–46.
[13] Domke J, Radmacher M. Measuring the elastic properties of thin polymer films with the atomic force microscope. Langmuir 1998;14(12):3320–5.
[14] Parra A, Casero E, Lorenzo E, Pariente F, Vazquez L. Nanomechanical properties of globular proteins: lactate oxidase. Langmuir 2007;23(5):2747–54.
[15] Wang L. Towards revealing the structure of bacterial inclusion bodies. Prion 2009;3:6.
[16] García-Fruitós E, Martínez-Alonso M, González-Montalbán N, Valli M, Mattanovich D, Villaverde A. Divergent genetic control of protein solubility and conformational quality in *Escherichia coli*. J Mol Biol 2007;374(1):195–205.
[17] Faucheux N, Schweiss R, Lützow K, Werner C, Groth T. Self-assembled monolayers with different terminating groups as model substrates for cell adhesion studies. Biomaterials 2004;25(14):2721–30.
[18] Webb K, Hlady V, Tresco PA. Relative importance of surface wettability and charged functional groups on NIH 3T3 fibroblast attachment, spreading, and cytoskeletal organization. J Biomed Mater Res 1998;41(3):422–30.
[19] Andrade J, Hlady V. Protein adsorption and materials biocompatibility: a tutorial review and suggested hypotheses. In: Biopolymers/Non-Exclusion HPLC. Berlin: Springer; 1986. p. 1–63.
[20] Washburn NR, Yamada KM, Simon CG, Kennedy SB, Amis EJ. High-throughput investigation ofosteoblast response to polymer crystallinity: influence of nanometer-scale roughness on proliferation. Biomaterials 2004;25(7–8):1215–24.
[21] Yeung T, Georges P, Flanagan L, Marg B, Ortiz M, Funaki M, et al. Effects of substrate stiffness on cell morphology, cytoskeletal structure, and adhesion. Cell Motil Cytoskeleton 2005;60(1):24–34.
[22] Chen C-C, Hsieh PC-H, Wang G-M, Chen W-C, Yeh M-L. The influence of surface morphology and rigidity of the substrata on cell motility. Mater Lett 2009;63(21):1872–5.
[23] Hadjipanayi E, Mudera V, Brown RA. Close dependence of fibroblast proliferation on collagen scaffold matrix stiffness. J Tissue Eng Regen Med 2009;3(2):77–84.
[24] Cheung Yuk K, Azeloglu Evren U, Shiovitz David A, Costa Kevin D, Seliktar D, Sia Samuel K. Microscale control of stiffness in a cell-adhesive substrate using microfluidics-based lithography. Angew Chem Int Ed Engl 2009;48(39):7188–92.
[25] Teixeira AI, Ilkhanizadeh S, Wigenius JA, Duckworth JK, Inganäs O, Hermanson O. The promotion of neuronal maturation on soft substrates. Biomaterials 2009;30(27):4567–72.
[26] Saha K, Keung AJ, Irwin EF, Li Y, Little L, Schaffer DV, et al. Substrate modulus directs neural stem cell behavior. Biophys J 2008;95(9):4426–38.
[27] Engel A, Muller DJ. Observing single biomolecules at work with the atomic force microscope. Nat Struct Mol Biol 2000;7(9):715–8.
[28] Jaeger MS, Uhlig K, Clausen-Schaumann H, Duschl C. The structure and functionality of contractile forisome protein aggregates. Biomaterials 2008;29(2):247–56.
[29] Koenders MMJF, Yang L, Wismans RG, van der Werf KO, Reinhardt DP, Daamen W, et al. Microscale mechanical properties of single elastic fibers: the role of fibrillin–microfibrils. Biomaterials 2009;30(13):2425–32.
[30] Vinckier A, Semenza G. Measuring elasticity of biological materials by atomic force microscopy. FEBS Lett 1998;430(1–2):12–6.
[31] Heuberger M, Dietler G, Schlapbach L. Mapping the local Young's modulus by analysis of the elastic deformations occurring in atomic force microscopy. Nanotechnology 1995;6(1):12–23.
[32] del Mercato LL, Maruccio G, Pompa PP, Bochicchio B, Tamburro AM, Cingolani R, et al. Amyloid-like fibrils in elastin-related polypeptides: structural characterization and elastic properties. Biomacromolecules 2008;9(3):796–803.
[33] Radmacher M, Fritz M, Cleveland JP, Walters DA, Hansma PK. Imaging adhesion forces and elasticity of lysozyme adsorbed on mica with the atomic force microscope. Langmuir 2002;10(10):3809–14.
[34] Gasser B, Saloheimo M, Rinas U, Dragosits M, Rodriguez-Carmona E, Baumann K, et al. Protein folding and conformational stress in microbial cells producing recombinant proteins: a host comparative overview. Microb Cell Fact 2008;7(1):11.
[35] Garcia-Fruitos E, Aris A, Villaverde A. Localization of functional polypeptides in bacterial inclusion bodies. Appl Environ Microbiol 2007;73(1):289–94.
[36] Rodriguez F, Arsène-Ploetze F, Rist W, Rüdiger S, Schneider-Mergener J, Mayer MP, Bukau B. Molecular basis for regulation of the heat shock transcription factor alpha 32 by the DnaK and DnaJ chaperones. Mol Cell 2008;32(3):347–58.
[37] Mogk A, Deuerling E, Vorderwülbecke S, Vierling E, Bukau B. Small heat shock proteins, ClpB and the DnaK system form a functional triade in reversing protein aggregation. Mol Microbiol 2003;50(2):585–95.
[38] Carrio MM, Villaverde A. Localization of chaperones DnaK and GroEL in bacterial inclusion bodies. J Bacteriol 2005;187(10):3599–601.
[39] Martínez-Alonso M, Vera A, Villaverde A. Role of the chaperone DnaK in protein solubility and conformational quality in inclusion body-forming *Escherichia coli* cells. FEMS Microbiol Lett 2007;273(2):187–95.
[40] Gonzalez-Montalban N, Garcia-Fruitos E, Ventura S, Aris A, Villaverde A. The chaperone DnaK controls the fractioning of functional protein between soluble and insoluble cell fractions in inclusion body-forming cells. Microb Cell Fact 2006;5(1):26.
[41] Piszczek G, Rozycki J, Singh SK, Ginsburg A, Maurizi MR. The molecular chaperone, ClpA, has a single high affinity peptide binding site per hexamer. J Biol Chem 2005;280(13):12221–30.

Annex 3

Isolation of cell-free bacterial inclusion bodies

Escarlata Rodríguez-Carmona, Olivia Cano-Garrido, Joaquin Seras-Franzoso, Antonio Villaverde, Elena García-Fruitós

Microbial Cell Factories, Vol 9, 2010

Rodríguez-Carmona et al. Microbial Cell Factories 2010, 9:71
http://www.microbialcellfactories.com/content/9/1/71

MICROBIAL CELL FACTORIES

TECHNICAL NOTES Open Access

Isolation of cell-free bacterial inclusion bodies

Escarlata Rodríguez-Carmona[1,2], Olivia Cano-Garrido[1,2], Joaquín Seras-Franzoso[1,2], Antonio Villaverde[1,2], Elena García-Fruitós[2,1*]

Abstract

Background: Bacterial inclusion bodies are submicron protein clusters usually found in recombinant bacteria that have been traditionally considered as undesirable products from protein production processes. However, being fully biocompatible, they have been recently characterized as nanoparticulate inert materials useful as scaffolds for tissue engineering, with potentially wider applicability in biomedicine and material sciences. Current protocols for inclusion body isolation from *Escherichia coli* usually offer between 95 to 99% of protein recovery, what in practical terms, might imply extensive bacterial cell contamination, not compatible with the use of inclusion bodies in biological interfaces.

Results: Using an appropriate combination of chemical and mechanical cell disruption methods we have established a convenient procedure for the recovery of bacterial inclusion bodies with undetectable levels of viable cell contamination, below 10^{-1} cfu/ml, keeping the particulate organization of these aggregates regarding size and protein folding features.

Conclusions: The application of the developed protocol allows obtaining bacterial free inclusion bodies suitable for use in mammalian cell cultures and other biological interfaces.

Background

Bacterial inclusion bodies (IBs) are water-insoluble protein aggregates formed in the bacterial cytoplasm (and eventually periplasm) during the overproduction of recombinant proteins, especially those from viral or mammalian origin [1]. The diameter of these insoluble proteinaceous particles range from about 50 nm to 500 nm, depending on the background of the producer strain, harvesting time, culture conditions and recombinant protein [2]. Although IBs have traditionally been described as biologically inert protein clusters, recent insights show that these nanoparticles have not only an important level of molecular organization, but also that they are formed by a considerable extent of functional polypeptides [3-7]. In fact, IBs are pure [8], structurally organized [9], mechanically stable and biocompatible protein deposits [2], formed through stereospecific protein-protein cross-molecular interactions under amyloid-like schemes [9,10]. This turn in the understanding of IB biological nature has prompted to explore potential applications of such aggregates as straightforward bacterial products. One of the major IB applications is their use as particulate catalysts for different bioprocesses when formed by enzymes. It has been successfully proved with different enzyme-based IBs that these aggregates efficiently catalyse bioprocesses, becoming a promising alternative to classical enzyme immobilization [7,11]. In the completely different context of tissue engineering and regenerative medicine, it is widely accepted that the nano- and micro-modification of flat surfaces by different procedures, such as etching, lithography and particle decoration, can not only favour mammalian cell binding but also improve cell proliferation and substrate colonization [12]. In this regard, we have recently explored the performance of IBs as biocompatible particulate materials suitable for engineering surfaces roughness at a micro- and nano-scale level to stimulate, by mechano-transduction events, the growth of cultured mammalian cells [2,13,14].

On the other hand, a wide range of protocols for the purification of cytoplasmic IBs are available, all of them including bacterial lysis and IB washing steps. Bacterial lysis is achieved using either mechanical or non mechanical methods, or a combination of both, while washing

* Correspondence: elena.garcia.fruitos@uab.cat
[2]CIBER en Bioingeniería, Biomateriales y Nanomedicina (CIBER-BBN), Bellaterra, 08193 Barcelona, Spain
Full list of author information is available at the end of the article

steps include, among others, detergent and/or DNase treatments. These protocols have been mainly aimed to obtain IBs suitable for in vitro protein refolding attempts [15]. Since most of them permit the recovery of high amounts of pure IBs (usually representing between 90 and 95% of the total aggregated proteins), the presence of viable bacteria in the final sample is not routinely verified. Residual bacterial contamination may not be a critical issue when using IBs as the starting material for protein refolding procedures [16-18] (Table 1[19-58]). However, for applications in which IBs act as materials in biological interfaces, for instance in tissue engineering [2] or as biocatalysts [11], the presence of living bacteria would be not acceptable.

The aim of this study has been the development of an IB purification protocol rendering bacterial-free protein particles, which could not compromise the applicability of IBs as biomaterials for biomedical applications.

Results

To explore the efficiency of conventional IB purification protocols based on lysozyme treatment combined with repeated detergent washing steps, we have determined the number of viable bacterial cells before and after cell lysis, using different bacterial strains (MC4100, DnaK$^-$ and ClpP$^-$) carrying plasmids encoding different recombinant proteins (VP1GFP, VP1LAC and VP1NLSCt) (Figure 1). Our results indicate that the used standard protocol is inefficient concerning the complete removal of viable bacteria (Figure 1). The integrity of bacterial cells upon IB purification was confirmed by scanning electron microscopy (SEM) (Figure 2). Comparing the results obtained with *Escherichia coli* MC4100 carrying different plasmids, we noticed that, being the initial amount of bacteria around $1{\cdot}10^9$ cfu/ml in all cases, remaining viable cells after the protocol application ranged from $5{\cdot}10^7$ to $1{\cdot}10^3$ cfu/ml (Figure 1). In particular, we noted that the ClpP$^-$ strain carrying pTVP1GFP plasmid was the most resistant to cell lysis, since more than 10^7 cfu/ml remained after IB purification (Figure 1). Intriguingly, replicas of ClpP$^-$/pTVP1GFP and MC4100/pTVP1LAC cultures gave quite similar viable cell counts, but the lysis of DnaK$^-$/pTVP1GFP, MC4100/pTVP1GFP and MC4100/pTVP1NLSCt showed an important variability (Figure 1).

Because of the poor performance of the standard protocol cell lysis based on lysozyme, we decided to explore the effectiveness of other cell disruption protocols (Table 1). Viable bacteria were still observed after the application of lysis methods such as the French Press and freeze-thawing (data not shown). Specifically, we determined the viable cell concentration after using the French Press up to 7 rounds at 2,000 psi, observing a non significant decrease in the viable cell counts. Additionally, the effectiveness of freeze-thawing rounds was also not relevant. Thus, neither the physical nor the chemical methods tested were effective enough to obtain IBs free from bacterial contamination. Therefore, as the bacterial lysis was a bottleneck of the whole IB purification process, we decided to develop an improved protocol by combining both sonication and lysozyme treatment. After testing several combinations of these procedures and determining cell counts at the end of each process, the best protocol (Figure 3) combined both physical and chemical lysis methods with some washing steps and a DNase treatment (Figure 3). After the sonication step (Figure 3), no viable bacteria were observed in the sample containing purified IBs, regardless of the strain and plasmid used. However, the number of sonication cycles needed to eliminate all viable bacteria clearly depended on the particular protein encoded in the plasmid (Figure 4). Full lysis of *Escherichia coli* strains overproducing VP1GFP needed 5 sonication rounds of 10 min at 40% amplitude under 0.5 s cycles, independently of the genetic background (Figure 4). However, strains overproducing VP1LAC or VP1NLSCt proteins required 6 and 9 disruption cycles, respectively (Figure 4).

Since the IB-forming VP1GFP protein, encoded in all the plasmids used here, is a suitable model protein to easily determine functionality, IB architecture and mechanical stability [2,28], we evaluated the degree of IB purity as well as the functionality of the embedded protein, after IB isolation from MC4100/pTVP1GFP, DnaK$^-$/pTVP1GFP and ClpP$^-$/pTVP1GFP cells, by confocal microscopy. The obtained images confirmed that isolated IBs were still fluorescent and their morphology fully preserved. This demonstrates that the developed protocol does not significantly alter the final protein quality of highly pure IBs (Figure 5).

Discussion

The presence of bacteria in purified IB samples can be a major drawback when using these nanoparticles for biomedical and industrial applications. Although many IB purification protocols have been developed, their effectiveness regarding residual cell viability had not been tested. In this study we have explored different IB purification methods, focusing our attention on the lysis step, which seems to be decisive to obtain bacteria-free samples. The obtained results clearly show that IB purification methods based on lysozyme treatment, French press or freezing-thawing cycles are not effective concerning complete bacterial cell lysis, while the combination of both sonication and lysozyme treatments was the most effective option (Figure 3). Even though these methods have already been combined in different protocols, cell lysis efficiency remained unproved. Menzella and co-workers and Schrodel and collaborators used 5 min of sonication in order to obtain pure IBs [54,56].

Rodriguez-Carmona et al. Microbial Cell Factories 2010, 9:71
http://www.microbialcellfactories.com/content/9/1/71

Table 1 Bacterial lysis methods for IB purification

Lysis method		IB protein	DNase	Detergents	Tested viability	Reference
NON MECHANICAL LYSIS METHODS	LYSOZYME	LACVP1	Yes	Yes	No	[19-22]
		VP1LAC	Yes	Yes	No	[7-9,19-27]
		V2LAC	Yes	Yes	No	[22]
		TSP	Yes	Yes	No	[23]
		VP1GFP	Yes	Yes	No	[7,28-30]
		hDHFR	Yes	Yes	No	[7]
		Aβ42-BFP	Yes	Yes	No	[7]
		β-lactamase	Yes	Yes	No	[31]
		Prochymosin	No	Yes	No	[32]
		HET-s fungal prion	Yes	Yes	No	[33]
		Aβ42-GFP	Yes	Yes	No	[30,34]
		Aβ42-BFP	Yes	Yes	No	[30]
		MalE-Bla and MalE31-Bla	No	No	No	[35]
		MalE-PhoA and MalE31-PhoA	No	No	No	[35]
	NON-IONIC DETERGENTS	CBDclosN-SAA	No	Yes	No	[36]
		SAA-6HisC	No	Yes	No	[36]
		Maltodextrin phosphorylase	No	Yes	No	[37]
		CBD_{Clos}SabA	No	Yes	No	[38]
MECHANICAL LYSIS METHODS	HOMOGENIZER	rhBMP-2	No	Yes	No	[17,39]
		G-CSF	No	No	No	[40]
		rhMCSF	No	No	No	[41]
		rHEWL	No	Yes	No	[42]
		GFP	No	No	No	[43]
	FRENCH PRESS	EGD	No	No	No	[44]
		TvDAO	No	Yes	No	[45,46]
		NS3 protein	No	Yes	No	[47]
	SONICATION	IFN-α	No	No	No	[48]
		β-galactosidase	No	No	No	[49]
		pGH	No	No	No	[50]
		Pre-β-lactamase	No	No	No	[51]
		Procathepsin B	No	Yes	No	[52]
COMBINED LYSIS METHODS	SONICATION + HOMOGENIZER	N^{pro} fusion proteins	No	Yes	No	[53]
	SONICATION + LYSOZYME or LYSOZYME + SONICATION	Prochymosin	No	Yes	Yes	[54]
		Cro-β-gal	Yes	Yes	Yes	[55]
		His-GST-GFP	Yes	No	No	[56]
		Prochymosin B	No	Yes	No	[54]
		CLIPB14 Serine protease	Yes	Yes	No	[57]
	FRENCH PRESS + LYSOZYME or LYSOZYME + FRENCH PRESS	PHA synthase	Yes	Yes	No	[58]
		Class II PHA synthase	Yes	Yes	No	[58]

Rodriguez-Carmona *et al. Microbial Cell Factories* 2010, **9**:71
http://www.microbialcellfactories.com/content/9/1/71

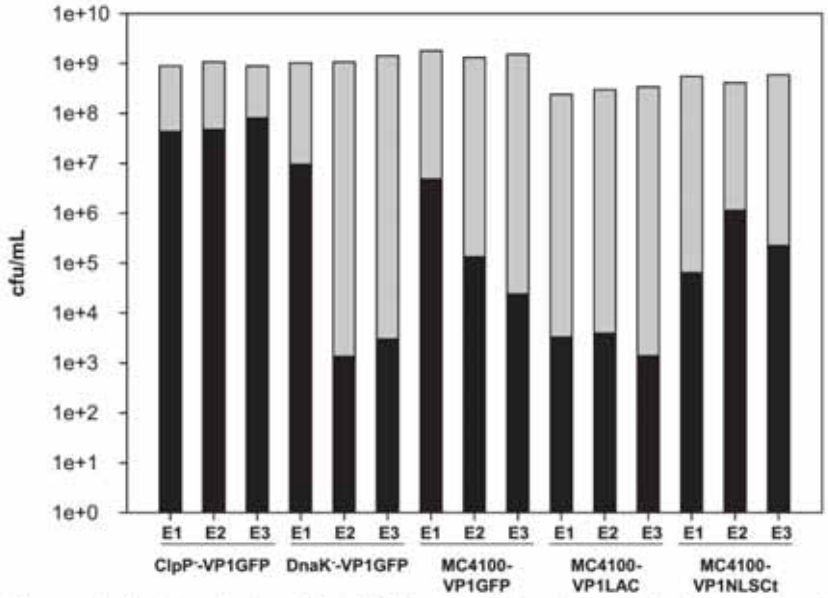

Figure 1 Viable cells counts before (grey bars) and after (black bars) cell lysis, using a standard protocol based on lysozyme and detergent treatment. E1, E2 and E3 correspond to three different replicas.

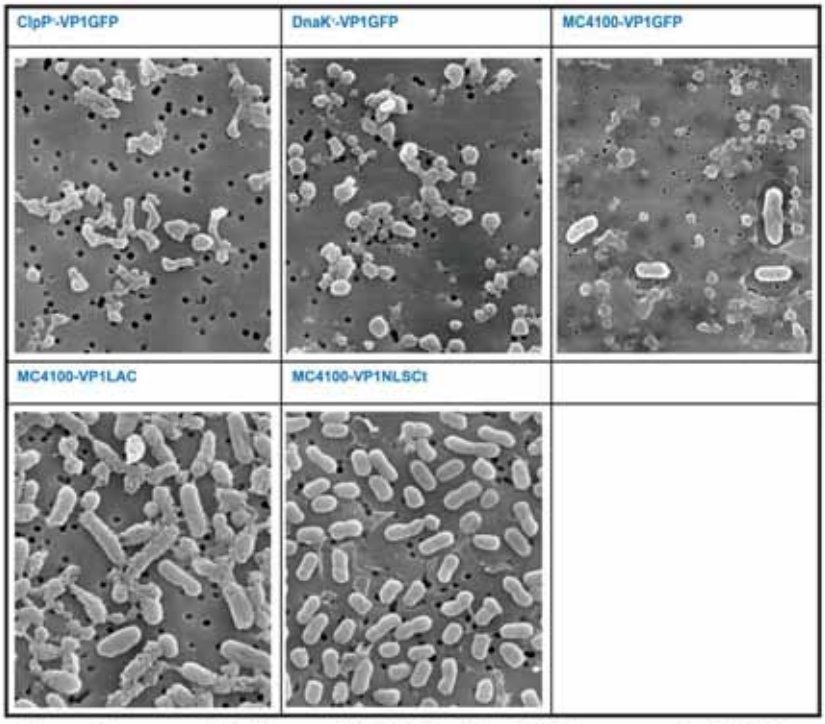

Figure 2 Scanning Electron Microscopy (SEM) images of MC4100, DnaK⁻ and ClpP⁻ overexpressing VP1GFP (top) and of MC4100 overexpressing VP1LAC and VP1NLSCt (bottom).

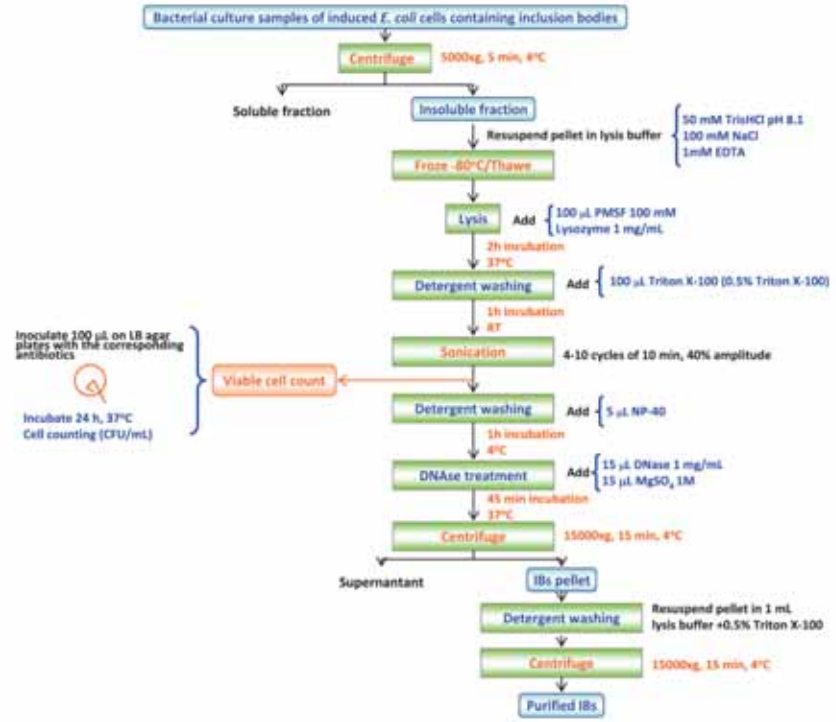

Figure 3 IB purification protocol: lysozyme-detergent, sonication and repeated detergent washing treatment.

However, our data clearly prove that at least 5 sonication cycles of 10 min at 40% amplitude under 0.5 s cycles are needed to reach a sample completely free from contaminating bacteria. Furthermore, the obtained results indicated that sonication cycles, sonication time but also lysozyme concentration must be determined for each specific protein (Figure 4).

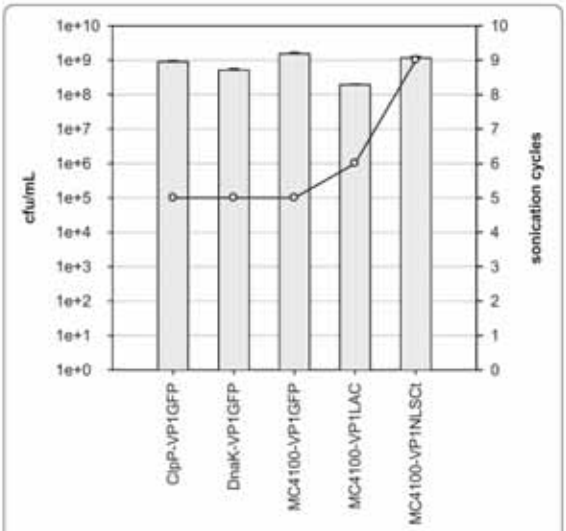

Figure 4 Viable cells counts in initial bacterial cultures (grey bars) and sonication cycles needed to eliminate all viable bacteria (white circles).

As mentioned before, our results showed a surprising variability among bacterial strains overproducing different recombinant proteins. Villa and collaborators have recently described that membrane lipids are dramatically influenced by the stress resulting from recombinant protein production [59]. Therefore, as the membrane protein composition and permeability in recombinant bacteria can be influenced by the specific produced protein [59,60], the observed variability regarding lysis efficiency could be accounted by different features of the recombinant polypeptide, that dissimilarly causes stress effects on the host cell.

Conclusion

Results presented here prove that the existing IB purification protocols may be not appropriate when those aggregates have to be used for both catalysis and biomedical purposes, due to residual but significant levels of metabolically active bacterial cells. In this context, a novel protocol developed in this study, which combines

Rodríguez-Carmona *et al. Microbial Cell Factories* 2010, **9**:71
http://www.microbialcellfactories.com/content/9/1/71

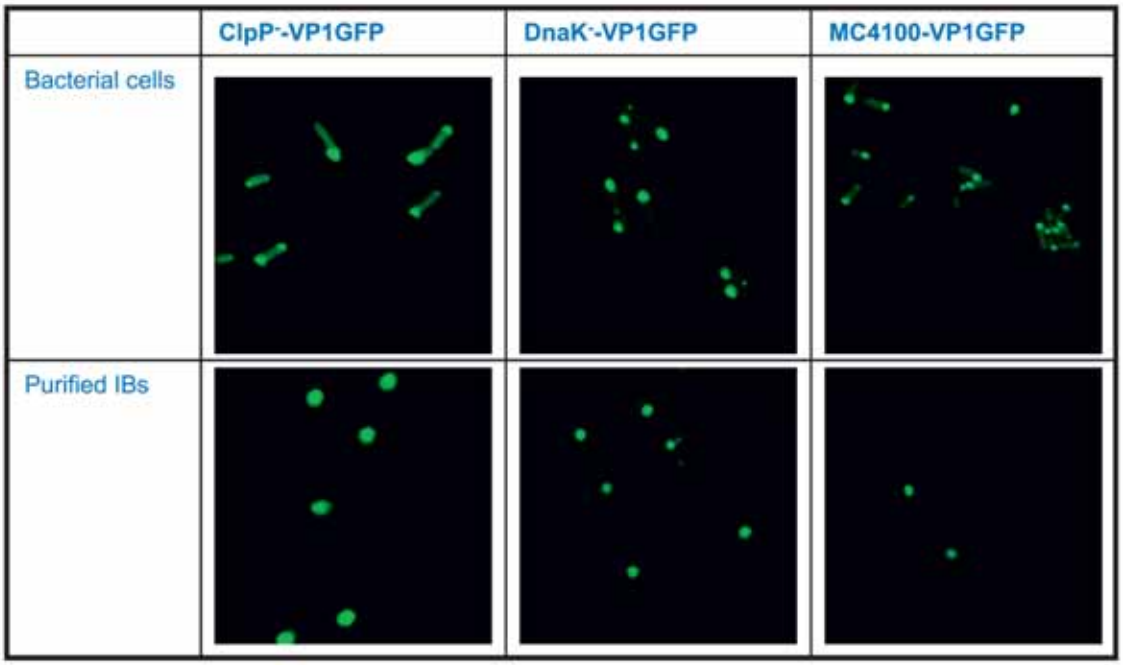

Figure 5 Confocal microscopy images of ClpP-, DnaK- and MC4100 cells overproducing VP1GFP (top). Confocal microscopy images of IBs purified from these strains (bottom).

both sonication-lysozyme treatment with DNase and detergent washing steps, has proved to be highly efficient regarding cell lysis and useful to obtain preparations of cell-free IBs.

Materials and methods

Strains and plasmids

The *Escherichia coli* strains used in this work were MC4100 (*araD139* Δ(*argF-lac*) *U169 rpsL150 relA1 flbB5301 deoC1 ptsF25 rbsR*, Strep^R) [61] and their derivatives JGT19 (*clpP::cat* Strep^R) and JGT20 (*dnak756 thr::Tn10*, Strep^R, Tc^R) [62]. The strain MC4100 was transformed with three different plasmids: pTVP1GFP, pTVP1LAC or pTVP1NLSCt encoding engineered versions of GFP and β-galactosidase [7] respectively. The three proteins were fused to the VP1 capsid protein of foot-and-mouth disease virus that dramatically reduces the solubility of the whole fusion, resulting in its aggregation as IBs [22]. JGT10 and JGT20 were only transformed with pTVP1GFP.

Culture conditions

Bacterial strains were cultured in shake flask cultures at 37°C and 250 rpm in LB rich medium [61] plus 100 μg/ml ampicillin for plasmid maintenance. Recombinant gene expression was induced when the optical density at 550 nm reached 0.5, by adding IPTG to 1 mM. Cell samples were taken at 3 h after induction of gene expression and were processed for bacterial counts, IB sampling and purification and microscopy analyses. Data for further analysis were obtained from three independent experiments.

Bacterial counts

The concentration of colony forming units (cfu/ml) was determined on LB plates with the corresponding antibiotics. After an appropriate dilution in Ringer 1/4, samples were inoculated on LB plates and incubated at 37°C o/n. Cell counting was always performed in triplicate.

IBs sampling and purification

Culture samples of 20 ml were taken 3 h after induction and IBs were purified by using two different purification protocols as follows.

Lysozyme and repeated detergent washing treatment: cells were harvested by centrifugation at 15,000 g at 4°C for 15 min and resuspended in 400 μl of lysis buffer (50 mM TrisHCl (pH 8.1), 100 mM NaCl and 1 mM EDTA,) and kept at -80°C o/n. After thawing, phenylmethanesulphonylfluoride (PMSF) (2.8 μl, 100 mM) and lysozyme (11.2 μl, 10 mg/ml) were added. After 45 min of incubation at 37°C, 4 μl of

Nonidet P40 (NP-40) were added and the mixture incubated at 4°C for 1 h. Then, 12 μl of DNase I (from a 1 mg/ml stock) and 12 μl of 1 M $MgSO_4$ were added and the resulting mixture was further incubated at 37°C for 45 min. Protein aggregates were separated by centrifugation at 15,000 g for 15 min at 4°C. Finally, IBs were washed once with 1 ml of the same lysis buffer containing 0.5% Triton X-100. After a final centrifugation at 15,000 g for 15 min at 4°C, pellets were stored at -80°C until analysis. All incubations were done under gentle agitation.

Lysozyme-detergent, sonication and repeated detergent washing treatment: samples of bacterial cultures (20 ml) were centrifuged at 4°C at 5,000 g for 5 min and resuspended in lysis buffer (20 ml, 50 mM TrisHCl (pH 8.1), 100 mM NaCl, and 1 mM EDTA) and frozen at -80°C o/n. After thawing, phenylmethanesulphonylfluoride (PMSF) (100 μl, 100 mM) and 1 mg/ml lysozyme (400 μl, 50 mg/ml) were added. After 2 h of incubation at 37°C, 100 μl of Triton X-100 were added (0.5% Triton X-100) and incubated at room temperature for 1 h. Then, the mixture was ice-jacketed, and sonicated between 4 and 10 cycles of 10 min at 40% amplitude under 0.5 s cycles. After sonication, an aliquot of 100 μl of the suspensions were inoculated on LB plates with the corresponding antibiotics and incubated at 37°C o/n. After that, 5 μl of Nonidet P40 (NP-40) were added to the rest of the suspension, and samples incubated at 4°C for 1 h. Then, DNA was removed with DNase (15 μl, 1 mg/ml) and $MgSO_4$ (15 μl, 1 M) for 45 min at 37°C. Finally, samples were centrifuged at 4°C at 15,000 g for 15 min, and the pellet containing pure IBs was washed once with 1 ml of lysis buffer containing Triton X-100 (0.5%). After a final centrifugation at 15,000 g for 15 min at 4°C, pellets were stored at -80°C until analysis. All incubations were done under agitation.

Microscopy analyses of bacteria and IBs

Fluorescence microscopy

At 3 h post-induction, VP1GFP-producing cells were fixed with 0.1% formaldehyde in phosphate buffered saline (PBS) and purified IBs were also resuspended in PBS and stored at 4°C until observed. Samples of bacterial cells or IBs were placed on a glass slide, fixed with a slide cover and observed with a Leica TCS SP2 AOBS confocal fluorescence microscope (Leica Microsystems Heidelberg GmbH, Mannheim, Germany) using a Plan-Apochromat objective (zoom 4 or 8; 1024 × 1024 pixels) and optical lens magnification (63×, NA 1.4 oil). Photomicrographs were obtained after excitation at 488 nm and at emission wavelengths between 500 and 600 nm.

Scanning Electron Microscopy

Bacterial samples and purified IBs were retained on a nuclepore membrane (Nuclepore Polycarbonate Track-etched Membrane, 0.2 μm pore size, Whatman Ltd.) and fixed with 2.5% phosphate buffered glutaraldehyde (Na_2HPO_4 0.9 M, $Na_2H_2PO_4$ 0.06 M, pH 8.0) for 1 h at 4°C. After that, the samples were dehydrated with increasing concentrations of ethanol in water (30, 50, 70, 90 and 100%) by consecutive 5 min washing steps. Ethanol was finally evaporated using the critical point method in a K850 CPD desiccator (Emitech, Ashford, UK). The dried membranes were sputtered with gold using a K550 Sputter Coater (Emitech, Ashford, UK) for observation. Microscopy was performed with a scanning microscope Hitachi S-570 (Hitachi LTD. Tokyo, Japan) using an acceleration between 0.5-30 kV.

Acknowledgements

The authors appreciate the financial support through MEC (BIO2007-61194, BFU2010-17450) and AGAUR (2009SGR-108). OCG is a recipient of a scholarship for initiation in research from CIBER-BBN, Spain. JSF is a recipient of a doctoral fellowship from UAB, Spain. We also appreciate the support from The Biomedical Research Networking Centre in Bioengineering, Biomaterials and Nanomedicine (CIBER-BBN, Spain), an initiative funded by the VI National R&D&i Plan 2008-2011, Iniciativa Ingenio 2010, Consolider Program, CIBER Actions and financed by the Instituto de Salud Carlos III with assistance from the European Regional Development Fund. Antonio P. Villaverde has been granted with an ICREA ACADEMIA award (from ICREA, Catalonia, Spain).

Author details

[1]Institut de Biotecnologia i de Biomedicina and Departament de Genètica i de Microbiologia, Universitat Autònoma de Barcelona, 08193 Bellaterra (Cerdanyola del Vallès), Barcelona, Spain. [2]CIBER en Bioingeniería, Biomateriales y Nanomedicina (CIBER-BBN), Bellaterra, 08193 Barcelona, Spain.

Authors' contributions

ERC performed most of the experiments and prepared the final data and figures. OCG and JSF purified inclusion bodies and analysed samples by fluorescence microscopy. AV and EGF conceived of the study. EGF directed the work and prepared the manuscript. All authors read and approved the final manuscript.

Competing interests

The authors declare that they have no competing interests.

Received: 8 May 2010 Accepted: 17 September 2010
Published: 17 September 2010

References

1. Marston FA: **The purification of eukaryotic polypeptides synthesized in *Escherichia coli*.** *Biochem J* 1986, **240**:1-12.
2. García-Fruitós E, Rodríguez-Carmona E, Díez-Gil C, Ferraz RM, Vázquez E, Corchero JL, *et al*: **Surface Cell Growth Engineering Assisted by a Novel Bacterial Nanomaterial.** *Adv Mater* 2009, **21**:4249.
3. Ventura S, Villaverde A: **Protein quality in bacterial inclusion bodies.** *Trends Biotechnol* 2006, **24**:179-185.
4. González-Montalbán N, García-Fruitós E, Villaverde A: **Recombinant protein solubility-does more mean better?** *Nat Biotechnol* 2007, **25**:718-720.
5. Peternel S, Grdadolnik J, Gaberc-Porekar V, Komel R: **Engineering inclusion bodies for non denaturing extraction of functional proteins.** *Microb Cell Fact* 2008, **7**:34.
6. Martínez-Alonso M, González-Montalbán N, García-Fruitós E, Villaverde A: **Learning about protein solubility from bacterial inclusion bodies.** *Microb Cell Fact* 2009, **8**:4.
7. García-Fruitós E, González-Montalbán N, Morell M, Vera A, Ferraz RM, Arís A, *et al*: **Aggregation as bacterial inclusion bodies does not imply inactivation of enzymes and fluorescent proteins.** *Microb Cell Fact* 2005, **4**:27.

8. Carrio MM, Corchero JL, Villaverde A: **Dynamics of in vivo protein aggregation: building inclusion bodies in recombinant bacteria.** *FEMS Microbiol Lett* 1998, **169**:9-15.
9. Carrio M, Gonzalez-Montalban N, Vera A, Villaverde A, Ventura S: **Amyloid-like properties of bacterial inclusion bodies.** *J Mol Biol* 2005, **347**:1025-1037.
10. Speed MA, Wang DI, King J: **Specific aggregation of partially folded polypeptide chains: the molecular basis of inclusion body composition.** *Nat Biotechnol* 1996, **14**:1283-1287.
11. Garcia-Fruitos E, Villaverde A: **Friendly production of bacterial inclusion bodies.** *Korean J Chem Eng* 2010, **27**:385-389.
12. Dalby MJ: **Nanostructured surfaces: cell engineering and cell biology.** *Nanomedicine-UK* 2009, **4**:247-248.
13. Diez-Gil C, Krabbenborg S, Garcia-Fruitos E, Vazquez E, Rodriguez-Carmona E, Ratera I, *et al*: **The nanoscale properties of bacterial inclusion bodies and their effect on mammalian cell proliferation.** *Biomaterials* 2010, **31**:5805-5812.
14. Garcia-Fruitos E, Seras-Franzoso J, Vazquez E, Villaverde A: **Tunable geometry of bacterial inclusion bodies as substrate materials for tissue engineering.** *Nanotechnology* 2010, **21**:205101.
15. Vallejo LF, Rinas U: **Strategies for the recovery of active proteins through refolding of bacterial inclusion body proteins.** *Microb Cell Fact* 2004, **3**:11.
16. Rudolph R, Lilie H: **In vitro folding of inclusion body proteins.** *FASEB J* 1996, **10**:49-56.
17. Vallejo LF, Brokelmann M, Marten S, Trappe S, Cabrera-Crespo J, Hoffmann A, *et al*: **Renaturation and purification of bone morphogenetic protein-2 produced as inclusion bodies in high-cell-density cultures of recombinant *Escherichia coli*.** *J Biotechnol* 2002, **94**:185-194.
18. Clark ED: **Protein refolding for industrial processes.** *Curr Opin Biotechnol* 2001, **12**:202-207.
19. Carrio MM, Corchero JL, Villaverde A: **Proteolytic digestion of bacterial inclusion body proteins during dynamic transition between soluble and insoluble forms.** *Biochim Biophys Acta* 1999, **1434**:170-176.
20. Carrio MM, Cubarsi R, Villaverde A: **Fine architecture of bacterial inclusion bodies.** *FEBS Lett* 2000, **471**:7-11.
21. Cubarsi R, Carrio MM, Villaverde A: **In situ proteolytic digestion of inclusion body polypeptides occurs as a cascade process.** *Biochem Biophys Res Commun* 2001, **282**:436-441.
22. Corchero JL, Viaplana E, Benito A, Villaverde A: **The position of the heterologous domain can influence the solubility and proteolysis of beta-galactosidase fusion proteins in *E. coli*.** *J Biotechnol* 1996, **48**:191-200.
23. Carrio MM, Villaverde A: **Protein aggregation as bacterial inclusion bodies is reversible.** *FEBS Lett* 2001, **489**:29-33.
24. Carrio MM, Villaverde A: **Role of molecular chaperones in inclusion body formation.** *FEBS Lett* 2003, **537**:215-221.
25. Petersson L, Carrio MM, Vera A, Villaverde A: **The impact of dnaKJ overexpression on recombinant protein solubility results from antagonistic effects on the control of protein quality.** *Biotechnol Lett* 2004, **26**:595-601.
26. Gonzalez-Montalban N, Garcia-Fruitos E, Ventura S, Aris A, Villaverde A: **The chaperone DnaK controls the fractioning of functional protein between soluble and insoluble cell fractions in inclusion body-forming cells.** *Microb Cell Fact* 2006, **5**:26.
27. Gonzalez-Montalban N, Natalello A, Garcia-Fruitos E, Villaverde A, Doglia SM: **In situ protein folding and activation in bacterial inclusion bodies.** *Biotechnol Bioeng* 2008, **100**:797-802.
28. Garcia-Fruitos E, Martinez-Alonso M, Gonzalez-Montalban N, Valli M, Mattanovich D, Villaverde A: **Divergent genetic control of protein solubility and conformational quality in *Escherichia coli*.** *J Mol Biol* 2007, **374**:195-205.
29. Martinez-Alonso M, Garcia-Fruitos E, Villaverde A: **Yield, solubility and conformational quality of soluble proteins are not simultaneously favored in recombinant *Escherichia coli*.** *Biotechnol Bioeng* 2008, **101**:1353-1358.
30. Morell M, Bravo R, Espargaro A, Sisquella X, Aviles FX, Fernandez-Busquets X, *et al*: **Inclusion bodies: specificity in their aggregation process and amyloid-like structure.** *Biochim Biophys Acta* 2008, **1783**:1815-1825.
31. Bowden GA, Paredes AM, Georgiou G: **Structure and morphology of protein inclusion bodies in *Escherichia coli*.** *Nat Biotechnol* 1991, **9**:725-730.
32. Taylor G, Hoare M, Gray DR, Marston FAO: **Size and Density of Protein Inclusion-Bodies.** *Nat Biotechnol* 1986, **4**:553-557.
33. Sabate R, Espargaro A, Saupe SJ, Ventura S: **Characterization of the amyloid bacterial inclusion bodies of the HET-s fungal prion.** *Microb Cell Fact* 2009, **8**:56.
34. Espargaro A, Sabate R, Ventura S: **Kinetic and thermodynamic stability of bacterial intracellular aggregates.** *FEBS Lett* 2008, **582**:3669-3673.
35. Arie JP, Miot M, Sassoon N, Betton JM: **Formation of active inclusion bodies in the periplasm of *Escherichia coli*.** *Mol Microbiol* 2006, **62**:427-437.
36. Nahalka J, Vikartovska A, Hrabarova E: **A crosslinked inclusion body process for sialic acid synthesis.** *J Biotechnol* 2008, **134**:146-153.
37. Nahalka J: **Physiological aggregation of maltodextrin phosphorylase from *Pyrococcus furiosus* and its application in a process of batch starch degradation to alpha-D-glucose-1-phosphate.** *J Ind Microbiol Biotechnol* 2008, **35**:219-223.
38. Nahalka J, Mislovicova D, Kavcova H: **Targeting lectin activity into inclusion bodies for the characterisation of glycoproteins.** *Mol Biosyst* 2009, **5**:819-821.
39. Vallejo LF, Rinas U: **Optimized procedure for renaturation of recombinant human bone morphogenetic protein-2 at high protein concentration.** *Biotechnol Bioeng* 2004, **85**:601-609.
40. Peternel S, Jevsevar S, Bele M, Gaberc-Porekar V, Menart V: **New properties of inclusion bodies with implications for biotechnology.** *Biotechnol Appl Biochem* 2008, **49**:239-246.
41. Tran-Moseman A, Schauer N, De Bernardez CE: **Renaturation of *Escherichia coli*-derived recombinant human macrophage colony-stimulating factor.** *Protein Expr Purif* 1999, **16**:181-189.
42. Batas B, Schiraldi C, Chaudhuri JB: **Inclusion body purification and protein refolding using microfiltration and size exclusion chromatography.** *J Biotechnol* 1999, **68**:149-158.
43. Novak S, Maver U, Peternel S, Venturini P, Bele M, Gaberscek M: **Electrophoretic deposition as a tool for separation of protein inclusion bodies from host bacteria in suspension.** *Colloid Surface A* 2009, **340**:155-160.
44. Tokatlidis K, Dhurjati P, Millet J, Beguin P, Aubert JP: **High activity of inclusion bodies formed in *Escherichia coli* overproducing *Clostridium thermocellum* endoglucanase D.** *FEBS Lett* 1991, **282**:205-208.
45. Nahalka J, Nidetzky B: **Fusion to a pull-down domain: a novel approach of producing *Trigonopsis variabilis* D-amino acid oxidase as insoluble enzyme aggregates.** *Biotechnol Bioeng* 2007, **97**:454-461.
46. Nahalka J, Dib I, Nidetzky B: **Encapsulation of *Trigonopsis variabilis* D-amino acid oxidase and fast comparison of the operational stabilities of free and immobilized preparations of the enzyme.** *Biotechnol Bioeng* 2008, **99**:251-260.
47. Li M, Pollakov A, Danielson UH, Su Z, Janson JC: **Refolding of a recombinant full-length non-structural (NS3) protein from hepatitis C virus by chromatographic procedures.** *Biotechnol Lett* 2003, **25**:1729-1734.
48. Babu KR, Swaminathan S, Marten S, Khanna N, Rinas U: **Production of interferon-alpha in high cell density cultures of recombinant *Escherichia coli* and its single step purification from refolded inclusion body proteins.** *Appl Microbiol Biotechnol* 2000, **53**:655-660.
49. Worrall DM, Goss NH: **The formation of biologically active beta-galactosidase inclusion bodies in *Escherichia coli*.** *Aust J Biotechnol* 1989, **3**:28-32.
50. Baranauskaite L, Sereikaite J, Gedminiene G, Bumeliene Z, Bumelis VA: **Refolding of porcine growth hormone from inclusion bodies of *Escherichia coli*.** *Biocatal Biotransfor* 2005, **23**:185-189.
51. Rinas U, Bailey JE: **Overexpression of bacterial hemoglobin causes incorporation of pre-beta-lactamase into cytoplasmic inclusion bodies.** *Appl Environ Microbiol* 1993, **59**:561-566.
52. Kuhelj R, Dolinar M, Pungercar J, Turk V: **The preparation of catalytically active human cathepsin B from its precursor expressed in *Escherichia coli* in the form of inclusion bodies.** *Eur J Biochem* 1995, **229**:533-539.
53. Kaar W, Ahrer K, Durauer A, Greinstetter S, Sprinzl W, Wechner P, *et al*: **Refolding of Npro fusion proteins.** *Biotechnol Bioeng* 2009, **104**:774-784.
54. Menzella HG, Gramajo HC, Ceccarelli EA: **High recovery of prochymosin from inclusion bodies using controlled air oxidation.** *Protein Expr Purif* 2002, **25**:248-255.
55. Kuczynska-Wisnik D, Zurawa-Janicka D, Narklewicz J, Kwiatkowska J, Lipinska B, Laskowska E: ***Escherichia coli* small heat shock proteins IbpA/B**

enhance activity of enzymes sequestered in inclusion bodies. *Acta Biochim Pol* 2004, **51**:925-931.
56. Schrodel A, de MA: **Characterization of the aggregates formed during recombinant protein expression in bacteria.** *BMC Biochem* 2005, **6**:10.
57. Schrodel A, Volz J, de Marco A: **Fusion tags and chaperone co-expression modulate both the solubility and the inclusion body features of the recombinant CLIPB14 serine protease.** *J Biotechnol* 2005, **120**:2-10.
58. Rehm BH, Qi Q, Beermann BB, Hinz HJ, Steinbuchel A: **Matrix-assisted in vitro refolding of *Pseudomonas aeruginosa* class II polyhydroxyalkanoate synthase from inclusion bodies produced in recombinant *Escherichia coli*.** *Biochem J* 2001, **358**:263-268.
59. Villa R, Lotti M, Gatti-Lafranconi P: **Components of the *E. coli* envelope are affected by and can react to protein over-production in the cytoplasm.** *Microb Cell Fact* 2009, **8**:32.
60. Ami D, Natalello A, Schultz T, Gatti-Lafranconi P, Lotti M, Doglia SM, *et al*: **Effects of recombinant protein misfolding and aggregation on bacterial membranes.** *Biochim Biophys Acta* 2009, **1794**:263-269.
61. Sambrook J, Fritsch E, Maniatis T: *Molecular Cloning, A Laboratory Manual* Cold Spring Harbor Laboratory Press, Cold Spring Harbor, NY 1989.
62. Thomas JG, Baneyx F: **Roles of the *Escherichia coli* small heat shock proteins IbpA and IbpB in thermal stress management: comparison with ClpA, ClpB, and HtpG In vivo.** *J Bacteriol* 1998, **180**:5165-5172.

doi:10.1186/1475-2859-9-71
Cite this article as: Rodriguez-Carmona *et al.*: Isolation of cell-free bacterial inclusion bodies. *Microbial Cell Factories* 2010 **9**:71.

Annex 4

Functional Inclusion Bodies Produced in Bacteria as Naturally Occurring Nanopills for Advanced Cell Therapies

Esther Vázquez, José L. Corchero, Joan F. Burgueño, Joaquin Seras-Franzoso, Ana Kosoy, Ramon Bosser, Rosa Mendoza, Joan Marc Martínez-Láinez, Ursula Rinas, Ester Fernández, Luis Ruiz-Avila, Elena García-Fruitós and Antonio Villaverde

Advanced Materials, 2012

Materials Views
www.MaterialsViews.com

ADVANCED MATERIALS
www.advmat.de

Functional Inclusion Bodies Produced in Bacteria as Naturally Occurring Nanopills for Advanced Cell Therapies

Esther Vázquez, José L. Corchero, Joan F. Burgueño, Joaquin Seras-Franzoso, Ana Kosoy, Ramon Bosser, Rosa Mendoza, Joan Marc Martínez-Láinez, Ursula Rinas, Ester Fernández, Luis Ruiz-Avila, Elena García-Fruitós, and Antonio Villaverde**

Bacterial inclusion bodies (IBs) are pseudo-spherical protein clusters, devoid of any coating layer that are often observed in recombinant bacteria but not in wild-type cells.[1] IBs are majorly formed by the recombinant protein (representing between 70 and 95% of their protein content), that self-assemble *in vivo* through stereospecific protein-protein interactions.[2] This generates a cotton-like amorphous matrix[3] and highly porous, mechanically stable protein particles with a large protein-solvent interface.[3,4] The nanoscale properties of IBs have recently characterized in detail.[5–7] Bacterial cell proteins, mainly chaperones, as well as lipids, lipopolysaccharides and nucleic acids are minor IB contaminants that might be further removed by convenient downstream procedures.[8,9] Being traditionally considered as waste side-products of protein production processes,[10] IBs have been mainly exploited as a pure source of proteins for *in vitro* refolding and further industrial or medical applications.[11–14] Recently, and because of their high mechanical stability,[7] and the tuneability of several nanoscale physical properties, including size,[7] geometry,[15] Z potential,[5] stiffness,[5] wettability[5] and density,[16] IBs have been also successfully adapted as inert nanostructured biomaterials to assist mammalian cell colonization and proliferation through surface decoration.[5–7,15] Essentially any protein species, as expressed at high rate from a recombinant form of its encoding gene, might form IBs in bacteria,[1] either spontaneously or assisted by the fusion of aggregation-prone, pull-down peptides.[17,18] Interestingly, IB proteins retain important extents of native-like secondary structure and biological activity[19] and IBs formed by enzymes efficiently perform as naturally immobilized catalysts.[20] The extent of functional recombinant protein in IBs depends on the particular protein species[21] and the genetic background of the producing bacteria.[22] The biological activity of IBs can be significantly enhanced by reducing the bacterial growth temperature[23,24] and in general, by manipulating a catalogue of factors known to favor proper protein folding *in vivo*.[25] In addition, significant amounts of properly folded functional proteins are released from IBs in aqueous media,[24,26] what prompts to presume an important bioavailability of functional protein in biological interfaces and the potential use of IBs as therapeutic agents for sustained release of protein drugs. However, the potential of IBs in protein replacement cell therapy has remained so far unexplored. In this study, and prompted by the mechanical and biological stability,[7] biocompatibility[5] and tuneability[27] of these protein particles as functional nanomaterials, we have explored whether IBs could act as natural vehicles of therapeutic proteins in protein replacement approaches. This has been addressed by exploring how functional IBs could rescue differently injured mammalian cells upon IB exposure, in an emerging concept of cell therapy based on nanoscale tablets produced in bacteria (nanopills).

First, we investigated how IBs in aqueous suspension interact with cultured mammalian cells, and at which extent these particles could be incorporated by them. For that, HeLa cell cultures were exposed to different concentrations of IBs formed by an aggregation-prone variant of the enhanced Green Fluorescent Protein (GFP)[22] used as convenient marker to monitor

Dr. E. Vázquez, Dr. J. L. Corchero, J. Seras-Franzoso, R. Mendoza, J. M. Martínez-Láinez, Dr. E. García-Fruitós, Prof. A. Villaverde
Institut de Biotecnologia i de Biomedicina
Universitat Autònoma de Barcelona
Bellaterra, 08193 Barcelona, Spain
E-mail: efruitos@ciber-bbn.es; antoni.villaverde@uab.cat

Dr. E. Vázquez, Dr. J. L. Corchero, J. Seras-Franzoso, J. M. Martínez-Láinez, Dr. E. García-Fruitós, Prof. A. Villaverde
Departament de Genètica i de Microbiologia
Universitat Autònoma de Barcelona
Bellaterra, 08193 Barcelona, Spain

Dr. E. Vázquez, Dr. J. L. Corchero, J. Seras-Franzoso, R. Mendoza, J. M. Martínez-Láinez, Dr. E. García-Fruitós, Prof. A. Villaverde
CIBER en Bioingeniería
Biomateriales y Nanomedicina (CIBER-BBN)
Bellaterra, 08193 Barcelona, Spain

DOI: 10.1002/adma.201104330

J. F. Burgueño, Prof. E. Fernández
Department of Cell Biology, Physiology and Immunology
Universitat Autònoma de Barcelona
Bellaterra, 08193, Barcelona, Spain

J. F. Burgueño, Prof. E. Fernández
CIBER de Enfermedades Hepáticas y Digestivas (CIBER-EHD)
CB06/04/0034, Bellaterra, 08193 Barcelona, Spain

Dr. A. Kosoy, Dr. R. Bosser, Dr. L. Ruiz-Avila
Janus Development SL, Parc Científic Barcelona
Torre R, Baldiri Reixach 4, 08028 Barcelona, Spain

Prof. U. Rinas
Institute of Technical Chemistry-Life Science
Leibniz University of Hannover
30167 Hannover, Germany

Prof. U. Rinas
Helmholtz Centre for Infection Research
Inhoffenstraße 7, 38124 Braunschweig, Germany

ADVANCED MATERIALS
www.advmat.de
www.MaterialsViews.com

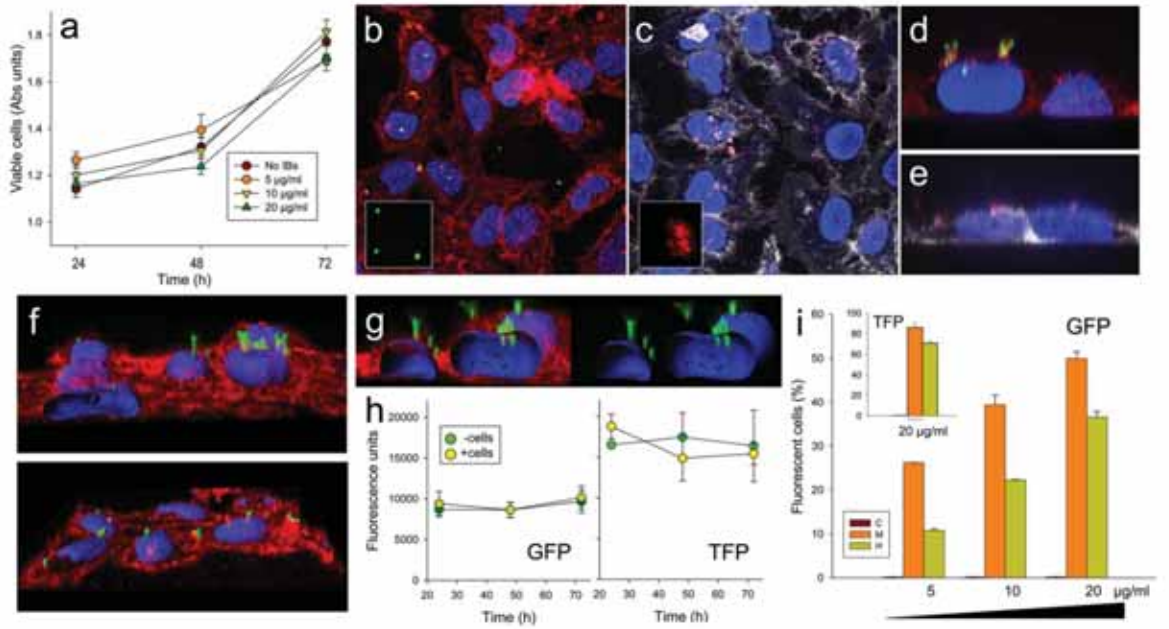

Figure 1. Cellular exposure to isolated IBs. A) Cultured HeLa cell growth (determined by MTT on polystyrene plates) in absence and in presence of increasing amounts of GFP IBs added to the culture media. B) Overlay confocal image (0.6 μm section) of HeLa cells exposed to GFP IBs for 20 h. In the inset, isolated GFP IBs before addition to the culture, with an average size of around 350 nm.[7] Nuclear membrane is seen in blue and cell membrane in red. GFP IBs are seen in green. C) Overlay confocal image (0.6 μm section) of HeLa cells exposed to TFP IBs for 20 h. In the inset, isolated TFP IBs before addition to the culture, with an average size estimated to be around between 400 nm, although their tendency to aggregation makes precise size determination highly difficult. Nuclear membrane is seen in blue and cell membrane in grey. TFP IBs are seen in red. D) *xzy* overlay of HeLa cells exposed to GFP IBs (20 h). E) *xzy* overlay of HeLa cells exposed to TFP IBs (20 h). F) Two confocal *xyz* stacks of 40 sections processed with Imaris 3D software (using the Isosurface module), showing intracellular penetration of GFP IBs. G) The embedment of IBs into the nuclear membrane is shown in two section stacks, showing the cell membrane (left) or excluding it from the picture (right). H) Intensity of fluorescence emitted by HeLa cell cultures at different times upon addition of either GFP or TFP IBs. As a control, fluorescence of IBs incubated in cell culture media in absence of cells is also shown. I) Percentage of fluorescent cell determined by flow cytometry at 4 h after addition of different amounts of GFP IBs. In the inset, the same is shown for the highest amount of TFP IBs. *C* represents cells in absence of IBs, *M* mild trypsin treatment to detach cells and *H*, harsh trypsin treatment to remove cell surface-attached protein.

intercellular imaging. Cultured cells proliferated with normality once exposed to GFP IBs (**Figure 1**a). Also, cells maintained their usual morphology and remained fully adhered to the substrate in absence of cytophatic effects, a fact that what was also confirmed by using Turbo Fluorescent Protein (Katushka, TFP635)[28] IBs (Figure 1b,c). On the other hand, both GFP and TFP IBs appeared intimately interacting with cell membranes (note the yellow and purple merging in Figure 1d,e, respectively, and Supporting Information Video 1). In addition, some protein particles were fully internalized by cells (Figure 1d,e). Both the intimate link between IBs and cell membranes as well as the cellular uptake were particularly well observed in 3D reconstructions, especially when using GFP IBs (Figure 1f). In these overviews and in the *xzy*-projections shown in Figure 1d, partial, sometimes even complete penetration of IBs into the cell nucleus was evidenced. This was fully confirmed in samples analyzed at major magnifications (Figure 1g and Supporting Information Videos 1 and 2). Most IBs interacting with the nucleus were visualized as trapped in the nuclear membrane (Figure 1d). Interestingly, the fluorescence intensity of IB proteins during prolonged incubation was not affected by cellular uptake (as fluorescence levels were comparable to those of IBs incubated in cell-free plates, Figure 1h). This indicated the stability, proteolytic resistance and functionality of the polypeptides forming IBs, in the extracellular media and also during internalization. In addition, these data indicate that IB proteins are not significantly metabolized during the experimental time (3 days).

At this stage we wondered which fraction of the cell population would have incorporated functional IBs. For that, we detached IB-exposed cells by mild trypsin treatment (M in Figure 1i) and the population of fluorescent cells was determined by flow cytometry. Between 28% and 50% of HeLa cells exposed to GFP IBs for 4 h were fluorescent in a dose-dependent fashion (Figure 1i), and these values were slightly higher for TFP IBs-exposed cells (up to almost 90%, inset). To discard externally attached fluorescence and to only resolve the fraction of cells into which IBs had been fully internalized, IB-exposed cells were treated with trypsin, using a harsh (H in Figure 1i), prolonged protocol which results in the total removal of surface-attached protein.[29] Upon this treatment, only a slight reduction in the number of fluorescent cells was observed, indicating efficient IB internalization in up to 38% and 70% of the cell population for GFP IBs and TFP IBs respectively (Figure 1i).

Adv. Mater. **2012**,
DOI: 10.1002/adma.201104330

Materials Views
www.MaterialsViews.com

ADVANCED MATERIALS
www.advmat.de

Then, only around 25% of the cell-interacting IBs remain externally associated to the cell membrane.

The lack of cytotoxicity of IBs, their stability and natural cell penetrability and that the fact that functional proteins are released from IBs under physiological conditions[24] prompted us to further explore the potential value of IBs as nanosized protein delivery systems for cell therapy (nanopills). This was approached by exposing differently injured cells to IBs formed by diverse enzymes and proteins with therapeutic potential. Four structurally and biologically distinct IB-forming human proteins were selected for the analyses, namely the chaperone Hsp70, the enzymes dihydrofolate reductase (DHFR) and catalase (CAT), and the growth factor leukemia inhibitory factor (LIF). Among other biological activities of therapeutic value, the human chaperone Hsp70 (monomer, 70 kDa) has shown an important anti-tumoral value,[30] being one of the first agents approved in China for the viral gene therapy of cancer.[31] In addition, Hsp70 is a potent inhibitor of cell apoptosis,[32] making the testing of their biological activity feasible under cell culture conditions. The antiapoptotic activity of Hsp70 is relevant both in the cytoplasm and in mitocondria.[33,34] DHFR (homodimer, 21.4 kDa per monomer), apart from being crucial in the regeneration of tetrahydrobiopterin and for the control or arterial pressure,[35] converts dihydrofolate into tetrahydrofolate, a methyl group shuttle required for the *de novo* synthesis of purines, thymidylic acid and certain amino acids.[36] Deficiencies or alterations of DHFR have been linked to megaloblastic anemia,[37] inherited spina bifida and related neurological disorders and cancer.[38] DHFR activity is located at the cytosol.[39] CAT (homotetramer, 59.7 kDa per monomer) efficiently catalyzes the decomposition of hydrogen peroxide to water and oxygen and it acts, in red blood cells, as a sink for hydrogen peroxide and superoxide removal.[40] CAT is envisaged for therapeutic use in a variety of diseases where there is a need to reduce hydrogen peroxide, such as in cancer,[41] viral-induced pneumonia,[42] ulcerative colitis and Crohn's disease,[43] and their activity is expected to be relevant in all cell compartments but especially in the cytosolic peroxisomes.[44] Finally, LIF a monomeric (19.7 kDa), four α-helix bundle protein activates a signaling cascade through interaction with its cell-surface membrane receptor LIFR[45,46] LIF is an interleukin 6 class cytokine that stimulates growth and differentiation of several cells types, and positively intervenes in blastocyte implantation,[47] showing potential as a drug in infertility treatments.[48] Biological activity of LIF is maintained when thioredoxin (TRX) is fused to the N-terminus of the growth factor.[49]

Bacterial IBs formed by all these model proteins, were added to the culture medium of differently challenged mammalian cell lines (see Experimental and Supplementary Information). All these four types of protein clusters (but not IBs formed by irrelevant proteins, IR in **Figure 2**) were able to produce, in all cases and in a dose-dependent fashion, positive physiological

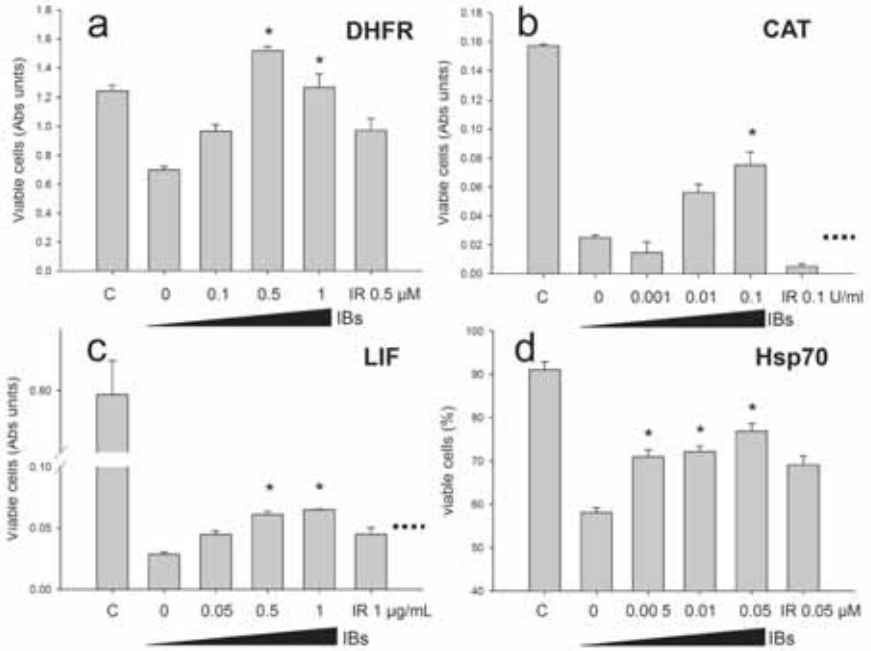

Figure 2. Rescue of damaged cells by exposure to therapeutic IBs. A) Recovery of DHFR-deficient cell viability by DHFR IBs. B) Recovery of cell viability by CAT IBs from oxidative stress. Dotted bar indicates the level of recovery achieved by comparable amounts of a soluble, commercially available CAT. C) Recovery of cell viability by LIF IBs upon growth factor removal from the medium. Dotted bar indicates the level of recovery achieved by comparable amounts of a soluble LIF version produced in bacteria along with IBs. D) Inhibition of cisplatin-induced apoptosis by Hsp70 IBs. Data from IB-treated cultures were compared with that of injured cultures non exposed to IBs (0), and significant differences ($p < 0.01$ in a Student's t test) are indicated by asterisks. Irrelevant (IR) IBs were formed by GFP for A) and B), FGF-2 for C) and LAC for D). U are enzymatic units and all the mentioned amounts or enzymatic units refer to the therapeutic protein in IBs. In all cases, the bar C represents healthy, non-insulted cells (in A, DHFR-defective CHO DG44 cells growing in the presence of the complete medium DG44, in C, TF-1 cells growing in RPMI-1640 medium supplemented with FBS and GM-CSF).

DOI: 10.1002/adma.201104330

ADVANCED MATERIALS
www.advmat.de
www.MaterialsViews.com

impacts on the treated cells. IB-treatment resulted in significantly enhancement of cell survival and/or proliferation under stress conditions (Figure 2a–c), or specifically, inhibition of apoptosis when formed by Hsp70 (Figure 2d). In particular, 0.5 μM DHFR IBs were able to double cell viability of cells missing purine precursors and to reach levels slightly higher than those achieved by supplemented cells (Figure 2a). A similar extent of cellular recovery was observed when administering 0.1 U/mL of CAT IBs (Figure 2b) and 1 μg/mL of LIF IBs (Figure 2c) to differently injured cell lines (see Supplementary information), or 0.05 μM of Hsp70 IBs to cisplatin-treated cells (Figure 2d). The increase of cell viability was statistically significant in all cases (Figure 2a–d) and comparable to, or even higher than that promoted by equimolar amounts of the soluble version of therapeutic proteins incorporated as positive controls (commercial CAT and recombinant LIF). Intriguingly, at exception of in the CAT therapeutic model, IBs formed by irrelevant proteins slightly tended to improve cell viability although below statistically significant values (Figure 2a,c,d). Although this fact would require further investigation, we hypothesize that traces of other bacterial proteins, usually present in bacterial IBs,[50] could exhibit unspecific positive effects on damaged mammalian cells. This possibility would be especially plausible in conditions that can be ameliorated by folding-assistant proteins, as the chaperone DnaK, the bacterial homologue of Hsp70, is a recognized contaminant of IBs.[51] Again, no signs of toxicity, cytopathic effects or other undesired side effects were observed when exposing mammalian cells to any of the used IBs.

These results indicate that sufficient amounts of IB-forming protein can reach and maintain native or native-like conformation at an extent required for efficient therapeutic action at cellular level. More importantly, data shown in Figure 2 evidenced the bioavailability of IB proteins. In this regard, it is not clear from which IB form, rescued cells take IB proteins, namely internalized, free particles or membrane-associated IBs. Also, experimental data with LIF indicates that extracellular IB material and the released proteins act as an additional source of therapeutic proteins. Due to the observed binding of IBs to mammalian cell membranes (Figure 1) we speculate that most of therapeutic polypeptides might derive from a slow release of active protein from membrane-anchored IB particles. This possibility, again, is fully supported by previous *in vitro* studies in which spontaneous release of functional IB protein has been fully demonstrated,[24,26] and by the high porosity of IBs that generates enormous solvent-protein interfaces.[3]

To evaluate if the nanopill concept would be only limited to *ex vivo* cell context or if it could potentially be extended *in vivo*, we have primarily tested the systemic tolerance to IBs. As in any of the approved protein drugs produced in bacteria,[52] the presence of bacterial contaminants (ribosomal components, nucleic acids and lipopolysaccharide) often observed in IBs[53] might represent a potential source of toxicity. However, new-generation protocols recently implemented for IB separation[54] and especially those adapted to completely remove bacterial contaminants[8] produce highly pure, biocompatible protein particles. By using GFP IBs, we tested the IB tolerance to oral delivery, the most preferred way for drug administration,[55] as a preliminary way to gain information about IB biocompatibility and to evaluate potential future directions for the development of the nanopill concept. In repeated administration, GFP IBs were well tolerated by all animals showing no weight loss (**Figure 3**a), normal food intake (Figure 3b), unaltered stool consistency (not shown) and no signs of discomfort, abdominal cramps or abdominal pain were observed up to 4 days

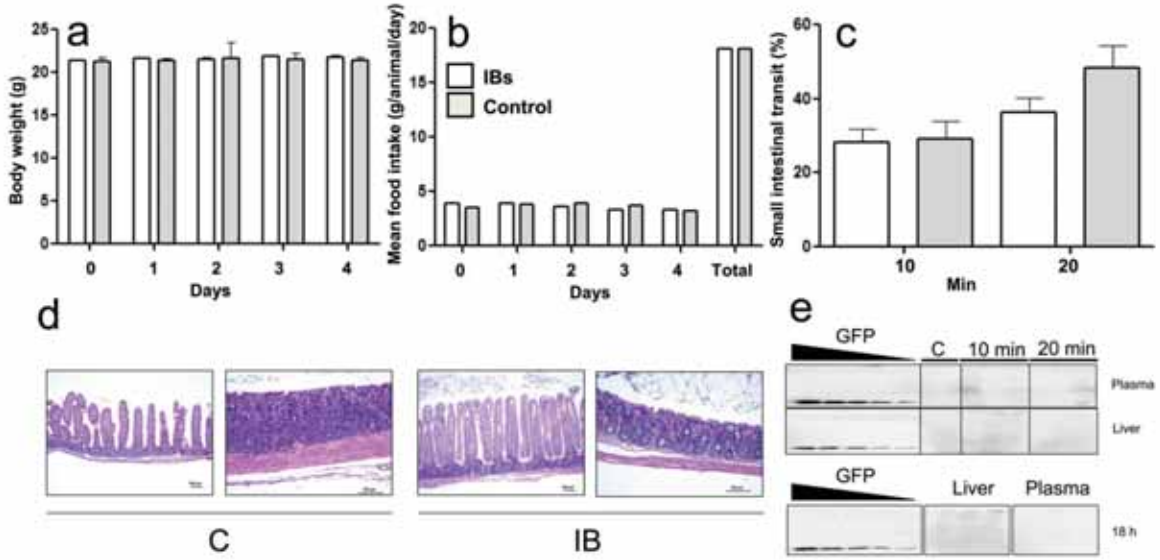

Figure 3. Tolerance of mice to oral GFP IB administration. A) Body weigh of animals during oral administration of GFP IBs compared with control animals. B) Food intake (per day and accumulated values) of animals during oral administration of GFP IBs compared with control animals. C) Intestinal transit (% total intestinal length) of bolus in IB-administered and control animals. D) Histological sections of the intestine of IB-administered animals (right) and control animals (left). E) Western blot immunodetection of GFP in plasma and liver of IB-administered and control animals (C). GFP represent 1/2 serial dilutions of commercial GFP from 500 to 37.5 ng.

Adv. Mater. **2012**,
DOI: 10.1002/adma.201104330

(not shown). The mean distance travelled by the IB bolus was slightly shorter compared to controls (Figure 3c), according to what expected for fluids containing caloric compounds (carbohydrates, proteins and lipids) that induce the release of gastrointestinal peptide hormones delaying gastric emptying.[56] The time in which we estimated IBs reaching the colon was about 1 h. No histological damage in the intestine was observed in IB-fed animals compared to controls receiving vehicle. Tissues were histologically indistinguishable (Figure 3d), again in the line of lack of IB toxicity. To explore potential penetration beyond the gastrointestinal tract, we performed western blot of selected tissues extracts, since autofluorescence was too high to allow straightforward fluorimetric monitoring. It must be noted that the intestinal content is highly abundant in porphirin-derived substances that once modified by the intestinal flora give rise to a wide variety of fluorescent compounds that emit in a broad wavelength spectrum which largely overlaps that of GFP.[57] GFP signals, although faint and diffuse because of protein excess in samples, were observed at early times in plasma and liver samples (10 and 20 min), and they remained for longer times solely in liver (Figure 3e). No traces of GFP were detected in spleen, kidney and lymph nodes (not shown). Although this fact suggested minor uptakes of GFP from the gastrointestinal tract, further analysis would be required to record quantitative data and to determine the biodistribution and pharmacokinetics of nanopill-carried protein upon oral administration.

In the present study, and by using IBs formed by Hsp70, CAT, DHFR, and LIF we have explored whether functional IBs produced in bacteria might act as natural protein delivery systems for cell therapy and at which extent mammalian cells exposed to IBs might gain phenotypic properties that rescue them from metabolic stress or other injures. The obtained data in cell culture, together with preliminary biocompatibility analysis in vivo levels provide solid support of these particles as functional nanostructured materials, which in form of nanopills show both affinity for biological membranes and high cellular penetrability. In the context of unconventional applications recently proposed for bacterial IBs[27,58,59] and the emerging needs of self-organizing biomaterials with tunable properties,[60–62] the bioavailability of IBs, whose therapeutic compound can be straightforward selected among the plethora of proteins with therapeutic potential, offers a new and highly intriguing conceptual platform that could fill important therapeutic gaps in nanomedicine and personalized medicines. The efficient and cost-effective bacterial production of these nano-micro-tablets, in which functional proteins can be even tailored by genetic engineering and produced in high cell-density bacterial cultures at industrial scale,[63] give full support to the further exploration of IBs as generic platforms for advanced drug formulation in cell therapy.

Experimental Section

Production and purification of bacteria IBs: Bacterial IBs were produced in *Escherichia coli* and purified by already described protocols. Details of plasmids, strains and proteins can be found in the Supporting Information.

Cell proliferation assay (MTT): After incubation of cells at 37 °C under selected conditions (described in the Supporting Information), variations in the number of metabolically active cells were determined using the EZ4U kit (Biomedica, GmbH) following manufacturer instructions, and samples analyzed in the multilabel reader VICTOR^3 V 1420 (Perkin Elmer). The reading absorbance was 450 nm, using 620 nm as reference, and the given values were standardized with respect to wells at exactly the same conditions but without cells.

Analytical procedures: All the analytical methods employed in this study (included those using animal models) are described in detail in the Supporting Information. All animal procedures had been approved by the Ethical Committee of the Universitat Autònoma de Barcelona (protocol number: CEEAH 1115).

Supporting Information

Supporting Information is available from the Wiley Online Library or from the author.

Acknowledgements

The authors appreciate the financial support to the design of advanced materials based on IBs through MICINN (BFU2010-17450) and AGAUR (SGR2009-108) to A.V., while J.F.B. and E.F. are supported by AGAUR (SGR2009-997). We also appreciate the financial support from from The Biomedical Research Networking Center in Bioengineering, Biomaterials and Nanomedicine, an initiative funded by the VI National R&D&i Plan 2008-2011, Iniciativa Ingenio 2010, Consolider Program, CIBER Actions and financed by the Instituto de Salud Carlos III with assistance from the European Regional Development Fund. We are indebted to the Protein Production Platform (CIBER-BBN) for helpful technical assistance and for protein production and purification services (http://bbn.ciber-bbn.es/programas/plataformas/equipamiento). We are also grateful to Antoni Iborra, Manuela Costa and Fran Cortés from the Cell Culture Unit of Servei de Cultius Cel.lulars, Producció d'Anticossos i Citometria (SCAC), and to Mónica Roldán from the Servei de Microscòpia, both at the UAB, for helpful technical assistance. A. V. has been granted with an ICREA ACADEMIA award (from ICREA, Catalonia, Spain) and E.G.F. is supported by the Programa Personal de Técnico de Apoyo (Modalidad Infraestructuras científco-tecnológicas, MICINN). *Competing interests*: E.V., J.L.C., E.G.F. and A.V. are co-inventors of a patent (WO2010131117A1) covering the use of IBs as therapeutic agents, that is currently licensed to Janus Development SL.

Received: November 11, 2011
Revised: December 25, 2011
Published online:

[1] A. Villaverde, M. M. Carrio, *Biotechnol. Lett.* **2003**, *25*, 1385.
[2] M. Morell, R. Bravo, A. Espargaro, X. Sisquella, F. X. Aviles, X. Fernandez-Busquets, S. Ventura, *Biochim. Biophys. Acta* **2008**, *1783*, 1815.
[3] S. Peternel, R. Komel, *Int. J. Mol. Sci.* **2011**, *12*, 8275.
[4] G. A. Bowden, A. M. Paredes, G. Georgiou, *Biotechnology* **1991**, *9*, 725.
[5] C. Diez-Gil, S. Krabbenborg, E. Garcia-Fruitos, E. Vazquez, E. Rodriguez-Carmona, I. Ratera, N. Ventosa, J. Seras-Franzoso, O. Cano-Garrido, N. Ferrer-Miralles, A. Villaverde, J. Veciana, *Biomaterials* **2010**, *31*, 5805.
[6] J. Seras-Franzoso, C. Diez-Gil, E. Vazquez, E. Garcia-Fruitos, R. Cubarsi, I. Ratera, J. Veciana, A. Villaverde, *Nanomedicine* **2012**, *7*, 79.
[7] E. García-Fruitós, E. Rodríguez-Carmona, C. Díez-Gil, R. M. Ferraz, E. Vázquez, J. L. Corchero, M. Cano-Sarabia, I. Ratera, N. Ventosa, J. Veciana, A. Villaverde, *Adv. Mater.* **2009**, *21*, 4249.

ADVANCED MATERIALS
www.advmat.de
www.MaterialsViews.com

[8] E. Rodriguez-Carmona, O. Cano-Garrido, J. Seras-Franzoso, A. Villaverde, E. Garcia-Fruitos, *Microb. Cell Fact.* **2010**, *9*, 71.
[9] G. Georgiou, P. Valax, *Methods Enzymol.* **1999**, *309*, 48.
[10] F. Baneyx, M. Mujacic, *Nat. Biotechnol.* **2004**, *22*, 1399.
[11] A. Jungbauer, W. Kaar, *J. Biotechnol.* **2007**, *128*, 587.
[12] S. M. Singh, A. K. Panda, *J. Biosci. Bioeng.* **2005**, *99*, 303.
[13] L. F. Vallejo, U. Rinas, *Microb. Cell Fact.* **2004**, *3*, 11.
[14] L. D. Cabrita, S. P. Bottomley, *Biotechnol. Annu. Rev.* **2004**, *10*, 31.
[15] E. Garcia-Fruitos, J. Seras-Franzoso, E. Vazquez, A. Villaverde, *Nanotechnology* **2010**, *21*, 205101.
[16] S. Peternel, S. Jevsevar, M. Bele, V. Gaberc-Porekar, V. Menart, *Biotechnol. Appl. Biochem.* **2008**, *49*, 239.
[17] W. Wu, L. Xing, B. Zhou, Z. Lin, *Microb. Cell Fact.* **2011**, *10*, 9.
[18] J. Nahalka, B. Nidetzky, *Biotechnol. Bioeng.* **2007**, *97*, 454.
[19] S. Ventura, A. Villaverde, *Trends Biotechnol.* **2006**, *24*, 179.
[20] E. Garcia-Fruitos, A. Villaverde, *Korean J. Chem. Eng.* **2010**, *27*, 385.
[21] E. Garcia-Fruitos, N. Gonzalez-Montalban, M. Morell, A. Vera, R. M. Ferraz, A. Aris, S. Ventura, A. Villaverde, *Microb. Cell Fact.* **2005**, *4*, 27.
[22] E. Garcia-Fruitos, M. Martinez-Alonso, N. Gonzalez-Montalban, M. Valli, D. Mattanovich, A. Villaverde, *J. Mol. Biol.* **2007**, *374*, 195.
[23] A. Vera, N. Gonzalez-Montalban, A. Aris, A. Villaverde, *Biotechnol. Bioeng.* **2007**, *96*, 1101.
[24] S. Peternel, J. Grdadolnik, V. Gaberc-Porekar, R. Komel, *Microbiol. Cell Fact.* **2008**, *7*, 34.
[25] N. Gonzalez-Montalban, E. Garcia-Fruitos, A. Villaverde, *Nat. Biotechnol.* **2007**, *25*, 718.
[26] E. Garcia-Fruitos, A. Aris, A. Villaverde, *Appl. Environ. Microbiol.* **2007**, *73*, 289.
[27] E. Garcia-Fruitos, E. Vazquez, C. Diez-Gil, J. L. Corchero, J. Seras-Franzoso, I. Ratera, J. Veciana, A. Villaverde, *Trends Biotechnol* **2012**, *30*, 65.
[28] D. Shcherbo, E. M. Merzlyak, T. V. Chepurnykh, A. F. Fradkov, G. V. Ermakova, E. A. Solovieva, K. A. Lukyanov, E. A. Bogdanova, A. G. Zaraisky, S. Lukyanov, D. M. Chudakov, *Nat. Methods* **2007**, *4*, 741.
[29] J. P. Richard, K. Melikov, E. Vives, C. Ramos, B. Verbeure, M. J. Gait, L. V. Chernomordik, B. Lebleu, *J. Biol. Chem.* **2003**, *278*, 585.
[30] S. K. Calderwood, J. R. Theriault, J. Gong, *Eur. J. Immunol.* **2005**, *35*, 2518.
[31] J. Guo, H. Xin. *Science* **2006**, *314*, 1232.
[32] C. Garrido, E. Schmitt, C. Cande, N. Vahsen, A. Parcellier, G. Kroemer, *Cell Cycle* **2003**, *2*, 579.
[33] C. Garrido, S. Gurbuxani, L. Ravagnan, G. Kroemer, *Biochem. Biophys. Res. Commun.* **2001**, *286*, 433.
[34] D. Lanneau, M. Brunet, E. Frisan, E. Solary, M. Fontenay, C. Garrido, *J. Cell Mol. Med.* **2008**, *12*, 743.
[35] T. Sugiyama, B. D. Levy, T. Michel, *J. Biol. Chem.* **2009**, *284*, 12691.
[36] J. R. Schnell, H. J. Dyson, P. E. Wright, *Annu. Rev. Biophys. Biomol. Struct.* **2004**, *33*, 119.
[37] H. Cario, D. E. Smith, H. Blom, N. Blau, H. Bode, K. Holzmann, U. Pannicke, K. P. Hopfner, E. M. Rump, Z. Ayric, E. Kohne, K. M. Debatin, Y. Smulders, K. Schwarz, *Am. J. Hum. Genet.* **2011**, *88*, 226.
[38] B. S. Askari, M. Krajinovic, *Curr. Genomics* **2010**, *11*, 578.
[39] H. Lodish, A. Berk, S. L. Zipursky, P. Matsudaira, D. Baltimore, J. Darnell, *Molecular Cell Biology*, 4th edition, W. H. Freeman and Company, New York, USA **2011**.
[40] L. Packer, E. Cadenas. *Free Radic. Res.* **2007**, *41*, 951.
[41] J. Goh, L. Enns, S. Fatemie, H. Hopkins, J. Morton, C. Pettan-Brewer, W. Ladiges, *BMC Cancer* **2011**, *11*, 191.
[42] X. L. Shi, Z. H. Shi, H. Huang, H. G. Zhu, P. Zhou, D. Ju, *Inflammation* **2010**, *33*, 166.
[43] B. Beltran, P. Nos, F. Dasi, M. Iborra, G. Bastida, M. Martinez, J. E. O'Connor, G. Saez, I. Moret, J. Ponce, *Inflamm. Bowel. Dis.* **2010**, *16*, 76.
[44] H. J. Geuze, J. W. Slot, P. A. van der Ley, R. C. Scheffer, *J. Cell Biol.* **1981**, *89*, 653.
[45] G. Skiniotis, P. J. Lupardus, M. Martick, T. Walz, K. C. Garcia, *Mol. Cell* **2008**, *31*, 737.
[46] R. C. Robinson, L. M. Grey, D. Staunton, H. Vankelecom, A. B. Vernallis, J. F. Moreau, D. I. Stuart, J. K. Heath, E. Y. Jones, *Cell* **1994**, *77*, 1101.
[47] C. L. Stewart, P. Kaspar, L. J. Brunet, H. Bhatt, I. Gadi, F. Kontgen, S. J. Abbondanzo, *Nature* **1992**, *359*, 76.
[48] W. Hu, Z. Feng, A. K. Teresky, A. J. Levine, *Nature* **2007**, *450*, 721.
[49] S. Imsoonthornruksa, P. Noisa, R. Parnpai, M. Ketudat-Cairns, *J. Biotechnol.* **2011**, *151*, 295.
[50] U. Rinas, J. E. Bailey, *Appl. Microbiol. Biotechnol.* **1992**, *37*, 609.
[51] M. M. Carrio, A. Villaverde, *J. Bacteriol.* **2005**, *187*, 3599.
[52] N. Ferrer-Miralles, J. Domingo-Espin, J. L. Corchero, E. Vazquez, A. Villaverde, *Microb. Cell Fact.* **2009**, *8*, 17.
[53] P. Neubauer, B. Fahnert, H. Lilie, A. Villaverde, in *Inclusions in Prokaryotes*, (Ed: J. M. Shively), Springer, Germany pp. 237, **2006**.
[54] S. Peternel, R. Komel, *Microb. Cell Fact.* **2010**, *9*, 66.
[55] Z. Antosova, M. Mackova, V. Kral, T. Macek, *Trends Biotechnol.* **2009**, *27*, 628.
[56] J. H. Meyer, in *Physiology of the gastrointestinal tract*, (Ed: L. R. Johnson LR). Raven Press, New York, USA, pp. 613, **1987**.
[57] Y. Miyabara, M. Tabata, J. Suzuki, S. Suzuki, *J. Chromatogr.* **1992**, *574*, 261.
[58] A. Mitraki, *Adv. Protein Chem. Struct. Biol.* **2010**, *79*, 89.
[59] E. Garcia-Fruitos, *Microb. Cell Fact.* **2010**, *9*, 80.
[60] A. Villaverde, *Microb. Cell Fact.* **2010**, *9*, 53.
[61] E. Rodriguez-Carmona, A. Villaverde, *Trends Microbiol.* **2010**, *18*, 423.
[62] E. Vazquez, A. Villaverde, *Microb. Cell Fact.* **2010**, *9*, 101.
[63] L. F. Vallejo, M. Brokelmann, S. Marten, S. Trappe, J. Cabrera-Crespo, A. Hoffmann, G. Gross, H. A. Weich, U. Rinas, *J. Biotechnol.* **2002**, *94*, 185.

Adv. Mater. **2012**,
DOI: 10.1002/adma.201104330

Annex 5

Bacterial inclusion bodies: making gold from waste

Elena García-Fruitós, Esther Vazquez, César Díez-Gil, José Luis Corchero,
Joaquin Seras-Franzoso, Imma Ratera, Jaume Veciana and Antonio Villaverde,

Trends in Biotechnology, Vol 30, 2012

Opinion

Cell PRESS

Bacterial inclusion bodies: making gold from waste

Elena García-Fruitós[1,2,3*], Esther Vázquez[1,2,3*], César Díez-Gil[3,4], José Luis Corchero[1,2,3], Joaquin Seras-Franzoso[1,2,3], Imma Ratera[3,4], Jaume Veciana[3,4] and Antonio Villaverde[1,2,3]

[1] Institute for Biotechnology and Biomedicine, Universitat Autònoma de Barcelona, Bellaterra, 08193 Barcelona, Spain
[2] Department of Genetics and Microbiology, Universitat Autònoma de Barcelona, Bellaterra, 08193 Barcelona, Spain
[3] CIBER de Bioingeniería, Biomateriales y Nanomedicina (CIBER-BBN), Bellaterra, 08193 Barcelona, Spain
[4] Department of Molecular Nanoscience and Organic Materials, Institut de Ciència de Materials de Barcelona (CSIC), Bellaterra, 08193 Barcelona, Spain

Many protein species produced in recombinant bacteria aggregate as insoluble protein clusters named inclusion bodies (IBs). IBs are discarded from further processing or are eventually used as a pure protein source for *in vitro* refolding. Although usually considered as waste byproducts of protein production, recent insights into the physiology of recombinant bacteria and the molecular architecture of IBs have revealed that these protein particles are unexpected functional materials. In this Opinion article, we present the relevant mechanical properties of IBs and discuss the ways in which they can be explored as biocompatible nanostructured materials, mainly, but not exclusively, in biocatalysis and tissue engineering.

Biology of bacterial inclusion bodies

Bacterial inclusion bodies (IBs) are protein aggregates that have been commonly observed in recombinant *Escherichia coli* since the implementation of recombinant DNA technologies. IBs were rapidly recognized as the major bottleneck in recombinant protein production and were assumed to be formed by unfolded or highly misfolded polypeptides that failed to reach their native conformation [1].

Solubility has been considered the main macroscopic signal of successful protein conformation and functional quality at the molecular level [2]. For instance, many recombinant proteins have been produced only (or almost only) as IBs and consequently discarded before further use. Thus, in biomedical research, among the wide spectrum of proteins identified as potential drugs, only a very limited fraction are actually produced, approved for use and marketed. In this context, a significant number of the therapeutic proteins in use have been obtained in yeasts or mammalian cells instead of *E. coli*. These systems allow post-translational modifications that are absent in bacteria and overcome massive aggregation [3].

Protein aggregation in bacteria has contributed to lower than expected success for recombinant DNA technologies because the yield of functional, soluble and stable polypeptides is often not cost-effective enough for industrial production. Even laboratory-scale production of many specific products for research purposes has a protein insolubility bottleneck. Minimization of protein aggregation through midstream approaches (by chaperone co-expression, protein engineering or by adjusting gene dosage, temperature or transcription rate) has yielded rather inconsistent and product-dependent results. Rational manipulation of foldase, protease and disaggregase activities to control protein solubility depends on metabolic engineering reaching the systems level. Unfortunately, the regulatory complexity, synergism and redundancy of the cellular quality control network make such a task currently unaffordable. At the downstream level, IBs are eventually used as a source of protein for *in vitro* refolding and recovery. This is because up to 90% of the total protein in IBs is recombinant protein and because IBs can easily be separated from cell debris by simple procedures. However, refolding strategies for proteins from isolated IBs need to be developed on a case-by-case basis and are weakly extendible to a wide spectra of products (insulin is among the exceptions). Consequently, IBs have been historically observed as undesired waste products of biotechnology processes [1].

Although recombinant protein aggregation in bacteria has been ignored as a scientific issue for decades and thus IB research has largely been neglected, a few seminal observations have revitalized both academic and industrial interest in IBs. Recent research in conformational stress of recombinant bacteria has provided insights into the physiology of IB formation and on the molecular architecture of these protein clusters. Emerging concepts regarding how bacteria survey the quality of soluble and insoluble protein species, the dynamics of protein aggregation–disaggregation, the functional characterization of IB polypeptides and the mechanical stability of IBs have unveiled unexpected potential for IBs in nanobiotechnology. In this Opinion article, we summarize these findings and support a new view on bacterial IBs. We propose reasons why IBs should not be discarded as waste byproducts of bioengineering processes. Instead, protein production processes might eventually be retargeted to obtain tailored IBs as desirable biomaterials for novel applications in industry and biomedicine.

Corresponding authors: Veciana, J. (vecianaj@icmab.es); Villaverde, A. (antoni.villaverde@uab.cat)
* These authors contributed equally contributed to this work.

0167-7799/$ - see front matter doi:10.1016/j.tibtech.2011.09.003 Trends in Biotechnology, February 2012, Vol. 30, No. 2

Inclusion bodies are highly dynamic and contain functional protein

Interest in IBs has recently resurfaced largely because of the findings that (i) protein deposition in recombinant cells is fully reversible and (ii) a relevant fraction of IB proteins is actually functional.

Protein deposition in recombinant cells is fully reversible

Already formed IBs spontaneously disintegrate in the cytoplasm of *E. coli* when *de novo* protein synthesis is arrested [4]. The process is highly dependent on chaperones and proteases, which indicates that IB proteins are actively removed from the clusters by cell components. More generically, cell-controlled IB disintegration also indicates that aggregates are not excluded from the conformational surveillance of the cell. In this regard, the main chaperone DnaK is a key controller of IB protein extraction and degradation, and uncoupling of DnaK and protease activities largely stabilizes aggregation-prone recombinant proteins [5]. Observations of soluble aggregates in recombinant bacteria largely support a continuum-of-forms model, under which bacteria contain the recombinant protein in a gradation of conformational states that steadily migrate between soluble and insoluble (virtual) cell fractions (Figure 1a) [6].

An important fraction of the IB-forming protein is functional

Enzyme activity in IBs was first associated with β-galactosidase [7] and endoglucanase D [8], but it was suspected that the activity was due to contamination. In 2005, functional protein species were clearly identified in IBs of the human granulocyte-colony stimulating factor formed in *E. coli* at suboptimal growth temperatures [9]. Such IBs were termed nonclassical inclusion bodies in the belief that these protein clusters were structurally anomalous and different from conventional protein aggregates. However, a parallel study using *E. coli* cells that produced green or blue fluorescent proteins, dihydrofolate reductase or an aggregation-prone version of β-galactosidase (at 37 °C) showed that conventional IBs were biologically active

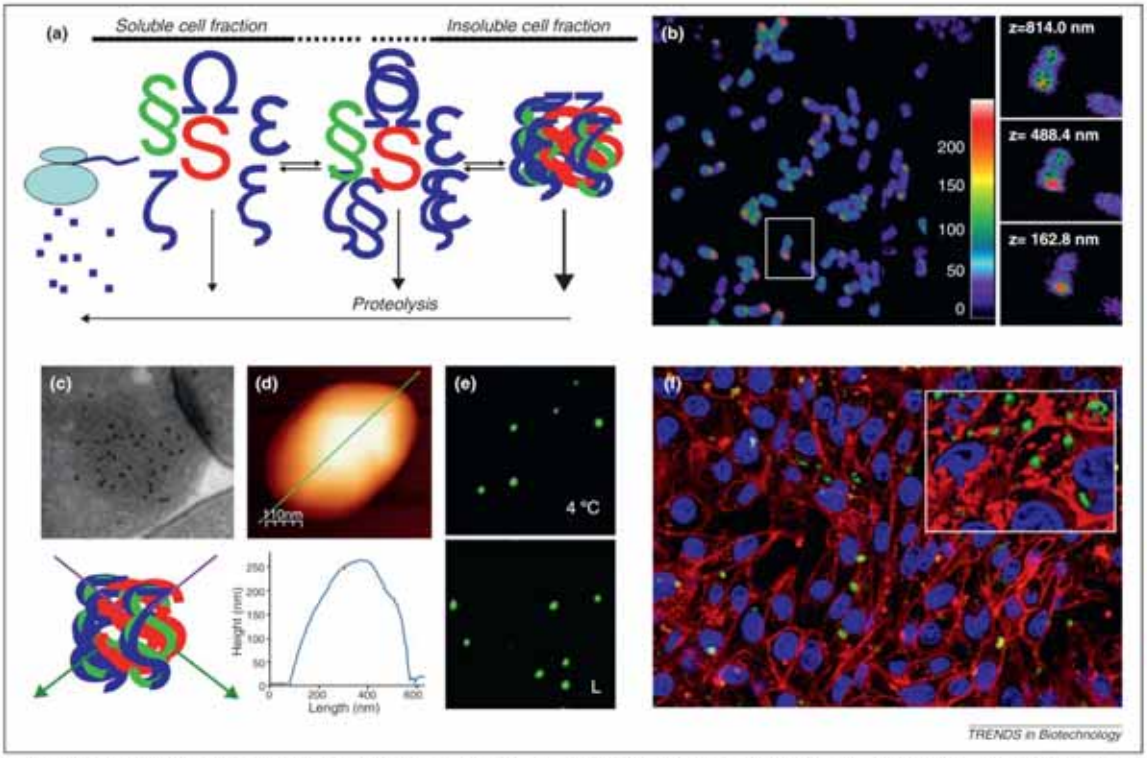

Figure 1. **(a)** A single recombinant protein produced in bacteria can fold into a wide spectrum of conformations, including the native conformation (red), functional isoforms (green) and inactive, largely misfolded protein forms (blue). All these species can reversibly aggregate via stereospecific crossmolecular interactions as soluble or insoluble clusters, through chaperone-modulated processes. Aggregated peptides are also substrates for proteases. **(b)** Confocal section of an *E. coli* culture producing GFP IBs. Magnified images of a single cell at different *z* values are also presented, which show the fluorescent core of the protein particles and the slightly less fluorescent surface layer. **(c)** Transmission electron micrograph of intracellular GFP IBs immunodetected with GFP-reactive antibodies. The porous architecture of IBs, which supports their high hydration and mechanical stability, is evident. Such a loose organization allows efficient mass transfer and permits diffusion of the substrate (purple lines) and release of the product (green lines) during enzymatic catalysis (bottom). **(d)** 3D AFM topographic image of a single GFP IB deposited on a mica surface. Its topographic cross-section indicated as a green line is shown at the bottom. **(e)** Confocal microscopy images of purified IBs formed by mGFP as in panel **(d)**, stored for 1 month at 4 °C (top) and after lyophilization and reconstitution (L, bottom). **(f)** Overlay of BHK cell culture growing on polystyrene plates decorated with mGFP IBs 75 h after cell seeding. The inset shows intimate cell membrane-IB contacts visualized by confocal xyz sections stack-processed using Imaris 3D software (modified from [22]; Copyright Wiley-VCH Verlag GmbH & Co. KGaA. Reproduced with permission).

[10]. Thus, even IBs produced using standard protocols can be considered as nonclassical regarding the functional quality of the embedded proteins. The extent of biological activity exhibited by IB proteins (measured as specific activity or fluorescence) depends on the specific protein, genetic background of the host bacteria and culture temperature [11], and ranges from undetectable amounts to levels even higher than those shown by soluble counterparts [10].

The biological activity of IB proteins requires protein folding and native or native-like secondary structure of the embedded protein (Figure 1a). Protein deposition as bacterial IBs is a sterospecific event, as suggested not only by the high protein purity of the aggregates, but also by the co-aggregation *in vitro* of homologous denatured proteins [12] and the sequence-specific seeding ability of isolated IBs [13]. Furthermore, sequence-specific contacts during IB formation have been fully proved *in vivo* through the mutually exclusive formation of IBs in cells that produce two heterologous protein species [14]. Stereospecific cross-molecular contacts require native-like secondary structure, and native-like conformation of IB proteins has been widely confirmed by IR spectroscopy [15]. Moreover, fine imaging analysis of GFP IBs revealed a more intense fluorescence in the core than at the IB surface [16]. Furthermore, fluorescence confocal section analysis of individual IBs within cells supports the functional nature of the IB core and suggests a structural role of native protein in the IB scaffold rather than superficial contamination (Figure 1b) [17].

Examinations of the inner architecture of IBs have benefited from amyloidosis clinical investigation with IR, circular dichroism, X-ray diffraction and other techniques for structural analysis. As a result, both native-like secondary structures and amyloid-like cross-molecular β-sheet architectures have been identified in IBs [13]. Proteinase K-resistant amyloidal fibers have been described as IB components. Although quantitative data are not available, such fibers probably represent a low proportion of the total IB mass [14]. How properly folded and amyloid-like protein stretches coexist and are organized within these protein particles remains an unsolved issue. However, structural studies on IBs have revealed that the relative abundance of cross-β regions is much lower than in conventional amyloid fibrils [18], which indicates that important segments of IB proteins are excluded from the tightly packed β-sheet architecture.

Inclusion bodies can be used as naturally immobilized enzymes in biocatalysis

The biological activity of bacterial IBs opens intriguing possibilities for their rational use in applications in which aggregation *per se* is not a major impediment [19]. Many recombinant enzymes, naturally immobilized as functional IBs, have been explored for industrial catalysis in a set of very elegant studies. So far, oxidases, reductases, phosphatases, kinases, aldolases, glucosidases, phosphorylases and others have been investigated as IB-based catalysts. *In vivo* immobilized enzymes might be advantageous because high yields of recombinant proteins can easily be driven to pure protein particles using selected peptides as pull-down tags [20]. In addition, the porous nature of IBs is expected to permit efficient mass transfer through the IB scaffold (Figure 1c), and their surface nanorugosity (Figure 1d) would be convenient for IB immobilization in solid phase catalysis. In addition, the production cost for pure IBs is estimated to be approximately 20 times lower than for easy-to-produce soluble proteins (García-Fruitós, unpublished data).

IBs are mechanically stable enough to withstand harvest by ultrasonication, high pressure or other harsh physical procedures applied to break cells [21]. This property is very convenient for industrial-scale manipulation in enzymatic reactors. In addition, very low amounts of the IB protein are released to aqueous media from freshly isolated IBs during the first minutes of incubation [16]. Beyond this point, IBs are extremely stable in long-term storage and incubation without perceivable changes in size, geometry and biological activity [22]. In addition, IBs show good tolerance of lyophilization and freezing–thawing (Figure 1e). In an enzymatic study, 90% of the initial maltodextrin phosphorylase activity was observed in naked IBs from *Pyrococcus furiosus* after 10 reaction cycles [23]. This excellent operational stability can be further enhanced by entrapping IBs in semi-permeable gel matrices or microcapsules [based on either agar–TiO_2, poly(methylene-co-guanidine), alginates and cellulose sulfate] [24,25], alone or in combination with crosslinking agents such as glutaraldehyde [26]. This approach minimizes eventual enzyme leakage and consequent product contamination. Finally, high-cell-density production of IBs is fully feasible and improved downstream protocols have been adapted to obtain highly pure protein particles [27,28].

Inclusion bodies are mechanically stable nanoparticulate materials

IBs are harvested from bacterial cultures by harsh mechanical procedures to disrupt the cell wall. On purification, IBs are observed as pseudospherical particles (Figure 1d) with limited size dispersion, ranging from 50 to 500 nm in diameter. IB average size depends on the particular protein species, genetic background of the cell and harvest time [22]. The biological origin, mechanical stability and regulatable size of IBs, together with the increasing demand for fully biocompatible and tunable nanostructured materials, raises the question of to what extent these protein particles can function as particulate biomaterials for biomedical applications.

In recent years, numerous studies have supported functionalization and nanostructuring of surfaces in tissue engineering and regenerative medicine [29]. Among the available approaches, the generation of nanostructured and nanopatterned surfaces with either inorganic or organic materials (Table 1) is especially appealing. These coatings not only improve cell adhesion and proliferation, but also influence more complex cellular processes such as cell differentiation and motility [30]. However, the need for complicated coating techniques, low versatility, limited physicochemical characteristics and cytotoxicity have delayed further progress in this area.

In bottom-up approaches to topographic engineering, IBs formed by irrelevant proteins successfully stimulate

Table 1. Most common materials for surface modification used in tissue engineering

Material	Properties*	Application	Deposition or presentation method	Ref.
Inorganic coatings (DLC, apatite, TiO_2, etc.)	Biocompatibility, nanophase materials, high Young's modulus (GPa)	Tissue engineering (mainly hard tissues such as bones)	Physical deposition, anodization, electrospun, chemical growth	[38]
Organic coatings (HA, FN, PL, PAA/PAM, PLGA, etc.)	Biocompatibility, versatile surface chemistry, controlled degradation	Tissue engineering (soft and hard tissues), drug or gene delivery	Layer by layer (LBL) deposition, electrospinning	[39]
Nanoparticles (metallic, magnetic, organic, ceramic, etc.)	Controlled size, versatile surface chemistry	Tissue engineering, drug or gene delivery, imaging	Chemical growth	[40]
Carbon nanotubes (CNTs)	Electroactive, high specific surface, functionalization, good mechanical properties	Tissue engineering, cell tracking and labeling, sensing of cellular behavior	Electrospinning, chemical vapor deposition (CVD)	[41]
IBs	Simple and cost-effective production, controlled size, biocompatibility, appropriate (and tunable) chemical and mechanical properties, nanoroughness	Tissue engineering	Dip coating and soft lithography techniques	[31]
IBs *	Simple and cost-effective production, controlled size, mechanical stability, porosity, reusability	Biocatalysis	Naked material, microencapsulation, gel embedment or crosslinking	[10]

*Additional properties of IBs as functional materials for catalysis are also indicated.

surface colonization by mammalian cells without any sign of cytotoxicity (Figure 1f) [22,31]. Because they are bioadhesive, IBs enhance cell retention on the decorated substrate. In addition, IBs activate filopodia-mediated cell sensing and suitable mechanotransduction circuits that stimulate proliferation via activation of the ERK pathway [32]. Acting as inert materials, their geometry, stiffness, Z-potential, wettability, size and morphology can be tuned by selective production using defined *E. coli* genetic backgrounds. In particular, deficiencies in chaperones, DnaK and ClpA, or in the protease ClpP lead to anomalous quality control and protein deposition patterns, which significantly affect the nanoscale properties of IBs produced in these mutants (Table 2) [17,22,31]. Interestingly, the impact of extracellular matrix hydrophobicity on stem cell adhesion, spread and differentiation was evaluated in a recent study by screening substrate variants with different properties [33]. The contact angle identified as optimal for surface colonization (57.99°) is within the range of angles exhibited by IBs and perfectly matches that of IB variants produced in $DnaK^-$ and $ClpA^-$ cells [31], which further supports the use of IBs as convenient substrate materials to favor mammalian cell colonization.

Surface patterning by microcontact printing with IBs influences the spatial distribution and performance of cultured cells [22]. Colloidal lithography produces a similar result. Here, dense short-range ordered arrays of circular gold holes in SiO_2 films are produced using dispersed colloidal monolayer masks. The hole diameter can be varied using a series of particles of sizes very similar to those of IBs. The gold holes can be modified using proteins (e.g. fibronectin or vitronectin) defined into patterns. In these studies, protein type and pattern size have an important effect on cell adhesion and spreading [34]. Compared to well-characterized hard materials such as TiO_2 particles, the reproducibility of cell responses to IB patterning has not been yet fully evaluated.

The density and porosity of isolated IBs can be modified by adjusting the pH (Table 2). Extreme chemical or physical changes to bacterial cultures influence the size and morphology of non-IB protein aggregates [35]. Whether these parameters could be useful in modulating IB properties at midstream or downstream levels deserves detailed investigation, as they might represent a way to minimize the heterogeneity of IB particles as natural products. Finally, the fact that polypeptides packaged as

Table 2. Biological and physicochemical nanoscale properties of bacterial IBs

Property*	Modulating factor	Ref.
Size	Tuneable by harvesting time and by the host genetic background	[22]
Geometry	Tuneable by the host genetic background	[17]
Stiffness	Tuneable by the host genetic background	[31]
Wettability	Tuneable by the host genetic background	[31]
Z-potential	Tuneable by the host genetic background	[31]
Bio-adhesiveness	Tuneable by the host genetic background	[32]
Proteolytic stability	Regulatable by harvesting time	[42]
Specific activity or specific fluorescence	Tuneable by production conditions (mainly by temperature) and by the host genetic background	[22]
Density/Porosity	Regulatable by pH	[43]
Release of functional proteins	Regulatable by production temperature	[36]

*All the properties listed are co-determined by the nature of the specific polypeptide forming the IBs.

non-classical IBs release high amounts of functional polypeptides under nondenaturing conditions [36] opens a possibility to use these materials as sustained protein delivery systems in cell–substrate interfaces, for instance, embedded in hydrogels.

The potential of IBs as promising advanced materials has been rapidly accepted by the scientific community [28,37]. However, full identification of the possibilities and drawbacks of these particulate materials requires more detailed investigations. Prematurely stopped, pioneering proteomic studies on IBs should be now completed. Global compositional analysis of IBs would potentially identify undesired contaminants that might compromise IB use in biological systems. This would help to improve downstream strategies to obtain cleaner materials. New-generation protocols to prepare IBs fully free from bacterial cells [27] already provide particles that do not exhibit any signs of toxicity when exposed to mammalian cell cultures [17,22].

Success of the applications of IBs as biocatalysts and as inert nanostructured materials tested so far for tissue engineering cannot be more promising. However, further multidisciplinary research is still needed to fully implement IB-based material platforms in emerging bionanotechonological applications.

Disclosure statement

A.V., E.G.F., E.V., J.V., I.R. and C.D.G. are co-inventors of a patent (P200900045) on the use of IBs as reagents for mammalian cell culture.

Acknowledgments

We are grateful for financial support of our research on bacterial inclusion bodies from MICINN (BFU2010-17450 and CTQ2010-19501), AGAUR (2009SGR-00108 and 2009SGR-00516) and CIBER de Bioingeniería, Biomateriales y Nanomedicina (CIBER-BBN, Spain) through projects NANOPILLS and NAINBO. CIBER-BBN is an initiative funded by the VI National R&D&i Plan 2008–2011, Iniciativa Ingenio 2010, Consolider Program, CIBER Actions and financed by the Instituto de Salud Carlos III with assistance from the European Regional Development Fund. J.S.F. is the recipient of a PIF doctoral fellowship from UAB and A.V. is the recipient of an ICREA ACADEMIA award.

References

1 Baneyx, F. and Mujacic, M. (2004) Recombinant protein folding and misfolding in *Escherichia coli*. *Nat. Biotechnol.* 22, 1399–1408

2 Gonzalez-Montalban, N. *et al.* (2007) Recombinant protein solubility – does more mean better? *Nat. Biotechnol.* 25, 718–720

3 Ferrer-Miralles, N. *et al.* (2009) Microbial factories for recombinant pharmaceuticals. *Microb. Cell Fact.* 8, 17

4 Carrio, M.M. and Villaverde, A. (2001) Protein aggregation as bacterial inclusion bodies is reversible. *FEBS Lett.* 489, 29–33

5 Martinez-Alonso, M. *et al.* (2009) Re-hosting bacterial chaperones for high-quality protein production. *Appl. Environ. Microbiol.* 75, 7850–7854

6 Ventura, S. and Villaverde, A. (2006) Protein quality in bacterial inclusion bodies. *Trends Biotechnol.* 24, 179–185

7 Worrall, D.M. and Goss, N.H. (1989) The formation of biologically active beta-galactosidase inclusion bodies in *Escherichia coli*. *Aust. J. Biotechnol.* 3, 28–32

8 Tokatlidis, K. *et al.* (1991) High activity of inclusion bodies formed in Escherichia coli overproducing *Clostridium thermocellum* endoglucanase D. *FEBS Lett.* 282, 205–208

9 Jevsevar, S. *et al.* (2005) Production of nonclassical inclusion bodies from which correctly folded protein can be extracted. *Biotechnol. Prog.* 21, 632–639

10 Garcia-Fruitos, E. *et al.* (2005) Aggregation as bacterial inclusion bodies does not imply inactivation of enzymes and fluorescent proteins. *Microb. Cell Fact.* 4, 27

11 Martinez-Alonso, M. *et al.* (2009) Learning about protein solubility from bacterial inclusion bodies. *Microb. Cell Fact.* 8, 4

12 Speed, M.A. *et al.* (1996) Specific aggregation of partially folded polypeptide chains: the molecular basis of inclusion body composition. *Nat. Biotechnol.* 14, 1283–1287

13 Carrio, M. *et al.* (2005) Amyloid-like properties of bacterial inclusion bodies. *J. Mol. Biol.* 347, 1025–1037

14 Morell, M. *et al.* (2008) Inclusion bodies: specificity in their aggregation process and amyloid-like structure. *Biochim. Biophys. Acta* 1783, 1815–1825

15 Doglia, S.M. *et al.* (2008) Fourier transform infrared spectroscopy analysis of the conformational quality of recombinant proteins within inclusion bodies. *Biotechnol. J.* 3, 193–201

16 Garcia-Fruitos, E. *et al.* (2007) Localization of functional polypeptides in bacterial inclusion bodies. *Appl. Environ. Microbiol.* 73, 289–294

17 Garcia-Fruitos, E. *et al.* (2010) Tunable geometry of bacterial inclusion bodies as substrate materials for tissue engineering. *Nanotechnology* 21, 205101

18 de Groot, N.S. *et al.* (2009) Amyloids in bacterial inclusion bodies. *Trends Biochem. Sci.* 34, 408–416

19 Garcia-Fruitos, E. (2010) Inclusion bodies: a new concept. *Microb. Cell Fact.* 9, 80

20 Wu, W. *et al.* (2011) Active protein aggregates induced by terminally attached self-assembling peptide ELK16 in *Escherichia coli*. *Microb. Cell Fact.* 10, 9

21 Georgiou, G. and Valax, P. (1999) Isolating inclusion bodies from bacteria. *Methods Enzymol.* 309, 48–58

22 Garcia-Fruitos, E. *et al.* (2009) Surface cell growth engineering assisted by a novel bacterial nanomaterial. *Adv. Mater.* 21, 4249–4253

23 Nahalka, J. (2008) Physiological aggregation of maltodextrin phosphorylase from *Pyrococcus furiosus* and its application in a process of batch starch degradation to alpha-D-glucose-1-phosphate. *J. Ind. Microbiol. Biotechnol.* 35, 219–223

24 Nahalka, J. *et al.* (2006) Bioenergy beads: a tool for regeneration of ATP/NTP in biocatalytic synthesis. *Artif. Cells Blood Substit. Immobil. Biotechnol.* 34, 515–521

25 Nahalka, J. *et al.* (2008) Encapsulation of *Trigonopsis variabilis* D-amino acid oxidase and fast comparison of the operational stabilities of free and immobilized preparations of the enzyme. *Biotechnol. Bioeng.* 99, 251–260

26 Nahalka, J. *et al.* (2008) A crosslinked inclusion body process for sialic acid synthesis. *J. Biotechnol.* 134, 146–153

27 Rodriguez-Carmona, E. *et al.* (2010) Isolation of cell-free bacterial inclusion bodies. *Microb. Cell Fact.* 9, 71

28 Peternel, S. and Komel, R. (2010) Isolation of biologically active nanomaterial (inclusion bodies) from bacterial cells. *Microb. Cell Fact.* 9, 66

29 Dalby, M.J. (2009) Nanostructured surfaces: cell engineering and cell biology. *Nanomedicine* 4, 247–248

30 Ferrari, A. *et al.* (2010) Neuronal polarity selection by topography-induced focal adhesion control. *Biomaterials* 31, 4682–4694

31 Diez-Gil, C. *et al.* (2010) The nanoscale properties of bacterial inclusion bodies and their effect on mammalian cell proliferation. *Biomaterials* 31, 5805–5812

32 Seras-Franzoso, J. *et al.* (2012) Bioadhesiveness and efficient mechanotransduction stimuli synergistically provided by bacterial inclusion bodies as scaffolds for tissue engineering. *Nanomedicine* 7, 79–93

33 Ayala, R. *et al.* (2011) Engineering the cell–material interface for controlling stem cell adhesion, migration, and differentiation. *Biomaterials* 32, 3700–3711

34 Malmstrom, J. *et al.* (2011) Focal complex maturation and bridging on 200 nm vitronectin but not fibronectin patches reveal different mechanisms of focal adhesion formation. *Nano Lett.* 11, 2264–2271

35 Natalello, A. *et al.* (2008) Physical and chemical perturbations induce the formation of protein aggregates with different structural features. *Protein Expr. Purif.* 58, 356–361

36 Peternel, S. *et al.* (2008) Engineering inclusion bodies for non denaturing extraction of functional proteins. *Microb. Cell Fact.* 7, 34
37 Mitraki, A. (2010) Protein aggregation from inclusion bodies to amyloid and biomaterials. *Adv. Protein Chem. Struct. Biol.* 79, 89–125
38 Whited, B.M. *et al.* (2011) Pre-osteoblast infiltration and differentiation in highly porous apatite-coated PLLA electrospun scaffolds. *Biomaterials* 32, 2294–2304
39 Chien, H.W. *et al.* (2009) Spatial control of cellular adhesion using photo-crosslinked micropatterned polyelectrolyte multilayer films. *Biomaterials* 30, 2209–2218
40 Hu, Y. *et al.* (2010) Layer-by-layer assembly of beta-estradiol loaded mesoporous silica nanoparticles on titanium substrates and its implication for bone homeostasis. *Adv. Mater.* 22, 4146–4150
41 Harrison, B.S. and Atala, A. (2007) Carbon nanotube applications for tissue engineering. *Biomaterials* 28, 344–353
42 Carrio, M.M. *et al.* (2000) Fine architecture of bacterial inclusion bodies. *FEBS Lett.* 471, 7–11
43 Peternel, S. *et al.* (2008) New properties of inclusion bodies with implications for biotechnology. *Biotechnol. Appl. Biochem.* 49, 239–246

References

1. Olempska-Beer,Z.S., Merker,R.I., Ditto,M.D., & DiNovi,M.J. Food-processing enzymes from recombinant microorganisms--a review. Regul. Toxicol. Pharmacol. 45, 144-158 (2006).

2. Das,A.P., Sukla,L.B., Pradhan,N., & Nayak,S. Manganese biomining: A review. Bioresour. Technol. 102, 7381-7387 (2011).

3. Pandey,A. et al. The realm of microbial lipases in biotechnology. Biotechnol. Appl. Biochem. 29 (Pt 2), 119-131 (1999).

4. Anfinsen,C.B. Principles that govern the folding of protein chains. Science 181, 223-230 (1973).

5. Karplus,M. The Levinthal paradox: yesterday and today. Fold. Des 2, S69-S75 (1997).

6. Dill,K.A. & Chan,H.S. From Levinthal to pathways to funnels. Nat. Struct. Biol. 4, 10-19 (1997).

7. Matagne,A. & Dobson,C.M. The folding process of hen lysozyme: a perspective from the 'new view'. Cell Mol. Life Sci. 54, 363-371 (1998).

8. Baldwin,R.L. Protein folding. Matching speed and stability. Nature 369, 183-184 (1994).

9. Dobson,C.M. Principles of protein folding, misfolding and aggregation. Semin. Cell Dev. Biol 15, 3-16 (2004).

10. Johnston,J.A., Ward,C.L., & Kopito,R.R. Aggresomes: a cellular response to misfolded proteins. J. Cell Biol. 143, 1883-1898 (1998).

11. Sukhanova,A., Poly,S., Shemetov,A., Bronstein,I., & Nabiev,I. Implications of protein structure instability: from physiological to pathological secondary structure. Biopolymers 97, 577-588 (2012).

12. Barnhart,M.M. & Chapman,M.R. Curli biogenesis and function. Annu. Rev. Microbiol. 60, 131-147 (2006).

13. Sawyer,E.B., Claessen,D., Haas,M., Hurgobin,B., & Gras,S.L. The assembly of individual chaplin peptides from Streptomyces coelicolor into functional amyloid fibrils. PLoS. One. 6, e18839 (2011).

14. Maji,S.K. et al. Functional amyloids as natural storage of peptide hormones in pituitary secretory granules. Science 325, 328-332 (2009).

15. Waegeman,H. & Soetaert,W. Increasing recombinant protein production in Escherichia coli through metabolic and genetic engineering. J. Ind. Microbiol. Biotechnol. 38, 1891-1910 (2011).

16. Hudault,S., Guignot,J., & Servin,A.L. Escherichia coli strains colonising the gastrointestinal tract protect germfree mice against Salmonella typhimurium infection. Gut 49, 47-55 (2001).

17. Ferens,W.A. & Hovde,C.J. Escherichia coli O157:H7: animal reservoir and sources of human infection. Foodborne. Pathog. Dis. 8, 465-487 (2011).

18. Toshifumi,T., Axel,M., Hanno,L., Pierre,G., & Bernd,B. Genetic dissection of the roles of chaperones and proteases in protein folding and degradation in the Escherichia coli cytosol. Molecular Microbiology 40, 397-413 (2001).

19. Basler,G., Grimbs,S., & Nikoloski,Z. Optimizing metabolic pathways by screening for feasible synthetic reactions. Biosystems 109, 186-191 (2012).

20. Kuba,H., Furukawa,A., Okajima,T., & Furukawa,K. Efficient bacterial production of functional antibody fragments using a phagemid vector. Protein Expr. Purif. 58, 292-300 (2008).

21. del Solar,G., Giraldo,R., Ruiz-Echevarria,M.J., Espinosa,M., & az-Orejas,R. Replication and control of circular bacterial plasmids. Microbiol. Mol. Biol. Rev. 62, 434-464 (1998).

22. Barnard,A., Wolfe,A., & Busby,S. Regulation at complex bacterial promoters: how bacteria use different promoter organizations to produce different regulatory outcomes. Curr. Opin. Microbiol. 7, 102-108 (2004).

23. Hannig,G. & Makrides,S.C. Strategies for optimizing heterologous protein expression in Escherichia coli. Trends Biotechnol. 16, 54-60 (1998).

24. Terpe,K. Overview of bacterial expression systems for heterologous protein production: from molecular and biochemical fundamentals to commercial systems. Appl. Microbiol. Biotechnol. 72, 211-222 (2006).

25. Studier,F.W. & Moffatt,B.A. Use of bacteriophage T7 RNA polymerase to direct selective high-level expression of cloned genes. J. Mol. Biol. 189, 113-130 (1986).

26. Guzman,L.M., Belin,D., Carson,M.J., & Beckwith,J. Tight regulation, modulation, and high-level expression by vectors containing the arabinose PBAD promoter. J. Bacteriol. 177, 4121-4130 (1995).

27. Kazemi,S.A., Norgaard,P., Palmqvist,E.A., Andersen,A.S., & Olsson,L. Modulating heterologous protein production in yeast: the applicability of truncated auxotrophic markers. Appl. Microbiol. Biotechnol.(2012).

28. Sorensen,H.P. & Mortensen,K.K. Advanced genetic strategies for recombinant protein expression in Escherichia coli. J. Biotechnol. 115, 113-128 (2005).

29. Seras-Franzoso,J. et al. Disulfide bond formation and activation of Escherichia coli beta-galactosidase under oxidizing conditions. Appl. Environ. Microbiol. 78, 2376-2385 (2012).

30. Miroux,B. & Walker,J.E. Over-production of proteins in Escherichia coli: mutant hosts that allow synthesis of some membrane proteins and globular proteins at high levels. J. Mol. Biol. 260, 289-298 (1996).

31. Valderrama-Rincon,J.D. et al. An engineered eukaryotic protein glycosylation pathway in Escherichia coli. Nat. Chem. Biol. 8, 434-436 (2012).

32. Garcia-Fruitos,E. et al. Divergent genetic control of protein solubility and conformational quality in Escherichia coli. J. Mol. Biol. 374, 195-205 (2007).

33. Lemaux,P.G., Herendeen,S.L., Bloch,P.L., & Neidhardt,F.C. Transient rates of synthesis of individual polypeptides in E. coli following temperature shifts. Cell 13, 427-434 (1978).

34. Nishihara,K., Kanemori,M., Yanagi,H., & Yura,T. Overexpression of

trigger factor prevents aggregation of recombinant proteins in Escherichia coli. Appl Environ Microbiol 66, 884-889 (2000).

35. Thomas,J.G. & Baneyx,F. Protein folding in the cytoplasm of Escherichia coli: requirements for the DnaK-DnaJ-GrpE and GroEL-GroES molecular chaperone machines. Mol Microbiol 21, 1185-1196 (1996).

36. Kuczynska-Wisnik,D. et al. The Escherichia coli small heat-shock proteins IbpA and IbpB prevent the aggregation of endogenous proteins denatured in vivo during extreme heat shock. Microbiology 148, 1757-1765 (2002).

37. Carrio,M.M. & Villaverde,A. Protein aggregation as bacterial inclusion bodies is reversible. FEBS Lett 489, 29-33 (2001).

38. Lee,I. & Suzuki,C.K. Functional mechanics of the ATP-dependent Lon protease- lessons from endogenous protein and synthetic peptide substrates. Biochim. Biophys. Acta 1784, 727-735 (2008).

39. Yu,A.Y. & Houry,W.A. ClpP: a distinctive family of cylindrical energy-dependent serine proteases. FEBS Lett. 581, 3749-3757 (2007).

40. Marston,F.A. The purification of eukaryotic polypeptides synthesized in Escherichia coli. Biochem. J. 240, 1-12 (1986).

41. Garcia-Fruitos,E. et al. Aggregation as bacterial inclusion bodies does not imply inactivation of enzymes and fluorescent proteins. Microb. Cell Fact. 4, 27 (2005).

42. Garcia-Fruitos,E., Aris,A., & Villaverde,A. Localization of functional polypeptides in bacterial inclusion bodies. Appl. Environ. Microbiol. 73, 289-294 (2007).

43. Garcia-Fruitos,E., Carrio,M.M., Aris,A., & Villaverde,A. Folding of a misfolding-prone beta-galactosidase in absence of DnaK. Biotechnol. Bioeng. 90, 869-875 (2005).

44. Carrio,M.M. & Villaverde,A. Localization of chaperones DnaK and GroEL in bacterial inclusion bodies. J. Bacteriol. 187, 3599-3601 (2005).

45. Gonzalez-Montalban,N., Garcia-Fruitos,E., & Villaverde,A. Recombinant protein solubility - does more mean better? Nat. Biotechnol 25, 718-720 (2007).

46. Peternel,S., Grdadolnik,J., Gaberc-Porekar,V., & Komel,R. Engineering inclusion bodies for non denaturing extraction of functional proteins. Microb. Cell Fact. 7, 34 (2008).

47. King,J., Haase-Pettingell,C., Robinson,A.S., Speed,M., & Mitraki,A. Thermolabile folding intermediates: inclusion body precursors and chaperonin substrates. FASEB J. 10, 57-66 (1996).

48. Carrio,M.M., Corchero,J.L., & Villaverde,A. Proteolytic digestion of bacterial inclusion body proteins during dynamic transition between soluble and insoluble forms. Biochim Biophys Acta 1434, 170-176 (1999).

49. Carrio,M.M. & Villaverde,A. Construction and deconstruction of bacterial inclusion bodies. J Biotechnol 96, 3-12 (2002).

50. Przybycien,T.M., Dunn,J.P., Valax,P., & Georgiou,G. Secondary structure

characterization of beta-lactamase inclusion bodies. Protein Eng 7, 131-136 (1994).

51. Tenidis,K. et al. Identification of a penta- and hexapeptide of islet amyloid polypeptide (IAPP) with amyloidogenic and cytotoxic properties. J Mol Biol 295, 1055-1071 (2000).

52. Carrio,M., Gonzalez-Montalban,N., Vera,A., Villaverde,A., & Ventura,S. Amyloid-like properties of bacterial inclusion bodies. J. Mol. Biol. 347, 1025-1037 (2005).

53. Morell,M. et al. Inclusion bodies: specificity in their aggregation process and amyloid-like structure. Biochim. Biophys. Acta 1783, 1815-1825 (2008).

54. Arie,J.P., Miot,M., Sassoon,N., & Betton,J.M. Formation of active inclusion bodies in the periplasm of Escherichia coli. Mol. Microbiol. 62, 427-437 (2006).

55. Taylor,G., Hoare,M., Gray,D.R., & Marston,F.A.O. Size and Density of Protein Inclusion-Bodies. Bio-Technology 4, 553-557 (1986).

56. Bowden,G.A., Paredes,A.M., & Georgiou,G. Structure and morphology of protein inclusion bodies in Escherichia coli. Biotechnology (N. Y.) 9, 725-730 (1991).

57. Carrio,M.M., Cubarsi,R., & Villaverde,A. Fine architecture of bacterial inclusion bodies. FEBS Lett 471, 7-11 (2000).

58. Carrio,M.M., Corchero,J.L., & Villaverde,A. Dynamics of in vivo protein aggregation: building inclusion bodies in recombinant bacteria. FEMS Microbiol Lett 169, 9-15 (1998).

59. Rinas,U. & Bailey,J.E. Overexpression of bacterial hemoglobin causes incorporation of pre-beta-lactamase into cytoplasmic inclusion bodies. Appl. Environ. Microbiol. 59, 561-566 (1993).

60. Georgiou,G. & Valax,P. Isolating inclusion bodies from bacteria. Methods Enzymol. 309, 48-58 (1999).

61. Conchillo-Sole,O. et al. AGGRESCAN: a server for the prediction and evaluation of "hot spots" of aggregation in polypeptides. Bmc Bioinformatics 8, (2007).

62. Peternel,S. & Komel,R. Isolation of biologically active nanomaterial (inclusion bodies) from bacterial cells. Microb. Cell Fact. 9, 66 (2010).

63. Gonzalez-Montalban,N., Garcia-Fruitos,E., Ventura,S., Aris,A., & Villaverde,A. The chaperone DnaK controls the fractioning of functional protein between soluble and insoluble cell fractions in inclusion body-forming cells. Microb. Cell Fact. 5, 26 (2006).

64. Peternel,S., Jevsevar,S., Bele,M., Gaberc-Porekar,V., & Menart,V. New properties of inclusion bodies with implications for biotechnology. Biotechnol. Appl. Biochem. 49, 239-246 (2008).

65. Jevsevar,S. et al. Production of nonclassical inclusion bodies from which correctly folded protein can be extracted. Biotechnol. Prog. 21, 632-639 (2005).

66. Vallejo,L.F. & Rinas,U. Strategies for the recovery of active proteins through refolding of bacterial inclusion body proteins. Microb. Cell Fact. 3, 11 (2004).

67. Espargaro,A., Villar-Pique,A., Sabate,R., & Ventura,S. Yeast prions form infectious amyloid inclusion bodies in bacteria. Microb. Cell Fact. 11, 89 (2012).

68. Garcia-Fruitos,E., Sabate,R., de Groot,N.S., Villaverde,A., & Ventura,S. Biological role of bacterial inclusion bodies: a model for amyloid aggregation. FEBS J. 278, 2419-2427 (2011).

69. Villar-Pique,A., Espargaro,A., Sabate,R., de Groot,N.S., & Ventura,S. Using bacterial inclusion bodies to screen for amyloid aggregation inhibitors. Microb. Cell Fact. 11, 55 (2012).

70. Nahalka,J., Gemeiner,P., Bucko,M., & Wang,P.G. Bioenergy beads: a tool for regeneration of ATP/NTP in biocatalytic synthesis. Artif. Cells Blood Substit. Immobil. Biotechnol 34, 515-521 (2006).

71. Nahalka,J. & Nidetzky,B. Fusion to a pull-down domain: a novel approach of producing Trigonopsis variabilisD-amino acid oxidase as insoluble enzyme aggregates. Biotechnol Bioeng 97, 454-461 (2007).

72. Nahalka,J., Vikartovska,A., & Hrabarova,E. A crosslinked inclusion body process for sialic acid synthesis. J Biotechnol 134, 146-153 (2008).

73. Garcia-Fruitos,E. et al. Surface Cell Growth Engineering Assisted by a Novel Bacterial Nanomaterial. Advanced Materials 21, 4249-+ (2009).

74. Nahalka,J. Physiological aggregation of maltodextrin phosphorylase from Pyrococcus furiosus and its application in a process of batch starch degradation to alpha-D-glucose-1-phosphate. J. Ind. Microbiol. Biotechnol. 35, 219-223 (2008).

75. Hung,C.F. et al. Ovarian Cancer Gene Therapy Using HPV-16 Pseudovirion Carrying the HSV-tk Gene. PLoS. One. 7, e40983 (2012).

76. Huang,Y. et al. Gene silencing of toll-like receptor 2 inhibits proliferation of human liver cancer cells and secretion of inflammatory cytokines. PLoS. One. 7, e38890 (2012).

77. Kim,J.H. et al. The use of biodegradable PLGA nanoparticles to mediate SOX9 gene delivery in human mesenchymal stem cells (hMSCs) and induce chondrogenesis. Biomaterials 32, 268-278 (2011).

78. Grande,D.A., Pitman,M.I., Peterson,L., Menche,D., & Klein,M. The repair of experimentally produced defects in rabbit articular cartilage by autologous chondrocyte transplantation. J. Orthop. Res. 7, 208-218 (1989).

79. Navsaria,H.A., Myers,S.R., Leigh,I.M., & McKay,I.A. Culturing skin in vitro for wound therapy. Trends Biotechnol. 13, 91-100 (1995).

80. Penn,M.S. et al. Autologous cell transplantation for the treatment of damaged myocardium. Prog. Cardiovasc. Dis. 45, 21-32 (2002).

81. Fodor,W.L. et al. Expression of a functional human complement inhibitor in a transgenic pig as a model for the prevention of xenogeneic hyperacute organ rejection. Proc. Natl. Acad. Sci. U. S. A 91, 11153-11157 (1994).

82. Phelps,C.J. et al. Production of alpha 1,3-galactosyltransferase-deficient pigs. Science 299, 411-414 (2003).

83. Okita,K. & Yamanaka,S. Intracellular signaling pathways regulating pluripotency of embryonic stem cells. Curr. Stem Cell Res. Ther. 1, 103-111 (2006).

84. Minguell,J.J., Erices,A., & Conget,P. Mesenchymal stem cells. Exp.

Biol. Med. (Maywood.) 226, 507-520 (2001).

85. Ventura Ferreira,M.S. et al. Cord blood-hematopoietic stem cell expansion in 3D fibrin scaffolds with stromal support. Biomaterials(2012).

86. Telles,P.D., Machado,M.A., Sakai,V.T., & Nor,J.E. Pulp tissue from primary teeth: new source of stem cells. J. Appl. Oral Sci. 19, 189-194 (2011).

87. Uysal,C.A., Tobita,M., Hyakusoku,H., & Mizuno,H. Adipose-derived stem cells enhance primary tendon repair: Biomechanical and immunohistochemical evaluation. J. Plast. Reconstr. Aesthet. Surg.(2012).

88. Susman,S. et al. Placental stem cell differentiation into islets of Langerhans-like glucagon-secreting cells. Rom. J. Morphol. Embryol. 51, 733-738 (2010).

89. Pittenger,M.F. et al. Multilineage potential of adult human mesenchymal stem cells. Science 284, 143-147 (1999).

90. Mackay,A.M. et al. Chondrogenic differentiation of cultured human mesenchymal stem cells from marrow. Tissue Eng 4, 415-428 (1998).

91. Wakitani,S., Saito,T., & Caplan,A.I. Myogenic cells derived from rat bone marrow mesenchymal stem cells exposed to 5-azacytidine. Muscle Nerve 18, 1417-1426 (1995).

92. Tang,D.Q. et al. In vivo and in vitro characterization of insulin-producing cells obtained from murine bone marrow. Diabetes 53, 1721-1732 (2004).

93. Woodbury,D., Schwarz,E.J., Prockop,D.J., & Black,I.B. Adult rat and human bone marrow stromal cells differentiate into neurons. J. Neurosci. Res. 61, 364-370 (2000).

94. Takahashi,K. & Yamanaka,S. Induction of pluripotent stem cells from mouse embryonic and adult fibroblast cultures by defined factors. Cell 126, 663-676 (2006).

95. Ye,L. et al. Induced pluripotent stem cells offer new approach to therapy in thalassemia and sickle cell anemia and option in prenatal diagnosis in genetic diseases. Proc. Natl. Acad. Sci. U. S. A 106, 9826-9830 (2009).

96. Ebert,A.D. et al. Induced pluripotent stem cells from a spinal muscular atrophy patient. Nature 457, 277-280 (2009).

97. Blum,B., Bar-Nur,O., Golan-Lev,T., & Benvenisty,N. The anti-apoptotic gene survivin contributes to teratoma formation by human embryonic stem cells. Nat. Biotechnol. 27, 281-287 (2009).

98. Liang,Y. et al. The Propensity for Tumorigenesis in Human Induced Pluripotent Stem Cells is Correlated with Genomic Instability. Chin J. Cancer(2012).

99. Langer,R. & Vacanti,J.P. Tissue engineering. Science 260, 920-926 (1993).

100. Freyman,T.M., Yannas,I.V., Yokoo,R., & Gibson,L.J. Fibroblast contraction of a collagen-GAG matrix. Biomaterials 22, 2883-2891 (2001).

101. Wang,Y., Kim,U.J., Blasioli,D.J., Kim,H.J., & Kaplan,D.L. In vitro cartilage tissue engineering with 3D porous

aqueous-derived silk scaffolds and mesenchymal stem cells. Biomaterials 26, 7082-7094 (2005).

102. Williams,D.F. On the nature of biomaterials. Biomaterials 30, 5897-5909 (2009).

103. Badylak,S.F., Freytes,D.O., & Gilbert,T.W. Extracellular matrix as a biological scaffold material: Structure and function. Acta Biomater. 5, 1-13 (2009).

104. Kakisis,J.D., Liapis,C.D., Breuer,C., & Sumpio,B.E. Artificial blood vessel: the Holy Grail of peripheral vascular surgery. J. Vasc. Surg. 41, 349-354 (2005).

105. Assad,M. et al. Porous titanium-nickel for intervertebral fusion in a sheep model: part 1. Histomorphometric and radiological analysis. J. Biomed. Mater. Res. B Appl. Biomater. 64, 107-120 (2003).

106. Assad,M. et al. Porous titanium-nickel for intervertebral fusion in a sheep model: part 2. Surface analysis and nickel release assessment. J. Biomed. Mater. Res. B Appl. Biomater. 64, 121-129 (2003).

107. Levine,J.P. et al. Bone morphogenetic protein promotes vascularization and osteoinduction in preformed hydroxyapatite in the rabbit. Ann. Plast. Surg. 39, 158-168 (1997).

108. Takahashi,Y., Yamamoto,M., & Tabata,Y. Osteogenic differentiation of mesenchymal stem cells in biodegradable sponges composed of gelatin and beta-tricalcium phosphate. Biomaterials 26, 3587-3596 (2005).

109. Pattnaik,S. et al. Chitosan scaffolds containing silicon dioxide and zirconia nano particles for bone tissue engineering. Int. J. Biol. Macromol. 49, 1167-1172 (2011).

110. Laurencin,C.T. & Freeman,J.W. Ligament tissue engineering: an evolutionary materials science approach. Biomaterials 26, 7530-7536 (2005).

111. Zong,X. et al. Electrospun fine-textured scaffolds for heart tissue constructs. Biomaterials 26, 5330-5338 (2005).

112. Chung,T.W., Wang,Y.Z., Huang,Y.Y., Pan,C.I., & Wang,S.S. Poly (epsilon-caprolactone) grafted with nano-structured chitosan enhances growth of human dermal fibroblasts. Artif. Organs 30, 35-41 (2006).

113. Coburn,J.M., Gibson,M., Monagle,S., Patterson,Z., & Elisseeff,J.H. Bioinspired nanofibers support chondrogenesis for articular cartilage repair. Proc. Natl. Acad. Sci. U. S. A 109, 10012-10017 (2012).

114. Zonari,A. et al. Endothelial differentiation of human stem cells seeded onto electrospun polyhydroxybutyrate/polyhydroxybutyrate-co-hydroxyvalerate fiber mesh. PLoS. One. 7, e35422 (2012).

115. Agarwal,M., Koelling,K.W., & Chalmers,J.J. Characterization of the degradation of polylactic acid polymer in a solid substrate environment. Biotechnol. Prog. 14, 517-526 (1998).

116. Agrawal,C.M. & Ray,R.B. Biodegradable polymeric scaffolds for musculoskeletal tissue engineering. J. Biomed. Mater. Res. 55, 141-150 (2001).

117. Dalby,M.J. et al. The control of human mesenchymal cell differentiation

using nanoscale symmetry and disorder. Nat. Mater. 6, 997-1003 (2007).

118. Dalby,M.J. Cellular response to low adhesion nanotopographies. Int. J. Nanomedicine. 2, 373-381 (2007).

119. Yao,C., Slamovich,E.B., & Webster,T.J. Enhanced osteoblast functions on anodized titanium with nanotube-like structures. J. Biomed. Mater. Res. A 85, 157-166 (2008).

120. Ergun,C. et al. Increased osteoblast adhesion on nanoparticulate calcium phosphates with higher Ca/P ratios. J. Biomed. Mater. Res. A 85, 236-241 (2008).

121. Park,G.E., Pattison,M.A., Park,K., & Webster,T.J. Accelerated chondrocyte functions on NaOH-treated PLGA scaffolds. Biomaterials 26, 3075-3082 (2005).

122. Kay,S., Thapa,A., Haberstroh,K.M., & Webster,T.J. Nanostructured polymer/nanophase ceramic composites enhance osteoblast and chondrocyte adhesion. Tissue Eng 8, 753-761 (2002).

123. Miller,D.C., Haberstroh,K.M., & Webster,T.J. Mechanism(s) of increased vascular cell adhesion on nanostructured poly(lactic-co-glycolic acid) films. J. Biomed. Mater. Res. A 73, 476-484 (2005).

124. Pham,Q.P., Sharma,U., & Mikos,A.G. Electrospinning of polymeric nanofibers for tissue engineering applications: a review. Tissue Eng 12, 1197-1211 (2006).

125. Hu,Y., Cai,K., Luo,Z., & Jandt,K.D. Layer-by-layer assembly of beta-estradiol loaded mesoporous silica nanoparticles on titanium substrates and its implication for bone homeostasis. Adv. Mater. 22, 4146-4150 (2010).

126. Whited,B.M., Whitney,J.R., Hofmann,M.C., Xu,Y., & Rylander,M.N. Pre-osteoblast infiltration and differentiation in highly porous apatite-coated PLLA electrospun scaffolds. Biomaterials 32, 2294-2304 (2011).

127. Keefer,E.W., Botterman,B.R., Romero,M.I., Rossi,A.F., & Gross,G.W. Carbon nanotube coating improves neuronal recordings. Nat. Nanotechnol. 3, 434-439 (2008).

128. Marcantonio,N.A. et al. The influence of tethered epidermal growth factor on connective tissue progenitor colony formation. Biomaterials 30, 4629-4638 (2009).

129. Moya,M.L. et al. The effect of FGF-1 loaded alginate microbeads on neovascularization and adipogenesis in a vascular pedicle model of adipose tissue engineering. Biomaterials 31, 2816-2826 (2010).

130. Zieris,A. et al. FGF-2 and VEGF functionalization of starPEG-heparin hydrogels to modulate biomolecular and physical cues of angiogenesis. Biomaterials 31, 7985-7994 (2010).

131. Bhang,S.H. et al. The effect of the controlled release of nerve growth factor from collagen gel on the efficiency of neural cell culture. Biomaterials 30, 126-132 (2009).

132. Visser,R., Arrabal,P.M., Becerra,J., Rinas,U., & Cifuentes,M. The effect of an rhBMP-2 absorbable collagen sponge-targeted system on bone formation in vivo. Biomaterials 30, 2032-2037 (2009).

133. Molnar,P., Wang,W., Natarajan,A., Rumsey,J.W., & Hickman,J.J. Photolithographic patterning of C2C12 myotubes using vitronectin as growth substrate in serum-free medium. Biotechnol. Prog. 23, 265-268 (2007).

134. Zouani,O.F., Chollet,C., Guillotin,B., & Durrieu,M.C. Differentiation of pre-osteoblast cells on poly(ethylene terephthalate) grafted with RGD and/or BMPs mimetic peptides. Biomaterials 31, 8245-8253 (2010).

135. Hennessy,K.M. et al. The effect of RGD peptides on osseointegration of hydroxyapatite biomaterials. Biomaterials 29, 3075-3083 (2008).

136. Berner,A. et al. Biomimetic tubular nanofiber mesh and platelet rich plasma-mediated delivery of BMP-7 for large bone defect regeneration. Cell Tissue Res. 347, 603-612 (2012).

137. Ghadiri,M.R., Granja,J.R., Milligan,R.A., McRee,D.E., & Khazanovich,N. Self-assembling organic nanotubes based on a cyclic peptide architecture. Nature 366, 324-327 (1993).

138. Hartgerink,J.D., Beniash,E., & Stupp,S.I. Self-assembly and mineralization of peptide-amphiphile nanofibers. Science 294, 1684-1688 (2001).

139. Claussen,R.C., Rabatic,B.M., & Stupp,S.I. Aqueous self-assembly of unsymmetric Peptide bolaamphiphiles into nanofibers with hydrophilic cores and surfaces. J. Am. Chem. Soc. 125, 12680-12681 (2003).

140. Vauthey,S., Santoso,S., Gong,H., Watson,N., & Zhang,S. Molecular self-assembly of surfactant-like peptides to form nanotubes and nanovesicles. Proc. Natl. Acad. Sci. U. S. A 99, 5355-5360 (2002).

141. Reches,M. & Gazit,E. Casting metal nanowires within discrete self-assembled peptide nanotubes. Science 300, 625-627 (2003).

142. Gorbitz,C.H. Nanotube formation by hydrophobic dipeptides. Chemistry. 7, 5153-5159 (2001).

143. Mitraki,A. Protein aggregation from inclusion bodies to amyloid and biomaterials. Adv. Protein Chem. Struct. Biol. 79, 89-125 (2010).

144. Griffith,L.G. & Naughton,G. Tissue engineering--current challenges and expanding opportunities. Science 295, 1009-1014 (2002).

145. Stevens,M.M. & George,J.H. Exploring and engineering the cell surface interface. Science 310, 1135-1138 (2005).

146. Khang,D., Carpenter,J., Chun,Y.W., Pareta,R., & Webster,T.J. Nanotechnology for regenerative medicine. Biomed. Microdevices. 12, 575-587 (2010).

147. Peternel,S., Grdadolnik,J., Gaberc-Porekar,V., & Komel,R. Engineering inclusion bodies for non denaturing extraction of functional proteins. Microb. Cell Fact. 7, 34 (2008).

148. Margreiter,G., Messner,P., Caldwell,K.D., & Bayer,K. Size characterization of inclusion bodies by sedimentation field-flow fractionation. J. Biotechnol. 138, 67-73 (2008).

149. Carrio,M.M. & Villaverde,A. Role of molecular chaperones in inclusion body formation. FEBS Lett 537, 215-221 (2003).

150. Weibezahn,J., Bukau,B., & Mogk,A. Unscrambling an egg: protein disaggregation by AAA+ proteins. Microb Cell Fact. 3, 1 (2004).

151. Rokney,A. et al. E. coli transports aggregated proteins to the poles by a specific and energy-dependent process. J. Mol. Biol. 392, 589-601 (2009).

152. Kantawong,F. et al. Whole proteome analysis of osteoprogenitor differentiation induced by disordered nanotopography and mediated by ERK signalling. Biomaterials 30, 4723-4731 (2009).

153. Tsuboi,Y. et al. Overexpression of extracellular signal-regulated protein kinase and its correlation with proliferation in human hepatocellular carcinoma. Liver Int. 24, 432-436 (2004).

154. Bastow,E.R. et al. Selective activation of the MEK-ERK pathway is regulated by mechanical stimuli in forming joints and promotes pericellular matrix formation. J. Biol. Chem. 280, 11749-11758 (2005).

155. Yim,E.K., Pang,S.W., & Leong,K.W. Synthetic nanostructures inducing differentiation of human mesenchymal stem cells into neuronal lineage. Exp. Cell Res. 313, 1820-1829 (2007).

156. Chen,W. et al. Nanotopography influences adhesion, spreading, and self-renewal of human embryonic stem cells. ACS Nano. 6, 4094-4103 (2012).

157. Redenti,S. et al. Retinal tissue engineering using mouse retinal progenitor cells and a novel biodegradable, thin-film poly(e-caprolactone) nanowire scaffold. J. Ocul. Biol. Dis. Infor. 1, 19-29 (2008).

158. Ge,C., Xiao,G., Jiang,D., & Franceschi,R.T. Critical role of the extracellular signal-regulated kinase-MAPK pathway in osteoblast differentiation and skeletal development. J. Cell Biol. 176, 709-718 (2007).

159. Biggs,M.J. et al. Adhesion formation of primary human osteoblasts and the functional response of mesenchymal stem cells to 330nm deep microgrooves. J. R. Soc. Interface 5, 1231-1242 (2008).

160. Biggs,M.J. et al. The use of nanoscale topography to modulate the dynamics of adhesion formation in primary osteoblasts and ERK/MAPK signalling in STRO-1+ enriched skeletal stem cells. Biomaterials 30, 5094-5103 (2009).

161. Yanes,O. et al. Metabolic oxidation regulates embryonic stem cell differentiation. Nat. Chem. Biol. 6, 411-417 (2010).

162. Engler,A.J., Sen,S., Sweeney,H.L., & Discher,D.E. Matrix elasticity directs stem cell lineage specification. Cell 126, 677-689 (2006).

163. Chiu,D.T. et al. Patterned deposition of cells and proteins onto surfaces by using three-dimensional microfluidic systems. Proc. Natl. Acad. Sci. U. S. A 97, 2408-2413 (2000).

164. McMurray RJ et al. Nanoscale Surfaces for the Long-Term Maintenance of Mesenchymal Stem Cell Phenotype and Multipotency. Nat Mater. 2011.

165. Doschak,M.R., Kucharski,C.M., Wright,J.E., Zernicke,R.F., &

Uludag,H. Improved bone delivery of osteoprotegerin by bisphosphonate conjugation in a rat model of osteoarthritis. Mol. Pharm. 6, 634-640 (2009).

166. Jaklenec,A. et al. Sequential release of bioactive IGF-I and TGF-beta 1 from PLGA microsphere-based scaffolds. Biomaterials 29, 1518-1525 (2008).

167. Madduri,S., di,S.P., Papaloizos,M., Kalbermatten,D., & Gander,B. Effect of controlled co-delivery of synergistic neurotrophic factors on early nerve regeneration in rats. Biomaterials 31, 8402-8409 (2010).

168. Liovic,M. et al. Inclusion bodies as potential vehicles for recombinant protein delivery into epithelial cells. Microb. Cell Fact. 11, 67 (2012).

169. Badtke,M.P., Hammer,N.D., & Chapman,M.R. Functional amyloids signal their arrival. Sci. Signal. 2, e43 (2009).

170. Garrido,C., Gurbuxani,S., Ravagnan,L., & Kroemer,G. Heat shock proteins: endogenous modulators of apoptotic cell death. Biochem. Biophys. Res. Commun. 286, 433-442 (2001).

171. Bikfalvi,A., Klein,S., Pintucci,G., & Rifkin,D.B. Biological roles of fibroblast growth factor-2. Endocr. Rev. 18, 26-45 (1997).

172. Peternel,S. & Komel,R. Active Protein Aggregates Produced in Escherichia coli. Int. J. Mol. Sci. 12, 8275-8287 (2011).

173. Maji,S.K. et al. Amyloid as a depot for the formulation of long-acting drugs. PLoS. Biol. 6, e17 (2008).

Acknowledgements

Acknowledgements

Això ja s'acaba i s'ha de dir que ha estat un procés molt difícil i dur però també divertit i enriquidor a molts nivells. Voldria agrair a totes aquelles persones que d'una manera o altre m'han ajudat a avançar durant aquests quatre anys. Pels qui em coneixeu ja sabreu que no sóc massa donat a discursos, així doncs demano disculpes per endavant per la qualitat del que escriuré a continuació, ja que mai podrà reflectir la magnitud de tot el que us dec.

Toni, moltíssimes gràcies per dipositar la teva confiança en mi i creure en la meva capacitat, per ajudar-me sempre que ho he necessitat i per oferir la teva experiència en els moments complicats. Gràcies per obrir-me les portes del grup, permetent-me així iniciar una de les etapes més enriquidores de la meva vida. Gràcies també per mostrar-me la grandesa dels cossos d'inclusió, sembla mentida que una cosa tan petita hagi tingut tanta influència en la meva existència.

Elena, a tu et va tocar ensenyar-me a moure'm pel laboratori sense fer masses destrosses, aguantar-me des dels meus inicis (sempre difícils), donar-me ànims i consell quan els experiments es torcien i una infinitat de coses més per les quals sempre t'estaré agraït. Gràcies per la teva paciència, per no donar-te mai per vençuda. Resulta molt fàcil treballar amb tu, sempre eficient però amable i alegre (que és encara més important). Per tot això gràcies infinites!

Esther, moltíssimes gràcies pel teu positivisme, durant el transcurs d'aquests quatre anys s'agraeix tenir gent al voltant amb tanta energia com tu. Gràcies per tots els ànims que m'has donat, pels consells a cultius cel·lulars i per ajudar en el que calgués quan era necessari.

Neus gràcies per tota la teva ajuda, sobretot per fer que donar les pràctiques resultés molt més senzill i divertit (cosa que té molt de mèrit). Gràcies també per estar sempre disposada a ajudar als altres i per tot el que he aprés de tu durant aquest temps.

Escar ha estat un plaer coincidir amb tu al laboratori, ets una persona amb la que sempre es pot comptar, amb la que es pot parlar obertament de qualsevol cosa, gràcies per fer més entretingut el dia a dia.

Pepe gracias por tu sentido del humor, siempre es bueno reír pero haciendo la tesis se convierte en algo indispensable para mantener juicio.

Rosa gràcies per facilitar-nos tant la vida, sense tu, la Vero i la Delia això no hagués estat possible. Gràcies per evitar que el laboratori s'ensorri i per aguantar-nos a tots nosaltres sense perdre mai la paciència (malgrat les bronques, per altra banda absolutament necessàries).

Vero muchísimas gracias por todo, eres la persona más alegre que he conocido y contagias esa alegría todos los que están a tu alrededor. Siempre estas ahí para charlar un rato y reír y reír y reír. Gracias por toda la ayuda que me has dado, por los ánimos y por tu experiencia. Ha sido increíblemente divertido trabajar contigo.

Joan que t'haig de dir, ha estat genial compartir aquesta experiència amb tu, sobretot pel que fa fondues, espaguetàs i demés, la veritat és que m'ho he passat sempre molt bé. Gràcies a més, per compartir un pensament crític amb el sistema que ens envolta. Fas que encara no perdi l'esperança que un món més just és possible. Salut i verduretes ecològiques!

Paolo, muchas gracias por hacer más divertidos los días, por estar siempre dispuesto a ayudar, por esperarme para echar el café y por aportar alegría al grupo. Tú sí que vales!

Ugutz, puede que sin darte cuenta, pero has aportado grandes dosis de humor durante estos cuatro años. Tu brutal sinceridad es desternillante (o por lo menos a mí me lo parece). Gracias por ayudarme cuando lo he necesitado y por tu clases aceleradas de IMARIS.

Olivia ha estat un plaer tenir-te de veïna de taula, gracies per posar música als nostres dies (i que no fos flaix fm!!) i compartir l'afició per la literatura fantàstica. Has fet la feina una mica menys monòtona, gràcies.

Joan Marc hem rigut molt, gràcies per entretenir-nos amb les teves historietes, però sobretot per la manera d'explicar-les, tot i que no sempre és fàcil entendre't!!!

Xu and Mireia I have shared a short period with you but it has been long enough to know you a little bit more. You are very nice people and I wish all the best for you in the future.

Monica i Nuria no vam compartir un període massa llarg però de les dues he aprés coses i m'enduc bons records, moltes gràcies.

Gracies a tu també Fela per la teva inestimable ajuda sobretot per les correccions dels textos en anglès. M'enduc també una recepta de guacamole que fa les delícies de tot aquell que el tasta.

Christoph and Karl thank you for being so patient with my English. In the end I think that we have done a good work together!

Fran, Sílvia, Paqui i tots aquells que han passat per cultius, moltes gràcies per la vostra ajuda. Sobretot a tu Fran que has patit en carn pròpia els meus estrambòtics experiments, sempre disposat a ajudar i fent que la feina resultés molt més interessant.

He aprés moltíssim amb tu i m'has ajudat a millorar enormement, gràcies també per totes les xerrades i els ànims que m'has donat durant aquests anys.

Haig d'agrair també al professor Jaume Veciana i al seu grup sobretot a la Imma, César i Witold per la seva inestimable ajuda a l'hora de portar endavant projectes comuns que han ajudat a definir aquesta tesi.

Uschi thank you very much, to you and your team: Maria, Ana and Zhaopeng for making of my stay in Hannover a really nice experience.

Matt thank you for the opportunity you gave me of doing a stay at your laboratory but also for your kindness and patience with me. It has been really great working in Glasgow. I want to thank also all the people at the CCE who helped me during my stay: Frank, Laura, Lewis, Caroline etc. but especially to you Monica. You taught me a lot of useful stuff and suffered most of my complaints and problems. I am really grateful you and Matt led my project there!

Muchas gracias a ti también Ángel por enseñarme la ciudad, donde estaban los mejores pubs y compartir unas cuantas pintas!!

No todo puede ser curro en esta vida! Gracias a toda mi familia por haberme apoyado no solo durante estos últimos cuatro años sino durante toda mi vida (es lo que toca, pero no por eso es menos meritorio), a mis padres porque sin ellos yo no estaría aquí y por lo tanto no podría escribir la tesis (ni existir). Gracias también por preocuparse por mi (a veces demasiado), por proporcionarme todo lo que he necesitado y ayudarme a crecer. También quiero agradecer a mis hermanitos, a la Roser y mis sobrinas por hacer de los domingos un día para desconectar y cargar pilas.

Gracias también a ti Carmen, por tu interés a lo largo del trabajo y todos los ánimos que nos has dado tanto a Andrea como a mi mismo.

No me olvido de los colegas Ivan, Furby y Elías con los que he compartido muy buenos momentos, la verdad es que nos lo pasamos muy bien, no sabría decir si habéis sido una buena influencia para el correcto desarrollo de la tesis… pero queda más que compensado!

També vull fer una menció especial als biotecs, no em posaré a dir noms perquè no acabaríem! Però junts hem descobert interessos comuns, ens hem fet grans i la hem liat en més d'una ocasió. Merci biotecs!!!

També et vull donar les gracies Teixi per tots els cops que m'has salvat la vida apropant-me de la Uni a Mataró i viceversa, per les partides de catan, per animar-me a escriure i els bons moments compartits!

Finalment et volia donar les gràcies a tu Andrea, per aguantar-me, per donar-me el teu suport i omplir de significat la meva vida. Sense tu estic segur que no hagués arribat fins aquí. Em coneixes millor que cap altre persona i saps perfectament què fer en cada moment, t'estaré eternament agraït (o fins que em mori, el que arribi abans). T' estimo.